DESIGN CRITERIA AND PERFORMANCE OF GAS TURBINES IN A COMBINED POWER AND POWER (CPP) PLANT FOR ELECTRICAL POWER GENERATION

QUSAI ZUHAIR MOHAMMED AL-HAMDAN

A thesis submitted in partial fulfilment of the
requirements of the University of Hertfordshire
for the degree of Doctor of Philosophy

The programme of research was carried out in the Department of
Aerospace, Automotive and Mechanical Engineering,
University of Hertfordshire

In collaboration with

The Royal Jordanian Air Force

June 2002

LIST OF CONTENTS

List of contents

ABSTRACT

The simple gas turbine engine operates on the basic Joule-Brayton cycle and it is notorious for its poor thermal efficiency. Several modifications have been made to the simple cycle in order to increase its thermal efficiency but, within the thermal and mechanical stress constrains, the efficiency still ranges between 28 and 35%. However, higher values of energy utilisation efficiency have been claimed in recent years by using low grade heat from the engine exhaust either for district heating or for raising low pressure steam for chemical processes. Both applications are not very attractive in hot countries.

The concept of using the low grade thermal energy from the gas turbine exhaust to raise steam in order to drive a steam turbine and generate additional electricity, i.e. the combined power and power or CPP plant would be more attractive in hot countries than the CHP plant. It was hypothesized that the operational parameters, hence the performance of the CPP plant, would depend on the allowable gas turbine entry temperature. Hence, the exhaust gas temperature could not be decided arbitrarily.

This thesis deals with the performance of the gas turbine engine operating as a part of the combined power and power plant. In a CPP plant, the gas turbine does not only produce power but also the thermal energy that is required to operate the steam turbine plant at achievable thermal efficiency.

Abstract

The combined gas turbine-steam turbine cycles are thermodynamically analysed. A parametric study for different configurations of the combined gas-steam cycles has been carried out to show the influence of the main parameters on the CPP cycle performance. The parametric study was carried out using realistic values in view of the known constraints and taking into account any feasible future developments.

The results of the parametric study show that the maximum CPP cycle efficiency would be at a point for which the gas turbine cycle would have neither its maximum efficiency nor its maximum specific work output. It has been shown that supplementary heating or gas turbine reheating would decrease the CPP cycle efficiency; hence, it could only be justified at low gas turbine inlet temperatures. Also it has been shown that although gas turbine intercooling would enhance the performance of the gas turbine cycle, it would have only a slight effect on the CPP cycle performance.

A graphical method for studying operational compatibility, i.e. matching, between gas turbine components has been developed for a steady state or equilibrium operation. The author would like to submit that the graphical method offers a novel and easy to understand approach to the complex problem of component matching. It has been shown that matching conditions between the compressor and the turbine could be satisfied by superimposing the turbine performance characteristics on the compressor performance characteristics providing the axes of both were normalised. This technique can serve as a valuable tool to determine the operating range and the engine running line. Furthermore, it would decide whether the gas turbine engine was operating in a region of adequate compressor and turbine efficiencies.

A computer program capable of simulating the steady state off-design conditions of the gas turbine engine as part of the CPP plant has been developed. The program was written in Visual Basic. Also, another program was developed to simulate the steady state off-design operation of the steam turbine power plant. A combination of both programs was used to simulate the combined power plant.

Finally, it could be claimed that the computer simulation of the CPP plant makes significant contribution to the design of thermal power plants as it would help in investigating the effects of the performance characteristics of the components on the performance of complete engines at the design and off-design conditions. This investigation of the CPP plat performance can be carried out at the design and engineering stages and thus help to reduce the cost of manufacturing and testing the expensive prototype engines.

ACKNOWLEDGEMENT

I would like to thank my project supervisors Prof. F. S. Bhinder and Dr S. Nasser for their invaluable guidance and for providing all the support needed to make this work possible. I would also like to express my thanks to my colleagues, Munzer Ebaid and Omar Al-Qura'n for their stimulating discussion and encouragement throughout the period of this research program.

Special gratitude to my family for their patience and encouragement throughout my study. The help of the administration office of STRC at the University of Hertfordshire will always be remembered.

Last but not least, I want to express my appreciation to the Royal Jordanian Air Force for their immense support and assistance.

NOMENCLATURE

Symbol	Meaning	Unit
C_P	Specific heat at constant pressure	kJ/kgK
C_V	Specific heat at constant volume	kJ/kgK
γ	Ratio of specific heats	------
$\dot{m}$	Mass flow rate	kg/s
q,Q	Heat supplied or rejected	$kJ/kg, kJ$
w,W	Specific work output, work output	$kJ/kg, kJ$
P	Pressure	N/m^2
T	Temperature	$K, ^oC$
S	Entropy	kJ/kg
r	Pressure ratio	------
η	Efficiency	------
θ	Ratio of maximum to minimum temperature	------
χ	Isentropic temperature ratio	------
h	Enthalpy	kJ/kg
LCV	Lower calorific value	kJ/kg
τ	Torque	$N.m$
M	Mach number	------
f	function	------
F	Fuel to air ratio	------
d	Diameter	m
Subscripts		
1,2,3	State points in the cycles	------
gt	Gas turbine	------
st	Steam turbine	------
s	Isentropic	------
∞	Polytropic	------
o	Stagnation	------
g	Gas	------

Nomenclature

a	Air	------
c	Compressor	------
t	Turbine	------
cc	Combustion chamber	------
P	Pump	------
B	Boiler	------
con	Condenser	------
mec	Mechanical	------
carnot	Carnot cycle	------
CPP	Combined power and power	------
H	Higher cycle	------
L	Lower cycle	------
max	Maximum	------
min	Minimum	------
O	Overall	------
Superscripts		
.	Rate	------

CHAPTER 1

INTRODUCTION

1.1 Energy Scenario

Energy is one of the primary needs of human societies for their survival. It is needed for growing food, providing comfort and catering for a host of other application in all fields of activity such as agriculture, industry, transportation, etc. The main sources of energy are fossil fuels, solar radiation fall out, winds, tidal, and geothermal. The conversion, distribution and utilisation of energy are the domain of engineering.

The demand for energy throughout the world is increasing sharply because of growing world population, rising living standards and emphasis on developing energy intensive industries in almost all newly emerging countries to boost their economies in order to combat poverty and hardship.

Fossil fuels, coal, oil and gas, currently, provide more than 95% of the world's energy need. However, the reserves of fossil fuels on planet earth are finite and they are depleting rapidly. It should be noted also that the use of fossil fuels through combustion pollutes the environmental with toxic gases and contributes to global warming. Hence the continuing use of fossil fuels is undesirable both for energy conservation as well as for environmental protection.

Although sources of renewable energies appear to offer a promising alternative, their contribution to the world's total energy demand is still less than 5% and it is unlikely to change substantially in the near future. Hence, in order to conserve fossil fuels, increasing the efficiency of the current power generation systems is of paramount importance. This may be achieved either by modifying the thermal plant configuration or by using advanced thermodynamic cycles for power generation. The main aim of the research reported in this thesis was to investigate the potential gains that might be made in the overall efficiency of electrical power generation by combining gas turbine and steam turbine driven plants. This thesis deals with the gas turbine plant and parallel research program covers the steam turbine plant.

1.2 The Gas Turbine Engine

The gas turbine is a rotodynamic internal combustion engine therefore its working cycle comprises four processes, namely: compression, heating, expansion and discharge. The performance of the engine, i.e. its thermal efficiency and specific work output, depends on the two principal operational variables: cycle pressure ratio and turbine entry temperature. The effect of these variables on the performance of a gas turbine engine can be shown, at least qualitatively, by sketching the cycle on the Temperature *vs.* Entropy (T-S) diagram as shown in Fig. 1.1(a) and 1.1(b).

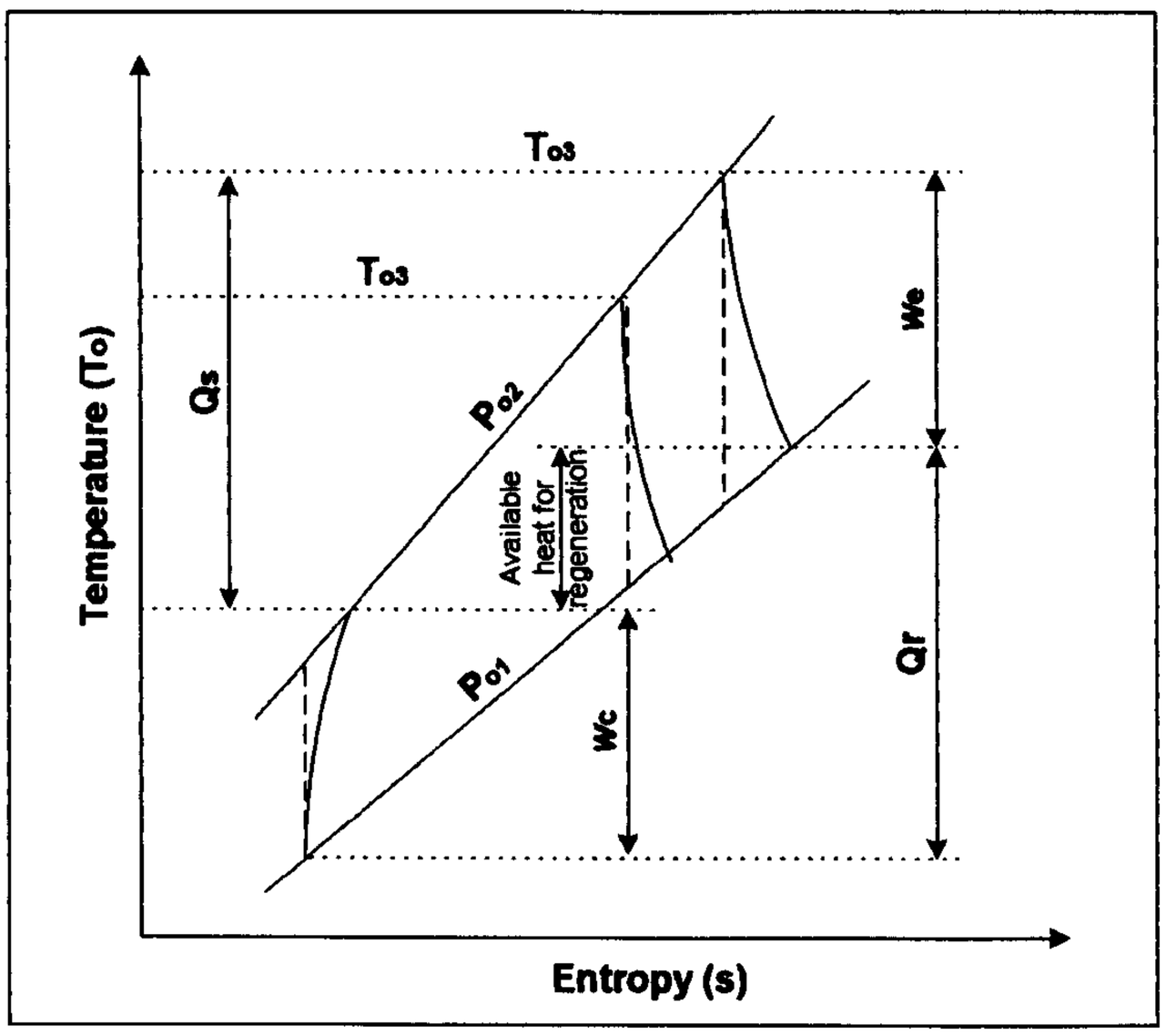

Fig. 1.1(a). The effect of varying turbine entry temperature at constant pressure ratio

For a fixed pressure ratio P_{02}/P_{01} as the turbine entry temperature T_{03} is increased the expansion work w_e increases because of the divergence of the constant pressure lines but the compression work w_c remains constant. Hence, specific work output, i.e. w_e - w_c, increases. Furthermore, because the constant pressure lines curve rise gradually to the left with increasing entropy, Q_r increases relatively more than Q_s therefore thermal efficiency also increases with increasing temperature.

Since permissible level of thermal stress determined by the construction materials limits the maximum value of the turbine entry temperature T_{03}, at a given value of T_{03} the effect of increasing P_{02}, i.e. cycle pressure ratio P_{02}/P_{01}, on performance can be seen qualitatively from Fig. 1.1(b). The values of both compression work and expansion work increase as P_{02} is increased but the relative increase in this case is not as obvious as in the previous case. Both heat supplied Q_s and heat rejected Q_r decrease with increasing P_{02} at constant T_{03} but the changes in the ratio Q_r/Q_s also are not that obvious. However, it is clear that the amount of recoverable heat that may be used for regenerative heating reduces sharply as pressure ratio is increased at constant turbine entry temperature.

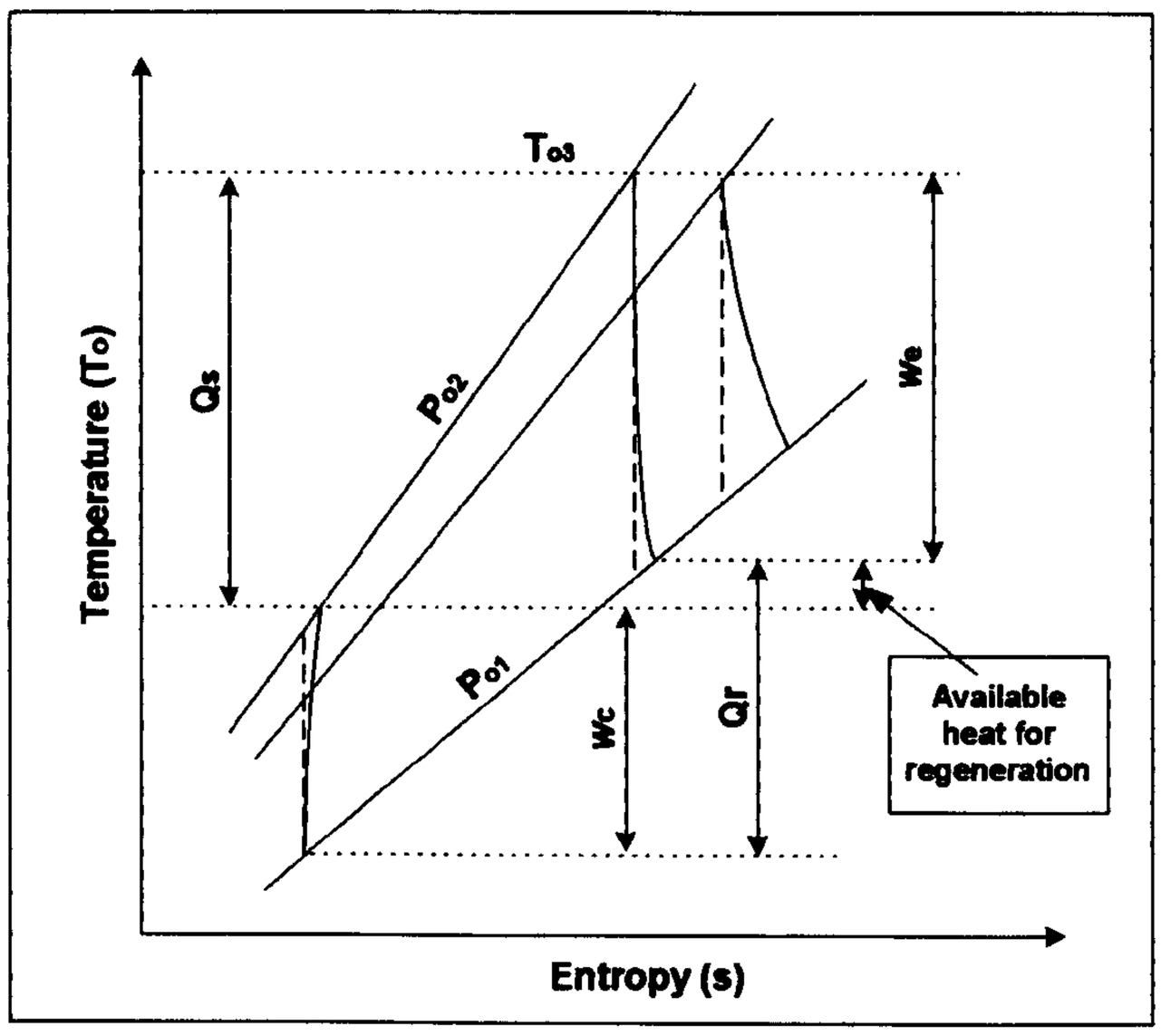

Fig. 1.1(b). The effect of varying pressure ratio at constant turbine entry temperature

Since the simple gas turbine engine is notorious for its poor thermal efficiency, numerous attempts have been made to raise thermal efficiency by modifying the principal cycle parameters. These modifications have included: (a) raising the turbine entry temperature; (b) designing for higher cycle pressure ratio and (c) exhaust heat recovery to heat the compressed air before it enters the combustion chamber i.e. re-generative heating. In spite of these changes, the thermal efficiency of gas turbine engines still remains between 28 to 38%.

Concepts such as *Total Energy* and *Combined Heat & Power*, CHP for short, were intended to recover low-grade exhaust heat for such purposes as district heating or raising low-pressure steam for process industries. The efficiencies as high as 80% for total energy or CHP plants have been claimed but care must be exercised when comparing one type of plant with another.

At this juncture it would be pertinent to define efficiency more precisely. The ambiguity may be avoided by defining efficiency as follows:

$$Energy\ utilisation\ efficiency\ =\ \frac{Work\ done\ +\ Exhaust\ heat\ recovered\ for\ CHP}{Enery\ released\ by\ the\ fuel\ through\ combustion}$$

$$Power\ generation\ efficiency = \frac{Work\ done}{Enery\ released\ by\ the\ fuel\ through\ combustion}$$

These definitions may help to understand that 80% efficiency of a CHP plant is not the power generation efficiency.

1.3 The Combined Power and Power Plant

The latest concept for increasing the power generation efficiency as well the total power output of thermal plants is the combined power and power or CPP plant. A block diagram of the CPP plant is shown in Fig. 1.2 while the Temperature-Entropy diagram of the CPP plant is shown in Fig. 1.5. Low-grade heat recovered from the exhaust gas of the gas turbine plant is used to raise high-pressure steam. This steam is then expanded through a steam turbine to generate additional electricity.

Preliminary estimate of the potential gains that might be made from the CPP plant, using typical values for the thermal efficiencies of the gas turbine and the steam turbine plant, are given in the following.

$$Gas\ turbine\ thermal\ efficiency = 30\%$$

Hence, assuming that the expansion is adiabatic, 70% of the energy released from the combustion of fuel may be extracted from the exhaust gas. Assuming that the steam turbine produces thermal efficiency of 40%, its efficiency in the CPP plant would be:

$$Steam\ tubine\ efficiency = 40\%\ of\ 70\% = 28\%$$

$$The\ overall\ power\ generation\ efficiency = (30 + 28) = 58\ \%$$

This value is significantly higher than either the efficiency of the gas turbine or the efficiency of the steam turbine. This simple calculation provides ample justification to study the CPP plant with aim of exploring its full potential for electrical power generation.

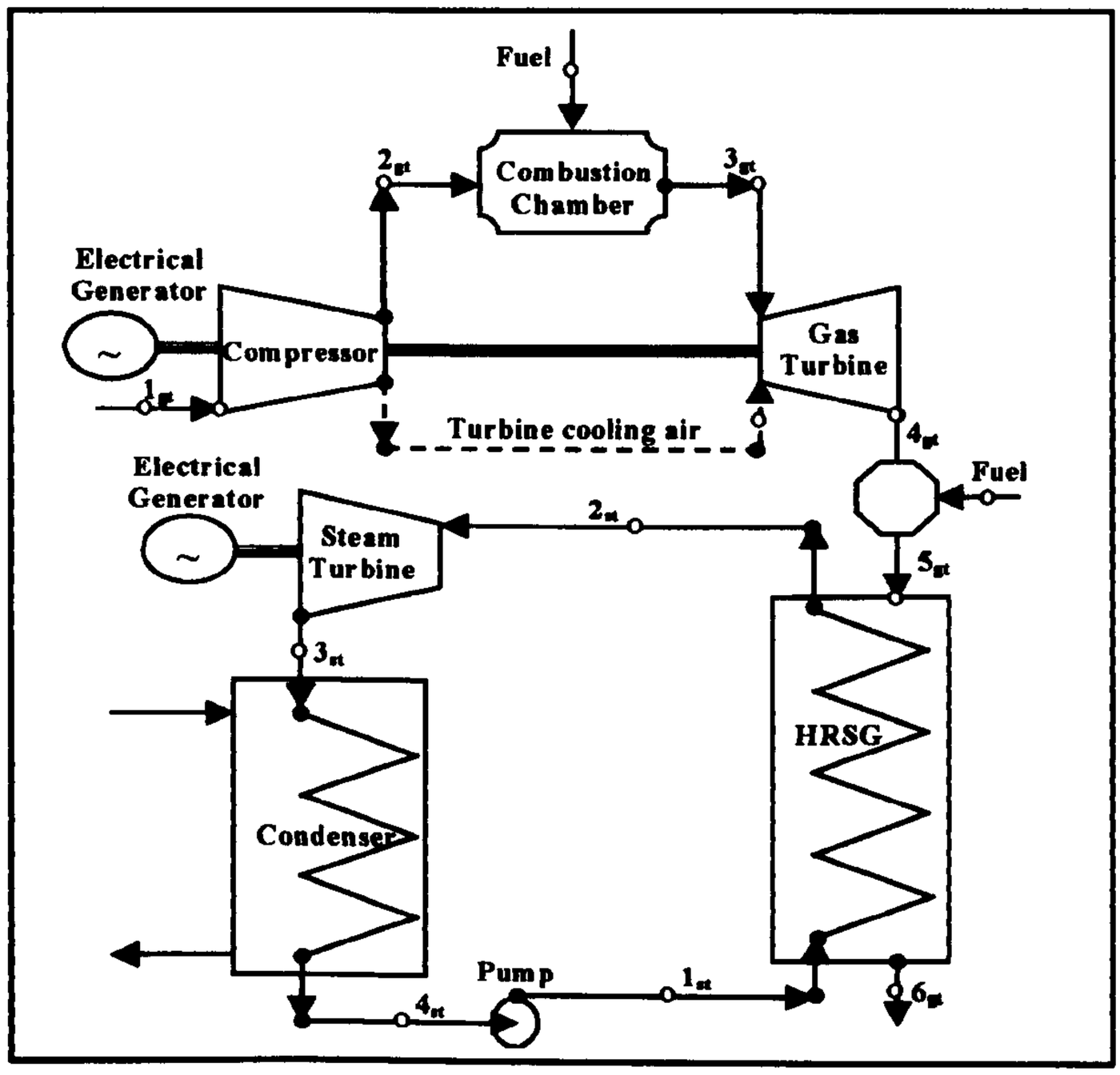

Fig. 1.2 Schematic diagram of a combined gas turbine-steam turbine power plant with a waste heat recovery boiler

For the sake of comparison, Table 1.1 is given below, which summarises different classes of application of gas turbine engines used for power generation, including

examples of actual engines used[38]. Figures 1.3 and 1.4 present the thermal efficiency and utilisation hours, i.e. typical number of hours per year that the plant was fired. Some of these applications, e.g. CHP plant are claimed to have yielded very high energy utilisation efficiency, however, it should be noted that data is not available to show that their power generation efficiency would exceed the efficiency that could accrue from the CPP plant.

Ident. No.	Plant type	Examples of applications	Examples of engines	Power per engine (MW)
1	Small scale turbo generator sets	-Aerospace applications (APU) -Hybrid vehicles	-TG50 -Garrett GTP85	0.04-0.2
2	Standby generators, simple cycle gas turbine	-Office block -Hospital	-Yanmar -AT36C, 60C -Turbomeca Astazou	0.25-1.5
3	Standby generators, diesel engine	-Office block -Hospital	-Caterpillar V12 -Mirrlees Blackstone	0.25-1.5
4	Small scale CHP, gas turbine combined with steam turbine	-Hospital -Small process factory	-EGT Tempest -NP PGT2 -Allison 501	0.5-10
5	Large scale CHP, gas turbine combined with steam turbine plant	-Electricity and district heating -Large process factory	-ABB STAL GT10 -GE LM2500 -Coberra 6000	10-50
6	Peak load units, simple cycle gas turbine	Supply to grid	-ABB GT10 -RR RB211	20-60
7	Mid merit power station, simple cycle gas turbine	Supply to grid	-GE LM6000 -RR Trent	30-60
8	Base load power station, CPP plant	Supply to grid	-WEC 501F -GE PG9331	50-450
9	Base load power station, coal fired steam plant	Supply to grid		200-800
10	Base load power station, nuclear powered steam plant	Supply to grid		800-2000

ABB = Asea Brown Boveri EGT = European Gas Turbines NP = Nuovo pignone
GE = General Electric WEC = Westinghouse Electric RR = Rolls-Royce

Table 1.1 Classes of power generation plants

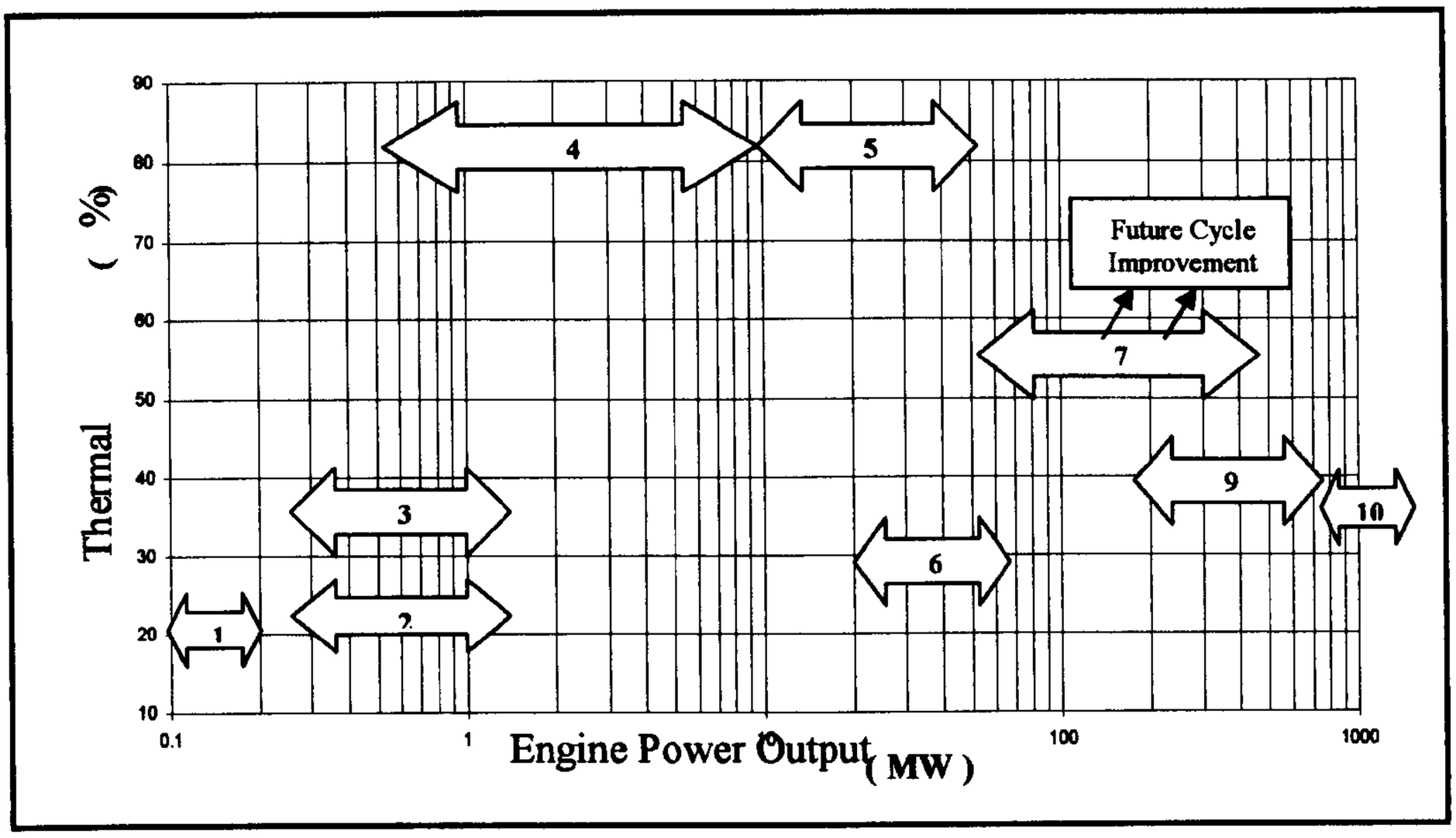

Fig. 1.3 Thermal efficiency vs. plant power output for classes of power generation plants summarised in Table 1.1

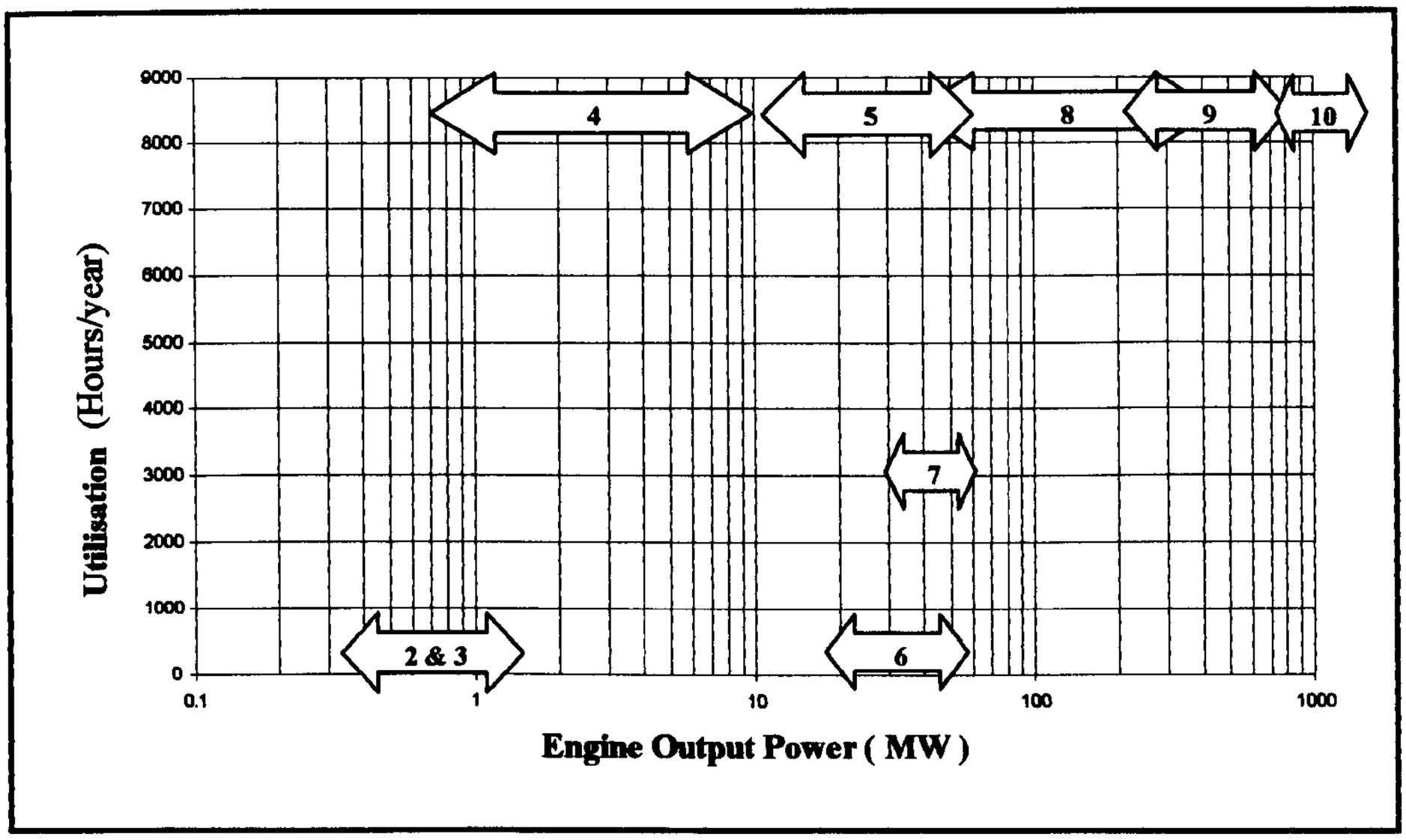

Fig. 1.4 Utilisation hours vs. plant power output for classes of power generation plants summarised in Table 1.1

The addition of an afterburner has been used in a number of retrofit cases in which a steam turbine already existed. The gas turbine and heat recovery steam generator were added to replace the boiler. The gas turbine generated extra electrical capacity and also provided hot exhaust gas to raise steam.

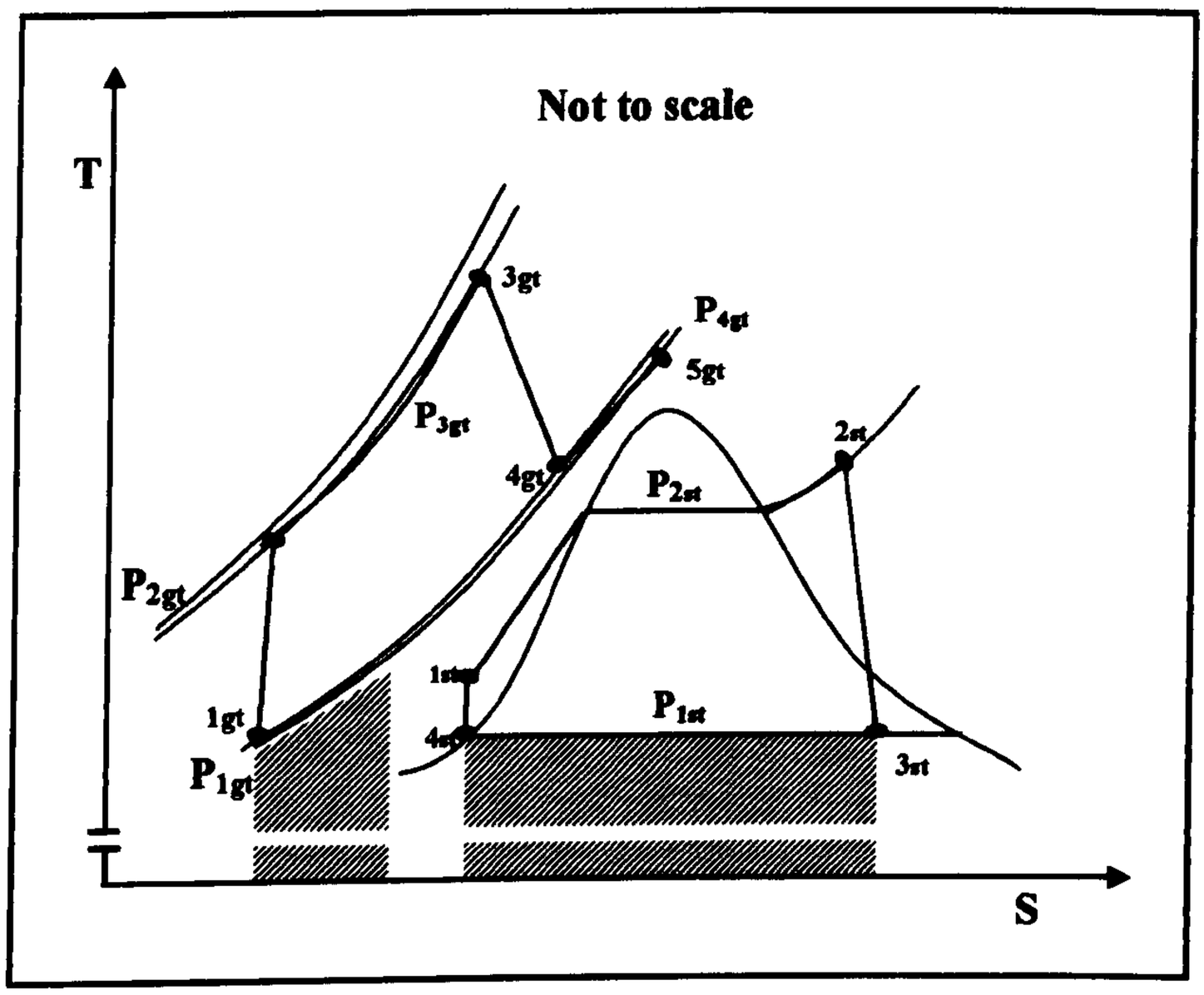

Fig. 1.5 Temperature-Entropy diagram of the CPP plant

1.4 Aims of Research

The aims of this study can be stated as follows:

i. To carry out a review of up to date published literature;
ii. To conduct a parametric study in order to explore the influence of design parameters of the gas turbine plant on its performance as part of the CPP plant;
iii. To produce a computer model to simulate the gas turbine power plant as a part of the CPP plant;
iv. To design and construct experimental facility, including instrumentation, in order to validate the parametric study and the simulation model by comparing the results with experimental data.

CHAPTER 2

LITERATURE REVIEW

2.1 Introduction

Gas turbine engines have been researched extensively during the last fifty years mainly because of their use in the aero industry. The aero engines must be lightweight, must have better power/weight ratio and must have a high thermal efficiency. To achieve these goals the aero engine development focused on raising the turbine entry temperature and cycle pressure ratio. High temperature materials and blade cooling techniques had to be developed to accept high turbine entry temperature[6,8].

The experience of the aero engine industry was followed by the gas turbine power generation industry; consequently the use of high temperature and high cycle pressure ratio became a norm in the power generation industry. High turbine entry temperature lead to high exhaust temperature hence recovery of low grade thermal energy from the exhaust gas became very attractive and other thermodynamic cycles such as combined heat and power, i.e. CHP, and combined Joule-Brayton/Rankine cycles started to gain popularity.

Although combined cycle researches dates back to the early part of the 20th century, research and development work on the combined gas turbine and steam turbine power generating plants started only in the late 1960s[9].

In this chapter a review of the studies relevant mainly to the gas turbine plants operating in the combined power and power cycle, CPP for short, are presented. A summary of the main observations from the literature is included in the last section. The steam turbine plant is being studied as a part of another parallel research project.

2.2 Review of Previous Work

Reviewing previous work related to the gas turbine power plants as part of the combined power and power plant would entail the following areas:

i. Gas turbine power plant thermodynamics and exergy analysis.
ii. Optimisation and parametric studies of combined power plants.

iii. Simulation and performance prediction of the gas turbine plant as part of the combined power plant.

iv. Off-design performance and control strategies of the gas turbine plant as a part of the combined power plant.

2.2.1 Gas Turbine Thermodynamics and Exergy Analysis

The goal of thermodynamic optimisation of power plant processes is determination of the most favourable combination of the process parameters with regard to efficiency and work output. The investigation and optimisation of the processes can be performed by an energy or exergy analysis.

In the energy analysis, energy-flows of various forms and qualities are used to determine the characteristic parameters of the process. Energy is a conserved quantity. When energy is converted from one form to another, a part of the ability to produce work is irreversibly lost, e.g. the energetic efficiency of the process is calculated from the ratio of the useful output to the energy input.

In the exergy analysis, the exergy-flows occurring in the process are used to calculate exergetic efficiencies and exergy losses. Exergy is a measure of the capacity of a fluid to perform work if it is reversibly brought into equilibrium with the surroundings. This can occur with interaction with the surroundings. Exergy has the character of a potential in a given environment. There is no low of conservation for exergy. Each irreversible state change represents the destruction of exergy.

From the thermodynamics point of view, the purpose of analysing any cycle is to identify the parameters that might reduce the thermal efficiency of the gas turbine engine.

Cohen, Kehlhofer, Haywood, Sonntag[2-5] and others used the thermodynamic laws to evaluate the performance of the gas turbine plant and to determine the dominant parameters. They concluded that the efficiency of a gas turbine plant was a function of many parameters as described below:

$$\eta_{gt} = f(\theta, r, C_p, \eta_c, \eta_{cc}, \eta_t, \eta_{mec}) \quad (2.1)$$

They studied different gas turbine cycle configurations to determine the best performance conditions. Their main conclusions are listed in below:

i. Heat exchange between the turbine exhaust and the compressor outlet, i.e. regenerative heating, will increase both the thermal efficiency and the specific work output of the gas turbine plant.
ii. Reheating between the turbine stages will increase specific work output but it will be at the expense of some reduction in thermal efficiency.
iii. Pre-cooling and inter-cooling the air will also increase the specific work output with some reduction in thermal efficiency.

Only Kehlhofer[3] studied gas turbine power plant as a part of the combined cycle power plant and concluded that raising the gas turbine efficiency would not necessarily produce the best overall efficiency of the combined power plant.

El-Masri[11-13] used the second law of thermodynamics and exergy analysis to locate and quantify the irreversibilities that cause loss of work output and of thermal efficiency of the gas turbine operating as a part of the combined power plant. His main conclusions are given below:

i. Compressor inter-cooling will lead to an increase in specific work output, but this will happen with some reduction in thermal efficiency.
ii. The dominant influence on cycle efficiency as turbine inlet temperature is raised will be the trade off between decreased combustion exergy losses and increased turbine blade cooling losses.

El-Masri studied only the effect of the irreversibilities in the system components on cycle performance. His investigations did not explore whether or not that heat generated by the irreversibilities could be used for generating steam as in CPP plant. His calculations assumed bleeding off as much as 24% of the compressed air for turbine blade cooling. Considering the size of the holes in turbine blades through which the cooling air flows, the figure of 24% seems to be unrealistic.

Kail[48] analysed and evaluated different trends in combined cycle gas turbine power plant configurations. The various configurations have been compared with the simple cycle combined gas turbine/steam turbine power plant. The studied configurations were as follows:

i. A combined reheat gas turbine/simple steam turbine power plant.
ii. A combined inter-cooled gas turbine/steam turbine power plant.
iii. A combined steam-cooled turbine blades gas turbine/steam turbine power plant.
iv. A combined gas turbine/simple steam turbine power plant where the gas turbine has a closed-loop combustion chamber cooling system.

In comparison with the 'simple' gas turbine, Kail concluded the followings:

i. Reheat of the gas turbine cannot transform its efficiency and output advantages into a lower cost of electrical power. The additional investments and higher maintenance costs overwhelm the thermodynamic advantages.
ii. Inter-cooling improves the efficiency and power output of the combined power plant.
iii. The concept of steam-cooled turbine blades places very stringent requirements on the blade materials, on the quality of the cooling steam and on the design of the closed cooling system.
iv. The gas turbine with a closed combustion chamber cooling system is less problematic than the gas turbine with a closed blade cooling system.
v. The simple combined gas turbine/steam turbine power plant achieves the lowest costs of electrical power and is therefore the best plant from an economic point of view.

Kail studied only the proposed configurations of the combined power plants. His investigations did not explore whether improvements could be implemented to the proposed plant configurations. It was not clear how the costs of imposed configurations were calculated.

2.2.2 Optimisation and Parametric Studies of Combined Power Plants

Optimisation of the combined power and power cycle involves long and laborious calculations. Several methods were employed by various researchers to analyse the combined power and power (CPP) cycle. All these methods were based on thermodynamic analyses to provide overall performance of the CPP plants. The results of those studies were published in a series of papers, which are reviewed in the following paragraphs.

Cerri[14] studied the CPP plant and proposed thermodynamic parameters or indices to quantify the plant performance. He varied the maximum gas turbine inlet temperature between 800° C and 1400° C, at the same time gas turbine pressure ratio was varied between 2 to 24. Afterburning was also taken into consideration. His calculations produced both the CPP plant thermal efficiency and the specific work output. Cerri summarised his findings in the form of the following conclusions.

i. The thermal efficiency of the CPP plant is independent of the gas turbine pressure ratio but it would be influenced slightly by the steam pressure if it was sufficiently high.
ii. The thermal efficiency of the CPP plant would be positively influenced by adding an afterburner only if the turbine inlet temperature was significantly low.

It is worth mentioning that the use of the proposed indices involved more assumptions thus complicating the calculations unnecessarily. Moreover, there was no verification of the assumptions.

Rufli[15] analysed the CPP plant also by using the basic thermodynamic calculations for both the gas turbine and the steam turbine cycles. The maximum gas turbine inlet temperature was varied between 900 °C to 1350 °C, at the same time the gas turbine pressure ratio was varied from 8 to 22. Afterburning was also taken into consideration. Rufli's calculations produced values of the CPP plant thermal efficiency and of the total heat transfer area of the heat recovery steam generator. These calculations were simple and straightforward. Rufli presented a simple method for selecting the optimum parameters for the steam operating in a combined power

and power plant cycle at any given gas turbine operating conditions. However, in order to counteract the adverse effect of high temperature, he introduced blade cooling air as a percentage of the total mass flow of air as shown in Fig. 2.1. The assumed proportions of the cooling air, as can be seen from the figure, were overestimated.

Bhinder and Mango[17] used thermodynamics analysis to study the CPP plant performance. Many assumptions were made to simplify the calculations of the cycle performance. Only a reheated gas turbine power plant configuration was used as the higher temperature plant. They concluded that the combined plant efficiency would be significantly higher than either the gas turbine efficiency or the steam turbine efficiency. The overall efficiency value of 60% for the CPP plant was shown to be achievable. In addition the thermal load on the environment was reduced to 59% of the gas turbine load working alone. The cycle calculations were simple and many of the losses were not included in the calculations. It would be difficult to achieve 60% thermal efficiency if all the losses were included in the calculations.

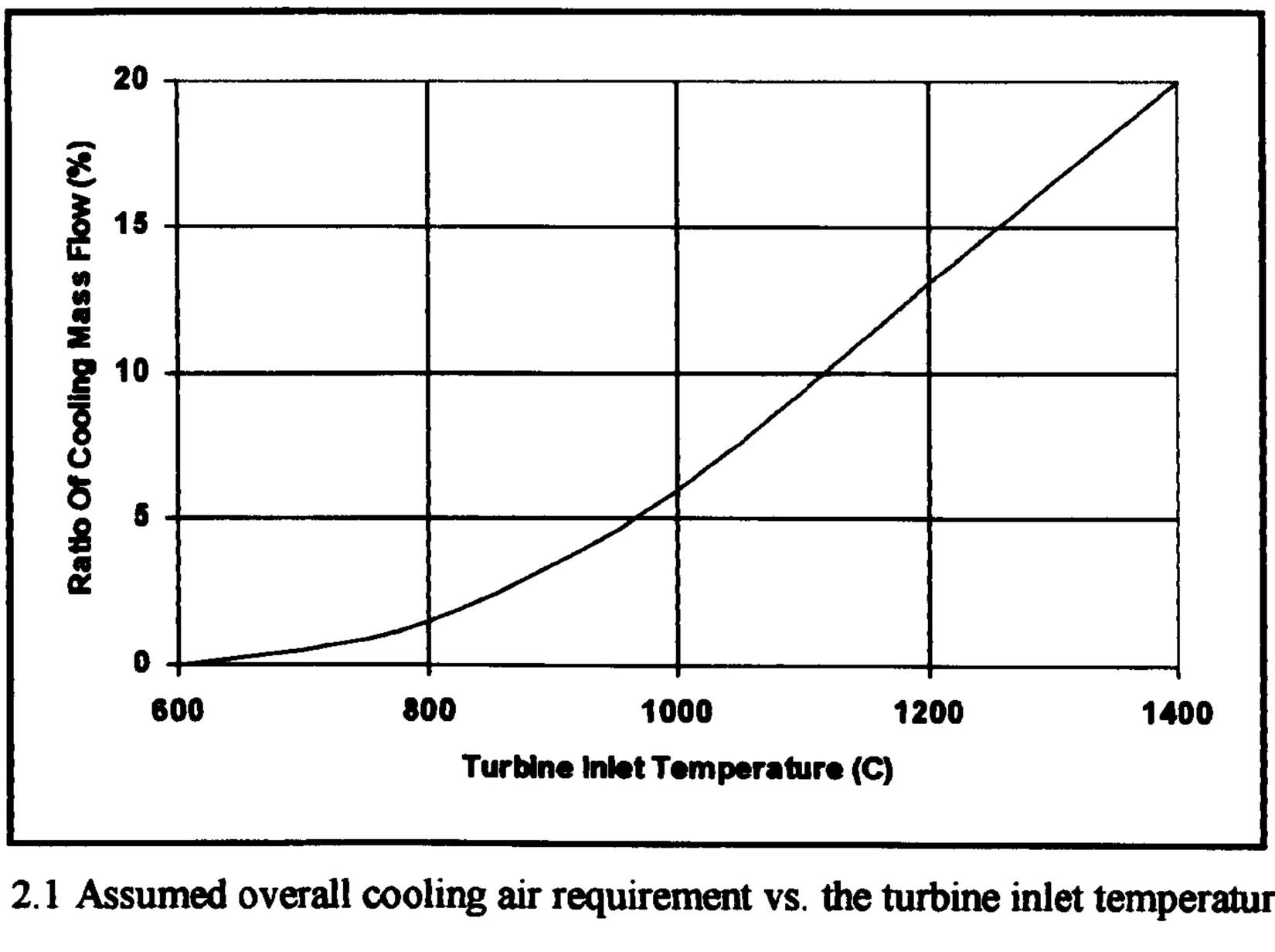

Fig. 2.1 Assumed overall cooling air requirement vs. the turbine inlet temperature[15]

Horloock[1][8-10] carried out an extensive study of combined power plants. The early history of combined plants was described. The recent developments and future

prospects for the combined gas turbine/steam turbine plant were described. He identified two lines for combined power plants developments: the first line used the aircraft engines and its technology in the combined power plants, the second line involved thinking about the combined plant as an integrated design from the beginning. He adopted a graphical method of predicting the performance of the gas turbine cycle, developed by Hawthorne and Davis[18] where their results shown in Fig. 2.2, to determine the optimum pressure ratio of the gas turbine that would give maximum overall efficiency of the combined power and power plant. Horloock's main conclusions can be summarised as follows:

i. In a combined power & power cycle the optimum pressure ratio for the gas turbine would be less than its pressure ratio for maximum efficiency in the conventional cycle but greater than the pressure ratio for the maximum specific work output of that cycle.
ii. Introduction of reheat for the gas turbine cycle would increase the pressure ratio required for maximum efficiency of CPP plant.
iii. Steam injection in the main stream of the gas turbine would increase both the gas turbine and the combined plant efficiencies.
iv. Steam cooling of high temperature gas turbine would decrease heat losses in the combined plant and therefore increase the combined plant efficiency.
v. The combined power and power efficiency decreases as the steam cycle efficiency is increased by the addition of feed heating.

The graphical method adopted by Horloock to optimise the combined power and power plant had its own limitations mainly because of the assumptions used in the steam power plant calculations, e.g. the assumption for the steam turbine work did not adequately cover single, dual and triple pressure steam raising; the assumed empirical constant value for the heat supplied would not be accepted for different steam cycle configurations.

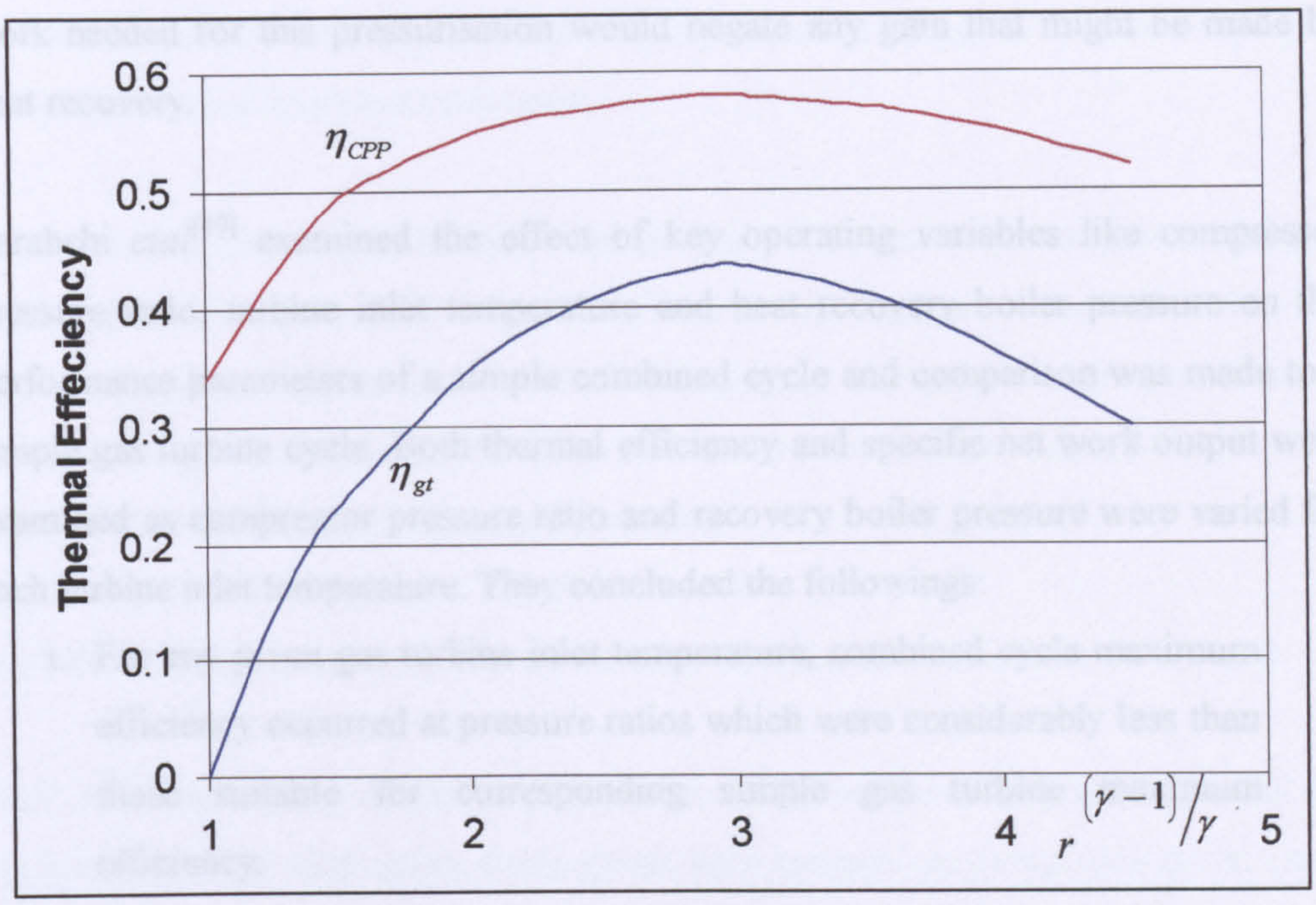

Fig 2.2 Hawthorne-Davis diagram for gas turbine and CPP plant[18]

Bannister *etal*[19-20] considered the techniques required to achieve energy conversion efficiencies greater than 60%. Their recommendations were improvements in operating process parameters for both gas turbine power plant and steam power plant. They listed the following four recommendations for possible CPP cycle improvements:

i. Raising the gas turbine inlet temperature to 1427° C.
ii. Introducing advanced cooling techniques in the gas turbine.
iii. Utilisation of both cycles heat losses through greater integration between the two plants.
iv. Improving component efficiencies.

It should be noted that component or process efficiencies have already reached their maximum values that could be achieved economically. Further increases would yield poor returns on investment and would not be acceptable to manufacturers who are working in a highly competitive energy market. Greater integration between the steam turbine and the gas turbine plants proposed by the authors involved using low pressure steam for reducing heat losses. They have not considered that in order to use this steam its pressure must be increased to the level of the gas stream pressure. The

work needed for this pressurisation would negate any gain that might be made by heat recovery.

Sarabchi *etal*[49] examined the effect of key operating variables like compressor pressure ratio, turbine inlet temperature and heat recovery boiler pressure on the performance parameters of a simple combined cycle and comparison was made to a simple gas turbine cycle. Both thermal efficiency and specific net work output were examined as compressor pressure ratio and recovery boiler pressure were varied for each turbine inlet temperature. They concluded the followings:

i. For any given gas turbine inlet temperature, combined cycle maximum efficiency occurred at pressure ratios which were considerably less than those suitable for corresponding simple gas turbine maximum efficiency.
ii. The combined cycle optimum pressure ratio is almost equal to the simple gas turbine optimum pressure ratio for maximum work output.
iii. The values of optimum pressure ratio and heat recovery boiler pressure for a combined cycle increased by increasing the gas turbine inlet temperature.

The cycle calculations were simple and many of the losses were not included in the calculations. Furthermore, the authors have not presented any experimental verification for the conclusions.

Bonzani *etal*[51] described a method for technical and economical optimisation of a 450 MW combined cycle power plant, consisting of two gas turbine V94.2 type associated with dual pressure heat recovery steam generator and one steam turbine. The optimisation process was based on the comparison between the investment cost of several alternatives and the economic evaluation of the associated performance. Improvements in gas turbine cycle efficiency have been achieved by raising the turbine inlet temperature to 1400 k as well as increasing the compressor pressure ratio to 15.

Bonzani *etal* concluded that there is no single optimal solution because customer needs and/or environmental requirements can give different results. They also

concluded that economically the heat recovery steam generator is the most important component in the optimisation process.

The optimisation process did not consider the off-design conditions were the gas turbine performance would be highly affected. Although, they concluded that the heat recovery steam generator is the most important component in the optimisation process, the gas exhaust pressure drop was assumed a constant value. This pressure drop would affect the gas turbine performance.

2.2.3 Modelling and Simulation of the Gas Turbine as Part of the CPP Plant

Dhar *etal*[22] described the development of a simulation program used to predict the performance of a CPP plant from given performance characteristics of its main components. The simulation technique was applied to a typical combined cycle power plant. The strategy of system simulation was obtained by linking the information flow diagrams of various components. Although Dhar *etal* claimed excellent results by comparing the computer program results with a typical CPP plant, they did not introduce the performance characteristics of the main components needed for components modelling and simulation. It is clear from the study that the turbine performance characteristics presented as a single line was an approximation which reduced the accuracy of performance calculations.

Bhinder and Ismail[24] described a procedure used to develop a computer program to simulate aircraft gas turbine engines. In this procedure both the analytical equations and the detailed performance characteristics of individual components were used to model the steady-state operation of the complete engine. Although they didn't compare the results obtained by calculations with test data, the trends of the results appeared to be acceptable.

Bhinder *etal*[25] described a procedure used to develop a computer program to simulate industrial gas turbine engines to aid in the design and application of fuel controllers. The program structure was explained and modelling of a simple two shaft industrial engine was given as an example. The program developed to simulate the gas turbine engines from the point of view of the fuel control system for the

steady state conditions. The work presented would not be helpful in simulating or predicting the performance of the gas turbine engine.

Roy-Aikins[26] analysed a computer program designed to simulate both the design point and off-design steady state performance. The program uses a computer-matching thermodynamic procedure to simulate any arbitrary Brayton, Rankine or combined cycle plants. Detailed performance characteristics of individual components should be used as input data for the computer program. Roy-Aikins presented a sample of calculations for a combined power plant without showing the performance characteristics of the individual components.

Perz[27] described a computer program used to simulate any thermodynamic power cycle. The modelling procedure involved algebraic equations to mathematically present the power cycles processes. The paper was an attempt to develop a generic program for modelling all thermal power cycles and did not appear to be relevant to the present study. Nevertheless, the methodology of approach was worthy of consideration.

El-Masri[28] described a programming code used to analyse the gas turbine systems. The program code performs exergy-balance analysis to break down and trace system inefficiencies to their source components and source processes within the components and the system optimisation trade-offs. Although, the results obtained by calculations have not been compared with test data, but the methodology of approach was different and worthy of consideration.

Najjar *etal*[39,45-46] described a procedure for modelling and simulation of gas turbine engines processes. The simulation program was used to predict the following:

i. The relative effect of ambient conditions on the engine performance.
ii. The part-load engine performance under different operating conditions.
iii. The content of engine exhaust, e.g. the engine production of NO_x.

A comparison of performance parameters for different gas turbine engines has been carried out to demonstrate the error percentages in predicting performance parameters by using the simulation program. Najjar *etal* claimed that the developed

computer programme was capable of accurately predicting the gas turbine engine performance at off-design and different operating conditions. His main conclusions can be summarised as follows:

i. Of the ambient conditions, the ambient temperature is the single most influencing factor in engine performance.
ii. The effect of relative humidity is insignificant on engine performance.
iii. Part load operation lower than 75% causes significant reductions in the thermal efficiency of the engine.
iv. Air extraction with any industrial process negatively affects engine performance.

This way of comparison had some major errors mainly because the engines log sheets and manufacturing catalogues had been used as the results of the experimental work. Furthermore, the computational model for the gas turbine engine has been presented without showing the performance characteristics of the individual components.

Erbes *etal*[50] presented a gas turbine simulation code, named GATE (GAs Turbine Evaluation). The GATE has been developed to evaluate the design and off-design performance of existing and advanced gas-turbine based systems for power plant applications. GATE can model a variety of gas turbine configurations and cooling technologies, and users can also interactively design and analyse an associated steam bottoming cycle. Although, Sample cases demonstrating the simulation code and its capabilities have been presented, the results obtained have not been compared with test data. The authors admitted that GATE simulation program was not capable of analysing the steam cycle off-design conditions; hence the code is not a good tool for investigating the combined power plants.

2.2.4 Off-Design Performance and Control Strategies of the Gas Turbine as Part of CPP Plant

The off-design performance of the combined power and power (CPP) plants has attracted more attention in recent studies due to the increased applications of these plants in power generation industry. The main concern remains that CPP plant, like

all gas turbine power plants, has a rapid and large reduction in its thermal efficiency at the part-load conditions.

Dechamps *etal*[29] described a method that can be used to evaluate the part-load performance of the CPP plants. This study agreed with the previous studies[30-31] on the importance of controlling the CPP plant using the variable inlet guide vanes (VIGV) before starting to reduce the fuel flow. It suggested that afterburning has a good efficiency advantage at part-load conditions despite its efficiency disadvantage at the design-point condition. However, the part-load effect on the gas turbine plant performance was not included in this study where it has a significant effect on the total off-design performance of the combined plant.

Kehlhofer[3] studied the response of the heat recovery steam generator (HRSG) and steam turbine plant to the load changes in the CPP plant. He suggested that the steam turbine power plant would be economically optimised if it was kept without controlling. The exhausted gas temperature and mass flow are the only control variables for the steam power plant. The CPP plant control system would depend largely on the fuel flow control system of the gas turbine power plant.

Gyarmthy[30] analysed a CPP plant consisting of a simple single pressure steam turbine plant (with preheating) and a simple gas turbine plant. The results indicated the merits of controlling the compressor mass flow by means of inlet guide vanes (IGV) adjustment. On the steam turbine side Gyarmthy agreed with Kehlhofer that no controls other than the regular steam turbine plant control would control the optimum efficiency.

Frutschi[31] analysed and compared different possible control techniques for the gas turbine plant operating in the CPP plant environment. The standard method was to control the fuel flow of the gas turbine plant for controlling the gas turbine inlet temperature, which would control the gas turbine exhaust temperature. Alternative methods involve recirculation of compressor air, intake throttling, inlet guide vanes control and compressor intake air control by heating the inlet air. Frutschi concluded that compressor throttling was not to be recommended and that inlet guide vanes

control, possibly coupled with inlet air preheating, was a useful control method for CPP plants.

Since compressor work is directly proportional to the inlet air temperature, preheating the air would increase compression work, hence reduce the efficiency of the gas turbine engine. This is foregone conclusion and any study to prove this would merely be a waste of time. Similarly throttling the compressor intake would increase axial thrust on the bearings and inevitably there would be a risk of compressor impeller damage. This too is a foregone conclusion and no experimental or theoretical work can be justified to prove this point.

Facchini[47] described a computer code to simulate the off-design operation of gas turbine power plants. This code is based on the simplified dimensionless model of different components (compressor, combustion chamber and turbine) and it allows simulation and comparison of several control system. The effects due to cooling in the first stages of the turbine are also taken into account in the model. Different control techniques have been applied during off-design simulation. These control systems included in the following:

i. Flow throttling at the compressor inlet.
ii. Variable flow guiding at the compressor inlet.
iii. Bleeding of the compressor's mass flow along the compression line.
iv. Mass flow compressor outlet recirculation at the inlet.
v. Variation of the fuel mass flow rate in the combustion chamber.

Facchini studied the influence of the various control systems on the thermal power of exhaust gases and therefore on the combined power and power plants.

Facchini concluded that variation of the fuel mass flow and the compressor inlet guide vanes are the most convenient control systems for gas turbine engines while the other systems will negatively affect the engine performance. These conclusions are forgone conclusions and no experimental or theoretical work can be justified to prove these points. Regarding the combined power and power plant, he admitted that more detailed simulation of global off-design performance should be made before a control system can be suggested.

2.3 Summary and Main Observations

- The thermodynamic analysis can be an important tool for thermal design of the CPP plant but supplementary practical data would always be needed to enhance its value.

- The thermodynamic analysis of the gas turbine power plant revealed that increasing both the pressure ratio and the turbine inlet temperature would increase the thermal efficiency if there were not significant losses due to turbine cooling. In the CPP plant configuration, increasing the thermal efficiency of the gas turbine plant will not necessarily mean an increase in the CPP plant thermal efficiency.

- The different combined cycle parametric studies, reviewed in the literature, gave different conclusions about the optimum conditions for the gas turbine cycle as part of the combined power and power cycle. Therefore, the choice of optimum parameters for the gas turbine plant operating in the CPP plant environment appears to be a matter of personal preference.

- The range of gas turbine power plant design parameters, particularly cycle pressure ratio, depends whether the plant is to be designed for maximum thermal efficiency or maximum specific work output. Therefore, the choice of optimum parameters between the maximum efficiency and the maximum specific work depends on the application. For the gas turbine engine operating in the CPP plant environment, the range of design parameters reduces sharply.

- Modelling the gas turbine plant requires the use of the performance characteristics of individual components, understanding the mechanical connections, and gas dynamics linkages within the plant as well as the thermodynamic analysis.

- The CPP plant, like all gas turbine power plants, has a rapid and large decrease in its thermal efficiency at the part-load conditions. Controlling of the CPP plant should be able to minimise the efficiency reduction, thus optimise the CPP plant performance.

CHAPTER 3

PARAMETRIC STUDY AND OPTIMISATION

3.1 Introduction

The gas turbine plant represents a complex system consisting of a number of rotational and stationary parts, each part is characterised by its own behaviour. The overall performance of the gas turbine plant depends on the performance of its individual components and component matching. A parametric study of the gas turbine cycle is an important tool for showing the influence of the principal design parameters on its performance.

In a combined power and power (CPP) plant, the gas turbine power plant produces electricity as well as exhaust heat that can be used to produce high pressure steam to operate a steam turbine plant and thus generate more electricity. Therefore, the design of a CPP plant will involve greater complexity especially because of the coupling between the two different types of power producing systems. Obviously the parametric study of the combined plant will be the first step in deciding the design criteria of both plants by understanding the influence of the main parameters on the CPP plant.

In the present chapter the thermodynamics of a parametric analysis of the gas turbine cycle performance and the CPP cycle performance are presented. A set of sample calculations is given in appendix A.

3.2 Theoretical Consideration of the CPP Cycle

This section deals with the theoretical aspects of power and power combined cycles. It starts with introducing some fundamental aspects of the Carnot cycle and subsequently presents some thermodynamic aspects of the gas turbine cycle, steam turbine cycle and combined power and power cycle. The aim of studying the thermodynamics of power plants is to determine the maximum achievable efficiency, i.e. Carnot efficiency, and the maximum work obtained from those plants by using the same amount of fuel.

The thermal efficiency of any insulated power cycle η_{th} can be calculated theoretically as follows

$$\eta_{th} = \frac{W_{net}}{Q_s} \tag{3.1}$$

where W_{net} = the net work produced and Q_s is the heat supplied to the plant.

3.2.1 Carnot Power Plant Performance

The efficiency of a thermal power plant operating on an ideal cycle i.e. Carnot cycle efficiency η_{Carnot}, represented on a temperature entropy (T-S) diagram as shown in Fig. 3.1 is the highest achievable efficiency of any thermal power cycle. It can be calculated as follows

$$\eta_{carnot} = \frac{W}{Q} = \frac{W}{Q_s} = \frac{Q_s - Q_r}{Q_s} \tag{3.2}$$

$$\eta_{carnot} = \frac{T_{\max}\Delta s - T_{\min}\Delta s}{T_{\max}\Delta s} \tag{3.3}$$

$$\eta_{carnot} = \frac{T_{\max} - T_{\min}}{T_{\max}} \tag{3.4}$$

$$\eta_{carnot} = 1 - \frac{T_{\min}}{T_{\max}} \tag{3.5}$$

where Q_s = the heat supplied at constant temperature $T_{\max}$

Q_r = the heat rejected at constant temperature $T_{\min}$.

It is quite clear from Eqn. 3.2 that increasing T_{max} or reducing T_{min} leads to higher efficiency, hence the Carnot cycle efficiency can also be expressed as a function of the temperatures T_{min} and T_{max}.

$$\eta_{carnot} = f(T_{min}, T_{max}) \tag{3.6}$$

Real power producing cycles do not achieve Carnot cycle efficiency for the following reasons:

i. The actual heat supply may not take place at the temperature T_{max}.

ii. The actual heat rejection may not take place at the temperature T_{min}.

iii. The compression and expansion processes are not reversible.

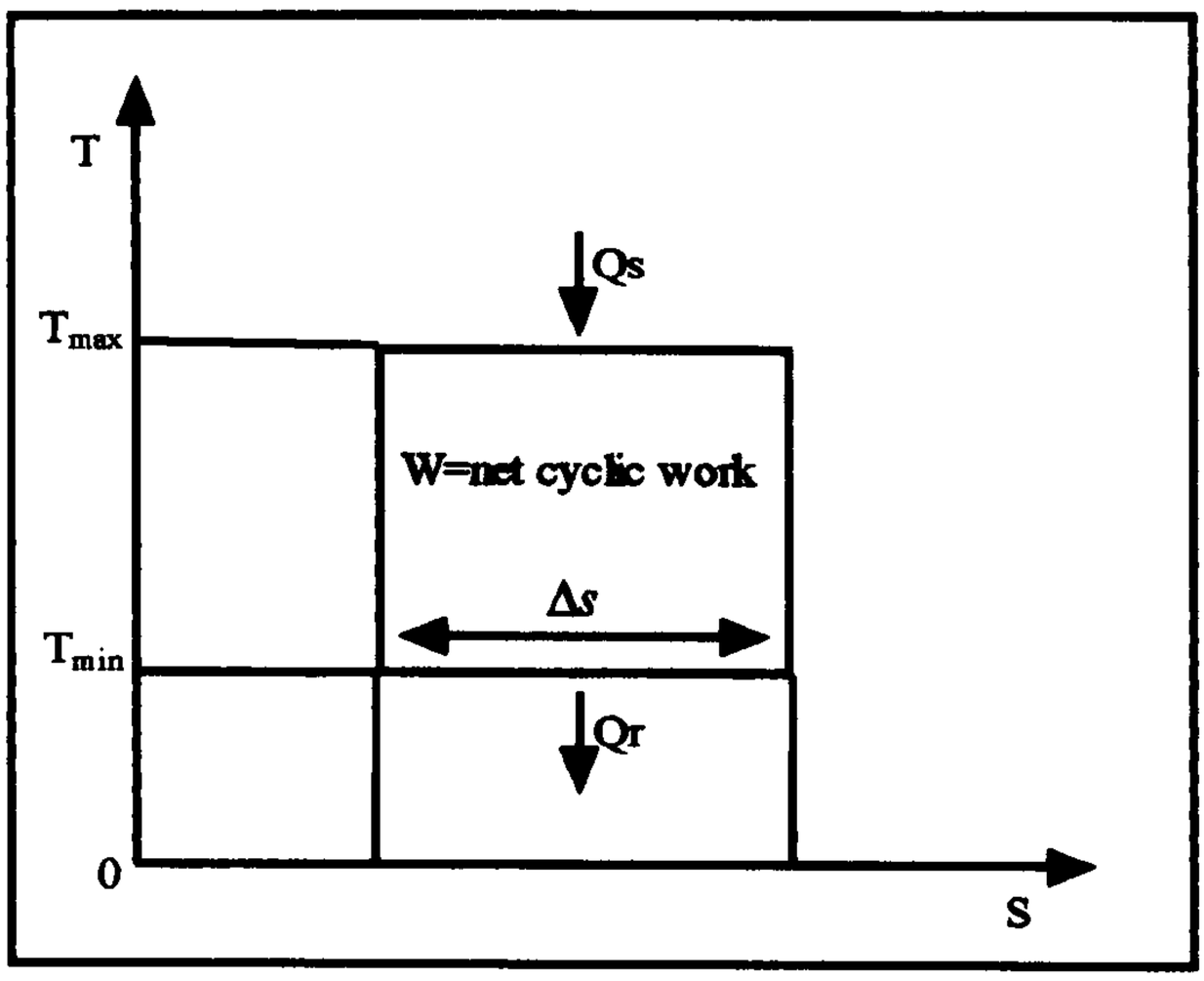

Fig. 3.1 Temperature-Entropy diagram for Carnot cycle power plant

3.2.2 Gas Turbine Power Plant

A simple gas turbine plant was depicted schematically in Fig. 3.2. This operates on the Joule/Brayton cycle and represented on the temperature entropy diagram as shown in Fig. 3.3. The gas turbine cycle thermal efficiency η_{gt} can be expressed as

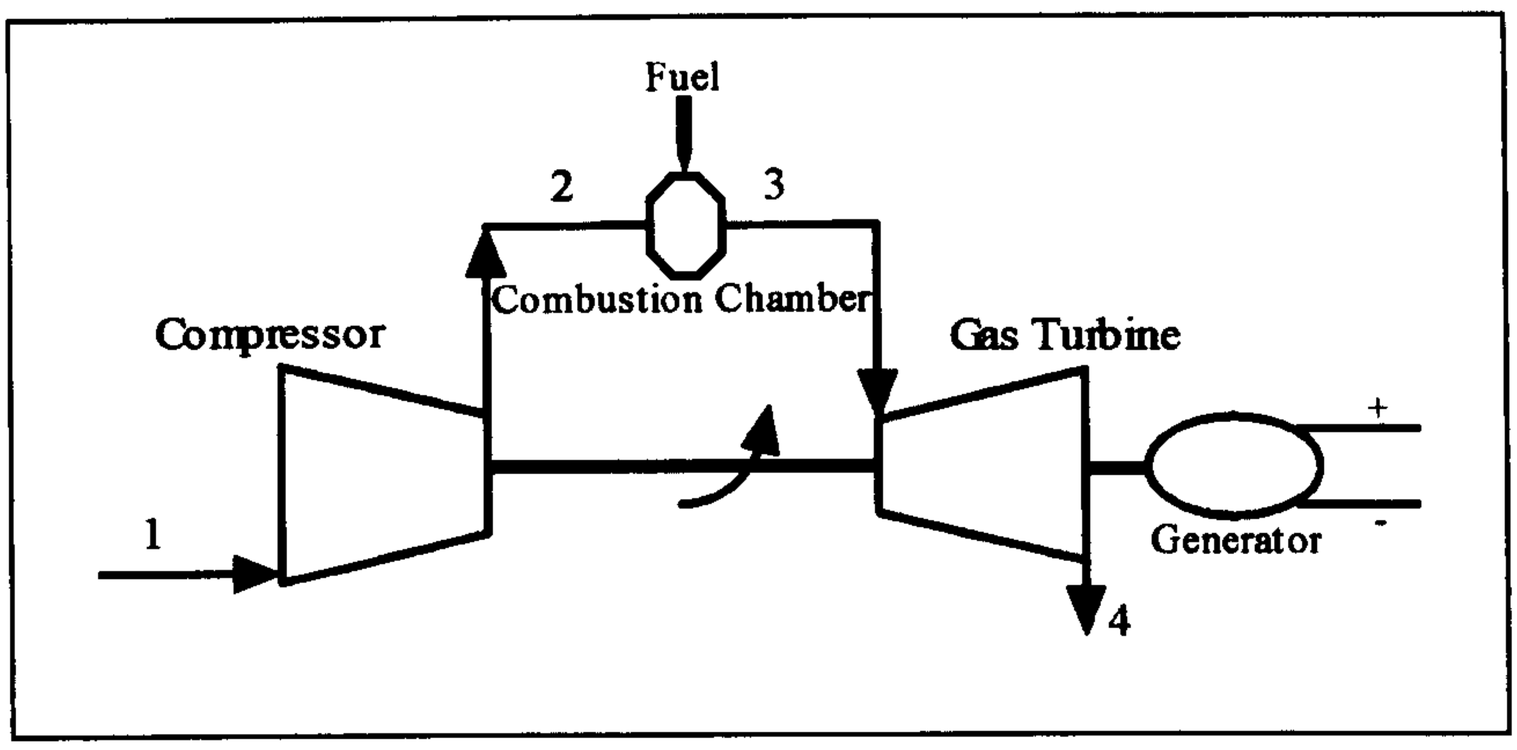

Fig. 3.2 Schematic diagram of a simple gas turbine power plant

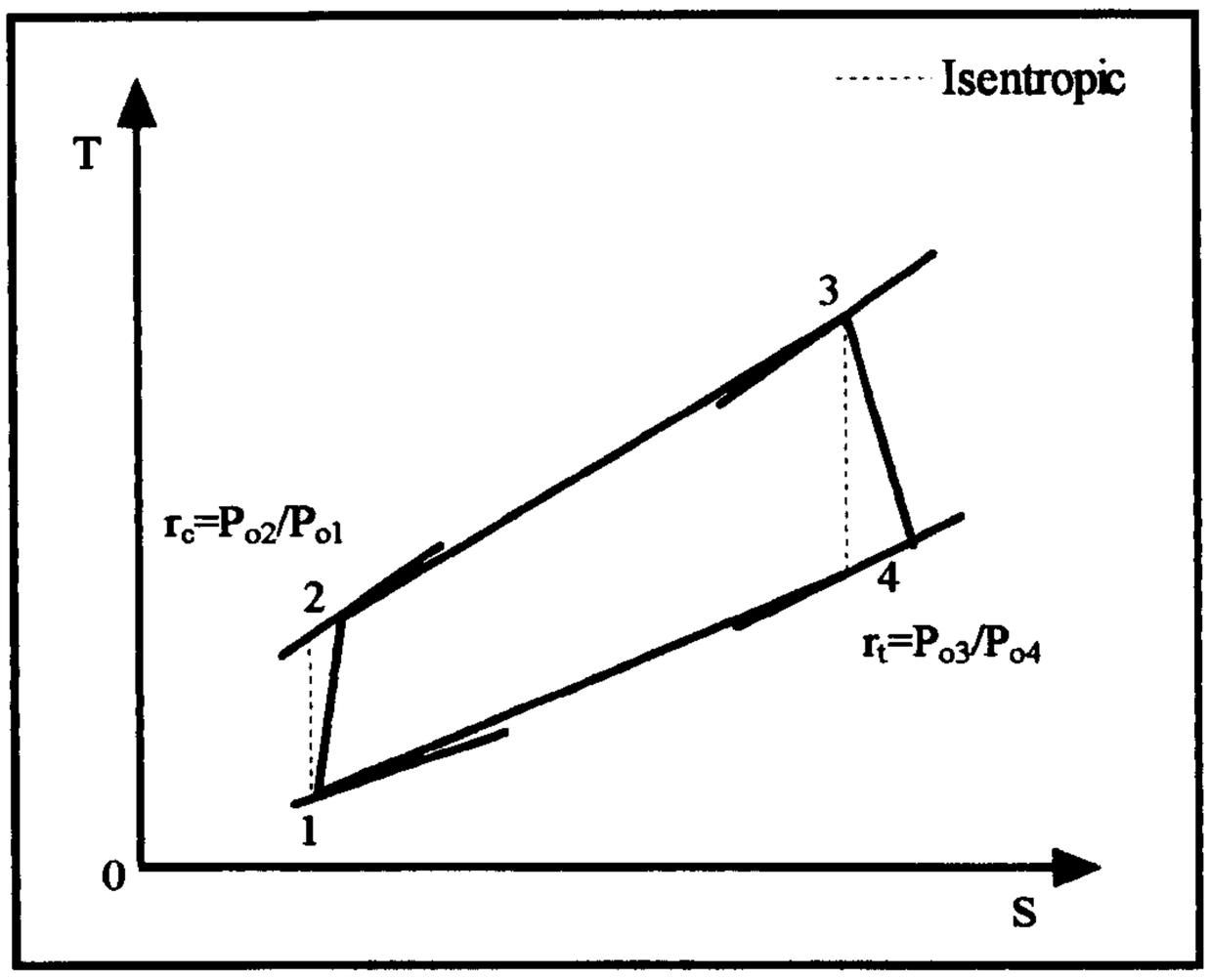

Fig. 3.3 Temperature-Entropy diagram of the gas turbine cycle

$$\eta_{gt} = \frac{Net\ \ power\ \ output}{Heat\ \ \text{sup}\ plied} \tag{3.7}$$

$$\eta_{gt} = \frac{Turbine\ \ power\ -\ Compressor\ \ power}{Heat\ \ \text{sup}\ plied} \tag{3.8}$$

$$\eta_{gt} = \frac{\dot{m}_g C_{pg}(T_{o3} - T_{o4}) - \dot{m}_a C_{pa}(T_{o2} - T_{o1})}{\dot{m}_g C_{pg}(T_{o3} - T_{o2})} \tag{3.9}$$

where $\dot{m}$ = the mass flow rate

C_p = the specific heat at constant pressure

T_o = the stagnation temperature.

To simplify the study of this cycle the following assumptions are made:

i. The working fluid has the same composition throughout the cycle and is a perfect gas with constant specific heats.

ii. The mass flow of the working fluid is constant throughout the cycle.

hence

$$\eta_{gt} = \frac{(T_{o3} - T_{o4}) - (T_{o2} - T_{o1})}{(T_{o3} - T_{o2})} \tag{3.10}$$

$$\eta_{gt} = 1 - \frac{\left[\left(\frac{T_{o4}}{T_{o3}}\right)\left(\frac{T_{o3}}{T_{o1}}\right) - 1\right]}{\left[\left(\frac{T_{o3}}{T_{o1}}\right) - \left(\frac{T_{o2}}{T_{o1}}\right)\right]} \tag{3.11}$$

but

$$\frac{T_{o4}}{T_{o3}} = \left(\frac{1}{P_{o3}/P_{o4}}\right)^{\eta_{\infty t}(\gamma-1)/\gamma} \qquad \text{or} \qquad \frac{T_{o4}}{T_{o3}} = 1 - \eta_t\left(1 - \left(\frac{1}{P_{o3}/P_{o4}}\right)^{(\gamma-1)/\gamma}\right)$$

$$\frac{T_{o2}}{T_{o1}} = \left(P_{o2}/P_{o1}\right)^{(\gamma-1)/\eta_{\infty c}\gamma} \qquad \text{or} \qquad \frac{T_{o2}}{T_{o1}} = 1 + \frac{1}{\eta_c}\left(\left(P_{o2}/P_{o1}\right)^{(\gamma-1)/\gamma} - 1\right)$$

where $\eta_{\infty c}$ = the compressor polytropic efficiency

$\eta_{\infty t}$ = the turbine polytropic efficiency

η = the isentropic efficiency

P = stagnation pressure and

γ = the ratio of specific heats

hence

$$\eta_{gt} = 1 - \frac{\left\{\theta\left[1-\eta_t\left(1-\frac{1}{\chi_t}\right)\right]-1\right\}}{\left[(\theta-1)-\frac{\chi_c-1}{\eta_c}\right]} \qquad (3.12)$$

where

$$\theta = \frac{T_{o3}}{T_{o1}},\ \chi_c = \left(P_{o2}/P_{o1}\right)^{(\gamma-1)/\gamma} \quad \text{and} \quad \chi_t = \left(P_{o3}/P_{o4}\right)^{(\gamma-1)/\gamma}$$

For the condition of no pressure losses in the turbine's inlet, the exhaust duct and in the combustion chamber, the compression ratios of the compressor r_c and the turbine r_t are equal and can be expressed as r

$$r = r_c = \frac{P_{o2}}{P_{o1}} = r_t = \frac{P_{o3}}{P_{o4}}$$

The thermal efficiency of the gas turbine can be calculated as follows

$$\eta_{gt} = \frac{(\eta_t\eta_c\theta - \chi)\left(\frac{\chi-1}{\chi}\right)}{\eta_c\theta - \eta_c - (\chi-1)} \qquad (3.13)$$

In the same way the specific work output of the gas turbine cycle can be calculated as follows

$$w_{gt} = C_p T_{o1}\frac{(\eta_c\eta_t\theta - \chi)(\chi-1)}{\eta_c\chi} \qquad (3.14)$$

It is clear from Eqn. 3.13 and Eqn. 3.14 that the gas turbine efficiency and specific work output are functions of many parameters

$$\eta_{gt} = f(\theta, r, C_p, \eta_c, \eta_{cc}, \eta_t, \eta_{mec}) \tag{3.15}$$

$$w_{gt} = f(\theta, r, C_p, \eta_c, \eta_{cc}, \eta_t, \eta_{mec}) \tag{3.16}$$

where η_{cc} = the combustion chamber efficiency

η_{mec} = the mechanical efficiency

Hence the efficiency of the gas turbine can be increased by

i. Increasing the temperature ratio θ.
ii. Increasing the pressure ratio r.
iii. Changing the cycle working fluid with a fluid of higher specific heat C_p.
iv. Increasing the components' efficiencies η_c, η_t and η_{cc}.

Other modifications to the cycle, for the purpose of increasing its efficiency, include reheating the working fluid in between the turbine stages and regenerative heating of the compressed gases prior to the entry to the combustion chamber using the turbine exhaust gases.

3.2.3 Steam Turbine Power Plant

The schematic diagram of a simple steam power plant operating on Rankine cycle is depicted in Fig. 3.4, and its corresponding cycle on the temperature entropy diagram is presented in Fig. 3.5. The thermal efficiency of the steam plant can be expressed as

$$\eta_{st} = \frac{Net\ power\ output}{Heat\ \text{sup}\ plied} \tag{3.17}$$

$$\eta_{st} = \frac{Turbine\ power\text{-}Pump\ power}{Heat\ \text{sup}\ plied}$$

$$\eta_{st} = \frac{(h_2 - h_3) - (h_1 - h_4)}{(h_2 - h_1)} \tag{3.18}$$

where h represents the enthalpy at various stages of the steam power plant cycle

In real steam power plant, loss occurs in every component of the plant, therefore the process is irreversible. The thermal efficiency of the steam power plant can be expressed as

$$\eta_{st} = \frac{\eta_{stt}(h_2 - h_{3s}) - \frac{1}{\eta_p}(h_{1s} - h_4)}{(h_2 - h_4)} \tag{3.19}$$

where η_p = feed pump efficiency

η_{stt} = steam turbine efficiency

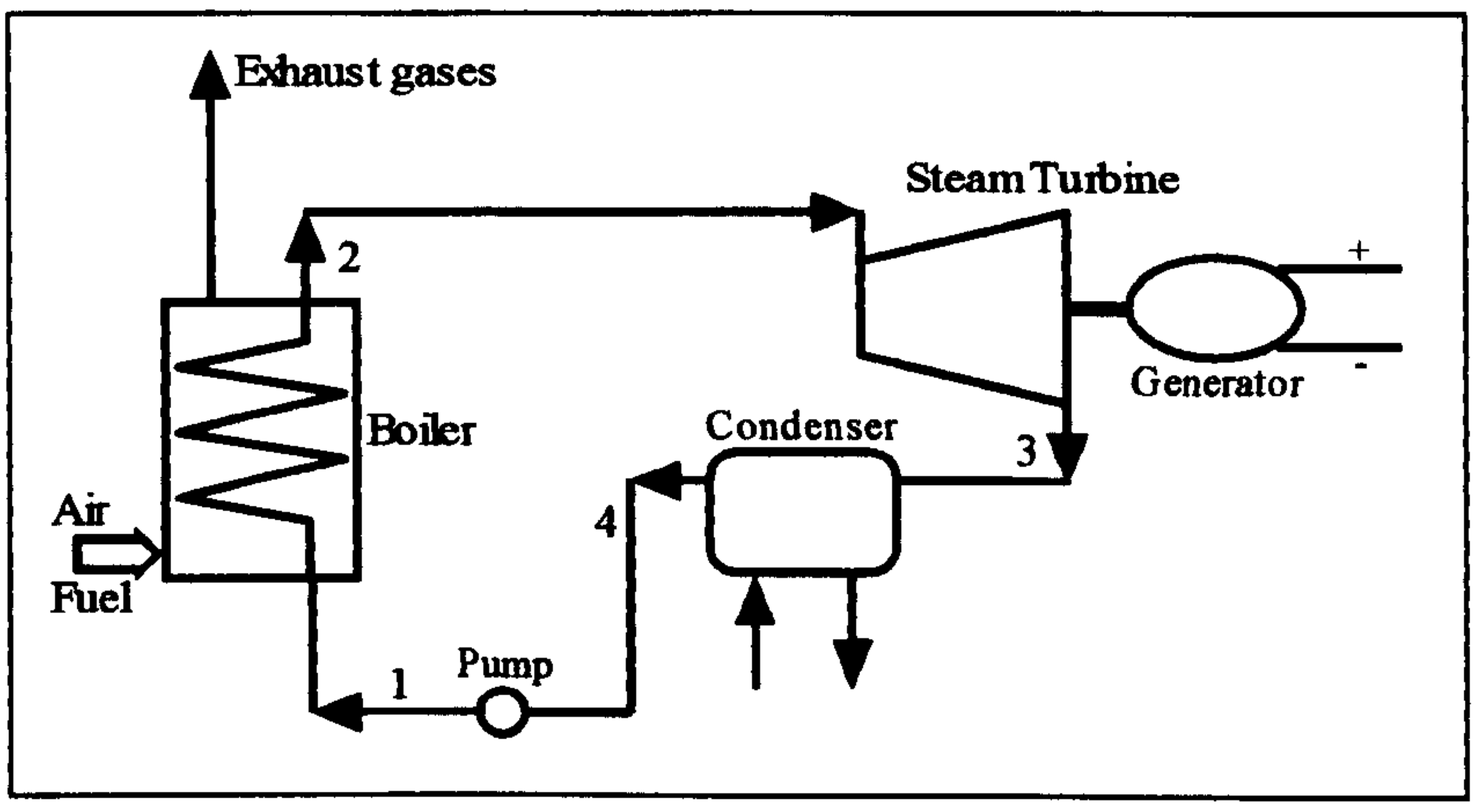

Fig. 3.4 Schematic diagram of a simple steam power plant

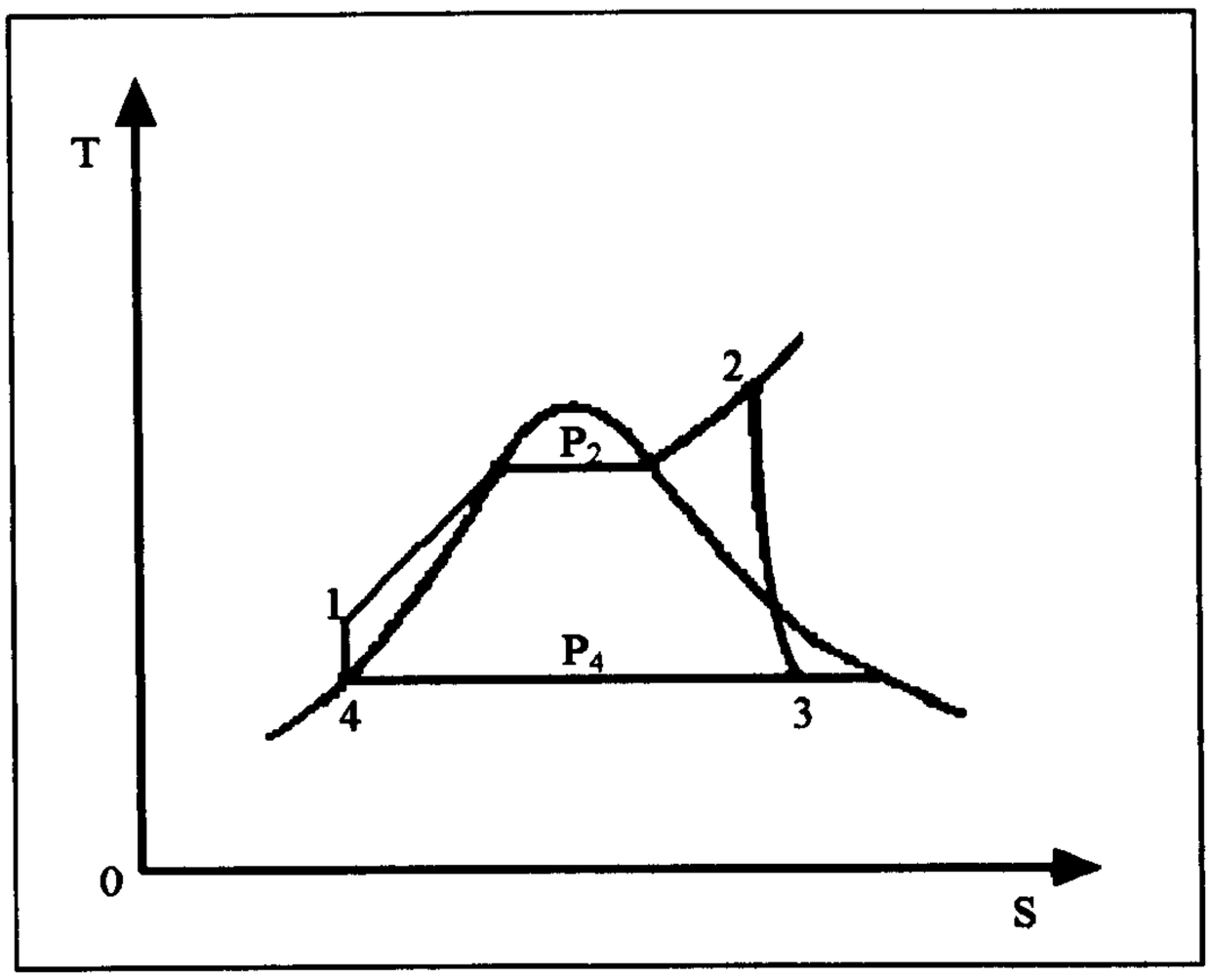

Fig. 3.5 Temperature-Entropy diagram of the simple steam turbine cycle

From Eqn. 3.19 it can be seen that the steam power plant efficiency is a function of steam turbine efficiency, pump efficiency, boiler pressure, condenser pressure and steam superheat temperature

$$\eta_{st} = f\left(\eta_{stt}, \eta_p, P_B, P_{con}, T_{2st}\right) \tag{3.20}$$

Introducing some modifications to the simple steam turbine cycle, such as reheating, regeneration or using an economiser, would increase the steam power plant thermal efficiency.

3.2.4 Gas Turbine and Steam Turbine Plants in Series

It has been shown that modifications and improvements to the gas turbine and steam turbine power plants individually would increase their efficiency. However, the cost of such modifications may be high because they invariably necessitate installation of new components. The alternative is to use the heat rejected by the gas turbine, hereafter named as the higher cycle, may be used to raise high pressure steam which is expanded in the steam turbine, hereafter known as the lower cycle.

The combined power plants reduce the mean temperature at which the heat is rejected

to the atmosphere. This recovery of heat that would otherwise be wasted increases the overall thermal efficiency of the combined plant and decrease $T_{\min}$ in Eqn. 3.5 at which heat is rejected to the environment, thus reducing the thermal load on the environment and the consequential green house effect.

The gas turbine-steam turbine combined power plant is the subject of this research. A block diagram of the simple combined power and power plant (CPP) is shown in Fig. 3.6. The higher plant H receives an amount of heat Q_A to produce work W_H and rejects the exhaust heat Q_{HL}. The lower plant L absorbs some of the heat rejected from the upper plant and produces work W_L. The thermal efficiency of the combined plant η_{CPP} can be calculated as follows

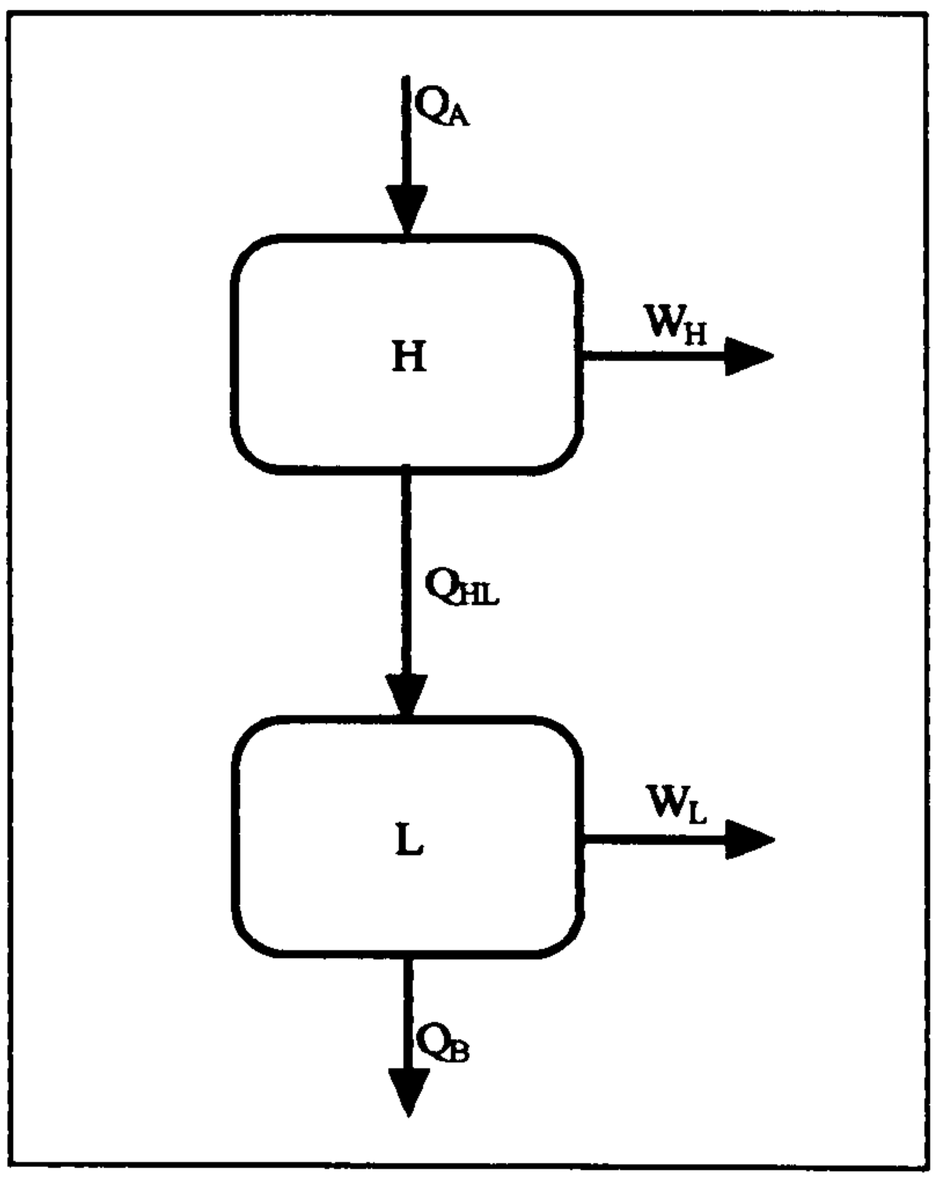

Fig. 3.6 Two plants in series

$$\eta_{CPP} = \frac{W_H + W_L}{Q_A} \tag{3.21}$$

but

$$W_H = \eta_H Q_A, \quad W_L = \eta_L Q_{HL} \qquad \text{and} \qquad Q_{HL} = Q_A(1-\eta_H)$$

hence

$$W_L = Q_A \eta_L (1-\eta_H) \tag{3.22}$$

Substituting the above expressions in Eqn. 3.21 will give

$$\eta_{CPP} = \frac{\eta_H Q_A + Q_A \eta_L (1-\eta_H)}{Q_A} \tag{3.23}$$

and finally,

$$\eta_{CPP} = \eta_H + \eta_L - \eta_H \eta_L \tag{3.24}$$

Considering a more realistic two combined plants in series where heat Q_{UN} lost to the environment through radiation and other effects before entering the lower plant. Further heat Q_{ab} may be added between the plants as shown in the block diagram in Fig. 3.7. The efficiency of such a plant can be defined as

$$\eta_{CPP} = \frac{W_H + W_L}{Q_A + Q_{ab}} \tag{3.25}$$

but

$$\eta_H = \frac{W_H}{Q_A} \qquad \text{and} \qquad \eta_L = \frac{W_L}{Q_L}$$

and

$$Q_L = Q_{ab} + Q_{HR} - Q_{UN} = Q_A(1-\eta_H) + Q_{ab} - Q_{UN} \tag{3.26}$$

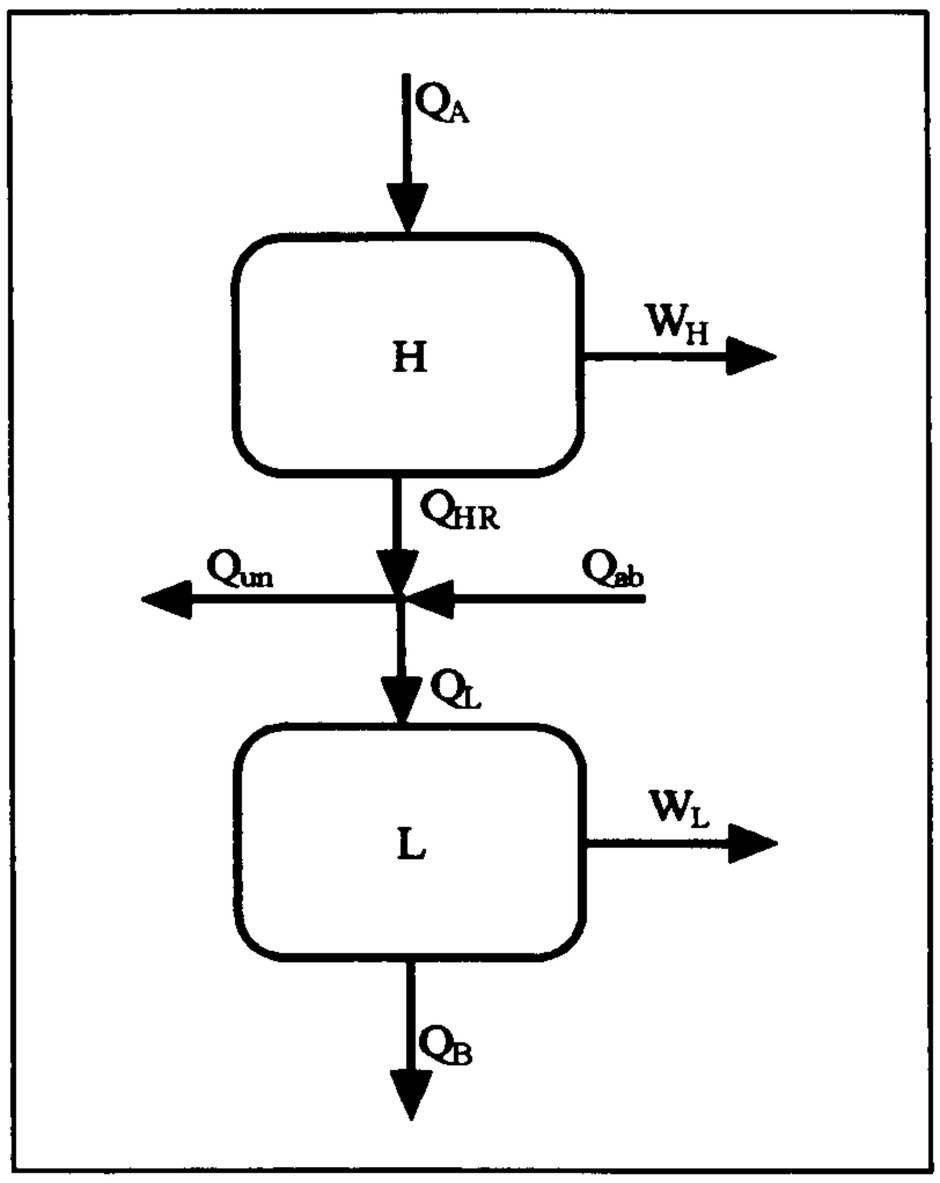

Fig. 3.7 Two plants in series with heat losses

Substituting the above expressions in Eqn. 3.21 will give

$$\eta_{CPP} = \frac{\eta_H + \dfrac{W_L}{Q_A}}{1 + \dfrac{Q_{ab}}{Q_A}} \tag{3.27}$$

but

$$W_L = \eta_L Q_L = \eta_L \left(Q_{ab} + Q_{HR} - Q_{UN}\right)$$

hence

$$\eta_{CPP} = \frac{\eta_H + \eta_L \left(\dfrac{Q_{ab}}{Q_A} + 1 - \eta_H - \dfrac{Q_{UN}}{Q_A} \right)}{1 + \dfrac{Q_{ab}}{Q_A}} \tag{3.28}$$

If $Q_{UN} = 0$ and $Q_{ab} = 0$ then η_{CPP} will be the same as Eqn. 3.24 obtained previously.

$$\eta_{CPP} = \eta_H + \eta_L - \eta_H \eta_L$$

From Eqn. 3.28 and with a constant higher cycle efficiency η_H of 0.3, the values of the combined efficiency η_{CPP} were calculated for a range of values of the lower cycle efficiency η_L at different values of supplementary heat ratios $\frac{Q_{ab}}{Q_A}$. The results have been plotted in Fig. 3.8.

Without supplementary heating, i.e. $\frac{Q_{ab}}{Q_A} = 0$, and by varying the higher cycle efficiencies η_H, Eqn. 3.28 was used also to calculate the lower cycle efficiency η_L at two constant combined cycle efficiencies η_{CPP} of 0.5 and 0.6. The calculated results versus the higher cycle efficiency have been plotted in Fig. 3.9 at two constant values, 0% and 10%, of percentage heat loss $\frac{Q_{UN}}{Q_A}$.

Figures 3.8 and Fig. 3.9 show that:

i. Supplementary heating would decrease the overall combined cycle efficiency except when the supplementary heating results in a significant increase in the lower cycle efficiency.
ii. To reach specified combined cycle efficiency, correct combination of the two cycle's efficiencies is necessary.
iii. The heat lost between the two plants Q_{UN} increases the importance of higher cycle efficiency in the combined plant.

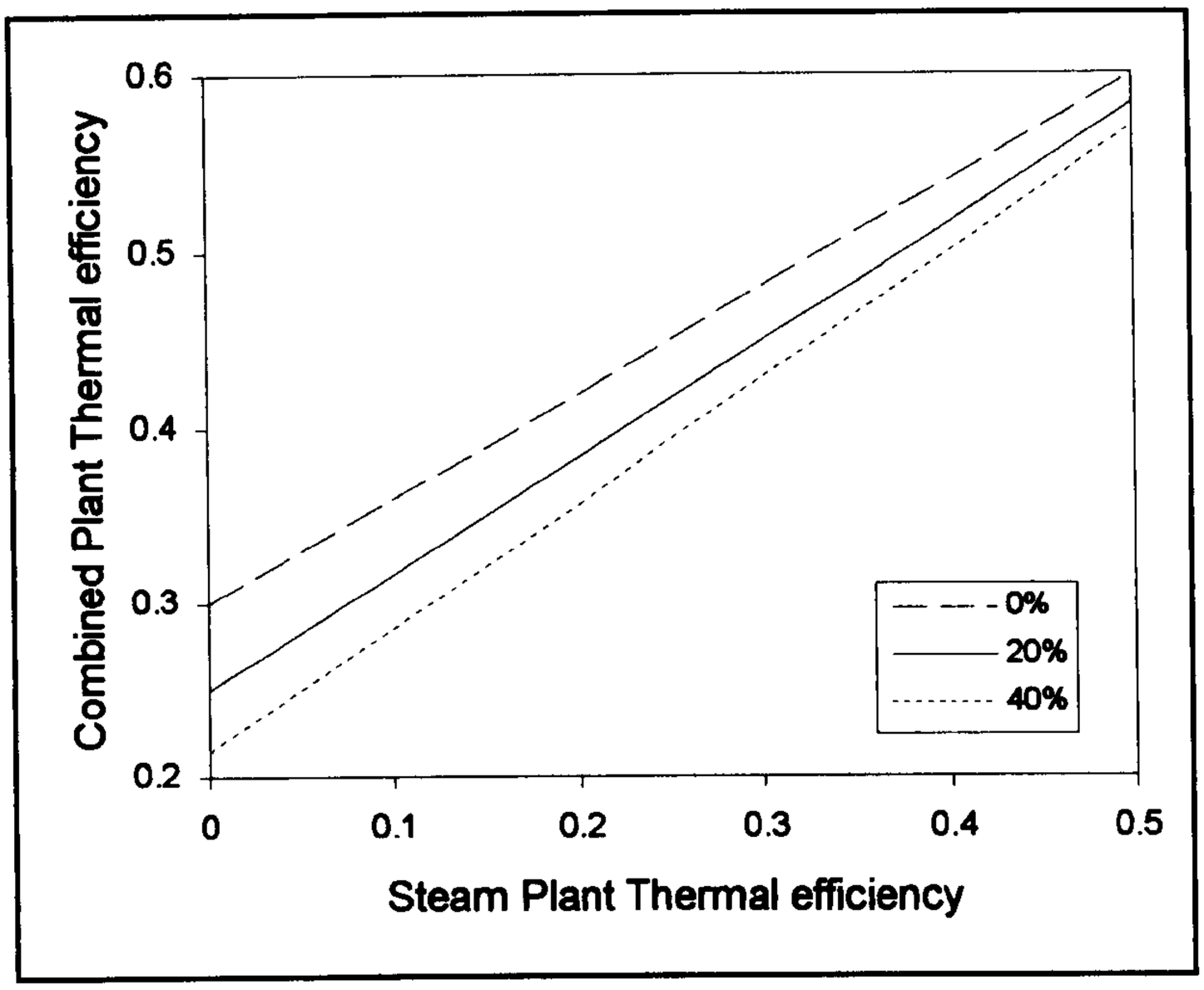

Fig. 3.8 Combined cycle efficiency versus lower cycle efficiency at constant supplementary heating ratios and 0.30 higher cycle efficiency

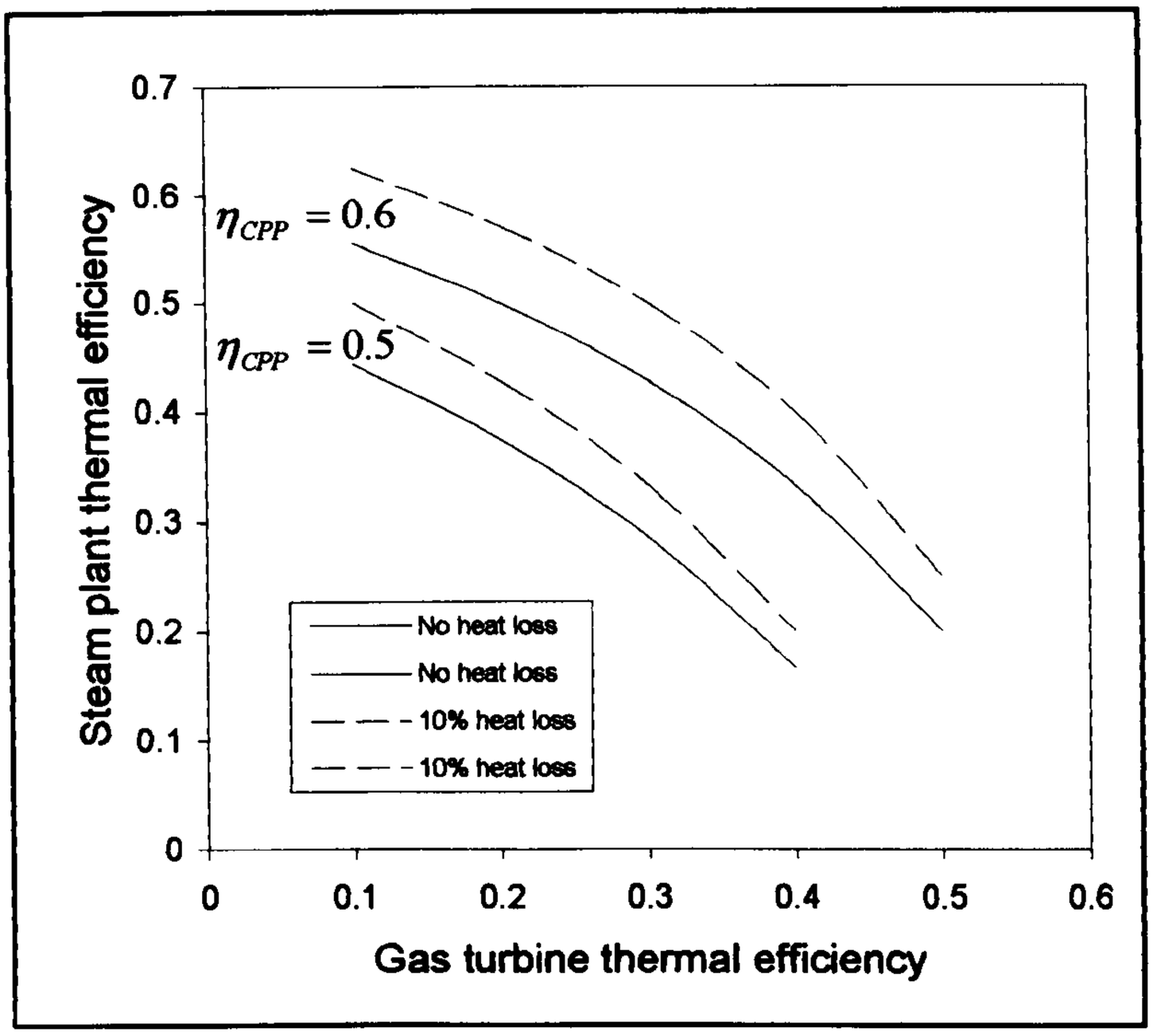

Fig. 3.9 Lower cycle efficiency versus higher cycle efficiency at constant heat loss ratios for 0.60 and 0.50 combined cycle efficiency

A simple combined gas/steam power plant has been discussed previously, but there can be many different configurations such as reheat gas turbine cycle with dual pressure steam cycle, inter-cooled gas turbine cycle with single or dual pressure steam turbine cycle etc. In the current parametric study different configurations for the combined cycle were investigated. The combined simple gas turbine cycle with single pressure steam cycle was thermodynamically analysed. The same analysis procedure may be applied to any of the following configurations:

i. Simple gas turbine cycle combined with simple steam cycle.
ii. Simple gas turbine cycle combined with dual pressure steam cycle.
iii. Reheat gas turbine cycle combined with simple steam cycle.
iv. Reheat gas turbine cycle combined with dual pressure steam cycle.
v. Gas turbine Inter-cooling cycle combined with simple steam cycle.
vi. Gas turbine Inter-cooling cycle combined with dual pressure steam cycle.

A schematic diagram of the combined plant consisting of a simple gas turbine and a single pressure steam turbine is shown in Fig. 3.10. The Temperature-Entropy diagram of the combined cycle is shown in Fig. 3.11.

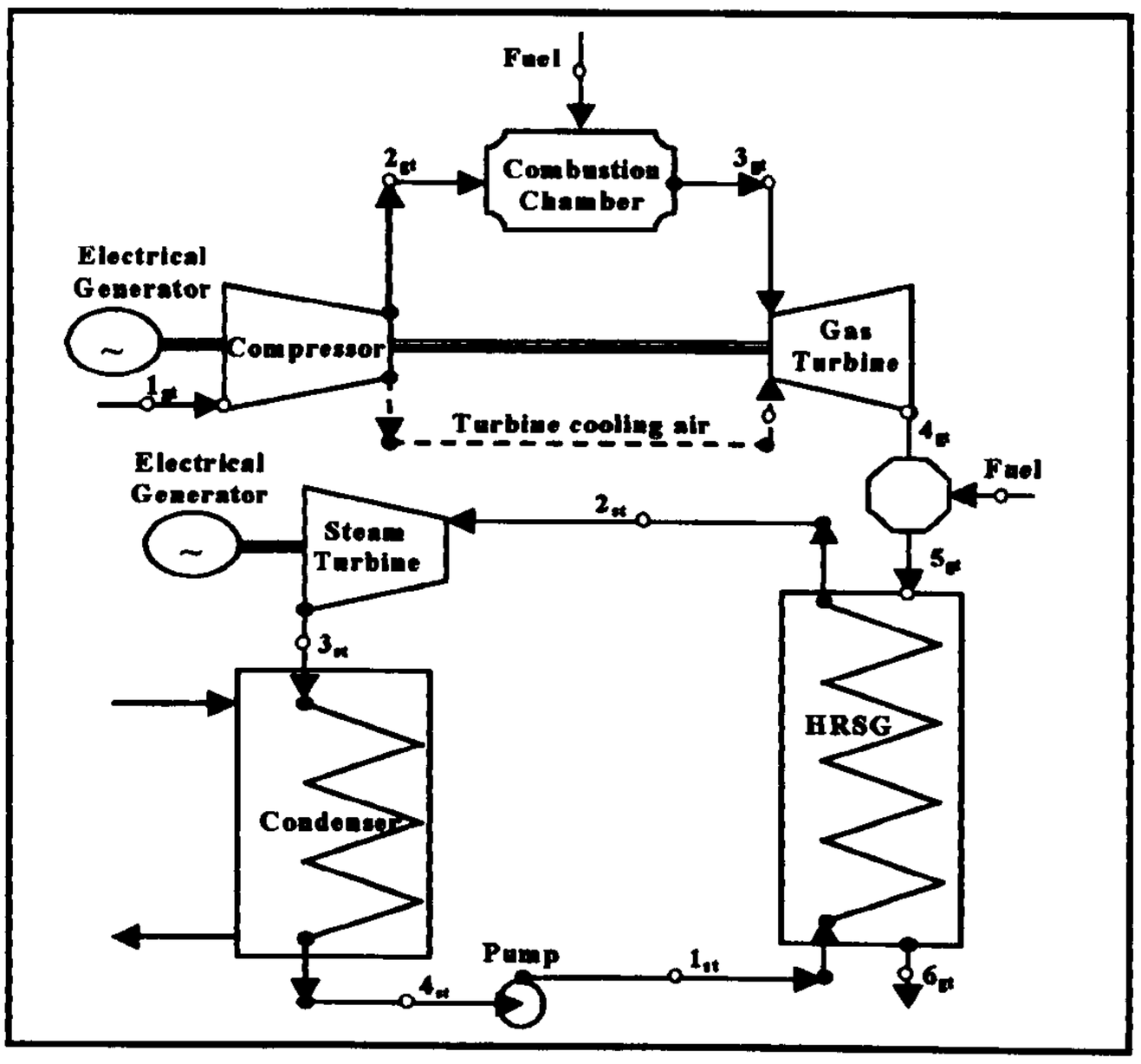

Fig. 3.10 Schematic diagram of a CPP plant with a waste heat recovery boiler

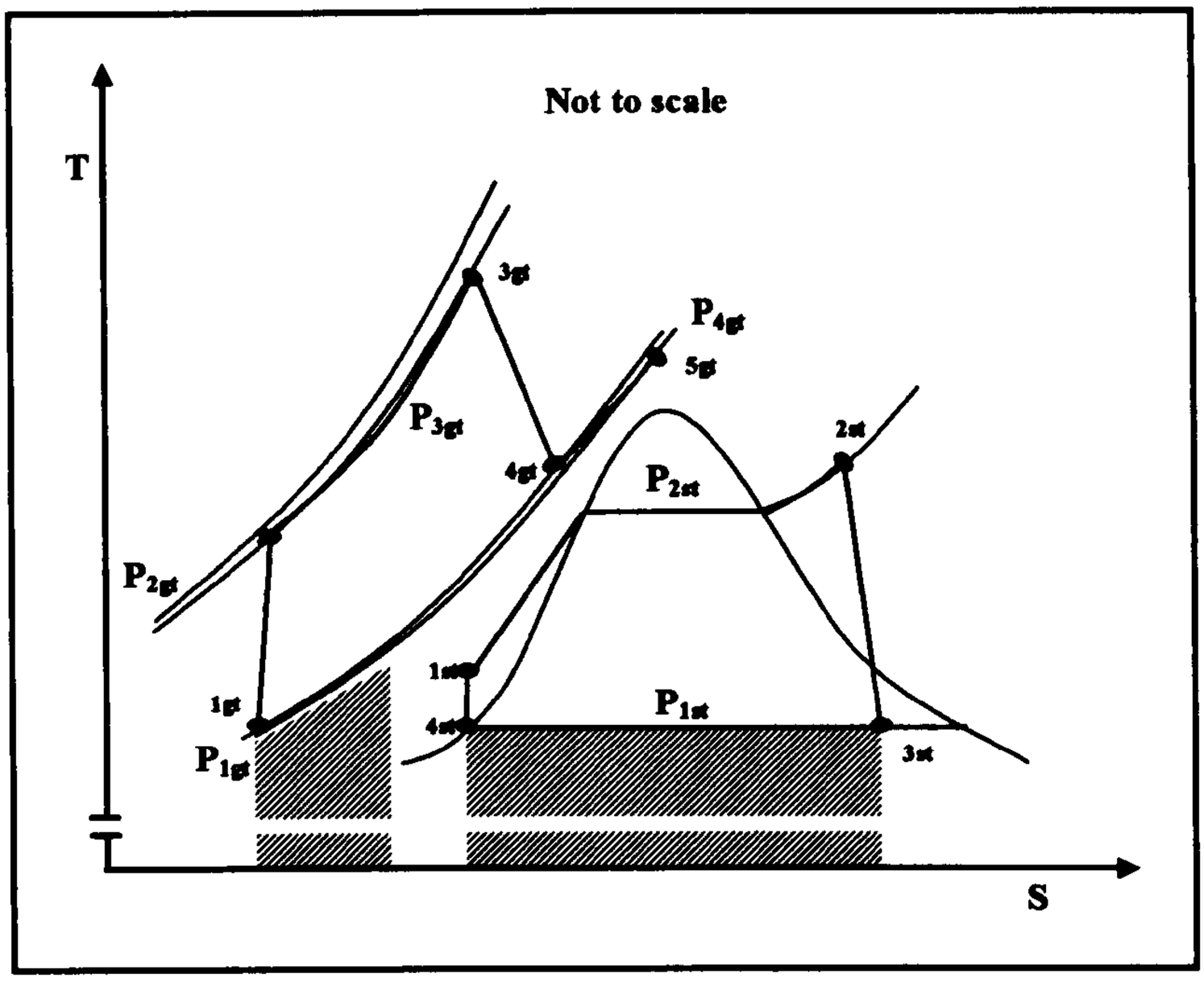

Fig. 3.11 Temperature-Entropy diagram of a combined gas-steam power cycle

3.2.5 Thermodynamic Analysis of the Gas Turbine Cycle

It has been shown previously that the gas turbine engine performance is a function of many parameters. The thermodynamic analysis of the engine may be simplified by making the following assumptions:

i. The air used by the gas turbine as well as the products of the combustion behave like perfect gas.
ii. The specific heat capacities are function of average temperature through each process.
iii. The loss of stagnation pressure in the compressor inlet is a constant percentage of the compressor inlet pressure.
iv. The loss of stagnation pressure in the combustion chamber is a constant percentage of the combustion chamber inlet pressure.

Within the framework of these assumptions, the engine performance may be calculated by means of a step-by-step analysis for each component in the engine. The procedure for calculating the values of specific heats is given in the next section.

3.2.5.1 Specific Heats of Air and Combustion Gases

The specific heats of air and combustion gases at various stages throughout the engine are calculated by considering variations of temperature but without dissociation.

The specific heat during the combustion process at constant pressure is considered to be a function of the temperature and the fuel/air ratio:

$$C_P = f(T, F) \tag{3.29}$$

Also gas constant (R) is a function of the fuel/air ratio:

$$R = f(F) \tag{3.30}$$

However, the variations of R with fuel/air ratio are negligible [5]; therefore R_{air} may be used in the calculations without the risk of serious error.

The specific heat at constant volume is given by:

$$C_V = C_P - R \tag{3.31}$$

The ratio of specific heats is given by:

$$\gamma = \frac{C_P}{C_V} \tag{3.32}$$

Tables containing the values of the specific heats against temperature variation have been published in many references such as Chappel and Cockshutt [38]. In the present work, to compute the values of specific heats at constant pressure and various temperatures for air and combustion gases, data from the tables were fitted with polynomial curves to obtain Equations 3.33 to 3.37. These equations provide the

details of the polynomials. Here T_a and T_g refer to the average temperatures during the compression and expansion processes in the compressor and turbine respectively.

For air at low temperature range of 200 to 800 K

$$C_{Pa} = 1.0189\times10^{3} - 0.13784T_a + 1.9843\times10^{-4}T_a^{\,2} + 4.2399\times10^{-7}T_a^{\,3} - 3.7632\times10^{-10}T_a^{\,4} \quad (3.33)$$

For air at high temperature range of 800 to 2200 K

$$C_{Pa} = 7.9865\times10^{2} + 0.5339T_a - 2.2882\times10^{-4}T_a^{\,2} + 3.7421\times10^{-8}T_a^{\,3} \quad (3.34)$$

For specific heats of products of combustion

$$C_{Pg} = C_{Pa} + (F/(1+F))B_T \quad (3.35)$$

where B_T at low temperature range of 200 to 800 K

$$B_T = -3.59494\times10^{2} + 4.5164T_g + 2.8116\times10^{-3}T_g^{\,2} - 2.1709\times10^{-5}T_g^{\,3} + 2.8689\times10^{-8}T_g^{\,4} - 1.2263\times10^{-11}T_g^{\,5} \quad (3.36)$$

and B_T at high temperature range of 800 to 2200 K

$$B_T = 1.0888\times10^{3} - 0.1416T_g + 1.916\times10^{-3}T_g^{\,2} - 1.2401\times10^{-6}T_g^{\,3} + 3.0669\times10^{-10}T_g^{\,4} - 2.6117\times10^{-14}T_g^{\,5} \quad (3.37)$$

3.2.5.2 Air Intake

The pressure loss in the compressor intake $\xi_{\text{int }ake}$ is assumed to be a percentage value of the atmospheric pressure therefore at the compressor inlet it can be expressed as:

$$P_{o1} = (1 - \xi_{\text{int }ake}) P_{atm} \tag{3.38}$$

3.2.6.3 Air Compression

The compression power W_c is given be the following equation:

$$W_c = \dot{m}_a C_{Pa} (T_{o2} - T_{o1}) = \dot{m}_a C_{Pa} T_{o1} \left(\frac{T_{o2}}{T_{o1}} - 1 \right)$$

This equation can be written as:

$$W_c = \dot{m}_a C_{Pa} \frac{T_{o1}}{\eta_c} \left[\left(\frac{P_{o2}}{P_{o1}} \right)^{\gamma_a - 1 / \gamma_a} - 1 \right] \tag{3.39}$$

The compressor specific work output equals to:

$$w_c = C_{Pa} \frac{T_{o1}}{\eta_c} \left[\left(\frac{P_{o2}}{P_{o1}} \right)^{\gamma_a - 1 / \gamma_a} - 1 \right] \tag{3.40}$$

The final stagnation temperature in the compression process T_{o2} equals to:

$$T_{o2} = T_{o1} + \frac{T_{o1}}{\eta_c} \left[\left(\frac{P_{o2}}{P_{o1}} \right)^{\gamma_a - 1 / \gamma_a} - 1 \right] \tag{3. 41}$$

As the air temperature rises through the compressor, its specific heat values would

change. Assuming constant specific heat for the whole range of pressure ratio could lead to significant errors in computing the compressor delivery temperature, compression work and isentropic efficiency of the compression process. For this reason in the current study variable specific heat and gama values were used. These values were computed, as has been described earlier, on the basis of the mean temperature across the compressor.

Similarly the final stagnation temperature T_{o2} at the end of the compression process cannot be computed directly from Eqn. 3.41. This is because the air specific heat ratio γ_a is a function of the mean stagnation temperature across the compression process. Therefore, in order to compute T_{o2} an iterative method was used. This method, named as **AIRPROP,** has been developed in the form of a computer subroutine for the purpose of this research. The flowchart of **AIRPROP** is shown in Fig. 3.12.

3.2.5.4 Combustion

Using the principles of mass and heat balance for the combustion process as shown in Fig. 3.13 and assuming complete combustion; Eqn. 3.42 was developed as follows:

$$\dot{m}_g C_{Pg}\left(T_{o3}-T_{o\_ref}\right)+\dot{m}_f \Delta h_f = \dot{m}_a C_{Pa}\left(T_{o2}-T_{o\_ref}\right)+\dot{m}_f C_{Pf}\left(T_{of}-T_{o\_ref}\right) \quad (3.42)$$

where $\dot{m}_a$ is net air mass flow delivered by the compressor without compressor bleed.

It is usual to assume that the fuel temperature T_{of} is equal to the reference temperature T_{o_ref}. Hence the result of the last term in Eqn. 3.42 approaches zero.

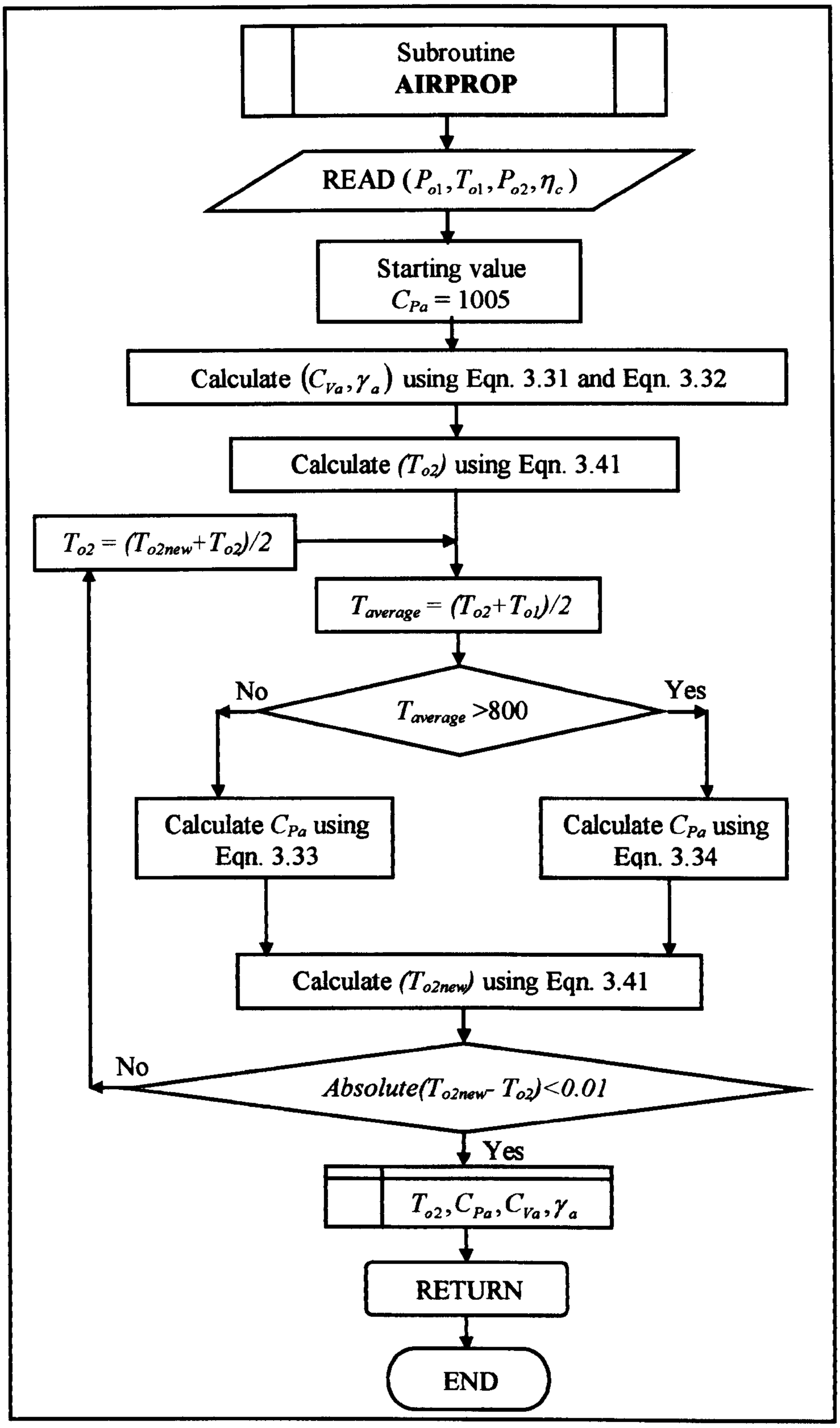

Fig.3.12 The flowchart for computing ($T_{o2}, C_{Pa}, C_{Va}, \gamma_a$)

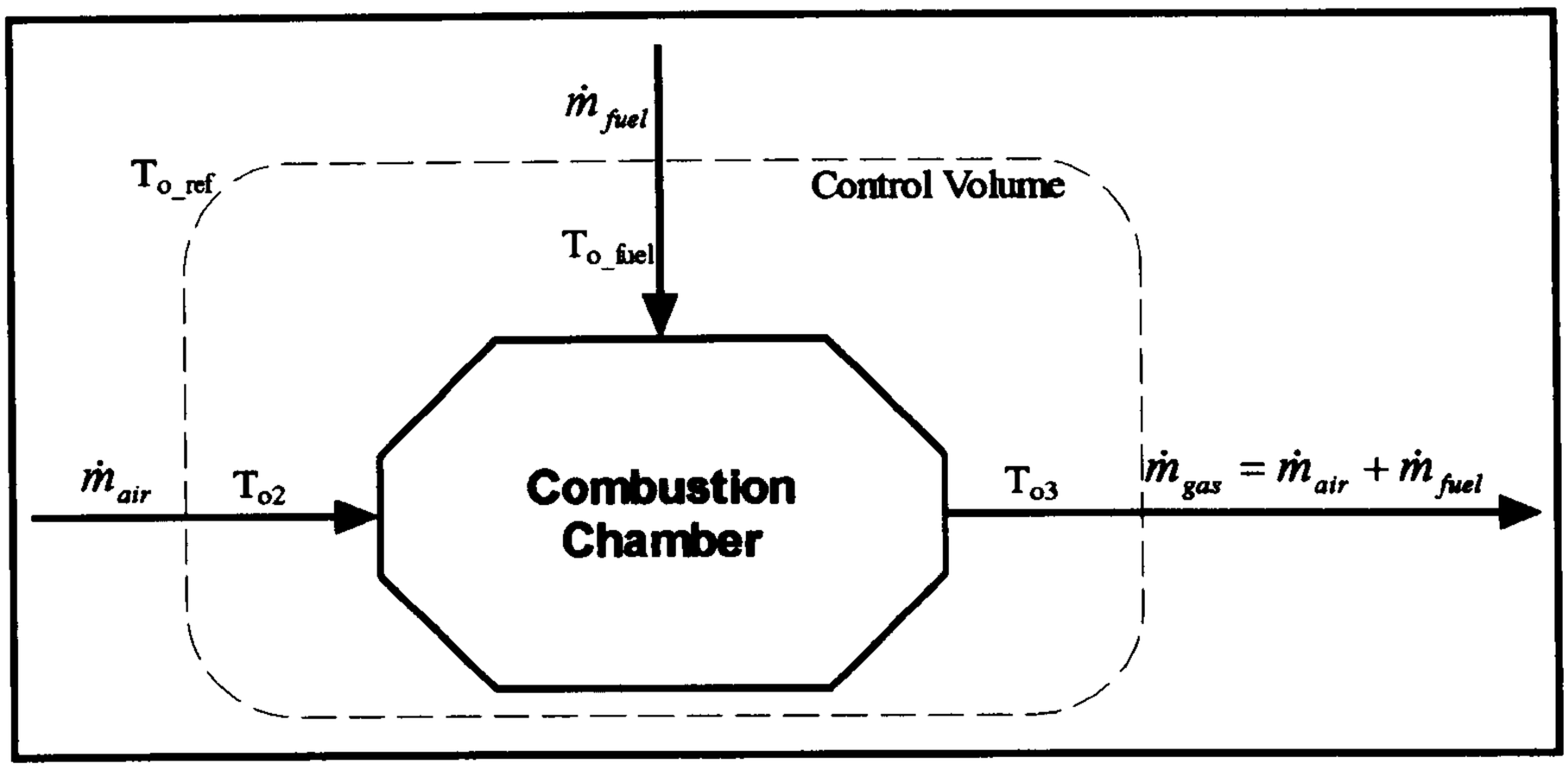

Fig. 3.13 Combustion chamber control volume

The efficiency of the combustion process may be expressed as

$$\eta_{cc} = \frac{Actual\ heat\ released\ to\ the\ gas}{Theoretical\ heat\ available\ in\ the\ fuel} \tag{3.43}$$

Using Eqn. 3.42 and Eqn. 3.43, the fuel/air ratio F in the combustion chamber can be calculated from Eqn. 3.44.

$$F = \frac{1}{\frac{\eta_{cc}(LCV)}{C_{Pg}(T_{o3} - T_{o2})} - 1} \tag{3.44}$$

The pressure loss in the combustion chamber ξ_{cc} is a constant percentage value of the compressor delivery pressure P_{o2}, therefore:

$$P_{o3} = (1 - \xi_{cc})P_{o2} \tag{3.45}$$

Due to a considerable rise of the gas temperature through the combustion chamber, an assumption of constant specific heat ratio for the whole range of combustion temperatures could lead to appreciable errors in computing the combustion chamber

pressure and temperature. For this reason an average specific heat ratio computed by using an average combustion chamber temperature was used in the current work.

For the same reason the fuel/air ratio F cannot be computed directly by using Eqn. 3.44 because the specific heat at constant pressure C_{pg} of the combustion gases is a function of the mean stagnation temperature across the combustion chamber. An iterative method was used to compute fuel/air ratio F. The method was developed for the purpose of this study in the form of a computer subroutine named **FARATIO**. The flowchart of the subroutine **FARATIO** is shown in Fig. 3.14.

3.2.5.5 Gas Expansion

The turbine power output W_t can be calculated from Eqn. 3.46 given below:

$$W_t = (1+F)\dot{m}_a C_{Pg}(T_{o3} - T_{o4}) = (1+F)\dot{m}_a C_{Pg} T_{o3}\left(1 - \frac{T_{o4}}{T_{o3}}\right)$$

$$W_t = (1+F)\dot{m}_a C_{Pg}\eta_t T_{o3}\left[1 - \left(\frac{P_{o4}}{P_{o3}}\right)^{\gamma_g - 1/\gamma_g}\right] \qquad (3.46)$$

The exhaust stagnation temperature T_{o4} in the expansion process was calculated by using Eqn. 3.47.

$$T_{o4} = T_{o3} - \eta_t T_{o3}\left[1 - \left(\frac{P_{o4}}{P_{o3}}\right)^{\gamma_g - 1/\gamma_g}\right] \qquad (3.47)$$

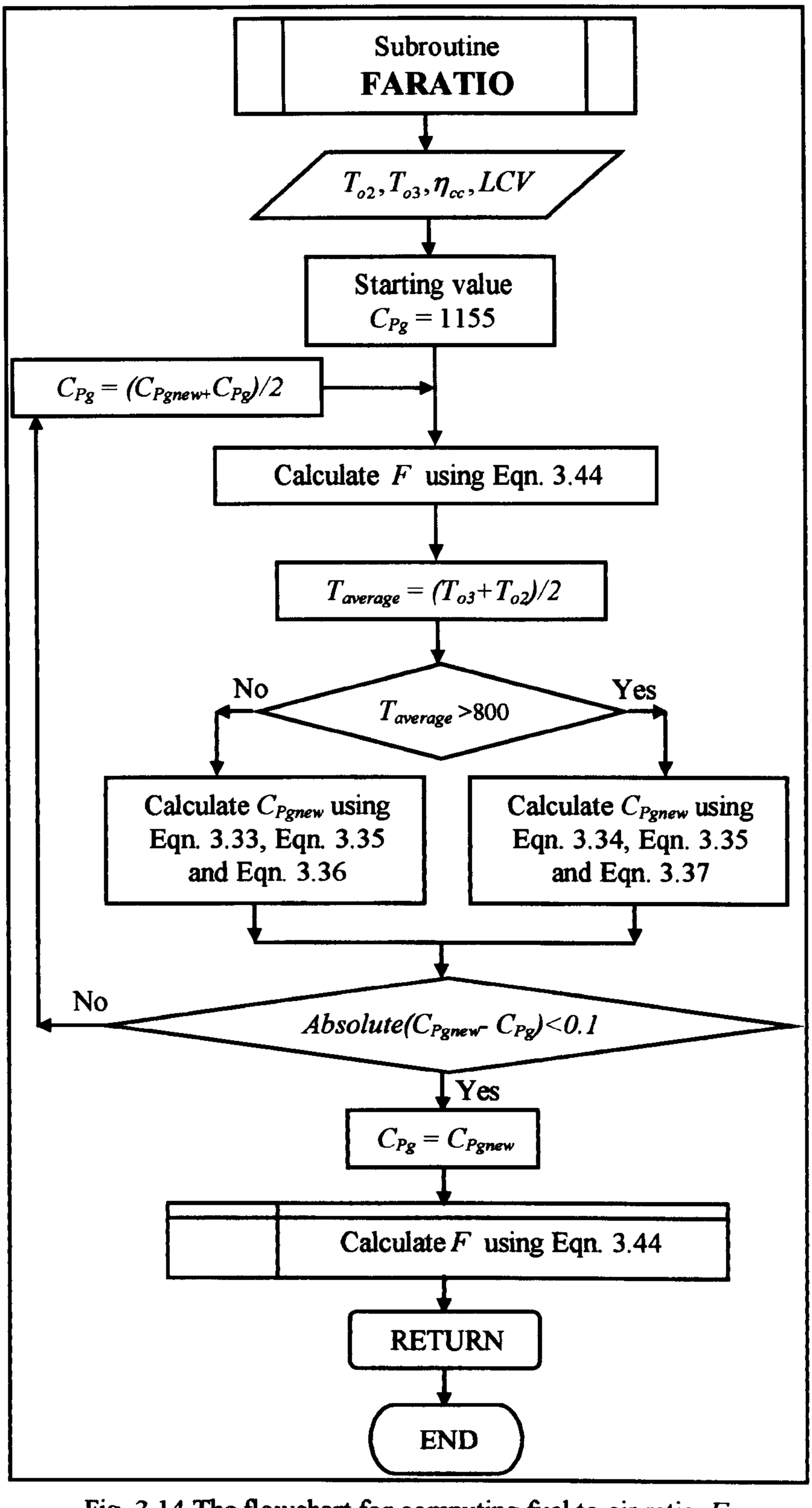

Fig. 3.14 The flowchart for computing fuel to air ratio F

The thermal efficiency of the gas turbine cycle η_{gt} can be calculated from Eqn. 3.48.

$$\eta_{gt} = \frac{W_t - W_c}{F\dot{m}_a(LCV)} \tag{3.48}$$

The work output W_{gt} and specific work output of the gas turbine cycle w_{gt} can be calculated from Eqn. 3.49 and Eqn. 3.50.

$$W_{gt} = W_t - W_c \tag{3.49}$$

$$w_{gt} = \frac{W_{gt}}{\dot{m}_a} \tag{3.50}$$

For the reasons explained earlier in this section, the values of the variable specific heat ratio were computed by using the mean temperature across the turbine. A computer subroutine named **GASPROP** was developed to calculate mean specific heat. The flowchart of subroutine **GASPROP** is shown in Fig. 3.15.

.

3.2.5.6 Electrical Alternators

Alternator efficiency is defined as the electrical power output divided by the shaft power input from the prime mover as follows:

$$\eta_{Alt} = \frac{W_{Alt}}{W_{gt}} = \frac{EMF \times I \times PF}{W_{gt}} \tag{3.51}$$

where EMF = the electromotive force in Volts

I = the current in Amps

PF = the power factor (PF=1 for electrical resistive load)

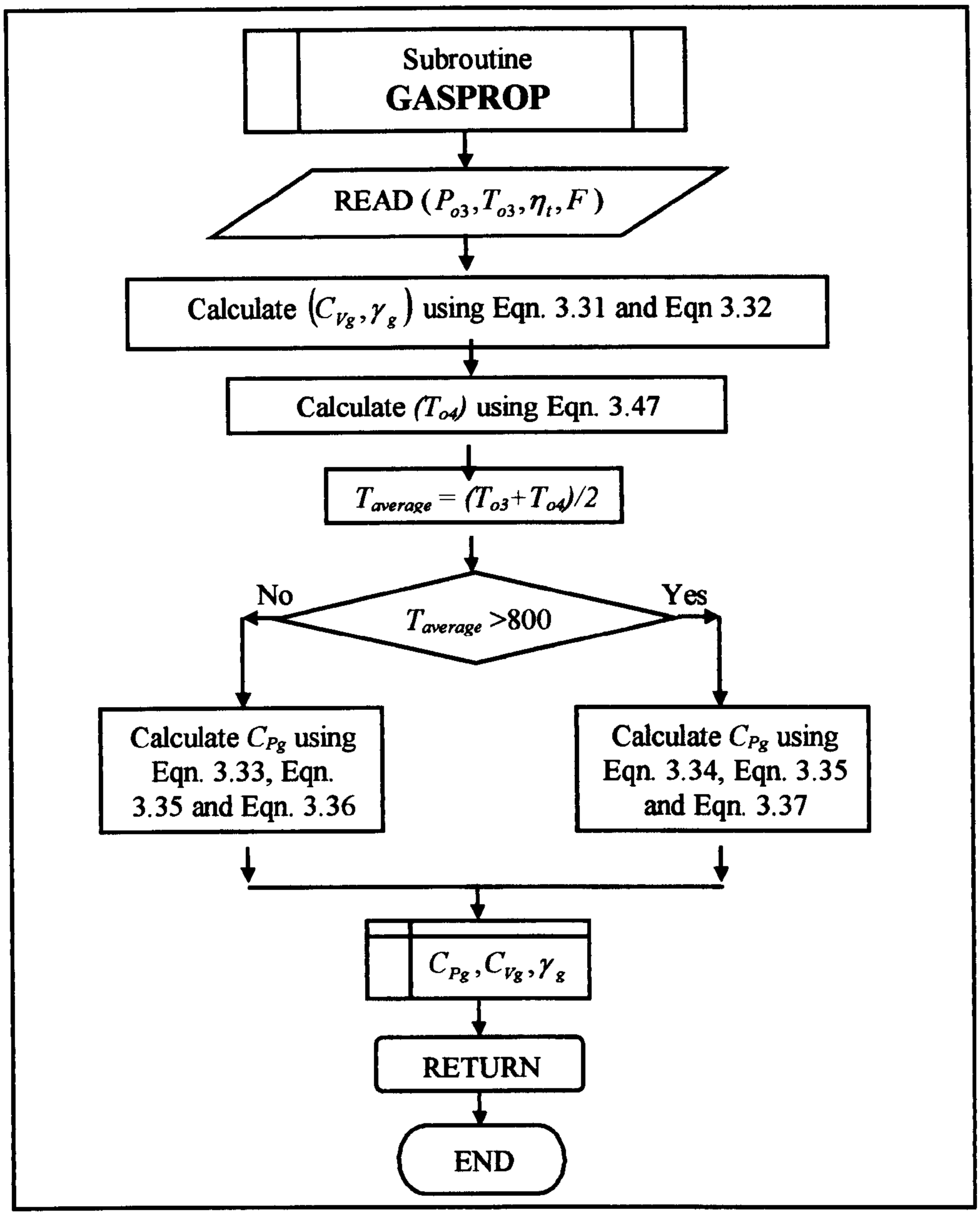

Fig. 3.15 The flowchart for computing $(C_{Pg}, C_{Vg}, \gamma_g)$

3.2.6 Thermodynamic Calculations of the Steam Turbine Cycle

A schematic diagram of a simple steam power plant operating on Rankine cycle and its corresponding temperature entropy diagram were shown in Fig. 3.4 and Fig. 3.5 respectively. The governing equations for the components are developed in the following section.

3.2.6.1 Thermodynamic Calculations of the Heat Recovery Steam Generator

The energy balance in the steam generator may be expressed as follows:

$$\dot{m}_a(1+F)C_{pg}(T_{o4(gt)} - T_{o6(gt)})\eta_B = \dot{m}_{st}(h_{2(st)} - h_{1(st)}) \quad (3.52)$$

The gas stack temperature $T_{o6(gt)}$ should be kept as low as possible, but at the same time condensation must be avoided to prevent corrosion. The lowest stack temperature is determined by the fuel type used, for instance sulphuric fuels should have a higher stack temperature.

The temperature-heat diagram of the heat recovery steam generator is shown in Fig. 3.16. The heat added to the water or the steam was supplied in three steps:

i. The economizing step where the temperature of water rises from $T_{1(st)}$ to the saturation liquid temperature at that boiler pressure.
ii. The evaporation step where water evaporates to steam by absorbing heat at a constant temperature.
iii. The superheating step where the temperature of steam increases from the saturation temperature to the desired maximum superheated temperature $T_{2(st)}$.

$$T_{2(st)} = \varepsilon_{sup}(T_{o4} - T_{2(st)sat}) + T_{2(st)sat} \quad (3.53)$$

where $T_{2(st)sat}$ is the saturated temperature at the $P_{2(st)}$

The enthalpy of the steam at the exit of the boiler $h_{2(st)}$ was given by Eqn. 3.54.

$$h_{2(st)} = f(T_{2(st)}, P_{2(st)}) \quad (3.54)$$

$$T_{o(evp)} = PP + T_{2(st)sat} \quad (3.55)$$

where $T_{o(evp)}$ is the gas temperature at the exit of the evaporator

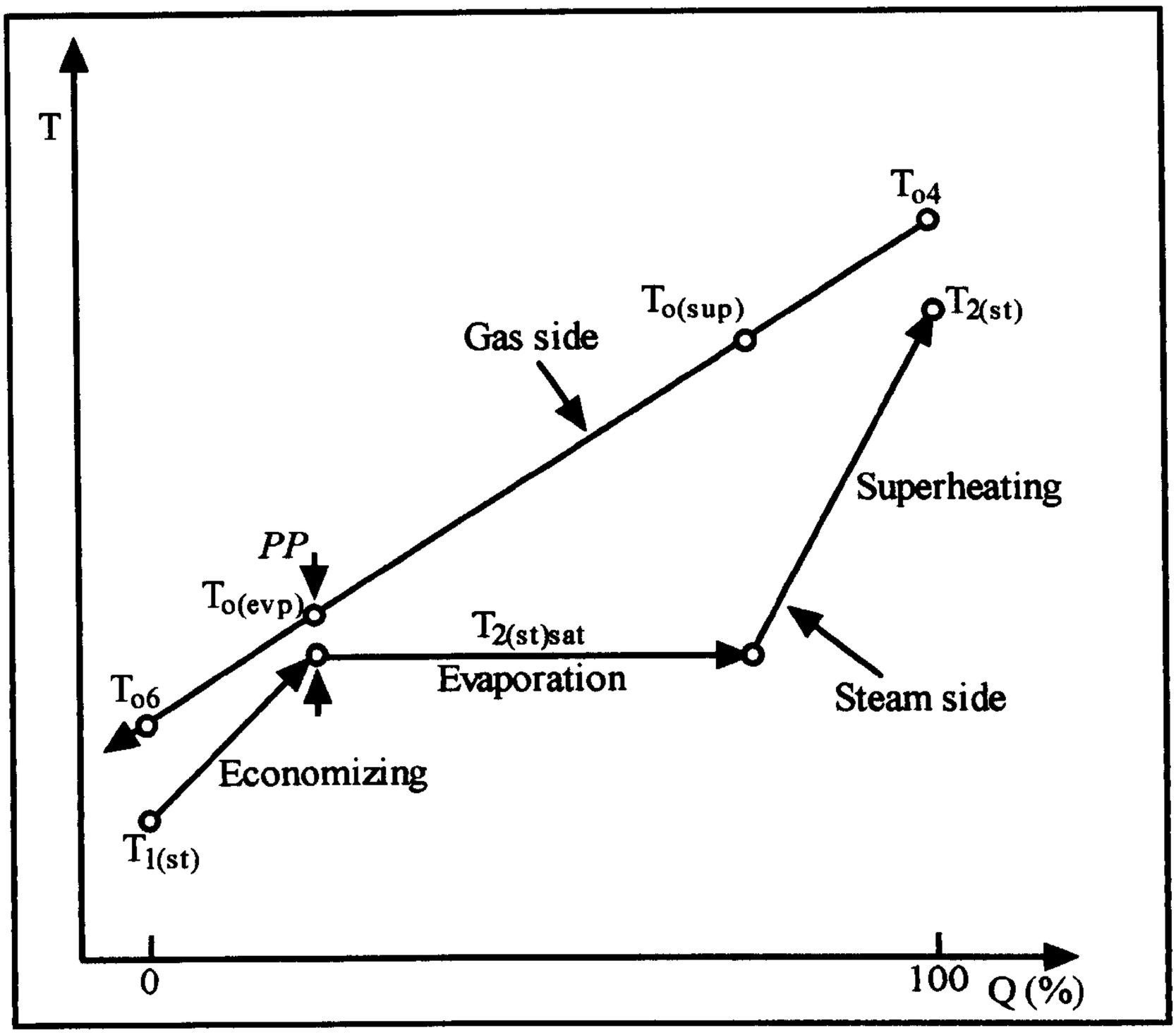

Fig. 3.16 Temperature variation in the heat recovery boiler

Finally,

$$\dot{m}_{st} = \frac{\dot{m}_a (1+F) \eta_B C_{Pg} (T_{o4} - T_{o(evp)})}{h_{2(st)} - h_{2(lq)sat}} \tag{3.56}$$

where $h_{2(lq)sat}$ is the saturated liquid enthalpy at $P_{2(st)}$

The enthalpy of the water at the pump exit $h_{1(st)}$ was calculated from Eqn. 3.57.

$$h_{1(st)} = f(P_{1(st)}, S_{4(st)}) \tag{3.57}$$

$$T_{o6} = T_{o(evp)} - \frac{\dot{m}_{st}\left(h_{2(st)satlq} - h_{1(st)}\right)}{\dot{m}_a\left(1+F\right)C_{Pg}} \tag{3.58}$$

The enthalpy of the steam at the exit of the steam turbine $h_{3(st)}$ was calculated by using Eqn. 3.59.

$$h_{3(st)} = f\left(P_{1(st)}, S_{3(st)}\right) \tag{3.59}$$

The enthalpy of the water at the exit of the condenser $h_{4(st)}$ was calculated as a function of $P_{1(st)}$ as shown in Eqn. 3.60.

$$h_{4(st)} = f\left(P_{1(st)}\right)$$

(3.60)

The heat exchange process in a counter flow heat recovery steam generator must satisfy the following conditions:

i. The gas stack temperature $T_{o6(gt)}$ must be greater than the inlet water temperature $T_{1(st)}$ at least by 10 °C.
ii. The gas temperature at the outlet of the evaporator $T_{o(evp)}$ must be greater than the liquid saturation temperature of the steam $T_{2(st)sat}$ by a minimum value (pinch point temperature difference PP).
iii. The superheated steam temperature $T_{2(st)}$ must be less than the gas turbine exhaust temperature $T_{o4(gt)}$.

The gas pressure loss in the heat recovery steam generator ξ_{HRSG} is a percentage value from the atmospheric pressure where the heat recovery steam generator inlet could be expressed as a function of the atmospheric pressure as shown in Eqn. 3.61.

$$P_{o4} = \left(1 - \xi_{HRSG}\right)P_{atm} \tag{3.61}$$

3.2.6.2 Water Pump Power

The water pump power W_P can be calculated as follows.

$$W_P = \frac{\dot{m}_{st}}{\eta_P}\left(h_{1(st)} - h_{4(st)}\right) \tag{3.62}$$

where the entropy at state 1 equals the entropy at state 4 ($S_{4(st)} = S_{1(st)}$).

3.2.6.3 Steam Expansion

The steam turbine power $W_{t(st)}$ can be calculated in terms of the turbine efficiency and the steam enthalpy drop across the turbine.

$$W_{t(st)} = \dot{m}_{st}\eta_{t(st)}\left(h_{2(st)} - h_{3(st)}\right) \tag{3.63}$$

where the entropy at state 2 equals the entropy at state 3 ($S_{2(st)} = S_{3(st)}$).

The efficiency of the steam turbine cycle η_{st} can now be calculated from Eqn. 3.64.

$$\eta_{st} = \frac{W_{st}}{Q_B} = \frac{W_{t(st)} - W_P}{\dot{m}_a(1+F)C_{pg}\left(T_{o4} - T_{o6}\right)} \tag{3.64}$$

3.2.7 The Combined Cycle Performance

The combined cycle total power W_{CPP} is given as:

$$W_{CPP} = W_{gt} + W_{st} \tag{3.65}$$

The combined cycle efficiency (η_{CPP}) can then be calculated from Eqn. 3.66.

$$\eta_{CPP} = \frac{W_{CPP}}{\dot{m}_a F(LCV)} \tag{3.66}$$

Finally, the specific work output of the combined cycle w_{CPP} can be calculated from Eqn. 3.67.

$$w_{CPP} = \frac{W_{CPP}}{\dot{m}_a} \tag{3.67}$$

3.2.8 Precautions for Using the Parametric Analysis

Equations 3.38 to 3.67 can be solved for every set parameters used in Eqn. 3.68 and Eqn. 3.69. One set of parameters and its numerical calculations is shown as an example in appendix A.

$$\eta_{CPP} = f(\theta, r, C_p, \eta_c, \eta_{cc}, \eta_{t(gt)}, \eta_{mec}, P_{con}, T_{2st}, P_B, \eta_{t(st)}, \eta_p, \eta_{HRSG}) \tag{3.68}$$

$$w_{CPP} = f(\theta, r, C_p, \eta_c, \eta_{cc}, \eta_{t(gt)}, \eta_{mec}, P_{con}, T_{2st}, P_B, \eta_{t(st)}, \eta_p, \eta_{HRSG}) \tag{3.69}$$

The parameters can be varied within the following thermodynamic, technological and physical constraints:

i. The temperature ratio θ can have any value starting from the value of the ratio T_{o2}/T_{o1} to a maximum value limited by the metallurgical considerations.
ii. The pressure ratio r can have any value starting from one to a maximum value determined by mechanical and aerodynamic factors such as stress and Mach number.
iii. The steam temperature can have any value starting from the saturation temperature at that pressure to a maximum value dependent on several

other factors such as thermal stresses, rotational stresses, etc, and economic factors.

iv. The steam pressure in the boiler and the condenser pressure are related to the wetness of the steam at the exit of the steam turbine, which should lie between 0.9 and 1.0. This is because wet steam can have detrimental effect on turbine blades.

v. The exhaust gas temperature in the boiler should be higher than the temperature of the steam by a minimum value where this value is dependent on the economic and the design parameters.

vi. The stack exhaust temperature should be higher than the condensation temperature of water vapour in exhaust gas in order to prevent corrosive condensation.

In the present parametric study the aforementioned precautions were taken into consideration. Table 3.1 displays the assumed values for the combined cycle parameters.

Parameter	Assumed value	Parameter	Assumed value
T_{atm}	288.15 K	η_{cc}	0.98
P_{atm}	101.325 kPa	$\eta_{t(gt)}$	0.88
$T_{o3(gt)}$	(1100 – 1700) K	$\eta_{t(st)}$	0.87
r	4 - 32	η_B	0.85
P_{2st}	10 – 100 bar	η_P	0.85
P_{1st}	0.2 bar	η_{mec}	0.98
$T_{3st(\max)}$	950 K	ξ	5%
$PP_{\min}$	25 K	$\varepsilon_{superheater}$	0.9
$D_{\min}$	0.88	LCV	43150 kJ/kg
η_c	0.86		

Table (3.1) Assumed parameters' values used in the parametric study

3.3 Gas Turbine Cycle Performance

The gas turbine cycle performance is determined by thermal efficiency and the specific work output. The efficiency and the specific work output are functions of many parameters as shown in Eqn. 3.15 and Eqn. 3.16. Hence a solution of Eqn. 3.38 to Eqn. 3.50 can be found for each set of values of T_{o3} and r.

$$\eta_{gt} = f(\theta, r, C_p, \eta_c, \eta_{cc}, \eta_t, \eta_{mec})$$

$$w_{gt} = f(\theta, r, C_p, \eta_c, \eta_{cc}, \eta_t, \eta_{mec})$$

3.4 Combined Gas Turbine/Steam Turbine Cycle Performance

The thermal efficiency and the specific work output can be used also to describe the combined gas turbine/steam turbine cycle performance. The efficiency and the specific work output are functions of many parameters as described by Eqn. 3.68 and Eqn. 3.69 where for each set of values of the parameters in Eqn. 3.68 or Eqn. 3.69 there is one solution for the combined efficiency and one for the specific work output.

$$\eta_{CPP} = f(\eta_{gt}, \eta_{st}) = f(\theta, r, C_p, \eta_c, \eta_{cc}, \eta_{t(gt)}, \eta_{mec}, P_{con}, T_{2st}, P_B, \eta_{t(st)}, \eta_p, \eta_{HRSG})$$

$$w_{CPP} = f(w_{gt}, w_{st}) = f(\theta, r, C_p, \eta_c, \eta_{cc}, \eta_{t(gt)}, \eta_{mec}, P_{con}, T_{2st}, P_B, \eta_{t(st)}, \eta_p, \eta_{HRSG})$$

There are many gas turbine/steam turbine cycle configurations, therefore studying the effect of each parameter on each configuration performance will be very difficult and tedious to achieve. In the present investigation only the following configurations were considered:

i. Simple gas turbine cycle combined with simple steam turbine cycle.
ii. Simple gas turbine cycle combined with dual pressure steam turbine cycle.
iii. Reheat gas turbine cycle combined with simple steam turbine cycle.

iv. Reheat gas turbine cycle combined with dual pressure steam turbine cycle.
v. Gas turbine pre-cooling cycle combined with simple steam turbine cycle.
vi. Gas turbine pre-cooling cycle combined with dual pressure steam turbine cycle.

Simultaneous variations of the main parameters in both cycles would show the effect of theses parameters on the combined cycle (CPP) performance. Calculations were made by varying some parameters and holding others constant. The assumed parameters for the calculations are shown in Table 3.1.

A computer program was written in Visual Basic language to solve Eqn. 3.38 to Eqn. 3.67 incorporating **AIRPROP**, **FARATIO** and **GASPROP** subroutines. The flowchart of the computer program is shown in Fig. 3.17(a) to Fig. 3.17(c). Figure 3.17(a) shows the solution of the gas turbine cycle and Fig. 3.17(b) shows the solution of the steam turbine cycle while Fig. 3.17(c) shows the solution of the combined gas steam cycle. The results of the analysis are presented in chapter 6 that deals with results and discussion.

UNIVERSITY OF HERTFORDSHIRE LRC

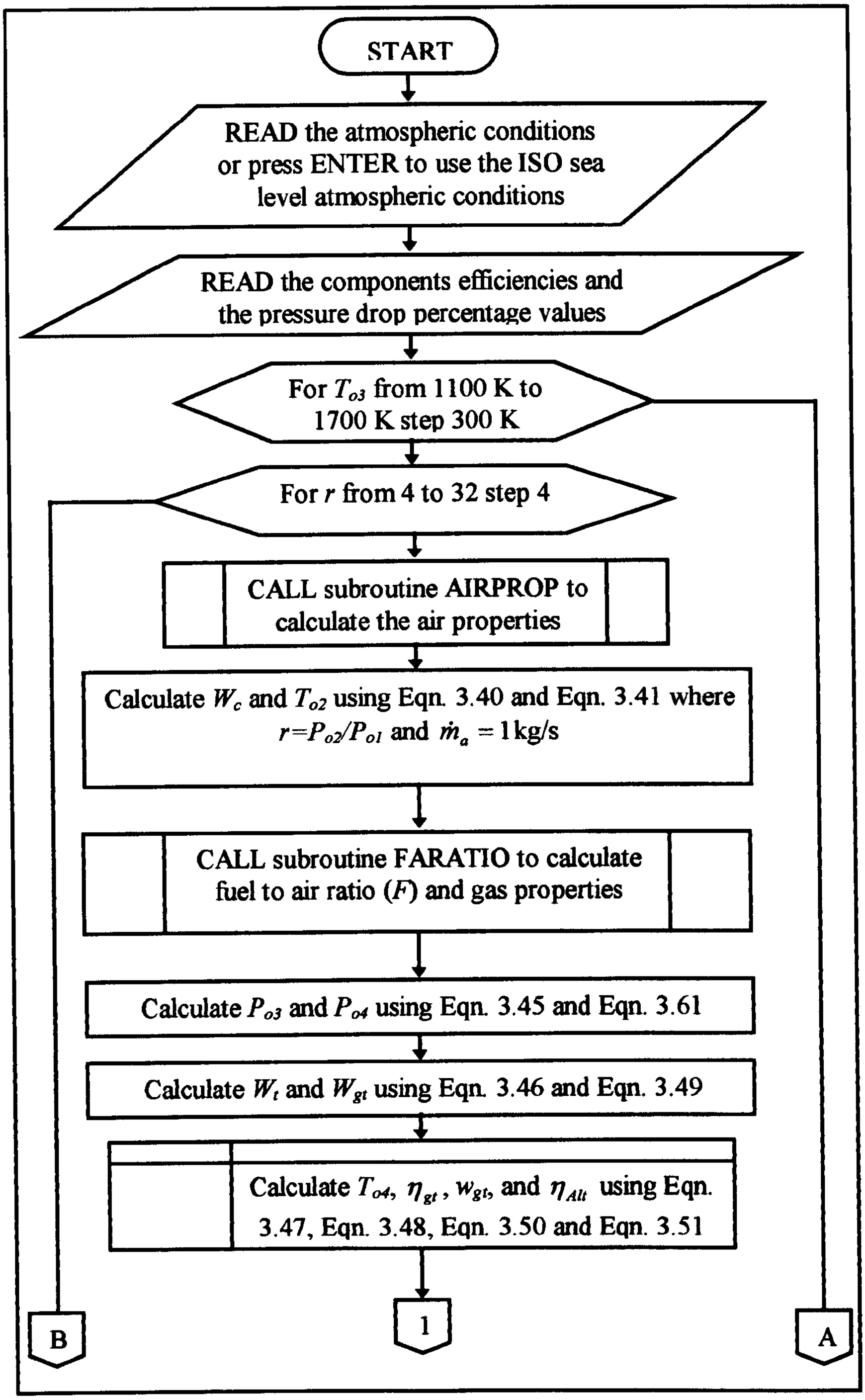

Fig. 3.17(a) Flowchart of gas turbine cycle calculations

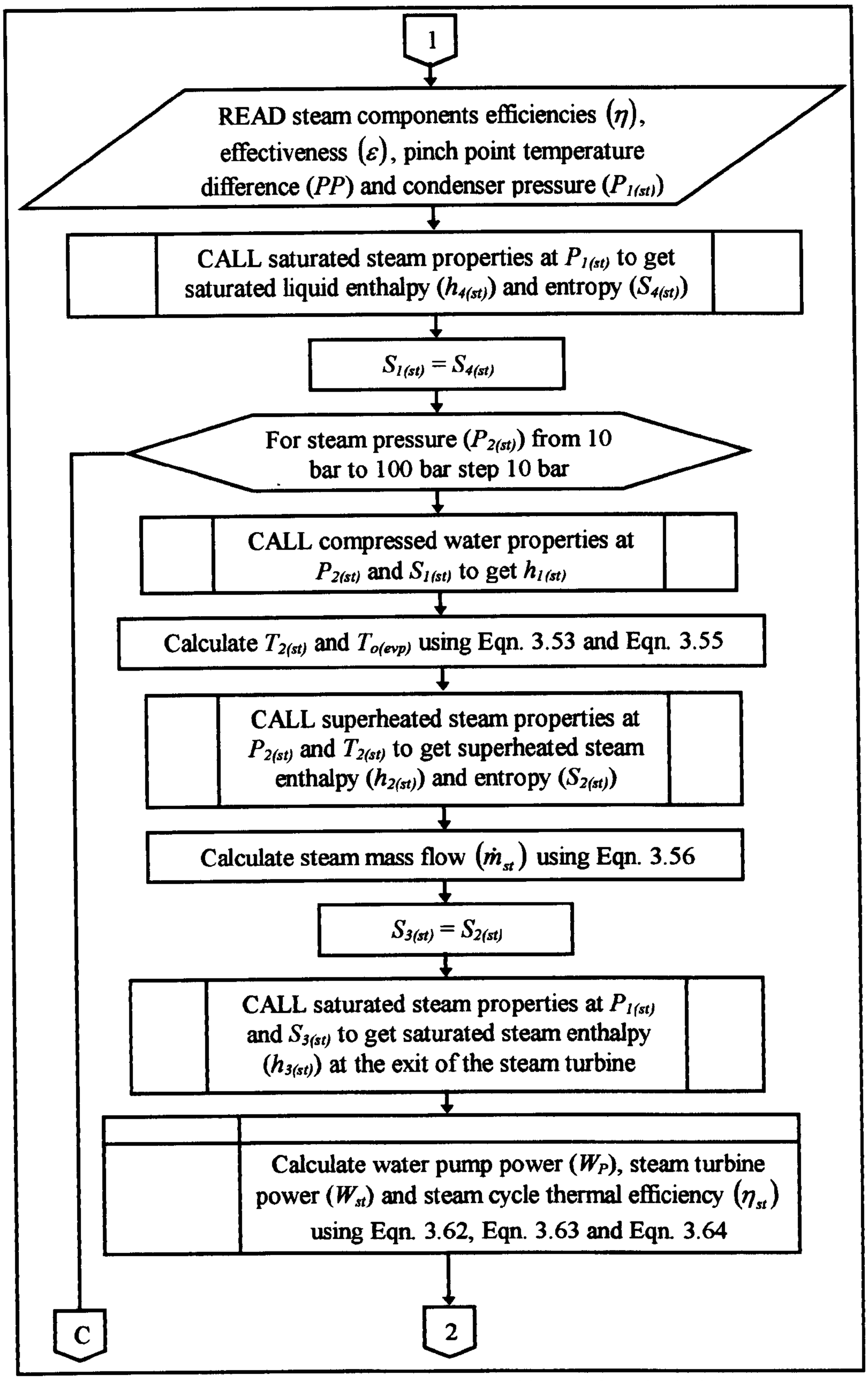

Fig. 3.17(b) Flowchart of steam turbine cycle calculations

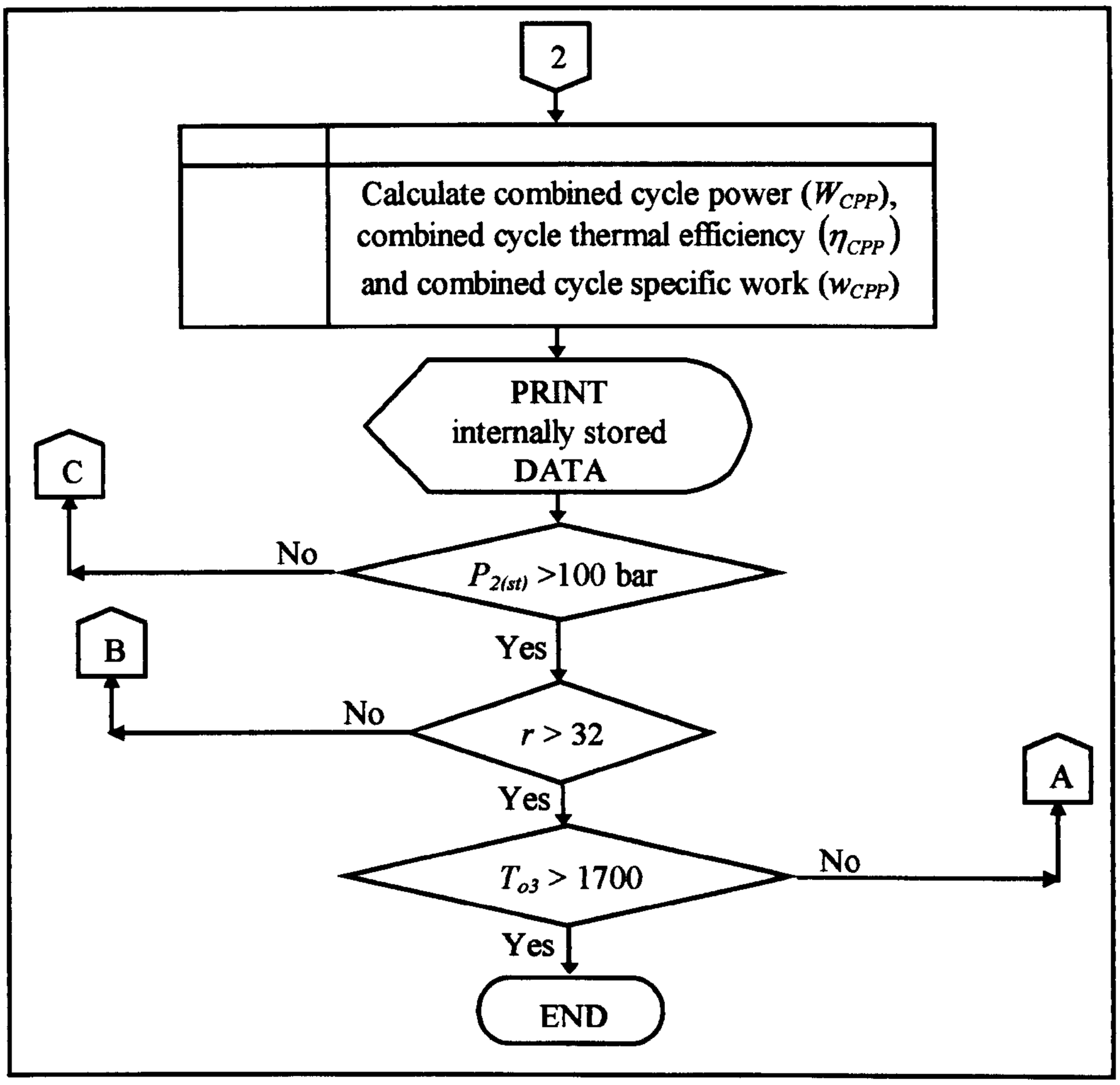

Fig. 3.17(c) Flowchart of combined cycle calculations

CHAPTER 4

MODELLING AND SIMULATION

4.1 Introduction

The gas turbine engine is a complex assembly of a variety of components that are designed on the basis of aero-thermodynamic laws. The design and operation theories of these individual components are complicated. The complexity of aero-thermodynamic analysis makes it impossible to mathematically solve the optimisation equations involved in various gas turbine cycles.

When gas turbine engines were designed during the last century, the need to evaluate the engines performance at both design point and off design conditions became apparent. Manufacturers and designers of gas turbine engines became aware that some tools were needed to predict the performance of gas turbine engines especially at off design conditions where its performance was significantly affected by the load and the operating conditions. Also it was expected that these tools would help in predicting the performance of individual components such as compressors, turbines, combustion chambers, etc.

At the early stage of developments, experimental tests of prototypes of either the whole engine or its main components were the only method available to determine the performance of either the engine or of the components. However, this procedure was not only costly, but also time consuming. Therefore, mathematical modelling using computational techniques were considered to be the most economical solution.

The first part of this chapter presents a discussion about the gas turbine modelling approach; the second part includes the gas turbine component matching while the last part includes the gas turbine computer simulation program and its philosophy.

4.2 Modelling of Gas Turbine Components

The aero derivative and industrial gas turbine engines are used for a variety of applications such as electrical power generation, driving pumps and compressors on gas and liquid fuels, etc. The engine configuration may vary to suit the application. The common configurations are: a single, twin or triple spool construction or a

single stage or multi stage construction. In this study only the gas turbines used for electrical power generation are considered.

A gas turbine engine essentially consists of the following component parts:

i. Intake
ii. Compressor(s)
iii. Combustion Chamber(s)
iv. Turbine(s)
v. Engine auxiliaries such as fuel pump, lubrication pump, electrical power supply, starting gear and control system.

A block diagram of the gas turbine engine showing theses components is given in Fig. 4.1.

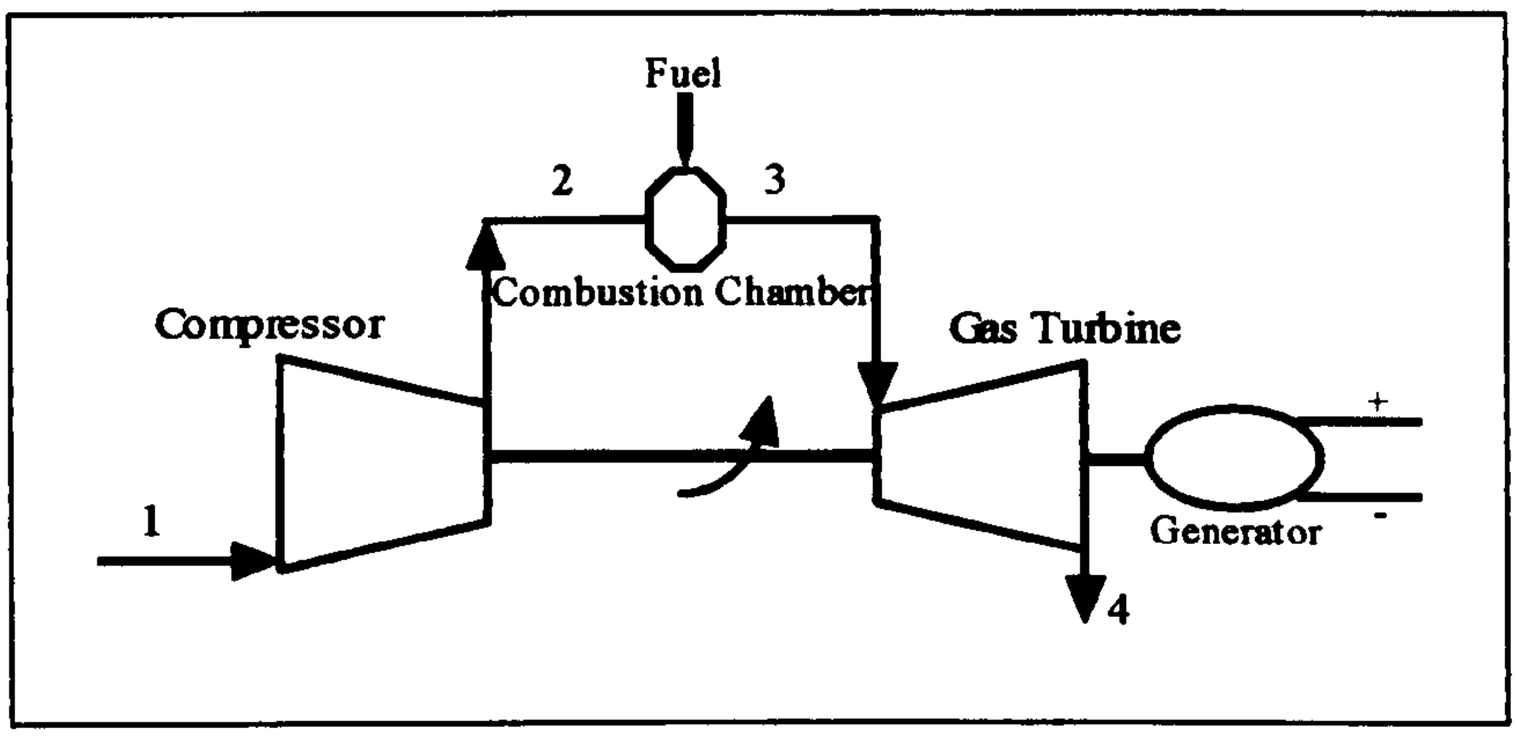

Fig. 4.1 block diagram of the simple gas turbine engine

The main components that determine the overall performance of the complete engine are i, ii, iii and iv. The mathematical model for each component was created using physical laws or input data when available.

There is an air intake prior to the compressor but it can be realistically considered that there is small change to the air conditions (pressure drop) through the air intake in case of gas turbine units used for electricity generation.

4.2.1 Compressor Modelling and Analysis

The performance of a compressor is fully described by a number of either dimensionless or normalized parameters. The dimensionless parameters would be the same for every system of units, e.g. SI system, FPS system or CGS system, but normalisation may be different depending on national practices. The dimensionless parameters and normalised parameters are shown in Table 4.1.

Parameters	Meaning
$\left(\frac{\dot{m}_a\sqrt{C_{Pa}T_{o1}}}{d_2^2P_{o1}}\right),\left(\frac{\dot{m}_a\sqrt{\theta}}{\delta}\right)$	Compressor dimensionless and normalised mass flow parameters
$\left(\frac{d_2N}{\sqrt{C_{Pa}T_{o1}}}\right),\left(\frac{N}{\sqrt{\theta}}\right)$	Compressor dimensionless and normalised speed parameters
$\left(\frac{\tau_c}{d_2^3P_{o1}}\right),\left(\frac{\tau_c}{\delta}\right)$	Compressor dimensionless and normalised torque parameters
$\left(\frac{P_{o2}}{P_{o1}}\right)$	Compressor dimensionless pressure ratio parameter
$\left(\frac{\left(\frac{P_{o2}}{P_{o1}}\right)^{\gamma_a-1/\gamma_a}-1}{\frac{T_{o2}}{T_{o1}}-1}\right)$	Isentropic compressor efficiency
$\left(\theta=\frac{T_{o1}}{T_{o\_ref}}\right)$	Normalised temperature parameter
$\left(\delta=\frac{P_{o1}}{P_{o\_ref}}\right)$	Normalised pressure parameter

Table 4.1 Dimensionless and Normalised Compressor Parameters

Compressor performance, sometimes called compressor map, is usually represented by overall performance characteristics. These maps are in general, obtained experimentally but sometimes they can be predicted with reasonable accuracy using

geometric properties of the components, i.e. intake, impeller, diffuser and the casing[2,40,41].

Figure 4.2(a) is the compressor pressure ratio vs. mass flow parameter and Fig. 4.2(b) is the compressor efficiency vs. mass flow parameter. Theses figures can be cross-plotted to obtain a general compressor performance map shown in Fig. 4.3.

Mathematically the compressor performance is described using the dimensionless or the normalised parameters as given below:

$$\frac{\tau_c}{d_2^3 P_{o1}} = \frac{1}{2\pi}\frac{1}{\eta_c}\left(\frac{d_2 N}{\sqrt{C_{Pa}T_{o1}}}\right)^{-1}\frac{\dot{m}_a\sqrt{C_{Pa}T_{o1}}}{d_2^2 P_{o1}}\left[\left(\frac{P_{o2}}{P_{o1}}\right)^{\gamma_a-1/\gamma_a}-1\right] \tag{4.1}$$

$$\frac{\tau_c}{\delta} = f\left(\eta_c, \frac{N}{\sqrt{\theta}}, \frac{\dot{m}_a\sqrt{\theta}}{\delta}, \frac{P_{o2}}{P_{o1}}\right) \tag{4.2}$$

Equation 4.1 is in complete dimensionless form and Eqn. 4.2 is the normalised general form.

The compression power W_c is given by

$$W_c = d_2^2 P_{o1}\sqrt{C_{Pa}T_{o1}}\,\frac{\dot{m}_a\sqrt{C_{Pa}T_{o1}}}{d_2^2 P_{o1}}\,\frac{1}{\eta_c}\left[\left(\frac{P_{o2}}{P_{o1}}\right)^{\gamma_a-1/\gamma_a}-1\right] \tag{4.3}$$

Using the compressor characteristics, if any two dimensionless parameters are known then the rest of the parameters can be determined easily.

The final stagnation temperature in the compression process T_{o2} can be calculated from the following equation:

$$T_{o2} = T_{o1} + \frac{T_{o1}}{\eta_c}\left[\left(\frac{P_{o2}}{P_{o1}}\right)^{\gamma_a - 1/\gamma_a} - 1\right] \tag{4.4}$$

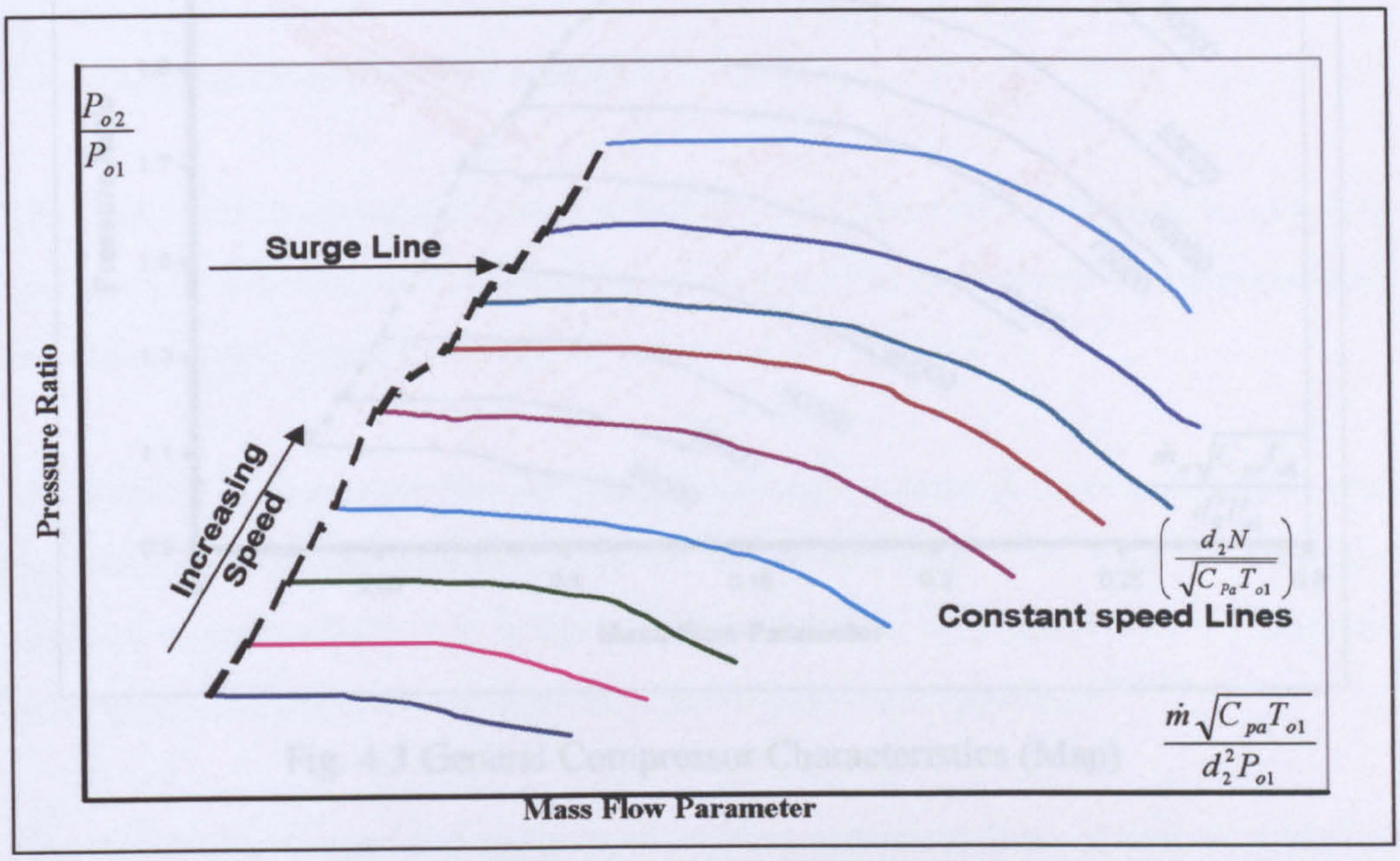

Fig. 4.2(a) Typical Compressor Pressure ratio vs. Mass Flow Parameter

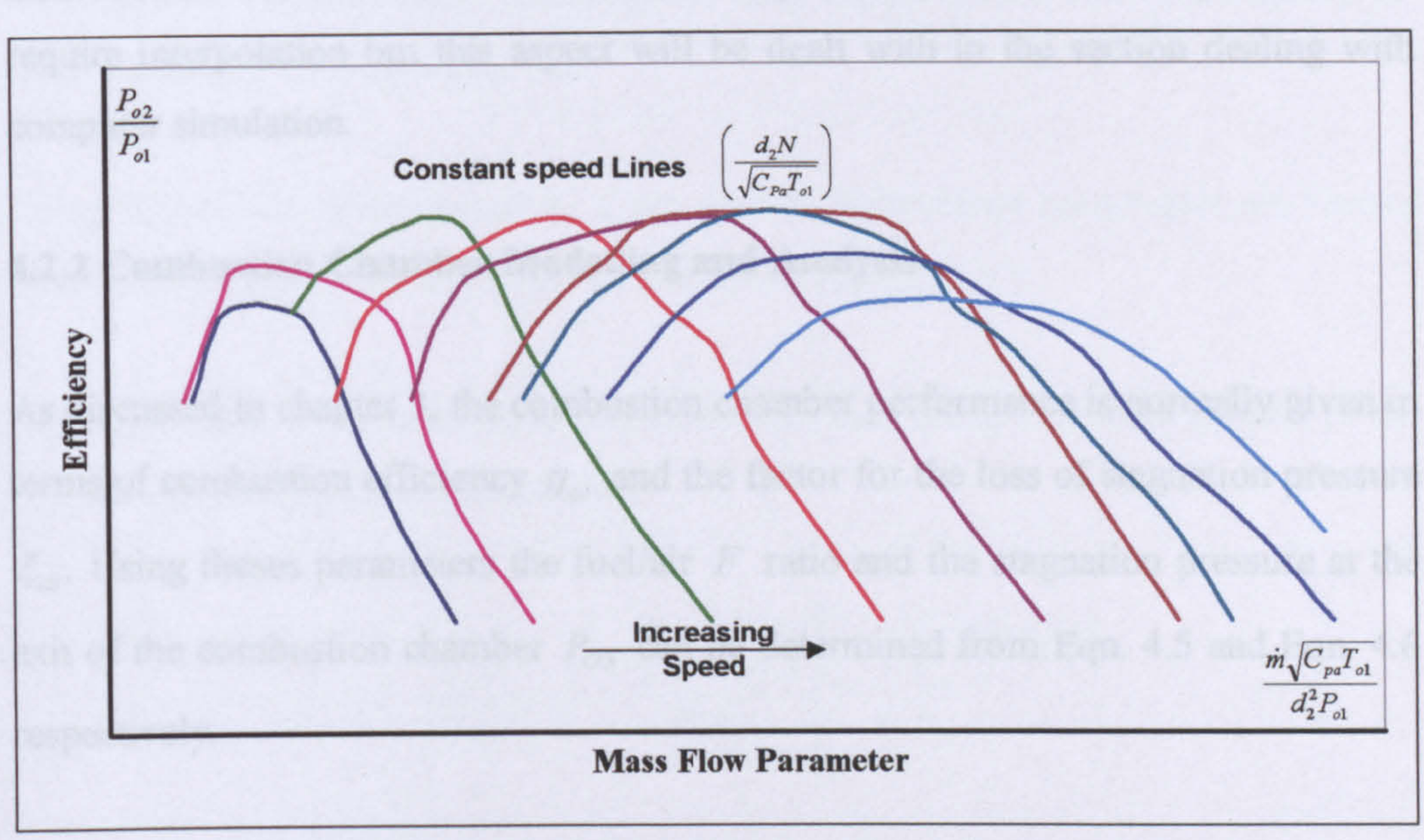

Fig. 4.2(b) Typical Compressor Efficiency vs. Pressure ratio

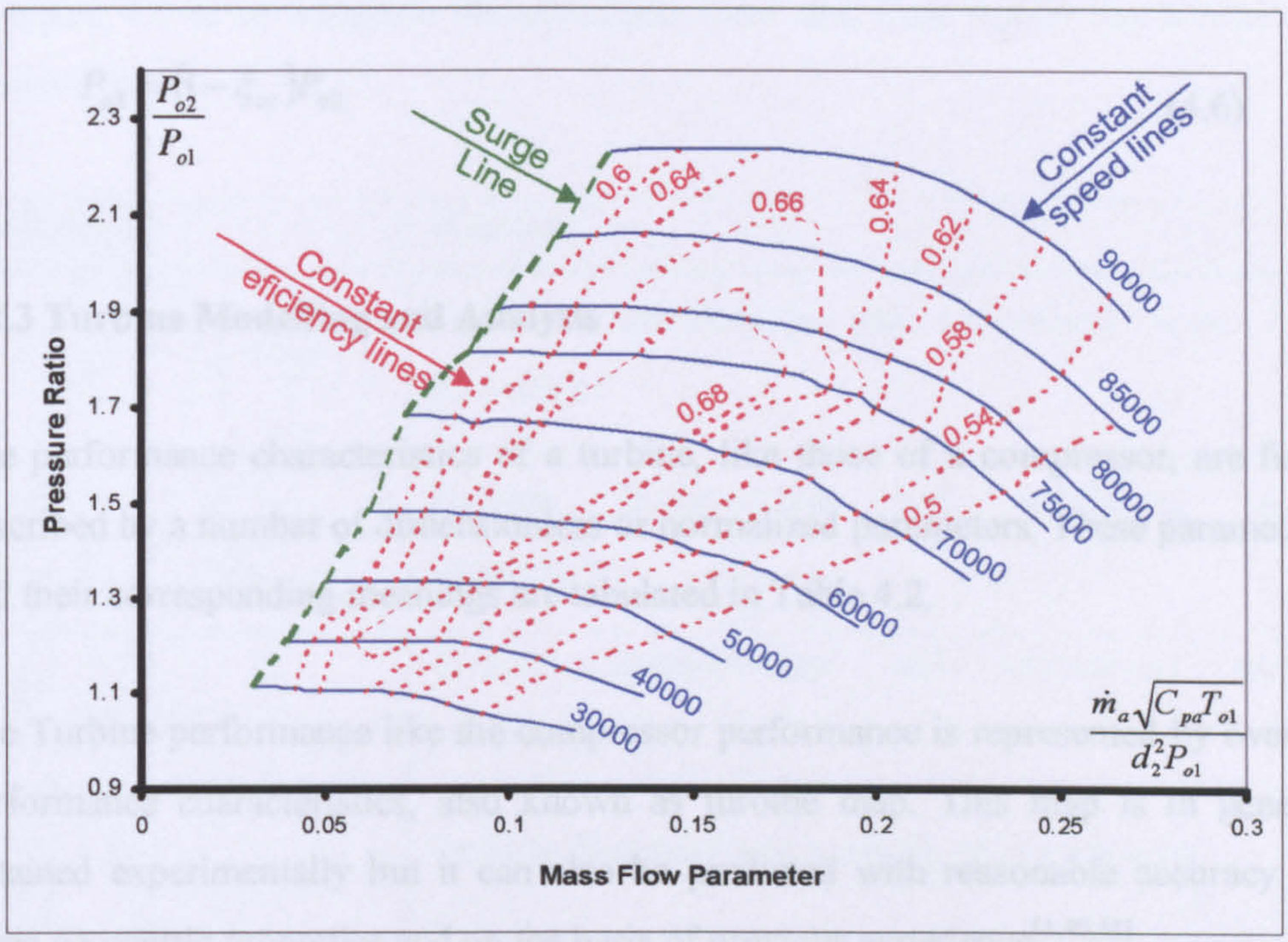

Fig. 4.3 General Compressor Characteristics (Map)

In order to solve Eqn. 4.1 to Eqn. 4.4 for any point in the compressor map, the input data needed can be obtained from the compressor performance map. This may require interpolation but this aspect will be dealt with in the section dealing with computer simulation.

4.2.2 Combustion Chamber Modelling and Analysis

As discussed in chapter 3, the combustion chamber performance is normally given in terms of combustion efficiency η_{cc} and the factor for the loss of stagnation pressure ξ_{cc}. Using theses parameters the fuel/air F ratio and the stagnation pressure at the exit of the combustion chamber P_{O3} can be determined from Eqn. 4.5 and Eqn. 4.6 respectively.

$$F = \frac{1}{\frac{\eta_{cc}(LCV)}{C_{Pg}(T_{o3} - T_{o2})} - 1} \tag{4.5}$$

$$P_{o3} = (1 - \xi_{cc}) P_{o2} \tag{4.6}$$

4.2.3 Turbine Modelling and Analysis

The performance characteristics of a turbine, like those of a compressor, are fully described by a number of dimensionless or normalized parameters. These parameters and their corresponding meanings are tabulated in Table 4.2.

The Turbine performance like the compressor performance is represented by overall performance characteristics, also known as turbine map. This map is in general obtained experimentally but it can also be predicted with reasonable accuracy by using geometric properties and on the basis of previous experience[1,40,41].

Figure 4.4 shows typical turbine performance characteristics: 4.4(a) is a plot of turbine pressure ratio vs. mass flow parameter and 4.4(b) gives a plot of turbine efficiency vs. pressure ratio. The complete map can be drawn from these figures by cross plotting as shown in Fig. 4.5.

Using the turbine characteristics, if any two dimensionless parameters are known then the rest of the parameters can be determined easily.

Mathematically the turbine performance is described using the dimensionless or the normalised parameters as given below:

$$\frac{\tau_t}{d_2^3 P_{o3}} = \frac{1}{2\pi} \eta_t \left(\frac{d_2 N}{\sqrt{C_{Pg} T_{o3}}} \right)^{-1} \frac{\dot{m}_g \sqrt{C_{Pg} T_{o3}}}{d_2^2 P_{o3}} \left[1 - \left(\frac{P_{o4}}{P_{o3}} \right)^{\gamma_g - 1 / \gamma_g} \right] \tag{4.7}$$

$$\frac{\tau_t}{\delta} = f\left(\eta_t, \frac{N}{\sqrt{\theta}}, \frac{\dot{m}_g \sqrt{\theta}}{\delta}, \frac{P_{o3}}{P_{o4}} \right) \tag{4.8}$$

Equation 4.7 is in complete dimensionless form and Eqn. 4.8 is the normalised general form.

Parameters	Meaning
$\left(\frac{\dot{m}_g\sqrt{C_{Pg}T_{o3}}}{d_2^2P_{o3}}\right),\left(\frac{\dot{m}_g\sqrt{\theta}}{\delta}\right)$	Turbine dimensionless and normalised mass flow parameters
$\left(\frac{d_2N}{\sqrt{C_{Pg}T_{o3}}}\right),\left(\frac{N}{\sqrt{\theta}}\right)$	Turbine dimensionless and normalised speed parameters
$\left(\frac{\tau_t}{d_2^3P_{o3}}\right),\left(\frac{\tau_t}{\delta}\right)$	Turbine dimensionless and normalised torque parameters
$\left(\frac{P_{o3}}{P_{o4}}\right)$	Turbine dimensionless pressure ratio parameter
$\left(\frac{\left(\frac{P_{o3}}{P_{o4}}\right)^{\gamma_g-1/\gamma_g}-1}{\frac{T_{o3}}{T_{o4}}-1}\right)$	Isentropic turbine efficiency
$\left(\theta=\frac{T_{o3}}{T_{o\_ref}}\right)$	Normalised temperature parameter
$\left(\delta=\frac{P_{o3}}{P_{o\_ref}}\right)$	Normalised pressure parameter

Table 4.2 Dimensionless and Normalised Turbine Parameters

The expansion power W_t and the final stagnation temperature T_{o4} in the expansion process are calculated using Eqn. 4.9 and Eqn. 4.10 respectively.

$$W_t = d_2^2P_{o3}\sqrt{C_{Pg}T_{o3}}\frac{\dot{m}_g\sqrt{C_{Pg}T_{o3}}}{d_2^2P_{o3}}\eta_t\left[1-\left(\frac{P_{o4}}{P_{o3}}\right)^{\gamma_g-1/\gamma_g}\right] \qquad (4.9)$$

$$T_{o4} = T_{o3} - T_{o3}\eta_t\left[1-\left(\frac{P_{o4}}{P_{o3}}\right)^{\gamma_g - 1/\gamma_g}\right] \tag{4.10}$$

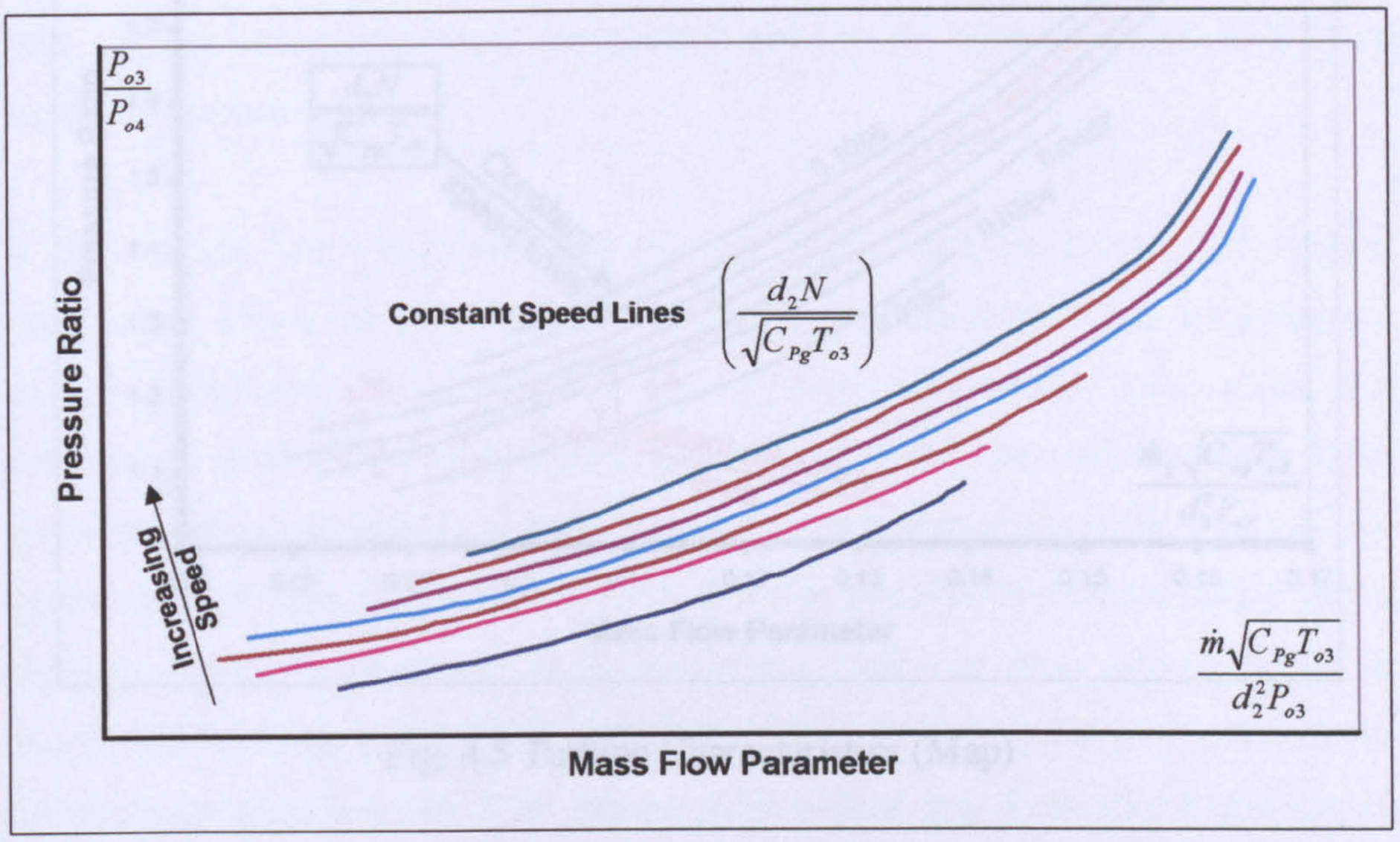

Fig. 4.4(a) Typical Turbine Pressure ratio vs. Mass Flow Parameter

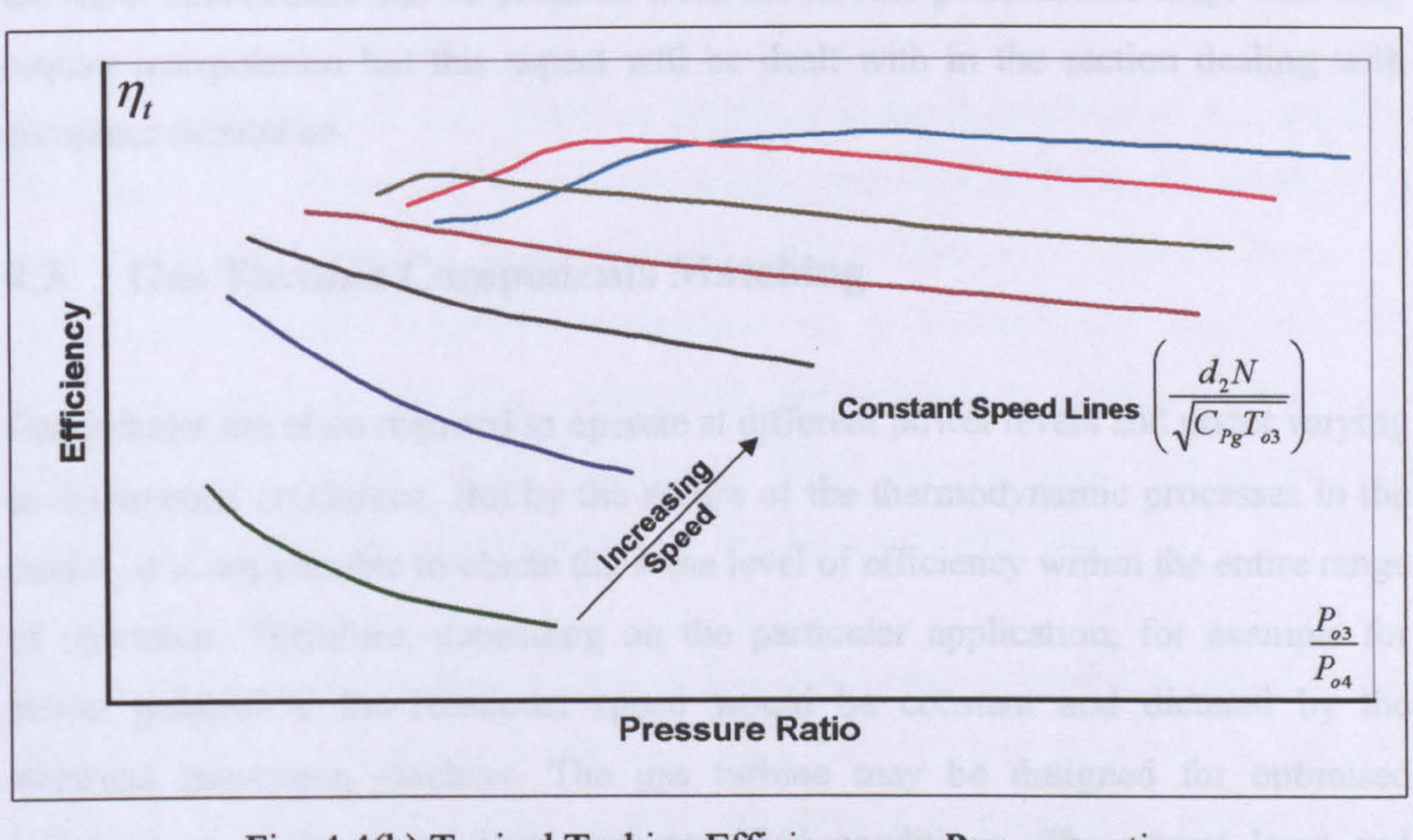

Fig. 4.4(b) Typical Turbine Efficiency vs. Pressure ratio

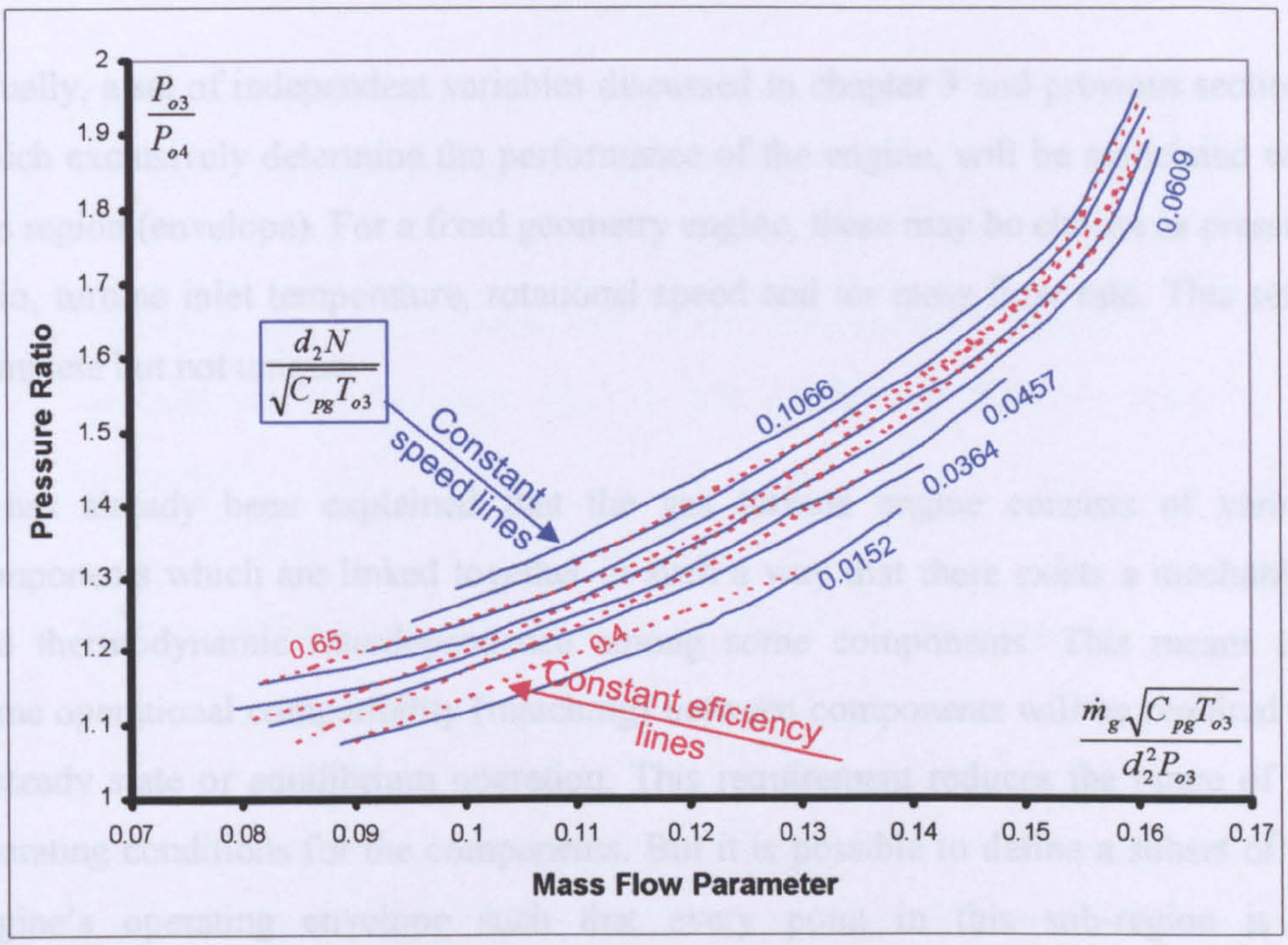

Fig. 4.5 Turbine Characteristics (Map)

In order to solve Eqn. 4.7 to Eqn. 4.10 for any point on the turbine characteristics, the input data needed can be obtained from the turbine performance map. This may require interpolation but this aspect will be dealt with in the section dealing with computer simulation.

4.3 Gas Turbine Components Matching

Gas turbines are often required to operate at different power levels and under varying environmental conditions. But by the nature of the thermodynamic processes in the engine, it is not possible to obtain the same level of efficiency within the entire range of operation. Therefore, depending on the particular application, for example for power generation, the rotational speed would be constant and dictated by the electrical generating machine. The gas turbine may be designed for optimised operation at given power level and specified conditions. The power level and expected thermal efficiency are chosen to correspond to those conditions under which the engine operates for most of its life. The values of the characteristic parameters at that point are termed as the design point.

Usually, a set of independent variables discussed in chapter 3 and previous sections, which exclusively determine the performance of the engine, will be associated with this region (envelope). For a fixed geometry engine, these may be chosen as pressure ratio, turbine inlet temperature, rotational speed and air mass flow rate. This set is complete but not unique.

It has already been explained that the gas turbine engine consists of various components which are linked together in such a way that there exists a mechanical and thermodynamic interdependence among some components. This means that some operational compatibility (matching) between components will be required for a steady state or equilibrium operation. This requirement reduces the range of the operating conditions for the components. But it is possible to define a subset of the engine's operating envelope such that every point in this sub-region is an equilibrium working point. These working points can be mapped on the respective components characteristics. The design point values are elements of this region which yield the best thermal efficiency. Any point in the region other than the design point represents an off-design condition.

The off-design problem may therefore be stated as the determination of a point in this region that corresponds to some specified conditions at which the equilibrium criteria would be satisfied but at reduced value of thermal efficiency. Since the operating points of the individual components can be determined by using the given values of some characteristic parameters, the off-design problem reduces to computing the values of these parameters which would satisfy the equilibrium criteria. This procedure is demonstrated in the analysis given below.

Considering a simple gas turbine consisting of three main components as an example used for electrical power generation application schematically shown in Fig. 4.1, and assuming that the performance of each component is completely known by its characteristics map shown in Fig. 4.3 and Fig. 4.5. In this gas turbine engine, the components matching should meet the following conditions:

i. The compressor speed is always the same as the turbine speed.

$$N_c = N_t$$

ii. The gas mass flow through turbine is the sum of the air mass flow through compressor and the fuel mass flow.

$$\dot{m}_g = \dot{m}_a + \dot{m}_f$$

iii. Assuming that the pressure loss in the combustion chamber is a constant small percentage (ξ_{cc}) of the combustion chamber inlet pressure.

$$P_{o3} = (1 - \xi_{cc}) P_{o2}$$

iv. Inlet and exhaust pressure losses are too small and can be ignored.

$$P_{o4} = P_{o1}$$

The second condition is subject to modification in that it is common practice to bleed air from the compressor at various stations to provide cooling air for bearings and turbine blade cooling. Quiet often it is sufficiently accurate to assume that the bleed air equals the fuel flow and therefore the mass flow is the same throughout the compressor and the turbine.

The steady state or equilibrium operation of this gas turbine engine can be achieved by the matching of its compressor and turbine. Matching the compressor and the turbine can be done by superimposing the turbine performance map on the compressor map while meeting the components matching conditions. This matching procedure is schematically shown in Fig. 4.6.

Superimposing the turbine map on the compressor map can not be totally accepted until both maps axes (the abscissa and the ordinate) are identical. The main difficulty here is that of temperatures: T_{o1} for the compressor and T_{o3} for the turbine. The procedure to overcome this problem was developed as part of investigation and it is described hereafter.

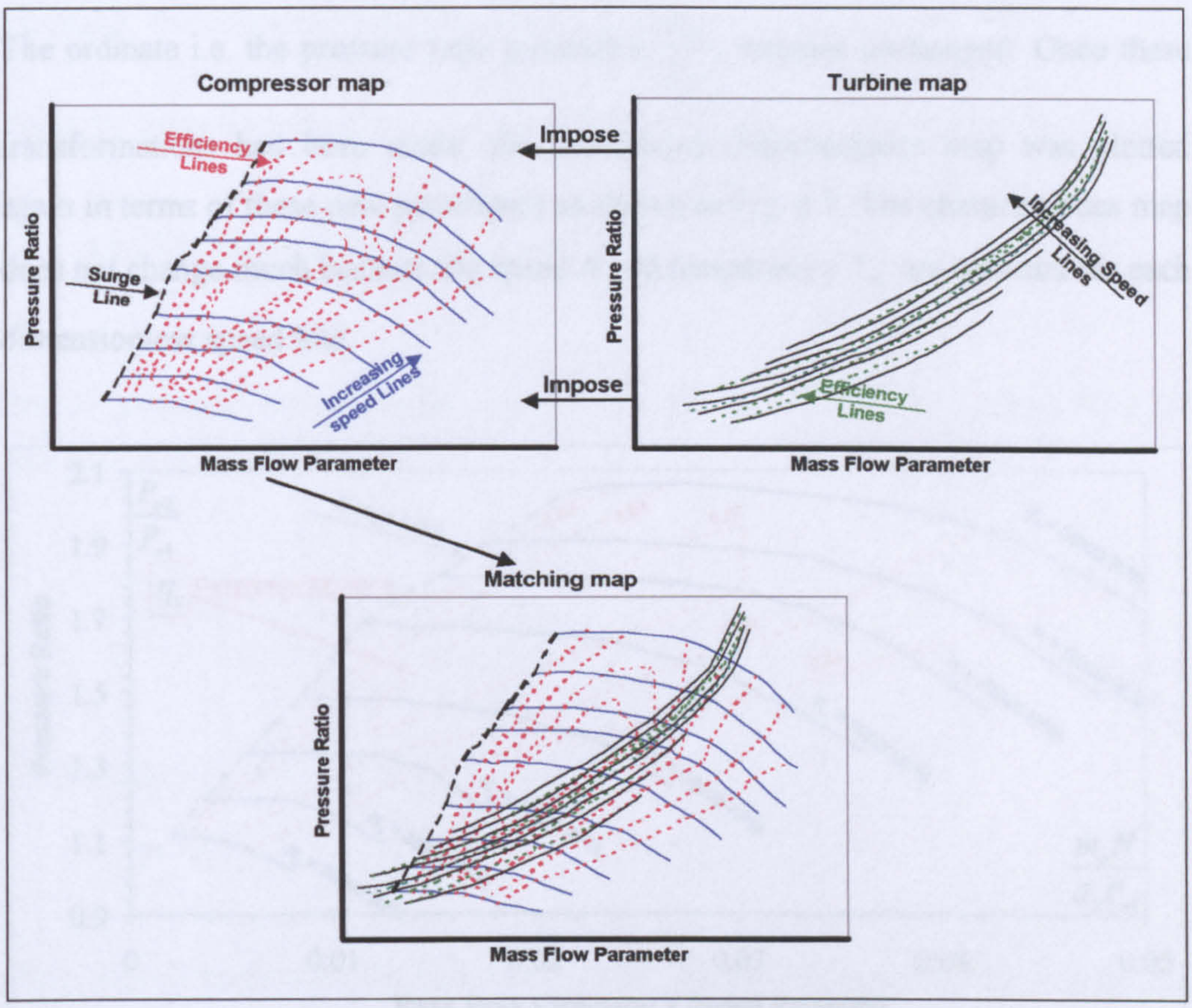

Fig. 4.5 Compressor turbine matching procedure

THE COMPRESSOR

The abscissa of the compressor characteristics i.e. the mass flow parameter $\frac{\dot{m}_a\sqrt{C_{pa}T_{o1}}}{d_2^2P_{o1}}$, matching was obtained by multiplying this parameter with the dimensionless speed parameter $\frac{d_2N}{\sqrt{C_{pa}T_{o1}}}$ as follows:

$$\left[\frac{\dot{m}_a\sqrt{C_{pa}T_{o1}}}{d_2^2P_{o1}}\right]\times\left[\frac{d_2N}{\sqrt{C_{pa}T_{o1}}}\right]=\left[\frac{\dot{m}_aN}{d_2P_{o1}}\right]$$

The output term $\frac{\dot{m}_aN}{d_2P_{o1}}$ is referred to as the mass flow matching parameter.

The ordinate i.e. the pressure ratio parameter $\frac{P_{o2}}{P_{o1}}$, remains unchanged. Once these transformations had been made, the compressor characteristics map was plotted again in terms of these new parameters as shown in Fig. 4.7. The characteristics map does not change much because the speed N and temperature T_{o1} are constant for each dimensionless speed line.

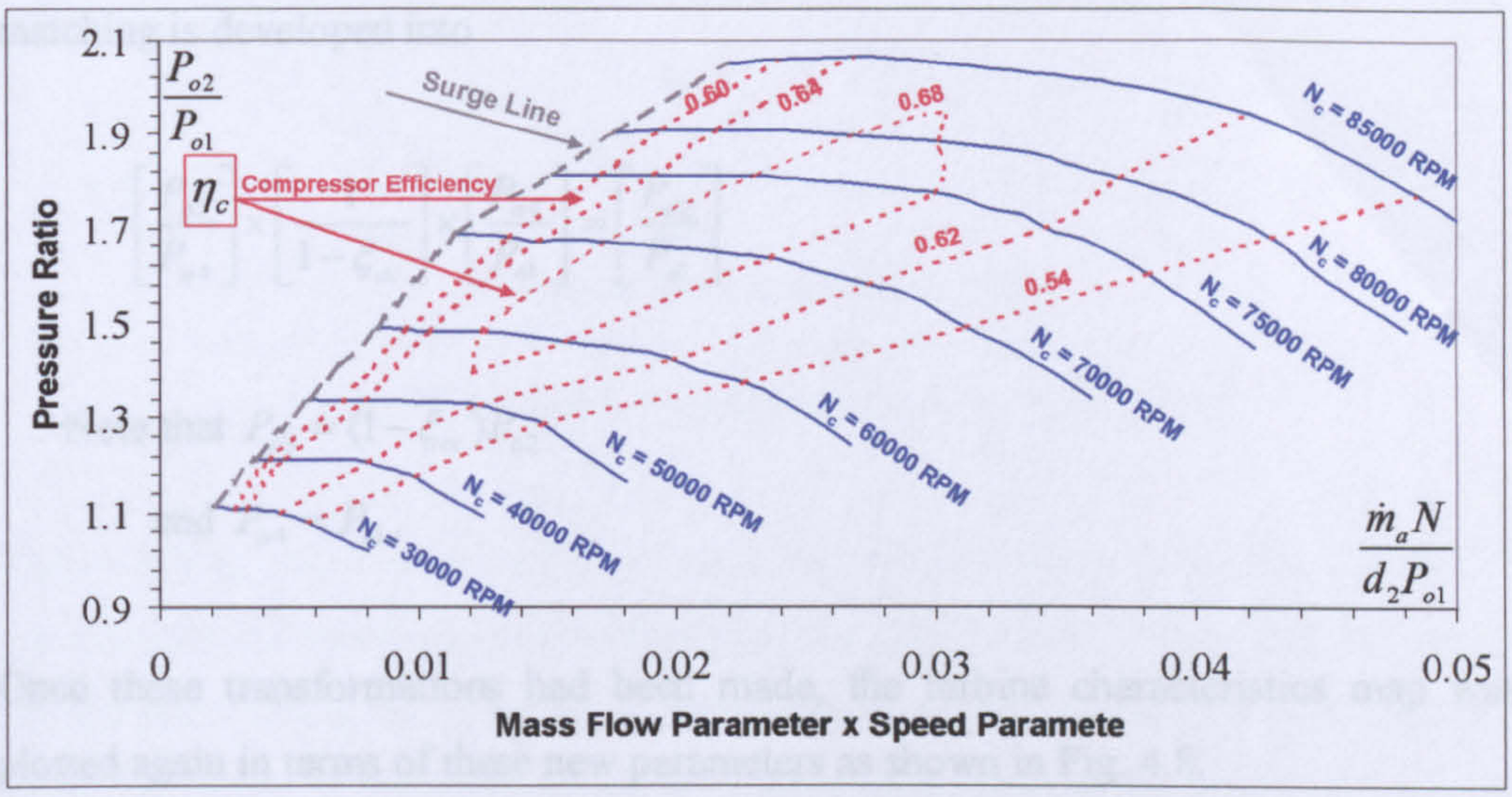

Fig. 4.7 Compressor map after transformation

THE TURBINE

The abscissa of the turbine characteristics i.e. the mass flow parameter $\frac{\dot{m}_g \sqrt{C_{pg} T_{o3}}}{d_2^2 P_{o3}}$, matching was obtained by multiplying this parameter with the dimensionless speed parameter and the pressure ratio as follows:

$$\left[\frac{\dot{m}_g \sqrt{C_{pg} T_{o3}}}{d_2^2 P_{o3}}\right] \times \left[\frac{d_2 N}{\sqrt{C_{pg} T_{o3}}}\right] \times \left[\frac{P_{o3}}{P_{o4}}\right] = \left[\frac{\dot{m}_g N}{d_2 P_{o4}}\right]$$

To satisfy the compressor-turbine matching conditions, i.e. $\dot{m}_g = \dot{m}_a$ and $P_{o4} = P_{o1}$.

Then the mass flow matching parameter of the turbine $\frac{\dot{m}_g N}{d_2 P_{o4}}$ is equal to the mass flow matching parameter of the compressor $\frac{\dot{m}_a N}{d_2 P_{o1}}$.

For the pressure ratio parameter, the ordinate axis of the turbine characteristics for matching is developed into

$$\left[\frac{P_{o3}}{P_{o4}}\right] \times \left[\frac{1}{1-\xi_{cc}}\right] \times \left[\frac{P_{o4}}{P_{o1}}\right] = \left[\frac{P_{o2}}{P_{o1}}\right]$$

Note that $P_{o3} = (1-\xi_{cc}) P_{o2}$

and $P_{o4} = P_{o1}$.

Once these transformations had been made, the turbine characteristics map was plotted again in terms of these new parameters as shown in Fig. 4.8.

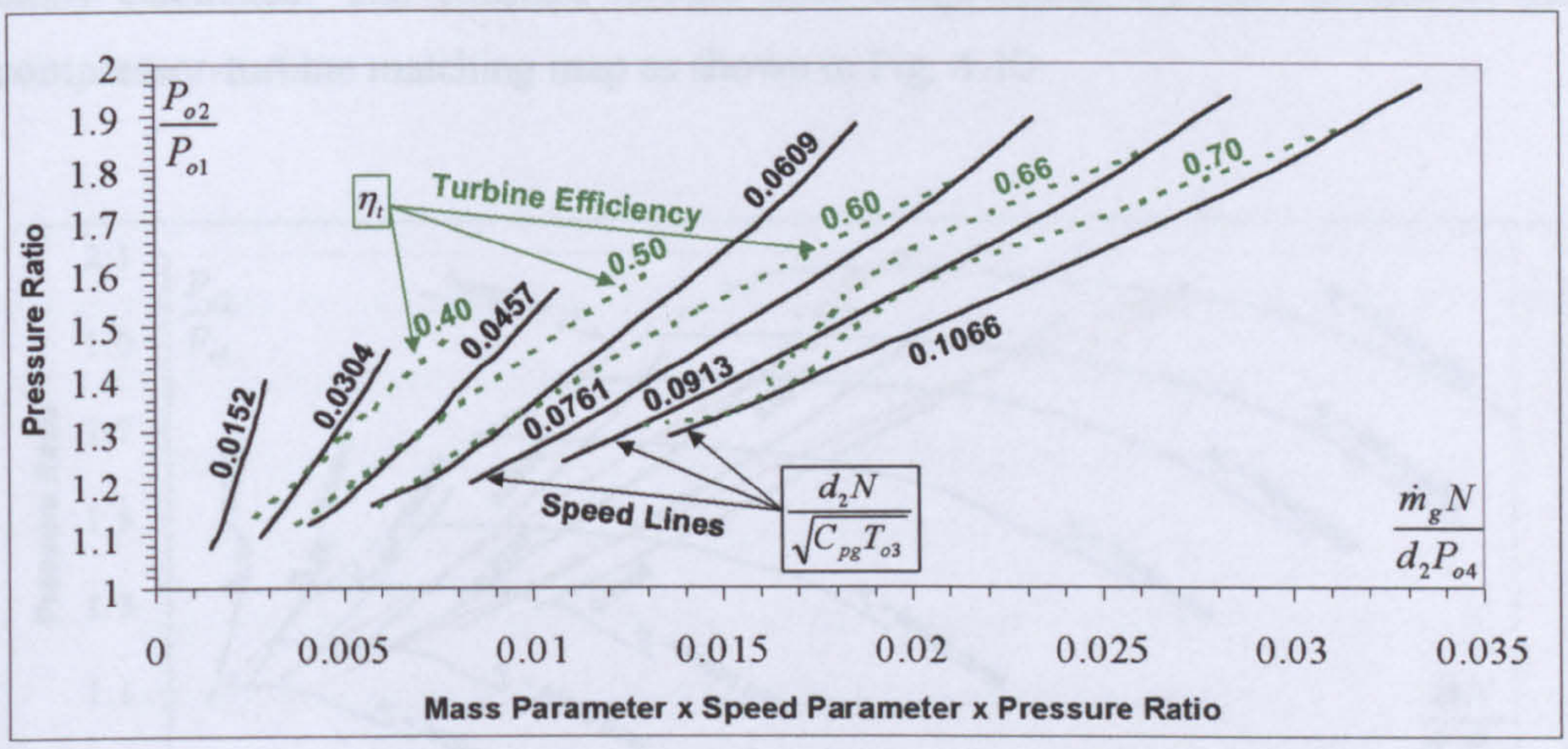

Fig. 4.8 Turbine map after transformation

It can be seen from the graphical plot of compressor and turbine performance maps that the abscissa and the ordinate of these maps are identical. Therefore, it is clear

that the turbine map could be superimposed on the compressor map to produce a complete compressor-turbine matching map as shown in Fig. 4.9.

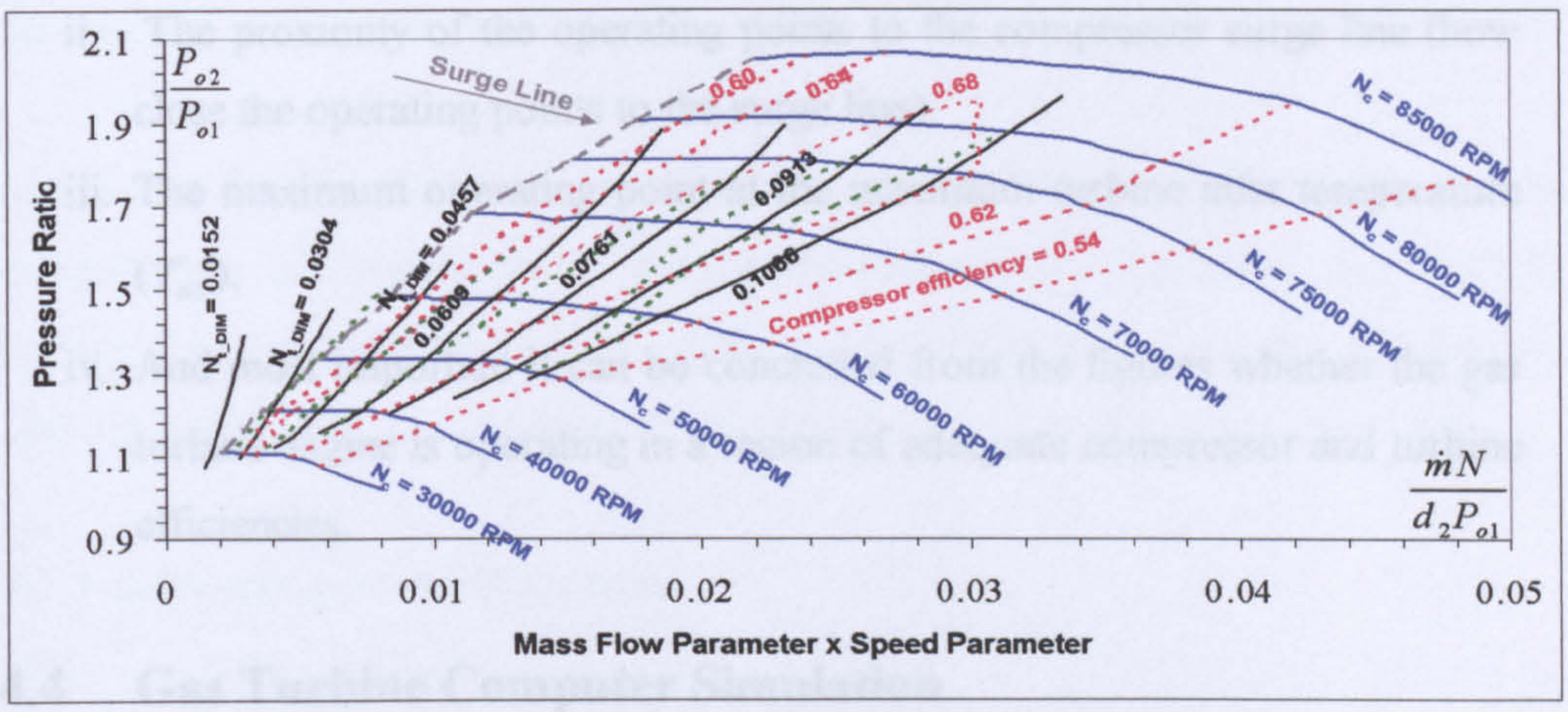

Fig. 4.9 Complete compressor-turbine matching map

The matching map shown in Fig. 4.9 is a very useful tool in predicting the overall performance of matched components, i.e. the gas turbine design and off-design performance. Using the compressor-turbine dimensionless speed intersection points, where the speed is the same ($N_c = N_t$), the turbine inlet temperatures T_{o3} can be easily calculated. The constant turbine inlet temperatures are then plotted in the compressor-turbine matching map as shown in Fig. 4.10.

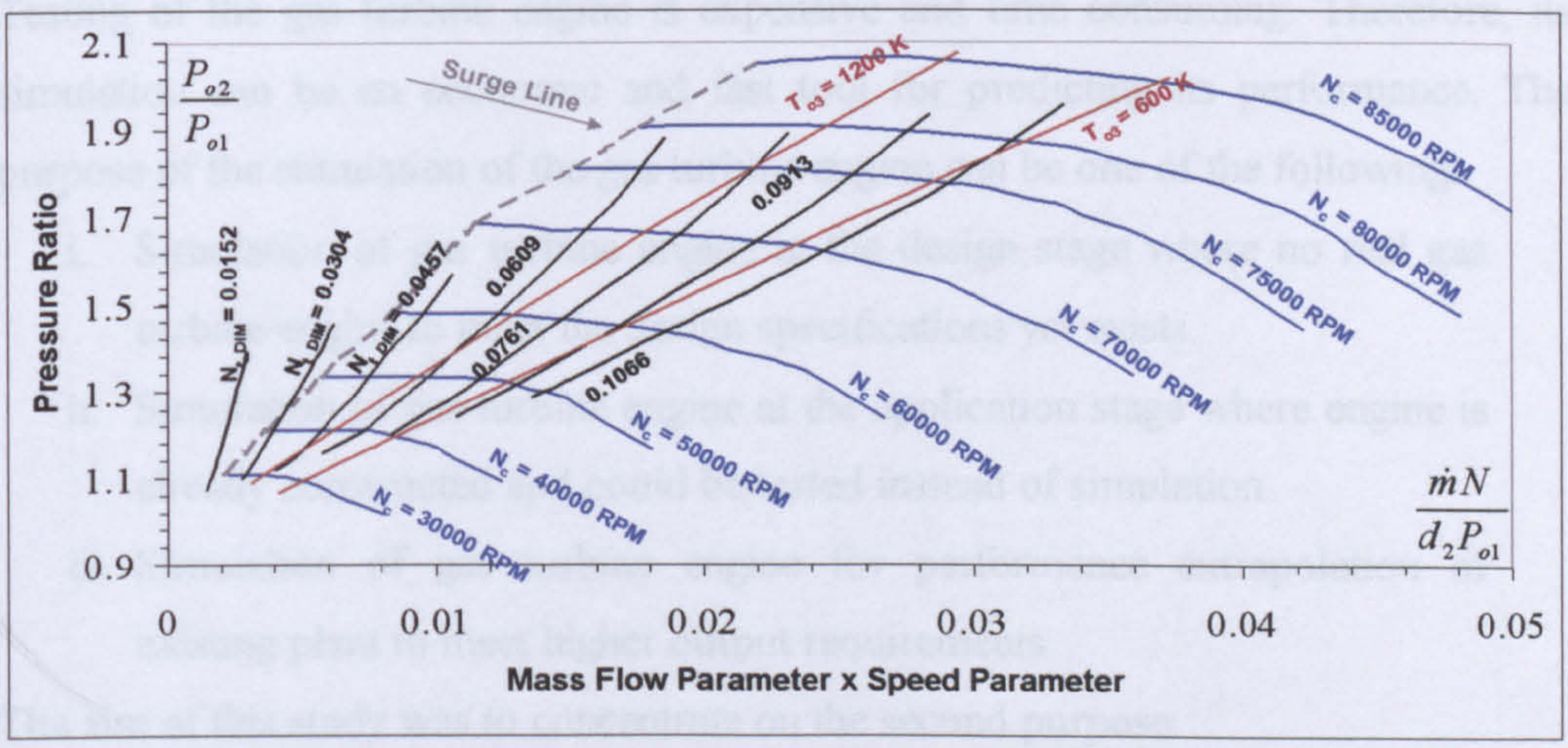

Fig. 4.10 Constant turbine inlet temperatures T_{o3} on the matching map

From Fig. 4.9 and Fig. 4.10, the following can be determined:

i. The operating range (envelope) and running line of the matched components.
ii. The proximity of the operating points to the compressor surge line (how close the operating points to the surge line).
iii. The maximum operating point at the maximum turbine inlet temperature (T_{o3}).
iv. And most important it can be concluded from the figures whether the gas turbine engine is operating in a region of adequate compressor and turbine efficiencies.

4.4 Gas Turbine Computer Simulation

A computer program for simulating a gas turbine engine would basically satisfy matching conditions analytically between the various components to produce the equilibrium running line. Representing this line either in the form of *lookup tables* or an *equation* is known as modelling and solving that equation with the help of a computer is computer simulation such that all energy and mass balances, all equations of state of working substances, and the performance characteristics of all components are satisfied.

Testing of the gas turbine engine is expensive and time consuming. Therefore, its simulation can be an economic and fast tool for predicting its performance. The purpose of the simulation of the gas turbine engine can be one of the following:

i. Simulation of gas turbine engine at the design stage where no real gas turbine engine to meet the design specifications yet exists.
ii. Simulation of gas turbine engine at the application stage where engine is already constructed and could be tested instead of simulation.
iii. Simulation of gas turbine engine for performance extrapolation of existing plant to meet higher output requirements.

The aim of this study was to concentrate on the second purpose.

The performance or control of the gas turbine plant at off-design conditions would always be of interest, so the gas turbine simulation program is run. That simulation run may pin-point the cause of operating problems or shows how the effectiveness of the gas turbine plant may be improved.

Essentially, the simulation of the transient operation of a gas turbine plant is more difficult than the simulation of the steady-state gas turbine plant. But unsteady operation of gas turbines is important for certain applications such as turbochargers. That field of study was considered to be outside the scope of present research.

4.4.1 Information-Flow Diagrams

For system simulation, fluid-flow and energy-flow diagrams are standard engineering tools. An equally useful tool is the information-flow diagram, for example, a block diagram of a control system is an information-flow diagram wherein a block signifies that an output can be calculated when the input is known. A centrifugal pump might appear in a fluid-flow diagram such as shown in Fig. 4.11(a), while in the information-flow diagram the blocks shown in Fig. 4.11(b). These figures represent functions or expressions that permit calculation of the outlet pressure for one block and the flow rate for the other. A block, as in Fig. 4.11(b), is called a transition function and may be an equation or may be tabular data to which interpolation would be applicable.

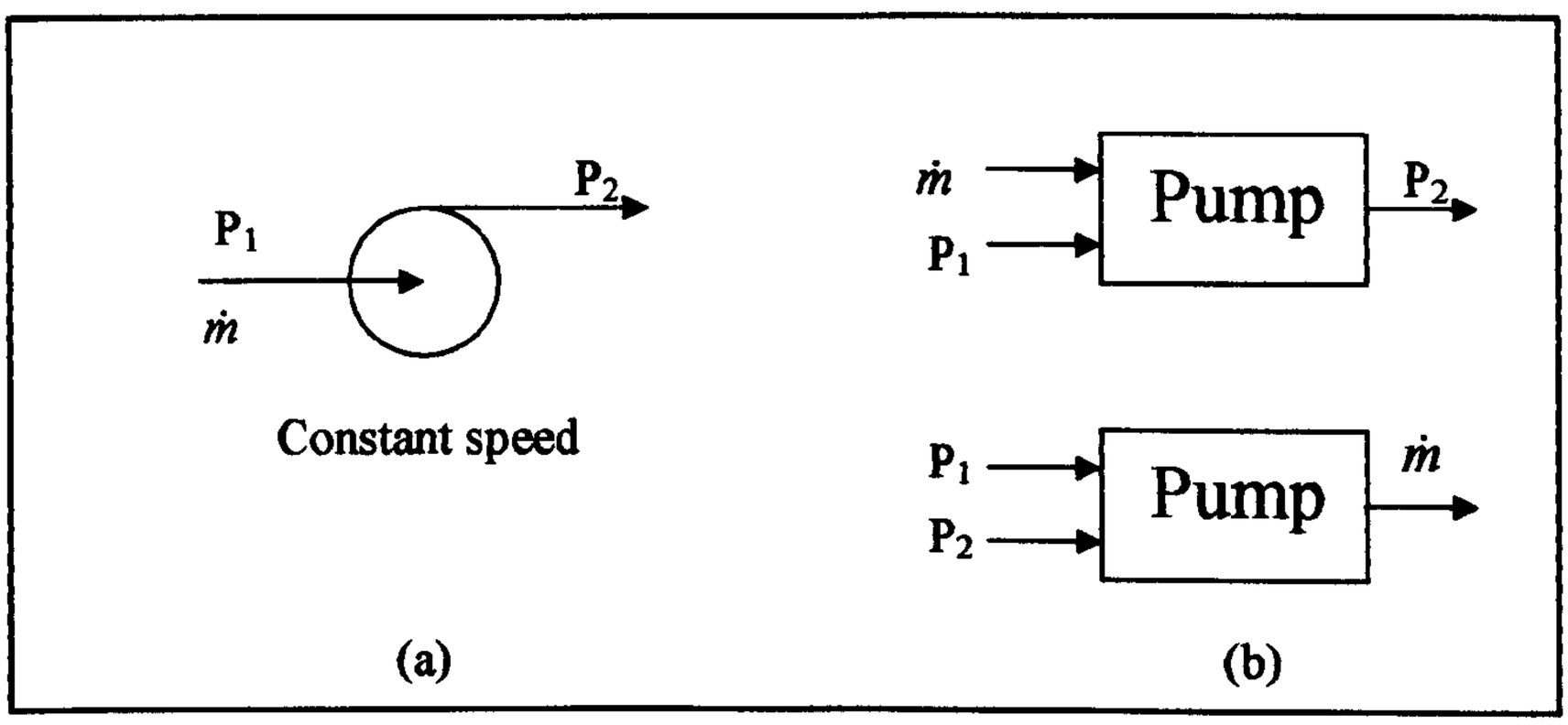

Fig. 4.11 (a) Centrifugal pump in fluid-flow diagram (b) Possible information-flow blocks representing pump

Figure 4.11 shows only one component. To illustrate how these individual blocks can build the information-flow diagram for a gas turbine plant, consider the simple gas turbine cycle in Fig. 4.1 shown earlier. The components in this cycle are the compressor, the combustion chamber and the turbine.

The information-flow diagram is arranged in Fig. 4.12 in a manner that might be used if the net power output W_{net} was to be calculated for the system with a given rate of fuel mass flow rate i.e. heat input at the combustion chamber. Further input information includes the ambient conditions T_{o1}, P_{o1} and rotational speed N.

The compressor block diagram signifies that when the rotational speed N_c, inlet pressure P_{o1}, inlet temperature T_{o1} and air flow rate $\dot{m}_a$ are specified, the outlet pressure P_{o2} and the compressor efficiency η_c can be determined from the compressor characteristics map as shown previously in Fig. 4.3. Furthermore, power W_c required by the compressor and outlet temperature T_{o2} can be calculated from Eqn 4.3 and Eqn 4.4 respectively.

The combustion chamber block diagram signifies that when the fuel flow rate $\dot{m}_f$, inlet temperature T_{o2} and inlet pressure P_{o2} are specified, the outlet pressure P_{o3} and the outlet temperature T_{o3} can be calculated from Eqn 4.5 and Eqn 4.6 respectively.

The turbine block diagram signifies that when the rotational speed N_t, inlet pressure P_{o3}, inlet temperature T_{o3} and gas flow rate $\dot{m}_g$ are specified, the outlet pressure P_{o4} and the turbine efficiency η_t can be determined from the tuurbine characteristics map as shown previously in Fig. 4.5. Furthermore, power W_t delivered by the turbine and outlet temperature T_{o4} can be calculated from Eqn 4.9 and Eqn 4.10 respectively.

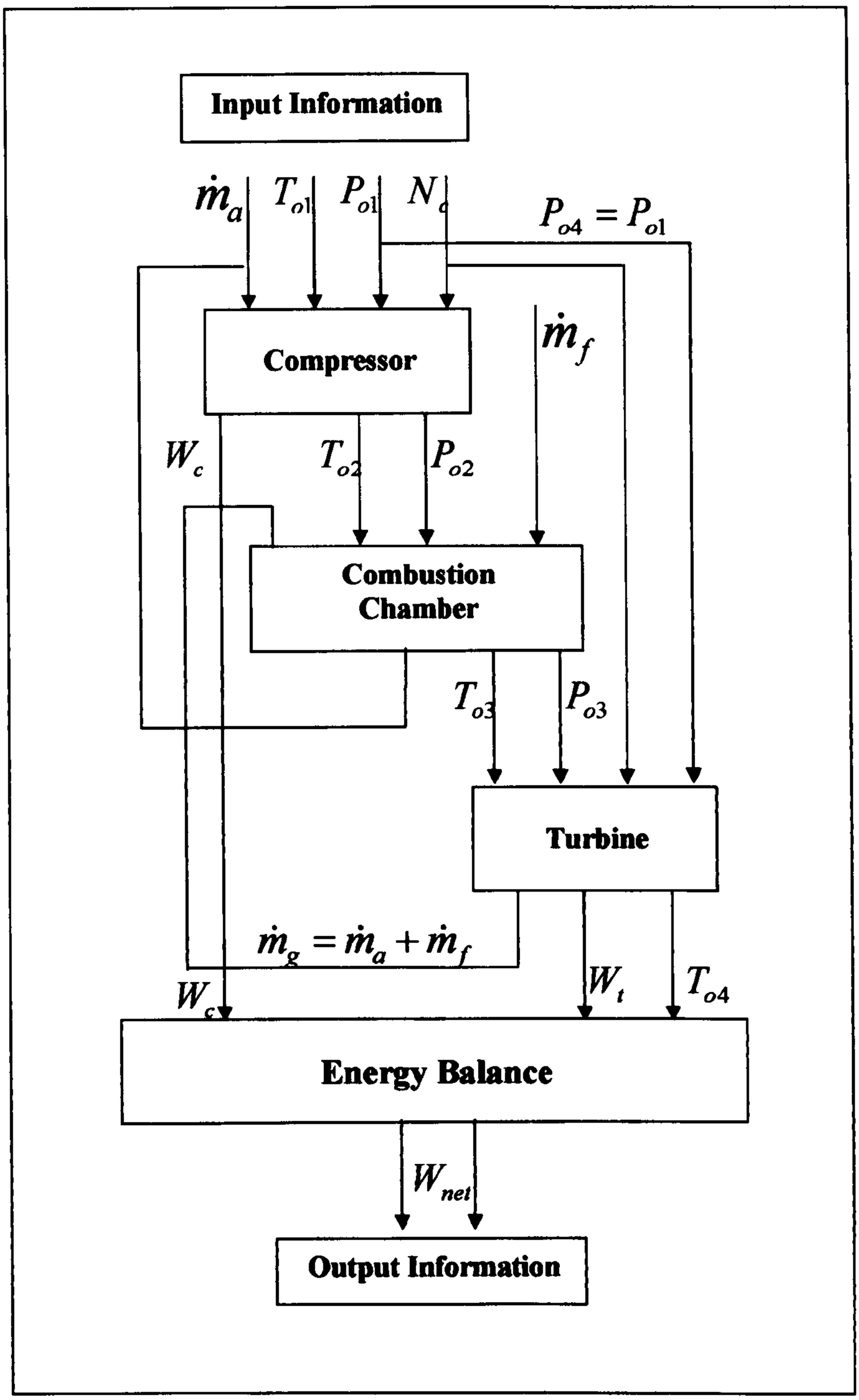

Fig. 4.12 Information-flow diagram of a simple gas turbine engine

Sometimes the arrangement of the system permits a direct numerical calculation for the first component of the system using input information. The output information for this first component is all that is needed to calculate the output information of the

next component and so on to the final component of the system whose output is the output information of the system. Such a system simulation consists of sequential calculations.

Before starting the design of the computer program for simulation purposes, it was necessary to identify its main features. Those features are summarised as follows:

i. The computer simulation should allow the user to simulate the components individually or as a complete plant.
ii. The simulation program should be modelled for the linking with another program to finally simulate the CPP plant. The outputs of this computer program should contain the needed parameters to start simulating the steam power plant, the other part of the CPP plant which is being studied as a part of parallel research.
iii. The simulation program should be modular so that various modules may be assembled to represent different gas turbine plant configurations.
iv. The simulation program should be user friendly and written in such manner that data can be transferred from one module to another easily and efficiently.

To produce running line analytically, the computer simulation program will use the components mathematical models as will as the components characteristics. That running line will be essential to compute the various gas turbine performance parameters.

In order to use these maps in a computer program it was necessary to have them in a special format. This format can take one of the following forms:

i. Deriving an equation to describe the performance of the component and solving this equation to calculate the performance parameters for any selected point on the performance map.
ii. Store the compressor characteristics in look-up tables and then use an interpolation or extrapolation technique to determine the values of the

performance parameters for any selected point on the performance map.

iii. Use a neural network technique to teach the computer the pattern of the component characteristics then compute the performance parameters for any selected point on the performance map.

In the present work, the second option was chosen as it produced a more reliable estimate of the parameters at any point on the component characteristics map.

4.4.2 Representing Compressor and Turbine Maps in the Computer Program

The compressor or turbine characteristics in the standard format as shown in Fig. 4.3 and Fig. 4.5 cannot be used directly in the computer program; they require some processing to convert the maps into a good numerical representation. There are many problems and difficulties associated with the numerical representation process.

4.4.2.1 Representing Compressor Maps in the Computer Program

It is not possible to read the compressor map parameters with given speed N_{Dim} and pressure ratio P_{o2}/P_{o1}, as there might be two values for the mass flow parameter $\dot{m}_{Dim}$ at given pressure ratio (see point A in Fig. 4.13). It is also not possible to determine the efficiency η_c from the compressor map with given speed N_{Dim} and mass flow parameter $\dot{m}_{Dim}$, because at some parts of the compressor map the speed lines can be vertical. Hence, there might be two values for the pressure ratio P_{o2}/P_{o1} at a single value of mass flow parameter $\dot{m}_{Dim}$ (see point B in Fig. 4.13).

Introducing a new coordinates, here called the BETA (β) lines, was the solution for this problem. This allowed an independent map reading using the shape of the parameter lines with the β line and speed parameter N_{Dim}.

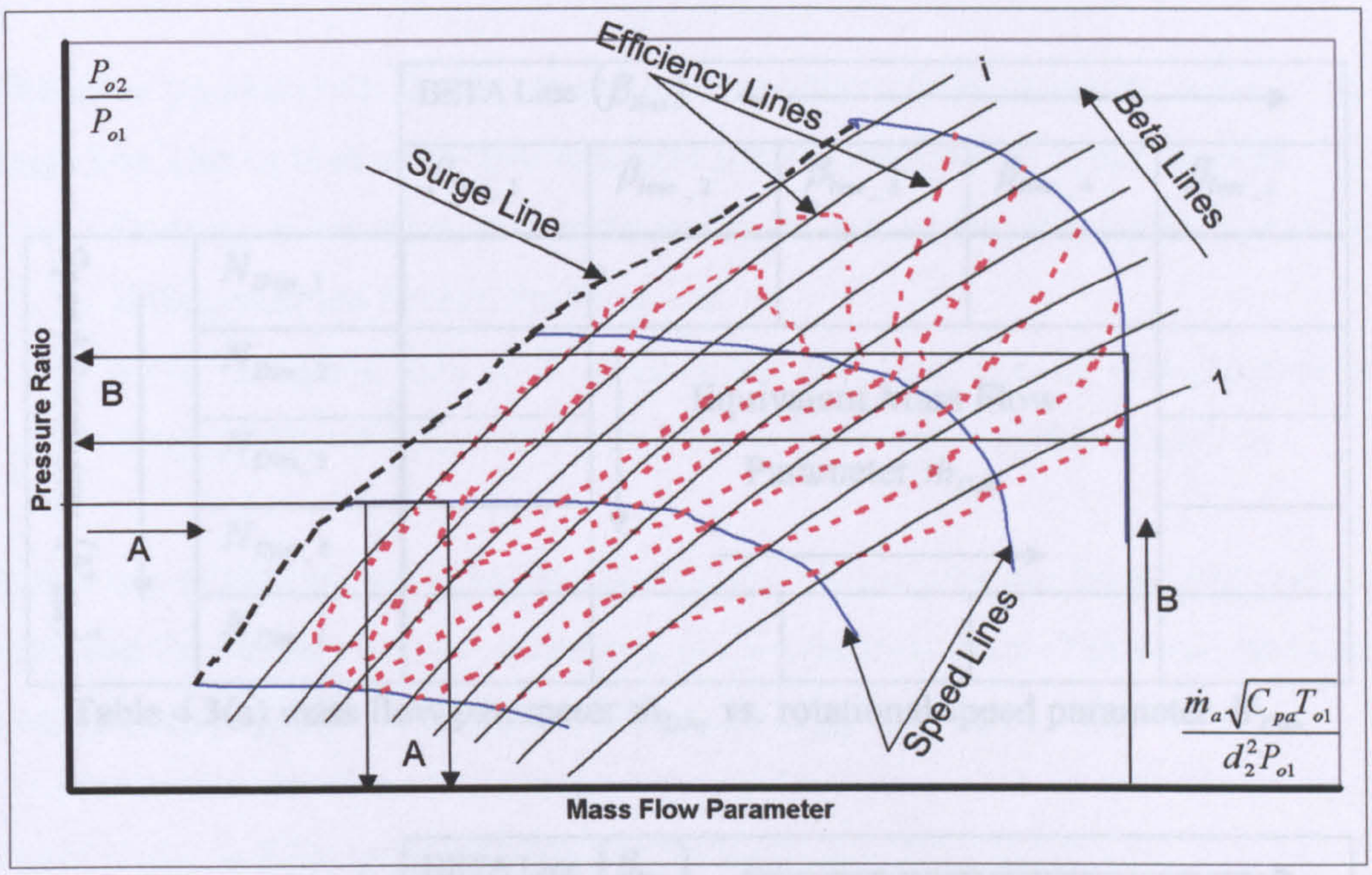

Fig. 4.13 Problems with reading compressor maps

The auxiliary coordinates (β lines) can be selected arbitrarily with only two conditions. First, there are no intersections between the β lines within the range of interest, and second the β lines are equally spaced. The β lines will have any numbers of lines with each line has a parameter number starting from 1. The β lines can be a parabolic lines or straight lines (straight lines are special parabolic lines).

Three-dimensional look-up tables, Tables 4.3(a), 4.3(b) and 4.3(c), were created to represent the compressor characteristics. These tables represented the mass flow parameter $\dot{m}_{Dim}$ vs. rotational speed parameter N_{Dim}, the pressure ratio P_{o2}/P_{o1} vs. rotational speed parameter N_{Dim} and the compressor efficiency η_c vs. rotational speed parameter N_{Dim}.

If the values of any parameter with β line parameter are specified, the program searches and picks the other two parameters from these look-up tables.

Speed Parameter (N_{Dim})	BETA Line (β_{line}) →				
	β_{line_1}	β_{line_2}	β_{line_3}	β_{line_4}	β_{line_i}
N_{Dim_1}					
N_{Dim_2}		Equivalent Mass Flow Parameter $\dot{m}_{Dim}$ →			
N_{Dim_3}					
N_{Dim_4}					
N_{Dim_i}					

Table 4.3(a) mass flow parameter $\dot{m}_{Dim}$ vs. rotational speed parameter N_{Dim}

Speed Parameter (N_{Dim})	BETA Line (β_{line}) →				
	β_{line_1}	β_{line_2}	β_{line_3}	β_{line_4}	β_{line_i}
N_{Dim_1}					
N_{Dim_2}		Equivalent pressure ratio P_{o2}/P_{o1} →			
N_{Dim_3}					
N_{Dim_4}					
N_{Dim_i}					

Table 4.3(b) pressure ratio P_{o2}/P_{o1} vs. rotational speed parameter N_{Dim}

Speed Parameter (N_{Dim})	BETA Line (β_{line}) →				
	β_{line_1}	β_{line_2}	β_{line_3}	β_{line_4}	β_{line_i}
N_{Dim_1}					
N_{Dim_2}		Equivalent compressor efficiency η_c →			
N_{Dim_3}					
N_{Dim_4}					
N_{Dim_i}					

Table 4.3(c) compressor efficiency η_c vs. rotational speed parameter N_{Dim}

The other problem with the numerical representation of the compressor map is the surge line. One or both of the following can achieve the solution to this problem:

i. Deriving an equation to describe surge line and solving this equation to check if the points are beyond the surge line.
ii. Store the surge line in look-up table and then use an interpolation or extrapolation technique to check if the points are beyond the surge line.

Either one of the two solutions can be efficient. In this program the second method was used for maintaining the consistency of the whole program. Table 4.4 shows the pressure ratio P_{o2}/P_{o1} vs. mass flow parameter $\dot{m}_{Dim}$ of the surge line.

Pressure Ratio P_{o2}/P_{o1}	Mass Flow Parameter $\dot{m}_{Dim}$

Pressure Ratio (P_{o2}/P_{o1}) ↓

Equivalent Mass Flow Parameter $(\dot{m}_{Dim})$ ↓

Table 4.4 Pressure ratio vs. mass flow parameter of the compressor surge line

Through the computer processing of all tables, linear interpolation technique was used to estimate the parameters values lying at intermediate points. This method of interpolation is followed in most books of numerical analysis.

4.4.2.2 Representing Turbine Maps in the Computer Program

As in the compressor case, the β lines must be introduced to the turbine maps to solve the problem of converting the maps into tabulated data. This can be seen clear in Fig. 4.5, where at the chocking condition and same speed parameter, more than one pressure ratio results from the same dimensionless mass flow parameter.

Three-dimensional look-up tables, as in the compressor case, have been developed and used to represent the turbine characteristics. These tables have the same forms as those of the compressor characteristics shown in Tables 4.3(a), 4.3(b) and 4.3(c). In these tables, linear interpolation technique was also used to compute the values lying at intermediate points.

4.4.3 Computer Simulation Program

The computer simulation program uses the components models based on either mathematical equations or performance characteristics to achieve matching between the various components in the gas turbine plant. This matching produces the engine equilibrium running line. The equilibrium running line can be used to calculate the different gas turbine performance parameters.

The principal advantages of gas turbine simulation program would be:

i. The computer simulation program can help in investigating the effects of the components performance characteristics on the performance of the complete engine. This investigation can be carried out at the design stage without bearing the cost of manufacturing and testing an expensive prototype.
ii. The conceptual designs of the engine can be studied and the choice of particular concept can be made to suit the specified operational requirements.
iii. The matching of the components can be explored for the design, off-design and transient conditions.
iv. The simulation program can serve as a valuable tool for investigating the performance of the gas turbine at off-design conditions. This investigation can help in designing an efficient control system for the gas turbine engine at that particular application such as being a part of the CPP plant.

The information flow diagram for the simple gas turbine cycle shown in Fig. 4.12 was used to create a computer simulation program. The flow chart for the program

logic is shown in Fig. 4.14. The program is suitable also for dealing with the simulation of other configurations discussed in Chapter 3. But for the sake of brevity the flow charts for each configuration have been omitted.

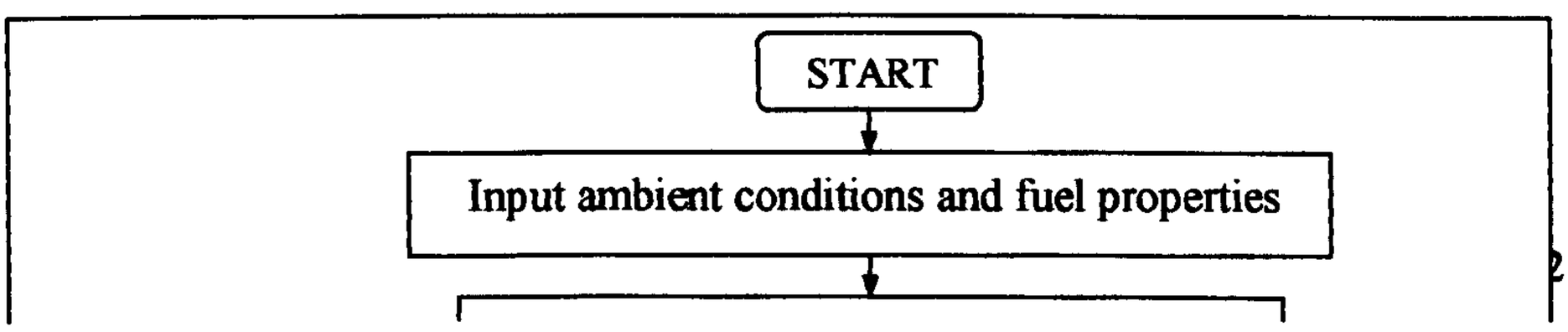

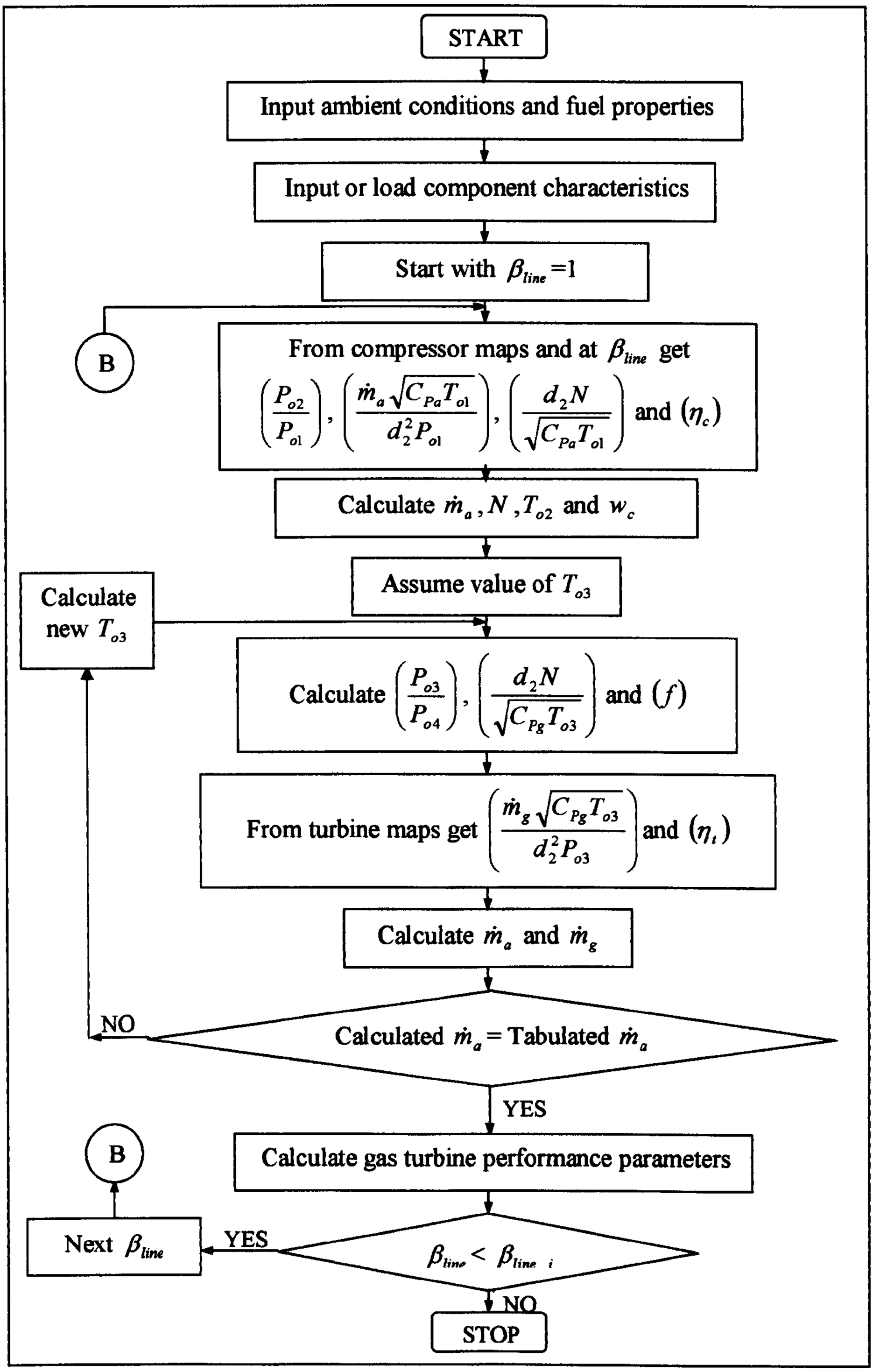

Fig. 4.13 Computer simulation flowchart

CHAPTER 5

DESIGN OF EXPERIMENTS AND EXPERIMENTAL FACILITY

5.1 Introduction

The preceding chapters concentrated on (a) the influence of the main parameters of the gas turbine cycle on the performance of the combined power and power cycle, (b) the performance of CPP design point calculations, and (c) the method for predicting the steady state off-design conditions of the gas turbine engine as part of the CPP plant. In order to verify the results of these studies, it was necessary to compare the predicted performance with the actual performance of the gas turbine engine measured experimentally.

Ideally the experimental work should be carried out on a gas turbine engine that has been either designed or selected for electrical power generation in the CPP plant. In order to get optimum performance, this design or selection of the engine must be based on the results of the parametric studies, modelling and simulation. However it was neither practically possible nor economically feasible to either design and manufacture or procure a real gas turbine engine. Therefore an alternative solution had to be found. It was decided to use an aircraft auxiliary power unit incorporating a small gas turbine. It was known that the results of the experiments would not demonstrate the full potential of the gas turbine for the CPP plant. Nevertheless, the test facility would provide a very good opportunity to design a high speed gearbox to couple the engine with the alternator, selection and calibration of instruments and finally system design as well as the setting up of the data acquisition equipment.

An experimental facility was build to run an electrical power generator. The generator was driven by an aircraft auxiliary power unit incorporating a small gas turbine engine. This chapter will have three main parts: the first will describe the details of the test facility; the second will describe the instruments and their calibration and the last part will describe the computerised data acquisition system.

5.2 Design of Experimental Facility

A schematic diagram of the test facility is shown in Fig. 5.1 showing the quantities to be measured and the locations of the measurement stations. The test facility was

designed according to the following minimum requirements:

i. The test facility should have the capability of measuring pressures, temperatures, mass flow rates, rotational speed, torque or thrust, etc at various stations shown in Fig. 5.1.
ii. The cost of the experimental facility should be as low as possible; therefore it was necessary to use, wherever possible, the available equipment within the Royal Jordanian Air Force (RJAF) facilities.
iii. Building the test facility should provide a valuable experience for developing a digital to analogue instrumentation for jet engine test facilities at present used by the RJAF.

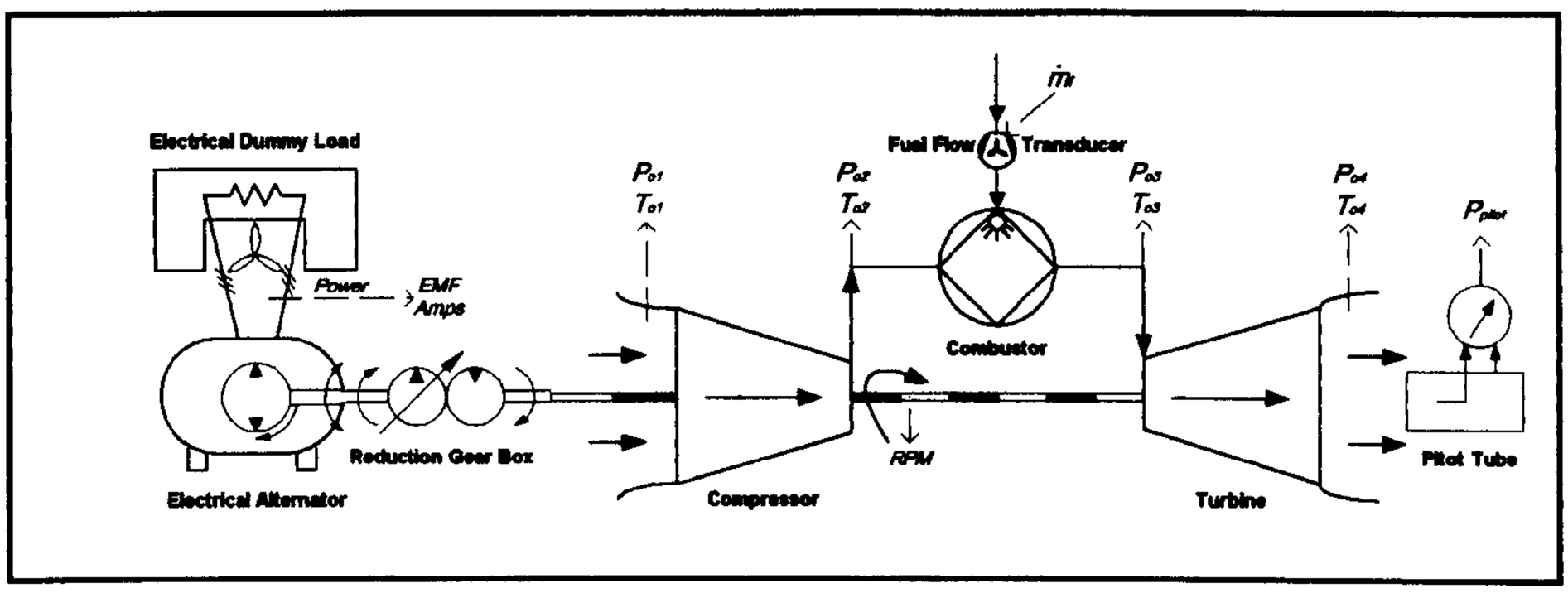

Fig. 5.1 Schematic diagram of the experimental test facility

The Garret aircraft auxiliary power unit of model JTCP-60A, shown in Fig. 5.2, was originally used to supply pressurised air and electrical power for jet engine starting and maintenance purposes of various airplanes used in the RJAF. In the current work the gas turbine plant should produce only electrical power output and not pressurised air. Therefore, some modifications and coupling of a new electrical alternator was necessary for the purpose of present research.

The modifications to the auxiliary power unit (APU) included the following:

i. Designing and manufacturing a new reduction gearbox to drive a larger electrical power generator than that provided with the APU.
ii. Modifying the APU stand for the adaptation of the reduction gearbox and the electrical generator.
iii. Modifying the components' casings for instrumentation.

The following sections will describe those modifications in detail.

Fig. 5.2 Garret aircraft auxiliary power unit of model JTCP-60A

5.2.1 Reduction Gearbox Design and Manufacturing

Gears are used in many applications to transmit motion from one shaft to another with constant angular velocity ratio. In some cases, the desired reduction in angular velocity is too great to achieve using only two gears. When this occurs, several gears must be connected together to give what is known as a gear train.

There are many types of gears including spur, helical, crossed-helical, herringbone, internal, bevel and worm gears. Spur gears are the simplest forms of gears. The tooth form is basic involute, the pressure angle is constant and the tooth dimensions are identical in all planes of rotation. The spur mesh doesn't have axial end thrust. They are applicable to all types of gear trains and a wide range of velocity ratios.

Helical gears are equivalent to the spur gears except for the added complication of the helix angle. They are appropriate to use if the gear train is high load and/or high speed. The helical mesh produces an axial thrust, which must be accommodated.

Crossed-helical gears give an advantage of skewed shafting but the sliding of a point contact limit the crossed helical gear mesh to a light load low speed applications.

Herringbone gears are double helical gears with opposite hand direction. The herringbone gears have the same advantages as the helical gears with an extra advantage of eliminating the axial thrust produced by each helical gear.

Bevel gears offer convenient angular drive but bevel gears have complicated tooth form that yields to difficulties in manufacturing. Worm gears offer right-angle skew shafts with high velocity ratio and high loads. On the other hand, the worm gear has a complicated noninvolute tooth form.

Table 5.1 summarises the main features of major types of gears, including the applications where the gears are used.

5.2.1.1 Gear Standards

Functional requirements can be used to determine tooth proportions, but this is not practical because it will produce various designs. Therefore it is better to use a limited number of standard tooth proportion designs and obtain the benefits of interchange ability, economy of common tooling, fewer design calculations and repeated use of the same designs.

The fundamental parameters of gears, such as basic tooth form, pressure angle, addendum and working depth have been standardised by many national institutions and associations. The British standards institution (BS) and the American gear manufacturers association (AGMA) produced standardised gear systems (e.g. BS436 and AGMA 170.01) as well as the necessary formulae needed to calculate the data required on a gear detail drawing for both manufacturing and inspection purposes. In the present work AGMA standardised gear systems are used for designing and manufacturing the reduction gearbox.

Gear type	Features	Applications	Comments
Spur	-Parallel shafting -High loads -High speeds -High efficiency	Applicable to all types of trains and a wide range of velocity ratios	Recommended for all gear meshes, except where very high speeds and loads or special features of other types, such as right-angle drive, cannot be avoided.
Helical	-Parallel shafting -Very high loads -Very high speeds -High efficiency	Most applicable to high speeds and loads; also used wherever spurs are used	Complications due to helix angle. Recommended for all high-speed and high-load meshes. Axial thrust component must be accommodated.
Crossed-helical	-Skewed shafting -Low loads -Low speeds -High sliding	Relatively low velocity ratio; low speeds and light loads only	Point contact limits capacity. Suitable for right angle drives if light load. Good lubrication essential.
Herringbone	-Parallel shafting -Very high loads -Very high speeds -High efficiency	Applicable to high speeds and loads; also used wherever spurs or helical are used	Equivalent quality to helical gears with the advantage of eliminating the axial thrust. Recommended for all high-speed and high-load meshes.
Internal	-Parallel shafting -High loads -High speeds	Requires high speeds and loads; offers high stress loading; long life	Not recommended because of the design and fabrication limitations.
Bevel	-Intersecting shafts -High loads -High speeds	Suitable for 1:1 and higher velocity ratios and for right-angle meshes (and other angles)	Good choice for right-angle drive, particularly low ratios. Complicated tooth form and fabrication limits the precision of bevel gears.
Worm	-Skewed shafting -High velocity ratio -High loads -High speeds -Low efficiency	Suitable for high velocity ratios; angular meshes; high loads	Best choice for combination high velocity ratio and right-angle drive. High sliding requires excellent lubrication.

Table 5.1 Summary and evaluation of gear types

In design and inspection of gear system, several special features must be known. These features will include the following:

i. The pitch diameter D.
ii. Metric Module M.
iii. Addendum a.
iv. Dedendum b.
v. Outside diameter D_o.
vi. Face width L.
vii. Centre distance c.
viii. Pressure angle ϕ.
ix. Velocity ratio VR.
x. Number of teeth n.
xi. Train value TV.
xii. Helix angle ψ.
xiii. Quality value, which determine the dimension tolerances.

Figure 5.3 identifies some of these features.

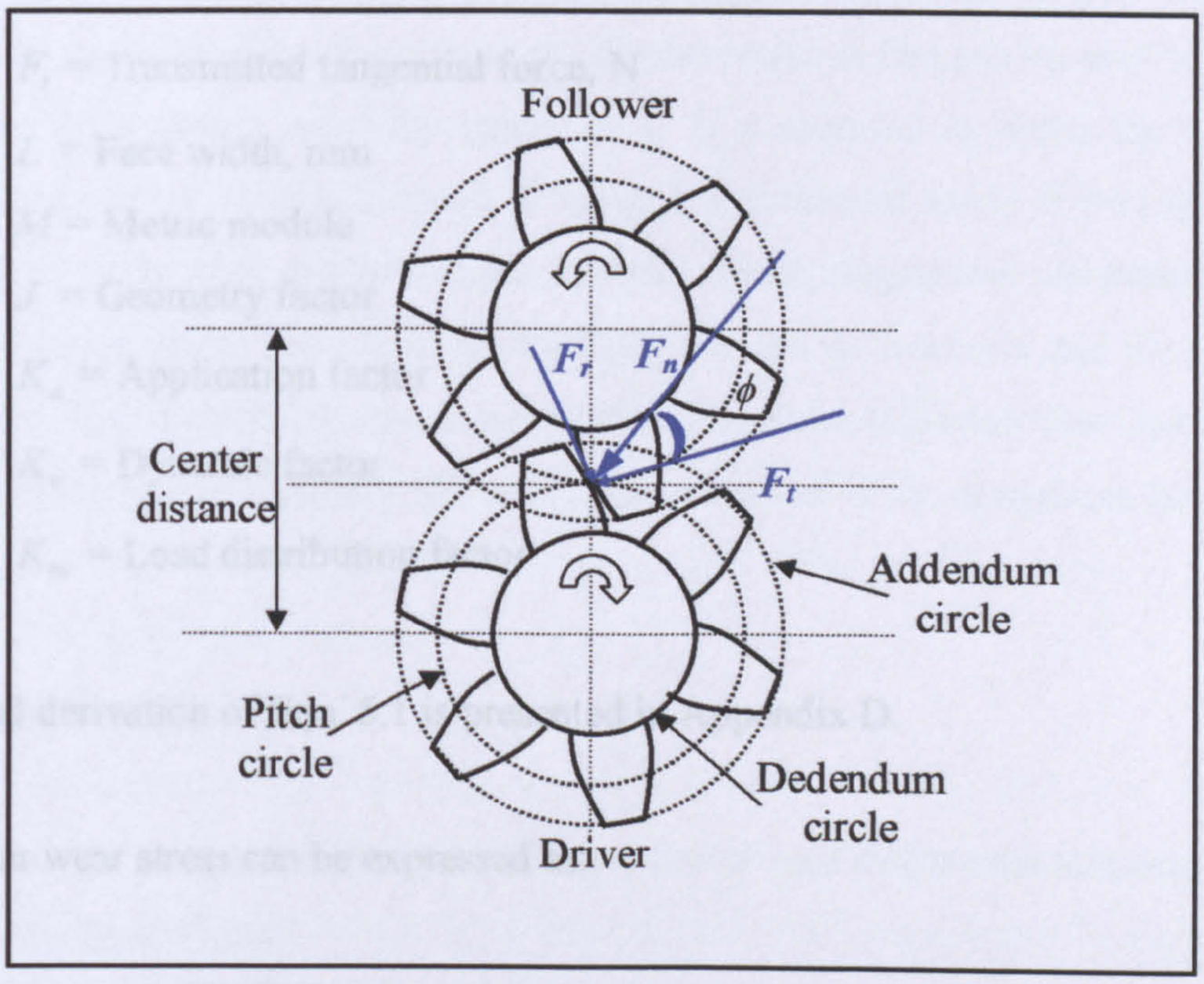

Fig. 5.3 Two gears in mesh

When two gears mesh, the smaller is called pinion and the larger is the gear. In this section the subscript P will be used to refer to the pinion while the subscript G will be used to refer to the gear.

Gears generally fail because the actual loads applied to the teeth are greater than the allowable loads based upon either the beam strength of the tooth (tooth fracture) or its wear strength (surface failure). Therefore, the stress analysis and the surface durability analysis of the gear teeth could be used to calculate the allowable stresses of the meshed gears. The stress values are useful in designing the appropriate gears. Equations 5.1 and 5.2, empirically modified by AGMA from Lewis equation, will be used to calculate the bending strength stress and surface wear stress, respectively.

The stress at the root of gear tooth is given as:

$$\sigma_t = \frac{F_t K_a}{K_v} \frac{K_m}{MLJ} \tag{5.1}$$

where σ_t = Calculated stress at root of tooth, MPa

F_t = Transmitted tangential force, N

L = Face width, mm

M = Metric module

J = Geometry factor

K_a = Application factor

K_v = Dynamic factor

K_m = Load distribution factor

Detailed derivation of Eqn. 5.1 is presented in Appendix D.

The gear wear stress can be expressed as:

$$\sigma_h = S_p \sqrt{\frac{S_a S_m F_t}{S_v LDI}} \tag{5.2}$$

where σ_h = Calculated wear stress, MPa

F_t = Transmitted tangential force, N

L = Face width, mm

D = Pitch diameter, mm

I = Geometry factor

S_a = Application factor

S_v = Dynamic factor

S_m = Load distribution factor

All K and S factors are empirical values provided by AGMA[33-54] in forms of tables and figures. Extracted figures and tables are included in Appendix D.

5.2.1.2 Gearbox Design

i. Factors Affecting the Design

Designing gears presents an extremely difficult problem because it is primarily a trial and error procedure. However, there are several methods that can be used to develop a design. In a design involving gear drives, it is required to know the following parameters, that is, rotational speed of the pinion, rotational speed of the gear and the amount of power that the drive must transmit. These parameters are determined by the application under consideration. Furthermore, the environment and the operating conditions to which the drive will be subjected must be understood so that the right empirical factors, provided by BS or AGMA, involved in the design can be correctly chosen.

ii. Design Specifications

In general, the design specifications of a gearbox should include the followings:

i. The type of gears.

ii. Their arrangements on the shafts.

iii. The gears material including their heat treatment.

iv. The geometry of the gears, which are the number of teeth, metric modules, pitch diameters, tooth form, faces width and quality numbers.

Furthermore, the design should account for the bending fatigue strength of the gear teeth and the wear resistance sometimes called surface durability.

There is no one best solution to a gear design problem; several good designs are possible. The creativity and the specific requirements of the application will greatly influence the selection of the final design. In the present work, the design procedure to be followed is to provide a mean of approaching the problem in order to have a reasonable design.

The final design of the gearbox should have the following characteristics:

i. Compact, safe and low in cost.
ii. Operate smoothly and quietly.
iii. Easy to manufacture and has a long life.
iv. Compatible with the other elements in the machine such as bearings, shafts, housing and the driven machine.

iii. Design Procedure

The design procedure is a trial and error methodology and it should have the following sequence order:

i. A proposed geometry that satisfies the required velocity ratio and application limitations such as centre distance and physical size.
ii. Selection of the type of material to be used (steel, cast iron etc).
iii. Choice of metric module.
iv. Determination of the loads and faces width.
v. Calculation of the bending stress. It should be noted here that if the output results satisfy the design requirements, the procedure continues, otherwise a new metric module is selected and the procedure is repeated starting from point iii.
vi. Computations of the contact wear stress on the surface of the teeth. If the output results satisfy the design requirements, the procedure continues,

otherwise a new material is selected and the procedure is repeated starting from point ii.

The sequence of the above design procedure can be illustrated in the flowchart depicted in Fig. 5.4.

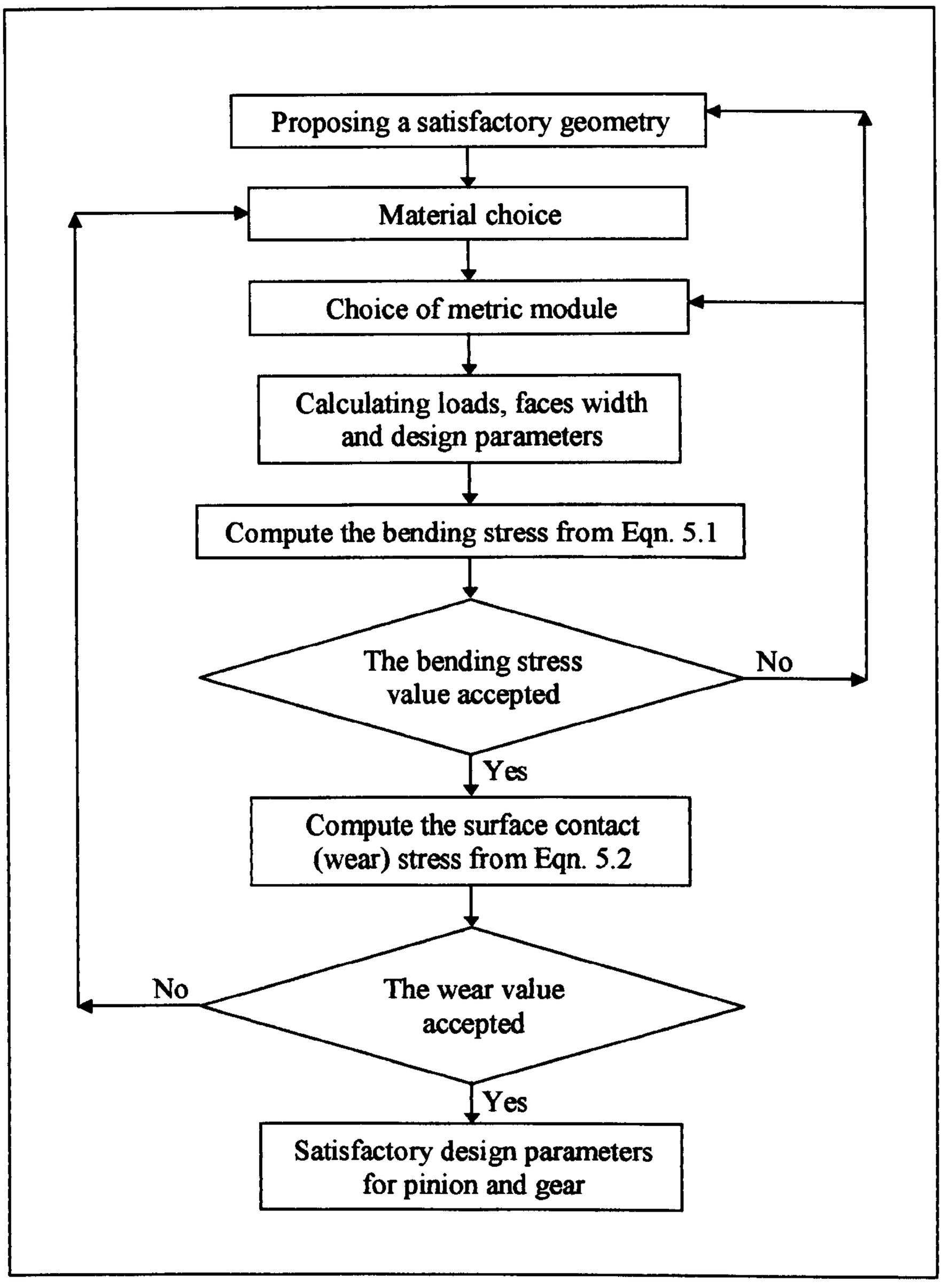

Fig. 5.4 Primary parts of gearbox design procedure

iv. Design Calculations

The requirements of the designed gearbox are:

A. Reducing the angular velocity at the output of the gas turbine engine from 42000 rpm to 1500 rpm which is the speed required by the electrical alternator.
B. The direction of rotation of the gas turbine engine is counter clock wise while the electrical alternator must rotate in clock wise direction.
C. The power that gearbox must transmit is 330 kW.

The design calculations will include the following:

A. The design calculations of the pinion and the gearbox.
B. The design calculations of the shaft.
C. The selection of the bearings.

A. The design calculations of the pinion and the gearbox.

The design calculation is a trial and error method and can be divided into the following steps:

1. Computing velocity ratio and rotational speed direction

The velocity ratio was calculated as follows

$$VR = \frac{\omega_P}{\omega_G} \qquad (5.3)$$

$$= \frac{42000}{1500} = 28$$

where ω = Angular velocity, rpm

Velocity ratio of 28 is difficult to achieve in one stage reduction gearbox, using two parallel shafts, due to the size of the produced gearbox. Therefore a gear train can be the solution to this problem. At the same time, the direction of rotation must be accounted for which should be opposite to the main shaft, see Fig. 5.5.

In order to produce a different rotational direction using a gear train, an even number of parallel shafts should be chosen. The suitable choice of the number of parallel shafts is selected to be four because increasing the number of parallel shafts will reduce the power transmission efficiency, increasing the cost and time of manufacturing. A schematic diagram of proposed four parallel shafts (triple reduction gearbox) is shown schematically in Fig. 5.5

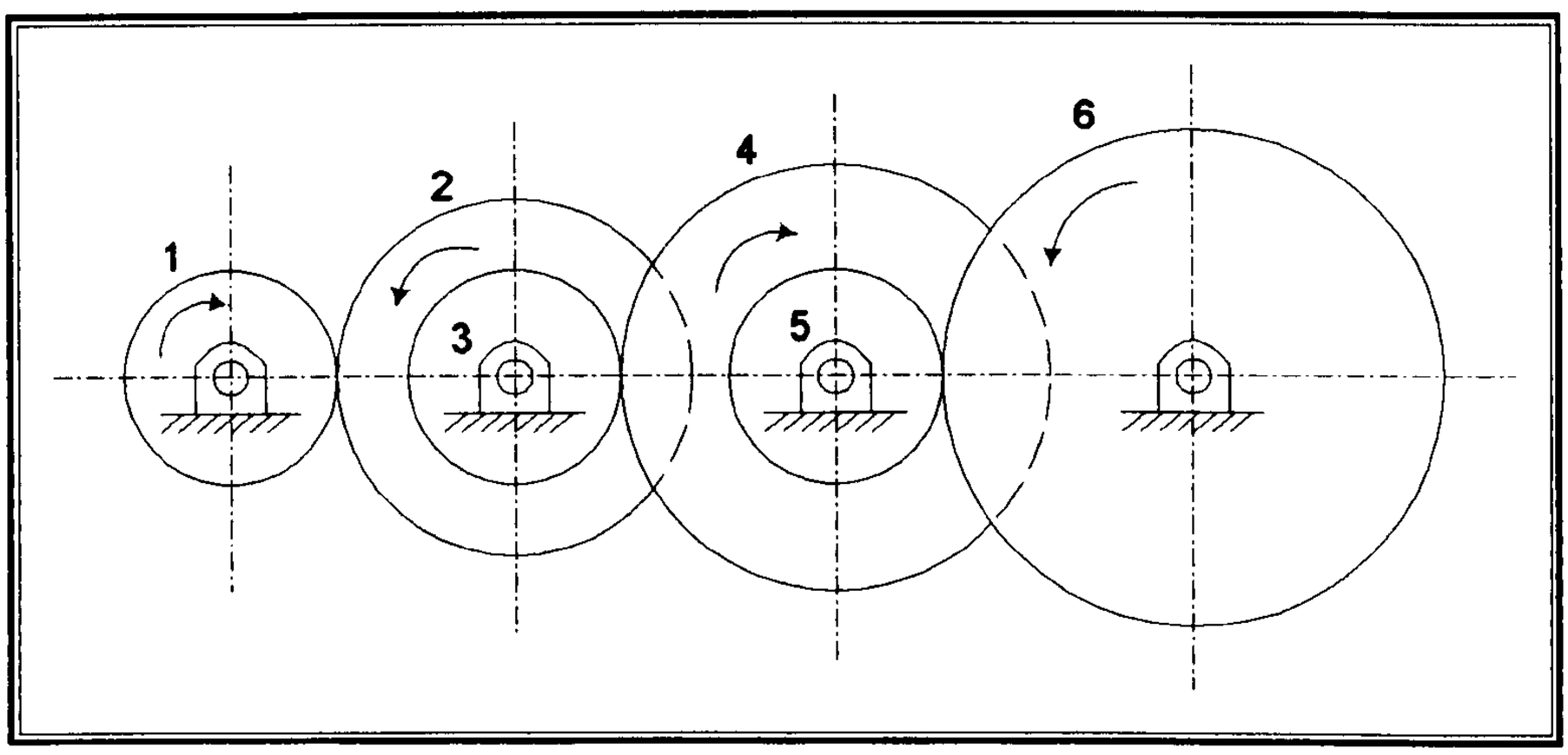

Fig. 5.5 Schematic diagram of triple reduction speed reducer

The gear train proposed will consist of three meshed gears and any combination of these three gear stages that produces a velocity ratio of 28 can be acceptable. In the present work the selected combination is listed in Table 5.2.

2. Specifying the geometry of the gears

Each stage of the gearbox will be designed using the same trial procedure, but for the sake of brevity, the design calculations of the first stage will be shown as an example to the next two stages.

Start by specifying the geometry of the pinion, which include: the type of gear, the normal metric module M, and the number of teeth n_p. The gear type is chosen to be a herringbone (refer to Table 5.1) with a helix angle ψ of 30° and normal pressure

angle ϕ of 20°, the metric module and the number of teeth are chosen to be 4 and 12, respectively.

Gear	Pinion Speed ω_p (rpm)	Gear Speed ω_g (rpm)	Velocity Ratio
First stage	42000	21000	2
Second stage	21000	5250	4
Third stage	5250	1500	3.5
Gear train	42000	1500	$2 \times 4 \times 3.5 = 28$

Table 5.2 Reduction gearbox stages

The pitch diameter D_P can be calculated from the definitions of the module in Eqn. 5.4 as follows:

$$D_P = \frac{n_P \times M_{normal}}{\cos\psi} \tag{5.4}$$

$$= \frac{12 \times 4}{\cos 30} = 55.43\,mm$$

Addendum a, dedendum b and outside diameter D_{oP} are calculated from Eqn. 5.5 to Eqn. 5.7.

$$a = 1.00 \times M \tag{5.5}$$

$$= 1.00 \times 4 = 4.00\,mm$$

$$b = 1.25 \times M \tag{5.6}$$

$$= 1.25 \times M = 5.00\,mm$$

$$D_{oP} = D_P + 2a \tag{5.7}$$

$$= 55.43 + 2 \times 4.00 = 63.43\,mm$$

By knowing the velocity ratio and the geometry of the pinion, the pitch diameter, the number of teeth and the outside diameter of the meshed gear can be calculated as follows:

$$D_G = D_P \times VR \tag{5.8}$$

$$= 55.43 \times 2 = 110.86\ mm$$

$$n_G = n_P \times VR \tag{5.9}$$

$$= 12 \times 2 = 24$$

$$D_{oG} = D_G + 2a \tag{5.10}$$

$$= 110.86 + 2 \times 4.00 = 118.86\ mm$$

The centre distance is computed from Eqn. 5.11 below.

$$c = \frac{D_P + D_G}{2} \tag{5.11}$$

$$= \frac{55.43 + 110.86}{2} = 83.145\ mm$$

3. Computing the pitch line velocity

The pitch line speed V_P in meters per second can be computed from Eqn. 5.12 below.

$$V_P = \frac{\pi D \omega_P}{60000} \tag{5.12}$$

$$= \frac{\pi \times 55.43 \times 42000}{60000} = 121.9\ m/s$$

4. Computing the transmission force

The transmission force F_t in Newton can be calculated as follows

$$F_t = \frac{P}{V_P} \tag{5.13}$$

$$= \frac{330000}{121.9} = 2707.2\,N$$

where P is the transmitted power in kW

5. Calculations of the bending stress

For the pinion, taking the face width L for the herringbone gear as 80 mm. The bending stress σ_{tP} can be calculated using Eqn. 5.1 with the AGMA empirical values as follows:

$$\sigma_{tP} = \frac{F_t K_a}{K_v}\frac{K_m}{MLJ} \tag{5.1}$$

$$= \frac{2707.2 \times 1.25}{0.48} \times \frac{1.6}{4 \times 80 \times 0.4} = 88.125\,MPa$$

Similarly for the Gear, the bending stress σ_{tG} can be calculated using Eqn. 5.1 with the AGMA empirical values as follows:

$$\sigma_{tG} = \frac{F_t K_a}{K_v}\frac{K_m}{MLJ} \tag{5.1}$$

$$= \frac{2707.2 \times 1.25}{0.48} \times \frac{1.6}{4 \times 80 \times 0.44} = 80.11\,MPa$$

Values of empirical factors K_a, K_m, K_v and J are selected based on figures and tables provided by AGMA given in Appendix D.

According to the availability of the material in the local market, AISI 4140 was chosen. This satisfies the calculated bending stresses condition for the pinion and the gear, respectively.

6. Calculations of the wear stress

The wear stress for the pinion σ_{hP} can be calculated using Eqn. 5.2 using the AGMA empirical values as follows:

$$\sigma_{hP} = S_p \sqrt{\frac{S_a S_m F_t}{S_v LDI}} \tag{5.2}$$

$$= 191 \times \sqrt{\frac{1.25 \times 1.6 \times 2707.2}{0.48 \times 80 \times 55.43 \times 0.085}} = 1045\, MPa$$

Similarly for the Gear, the wear stress σ_{hG} can be calculated using Eqn. 5.2 as follows:

$$\sigma_{hP} = S_p \sqrt{\frac{S_a S_m F_t}{S_v LDI}} \tag{5.2}$$

$$= 191 \times \sqrt{\frac{1.25 \times 1.6 \times 2707.2}{0.48 \times 80 \times 110.86 \times 0.1}} = 681.17\, MPa$$

The material was chosen before satisfies the calculated wear stresses for the pinion and the gear. Refer to figures and Tables in Appendix D.

B. The design calculations of the gearbox shafts

The diameter of the shaft can be calculated using Eqn. 5.14. Detail derivation of Eqn. 5.14 is shown in Appendix C.

$$d = (SF)\left[(64)\left(\frac{P}{\omega}\right)\left(\frac{1}{(\pi)(\sigma_{shear})}\right)\right]^{1/3} \tag{5.14}$$

where:

d = The diameter of the shaft, m

P = The power developed by the shaft, $Watt$.

ω = Angular velocity, rad/s .

σ_{shear} = Allowable shear stress, N/m^2 .

SF = Safety factor.

Note that $(\sigma_{shear})_{material} = \frac{1}{3}(\sigma_{stress})$ [55]

The selected material that was available in the local market is AISI 4140 and its yield strength is 1460 *MPa*.

$$d = (1.5)\left[(64)\left(\frac{330000 \times 60}{42000 \times 2 \times \pi}\right)\left(\frac{1}{(\pi)(\frac{1460 \times 10^6}{3})}\right)\right]^{1/3} = 0.0212\,m$$

$$= 21.2\,mm$$

The calculated value of the shaft diameter showed that 21.2 *mm* is the minimum value that satisfies the material specifications regarding stress values.

C. The selection of the bearings

The selection of bearings is based on three criteria: - (a) the type of load and its value (b) the rotational speed and (c) life cycle. Calculations of shaft diameter d showed that the most suitable bearing size for this design is equal to 25 *mm*. This size was selected because it was available in the local market and satisfies the load and the rotational speed of the shaft. The design load calculations of the bearings are outside the scope of this research work and can be found in any text or technical book.

Furthermore, it is important to specify the type of the bearing for the application used in this research work. However, it should be noted that there are several types of bearings that can satisfies the design specification of this application but the selection was based on the availability and cost wise. It was found that a deep groove bearing satisfies the selection criteria.

5.2.1.3 Complete Design Data

Similar procedure was carried out to calculate the remaining gears and shafts. The complete design data of the gearbox is listed in Table 5.3. Table 5.3(a) lists the design data of the gears and Table 5.3(b) lists the design data of the shafts and the selected bearings.

#	Pitch Diameter (*mm*)	Number of Teeth *n*	Pressure Angle ϕ	Module Number *M*	Helix Angle ψ	Outside Diameter (*mm*)	Gear Speed (*rpm*)	Tooth Width (*mm*)	Type of Material (*AISI*)
1	55.43	12	20	4	30	63.43	42000	2 x 40	4140
2	110.86	24	20	4	30	118.86	21000	2 x 40	4140
3	69.28	12	20	5	30	79.28	21000	2 x 45	4140
4	277.14	48	20	5	30	287.14	5250	2 x 45	4140
5	83.14	12	20	6	30	95.14	5250	2 x 50	4140
6	290.98	42	20	6	30	302.98	1500	2 x 50	4337

Table 5.3(a) Complete design data of the gears

Shaft #	Shaft Diameter (*mm*)	Type of Material (*AISI*)	Bearing Commercial Number	Bearing Inner Diameter (*mm*)	Bearing Outer Diameter (*mm*)	Bearing Thickness (*mm*)	Shaft Speed (*rpm*)
1	25	4140	6205	25	52	15	42000
2	25	4140	6205	25	52	15	21000
3	40	4140	6308	40	90	23	5250
4	65	4140	6213	65	120	23	1500

Table 5.3(b) Complete design data of the gearbox shafts and bearings

Various solid model views of the complete gearbox are shown in Figs. 5.6 to 5.9

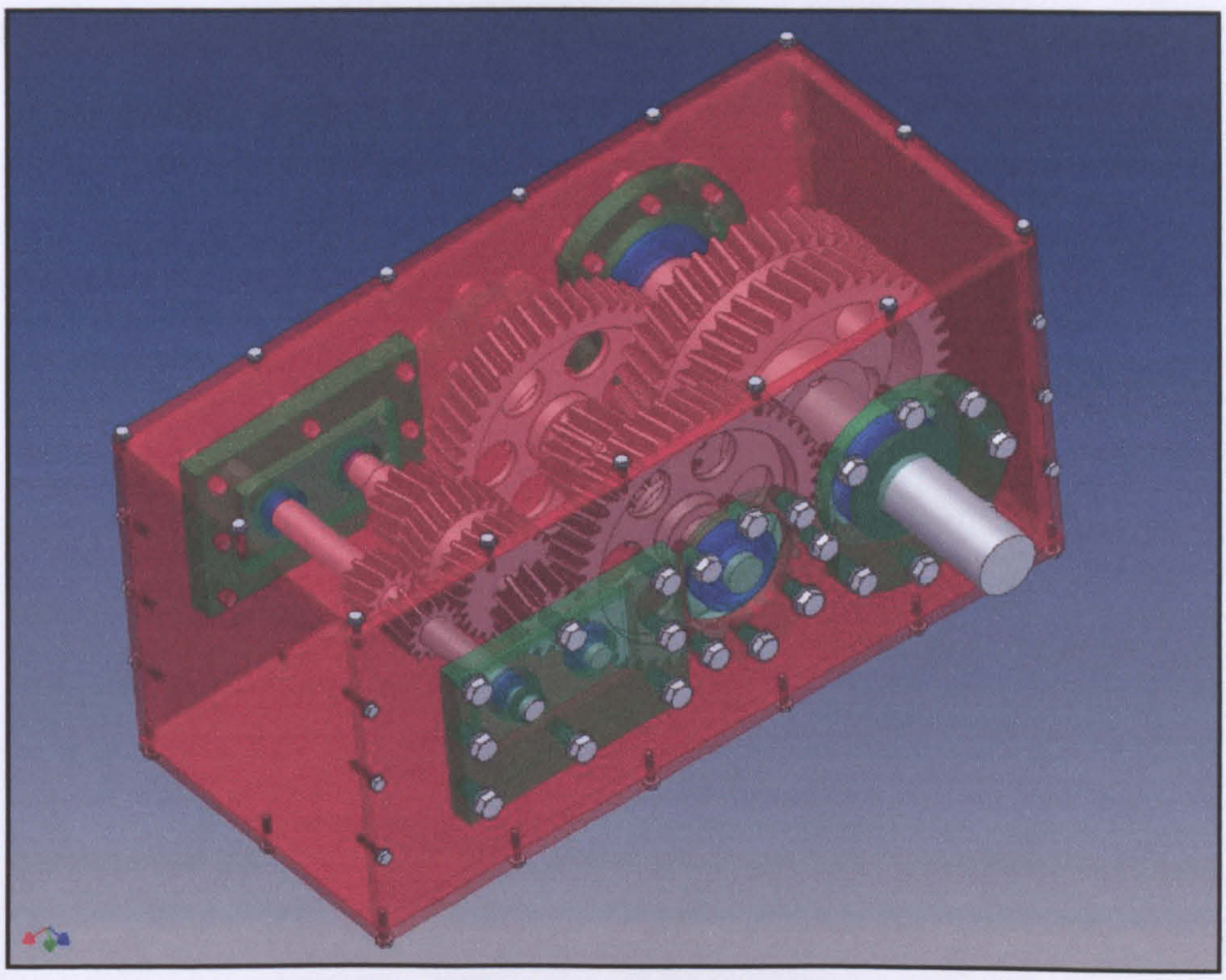

Fig. 5.6 Isometric view

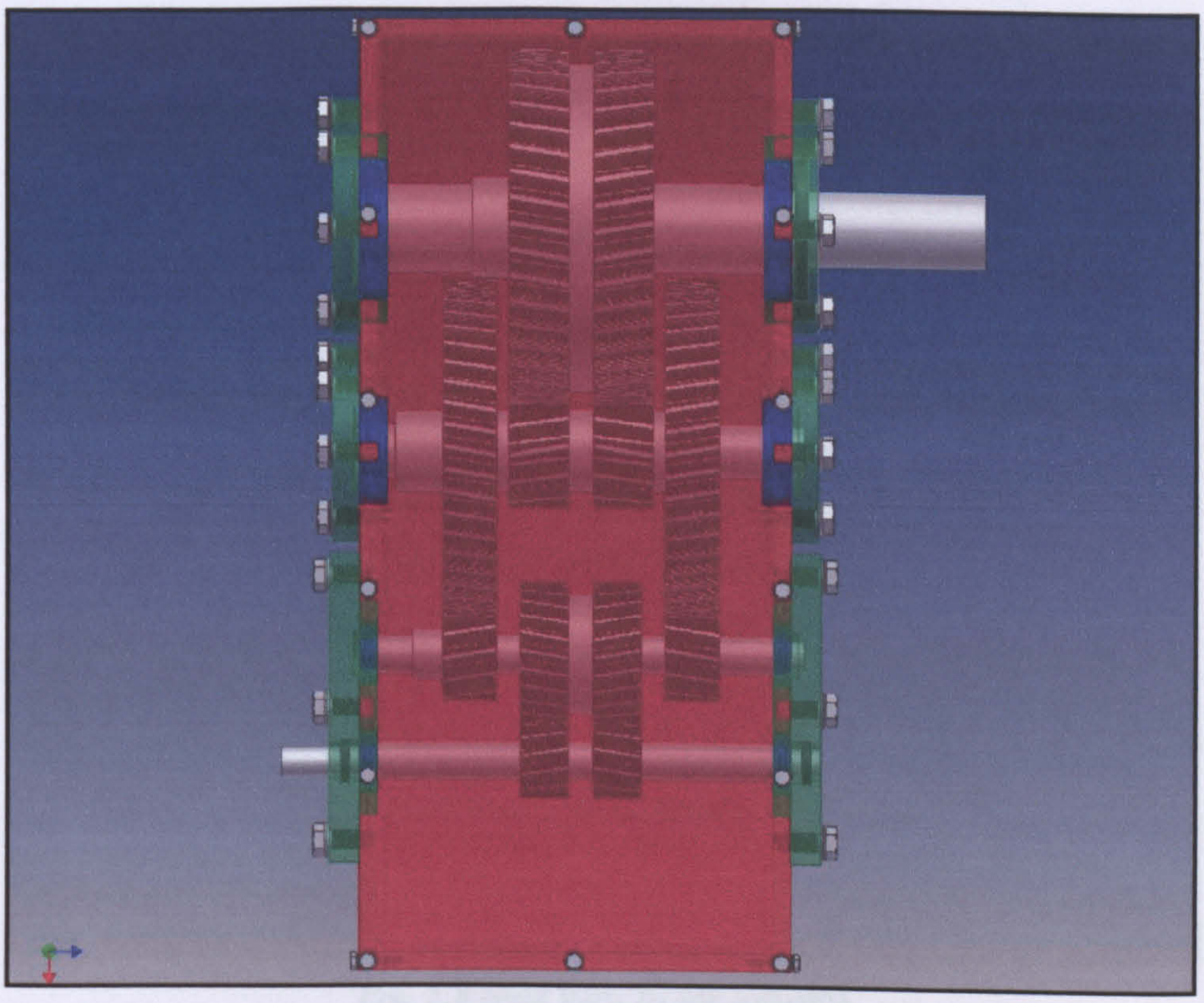

Fig. 5.7 Top view of the gearbox

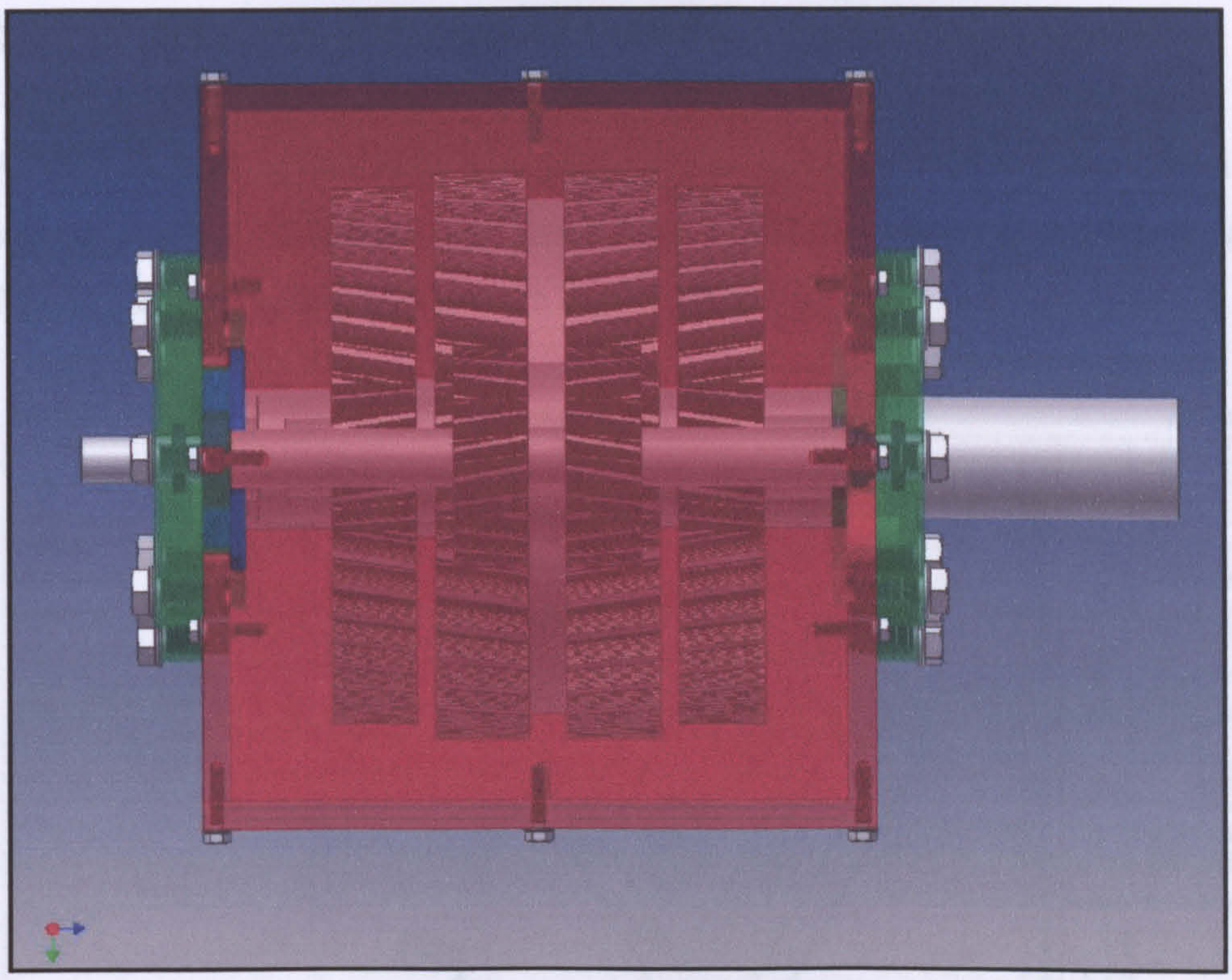

Fig. 5.8 Front view of the gearbox

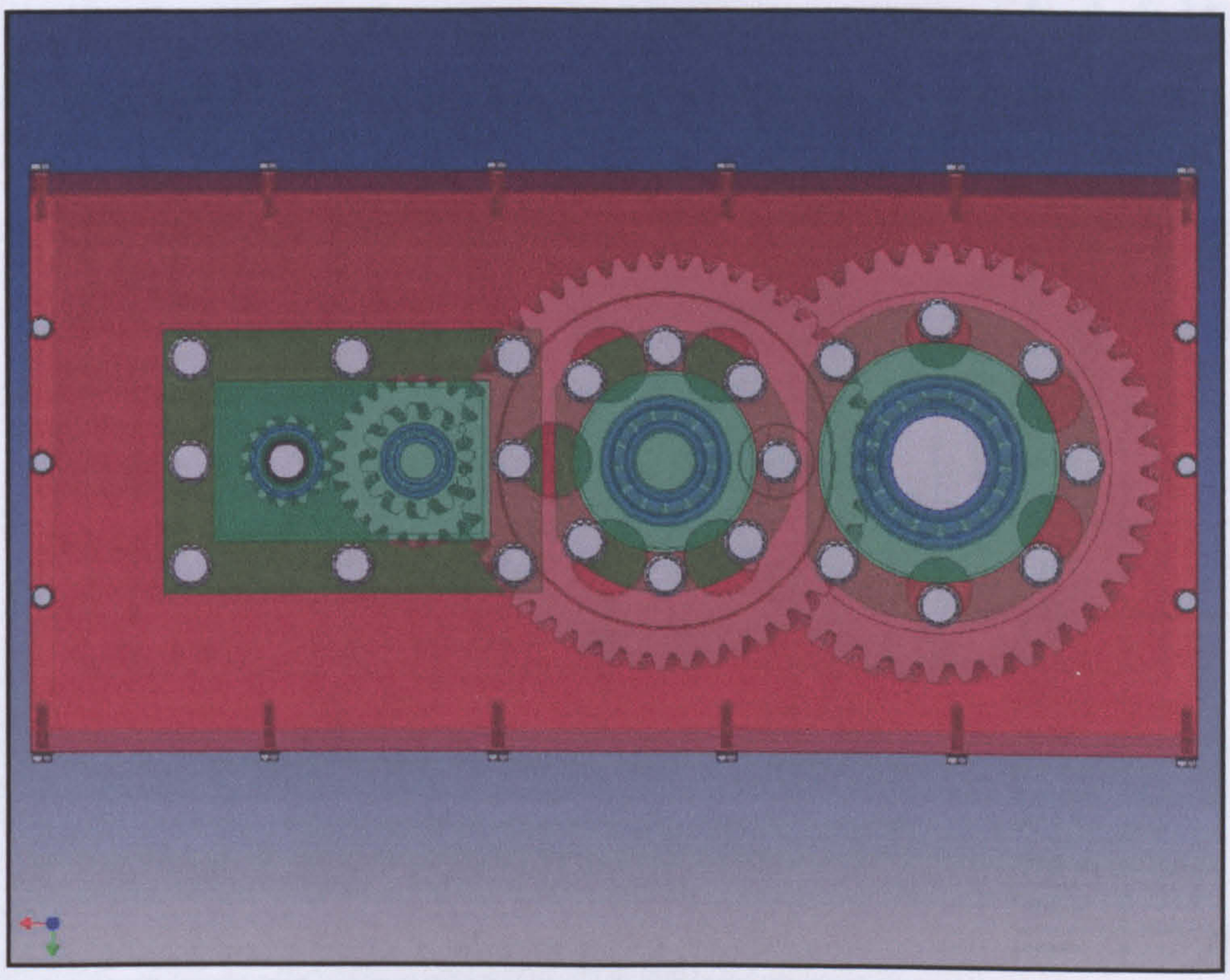

Fig. 5.8 Side view of the gearbox

5.2.1.4 Manufacturing of Reduction Gearbox

The manufacture of the reduction gearbox was carried out at the workshops of Jordan University of Science and Technology. Detail drawings of the various parts of the reduction gearbox are shown in Figs. 5.10 to 5.21.

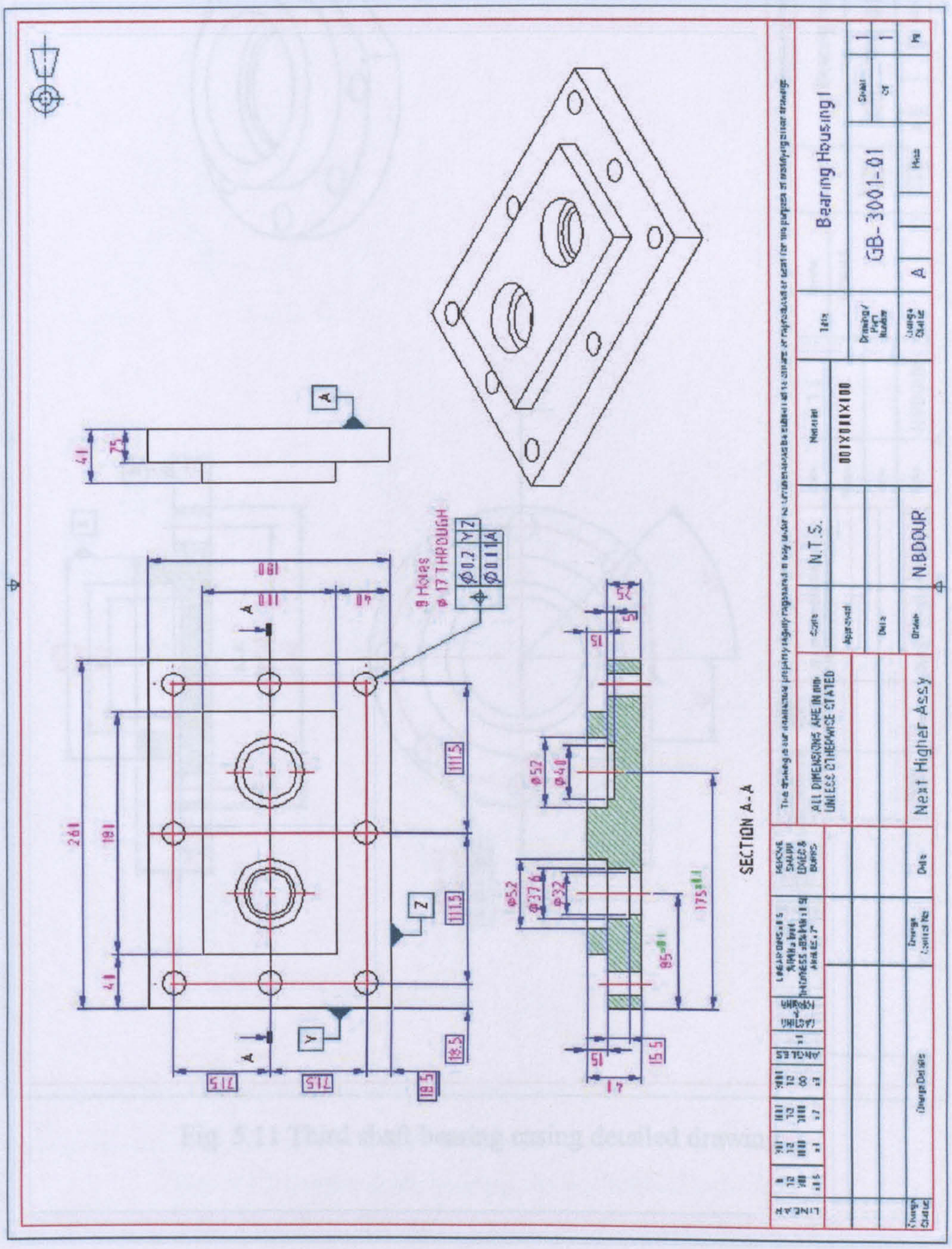

5.10 First and second shaft bearing casing detailed drawing

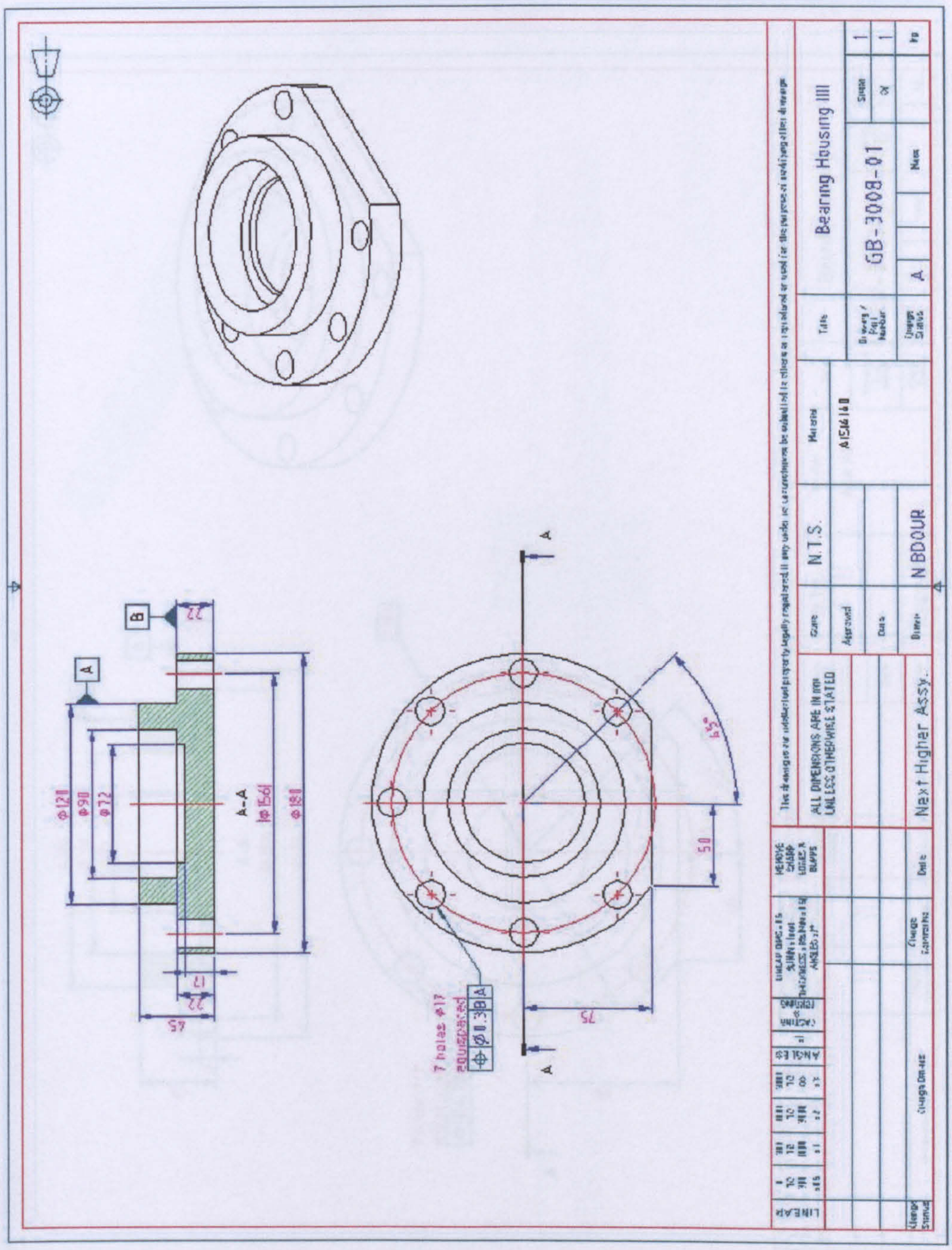

Fig. 5.11 Third shaft bearing casing detailed drawing

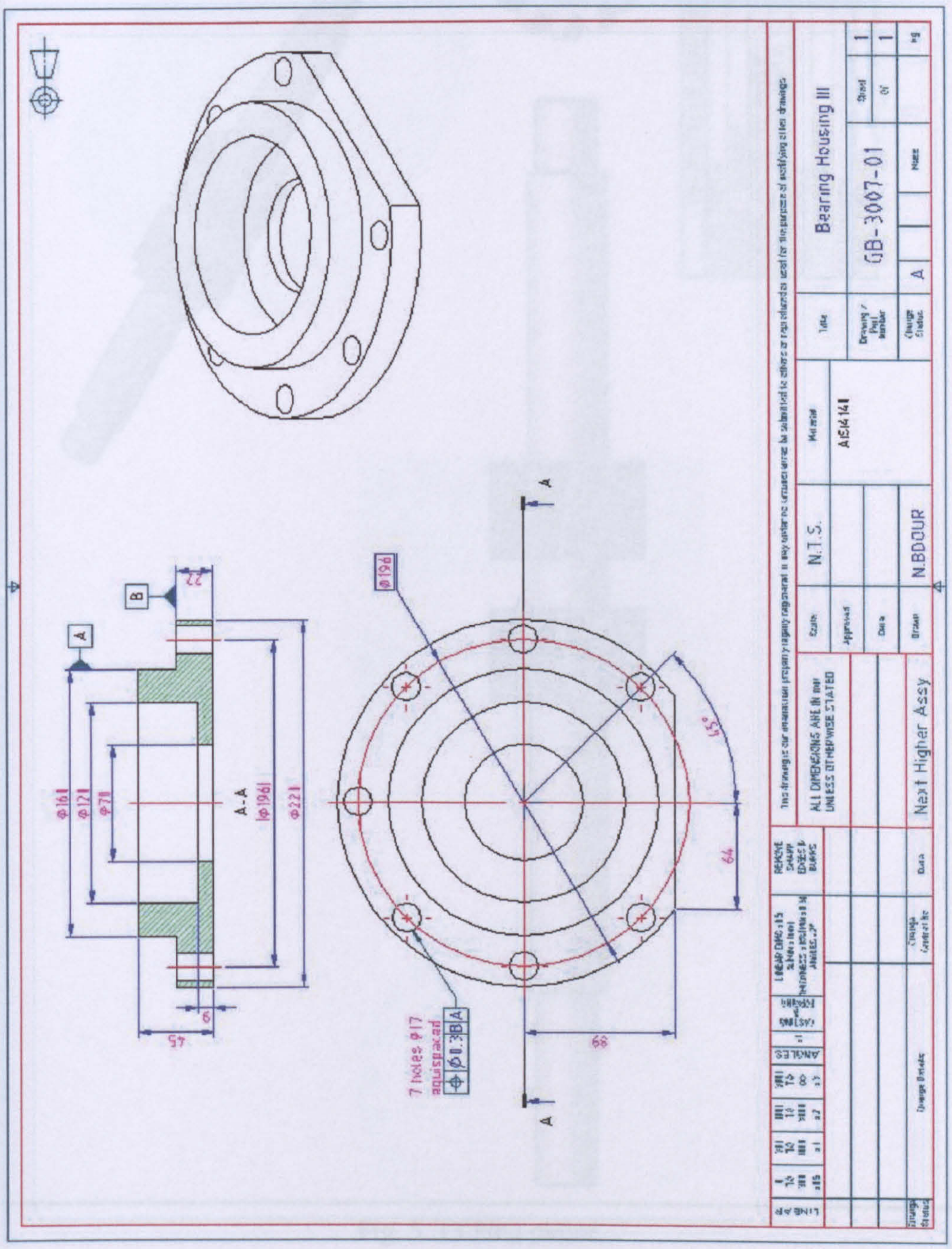

Fig. 5.12 Output shaft bearing casing detailed drawing

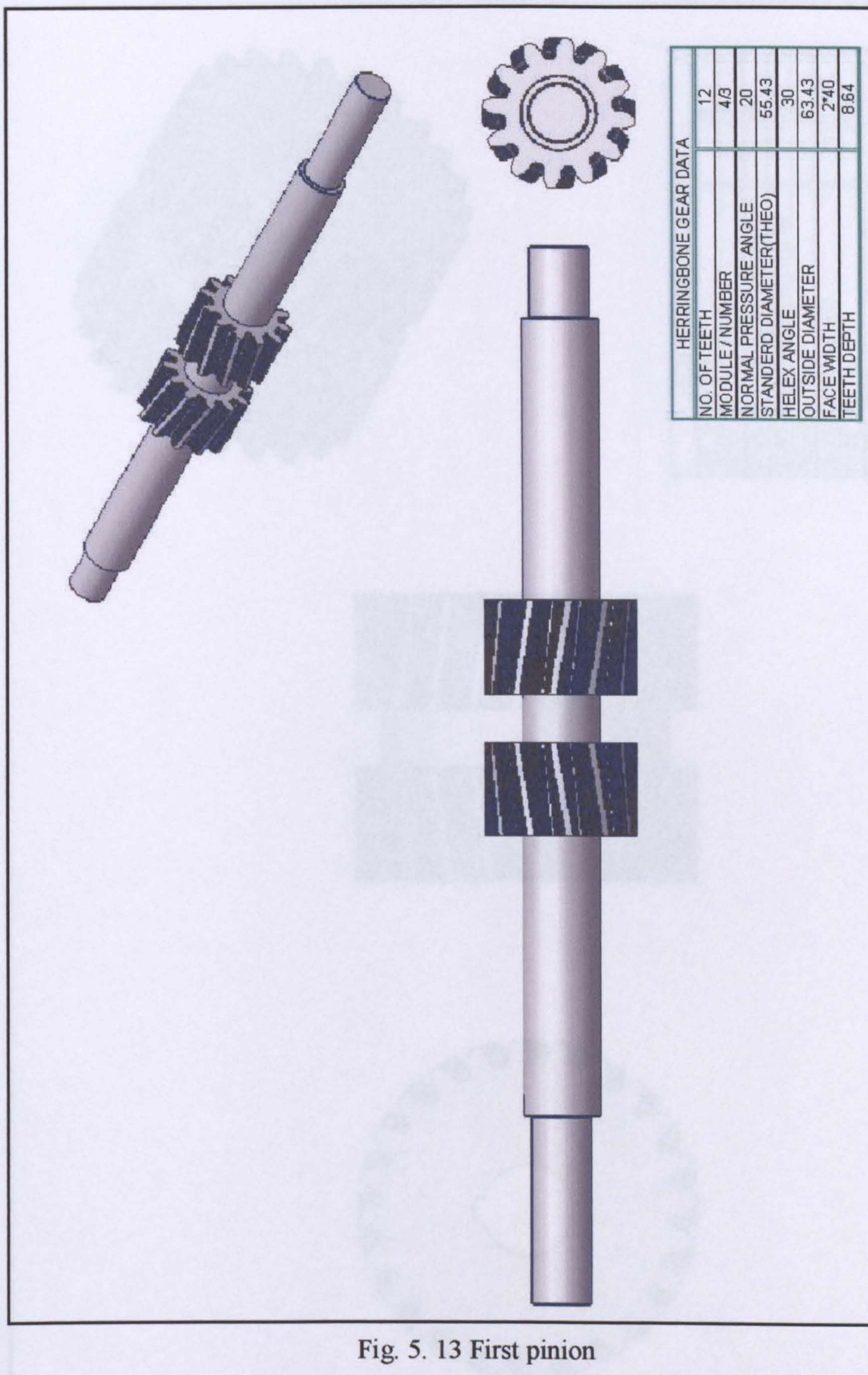

Fig. 5. 13 First pinion

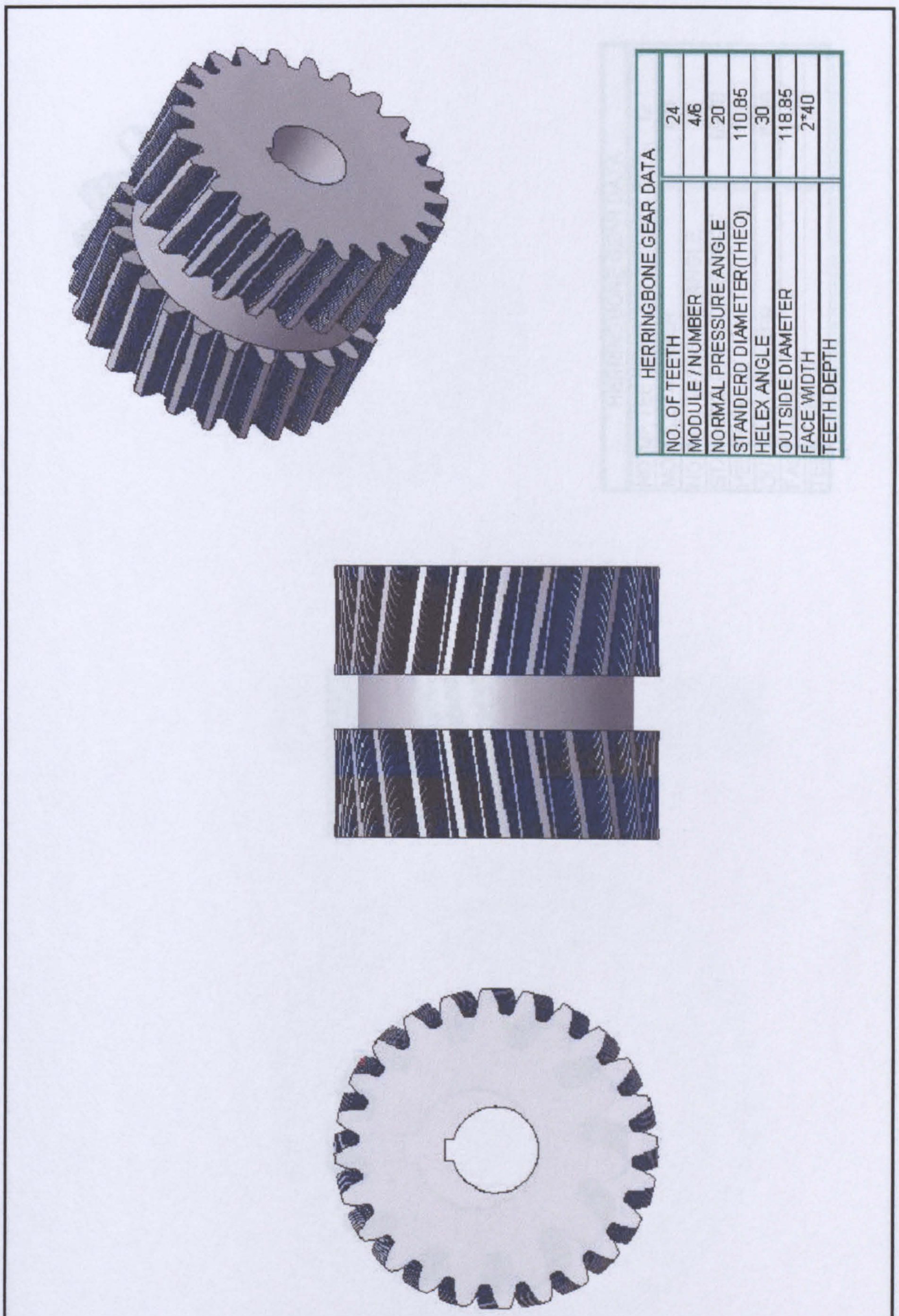

Fig. 5.14 First gear

HERRINGBONE GEAR DATA	
NO. OF TEETH	12
MODULE / NUMBER	5/3
NORMAL PRESSURE ANGLE	20
STANDERD DIAMETER(THEO)	69.28
HELEX ANGLE	30
OUTSIDE DIAMETER	79.28
FACE WIDTH	2*45
TEETH DEPTH	

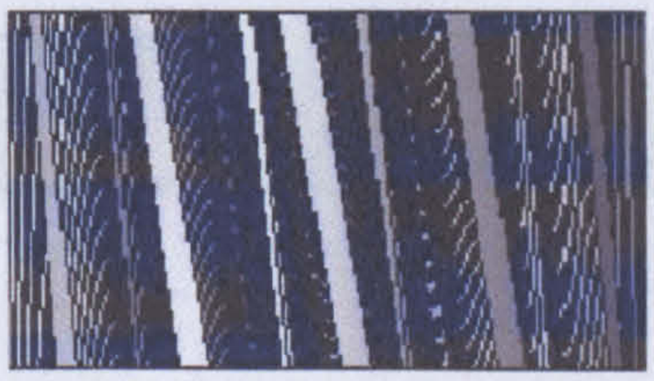

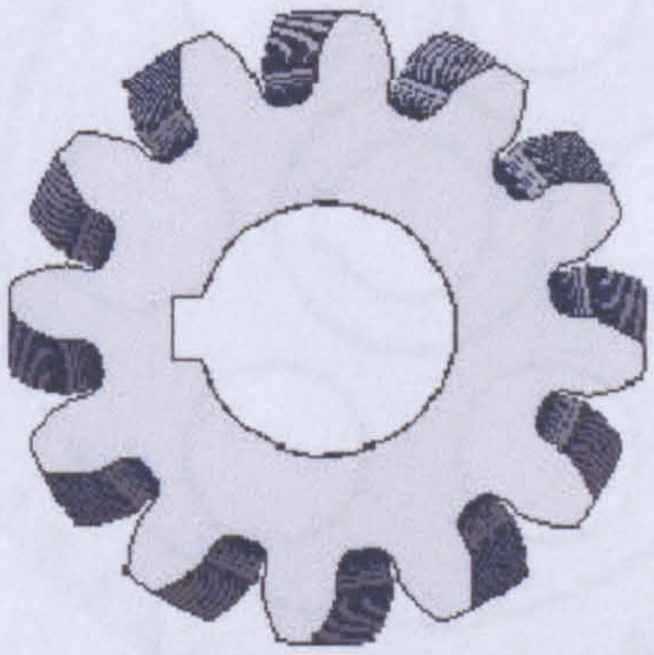

Fig. 5. 15 Second pinion

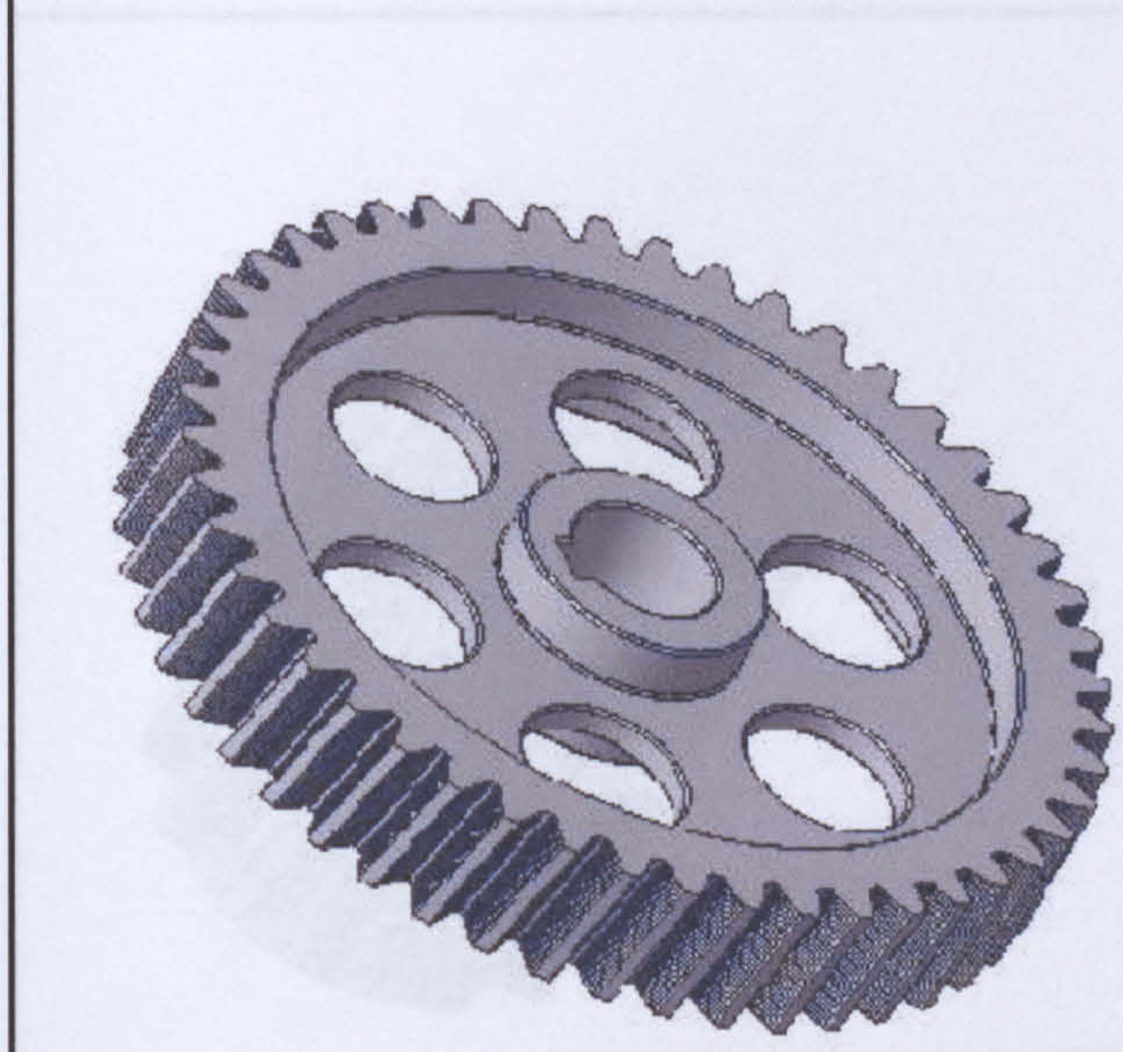

HERRINGBONE GEAR DATA	
NO. OF TEETH	48
MODULE / NUMBER	5/7
NORMAL PRESSURE ANGLE	20
STANDERD DIAMETER(THEO)	277.14
HELEX ANGLE	30
OUTSIDE DIAMETER	287.14
FACE WIDTH	2*45
TEETH DEPTH	

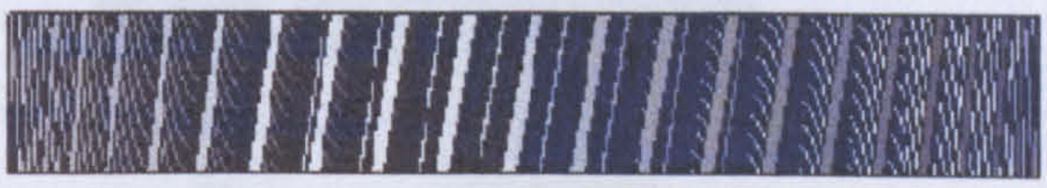

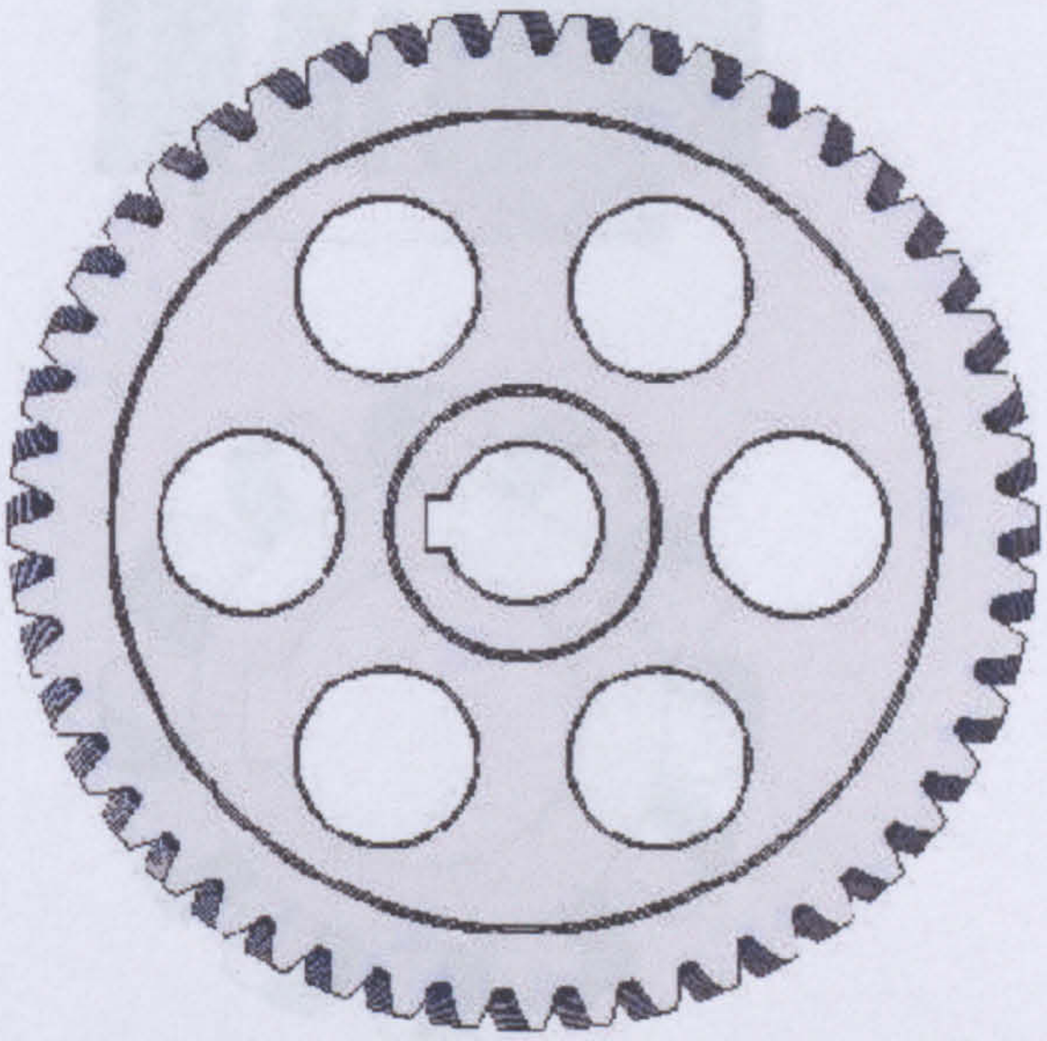

Fig. 5.16 Second gear

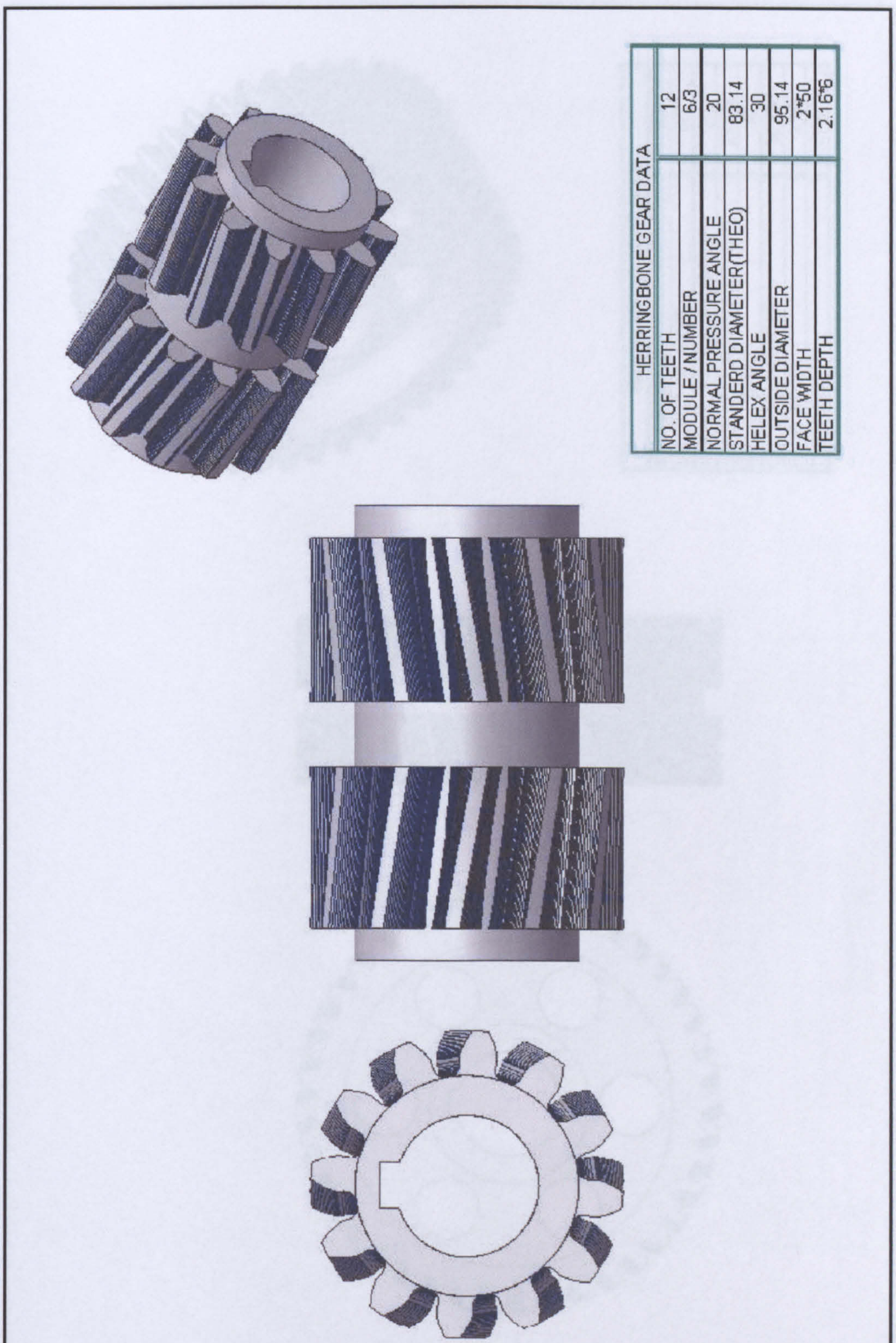

Fig. 5.17 Third pinion

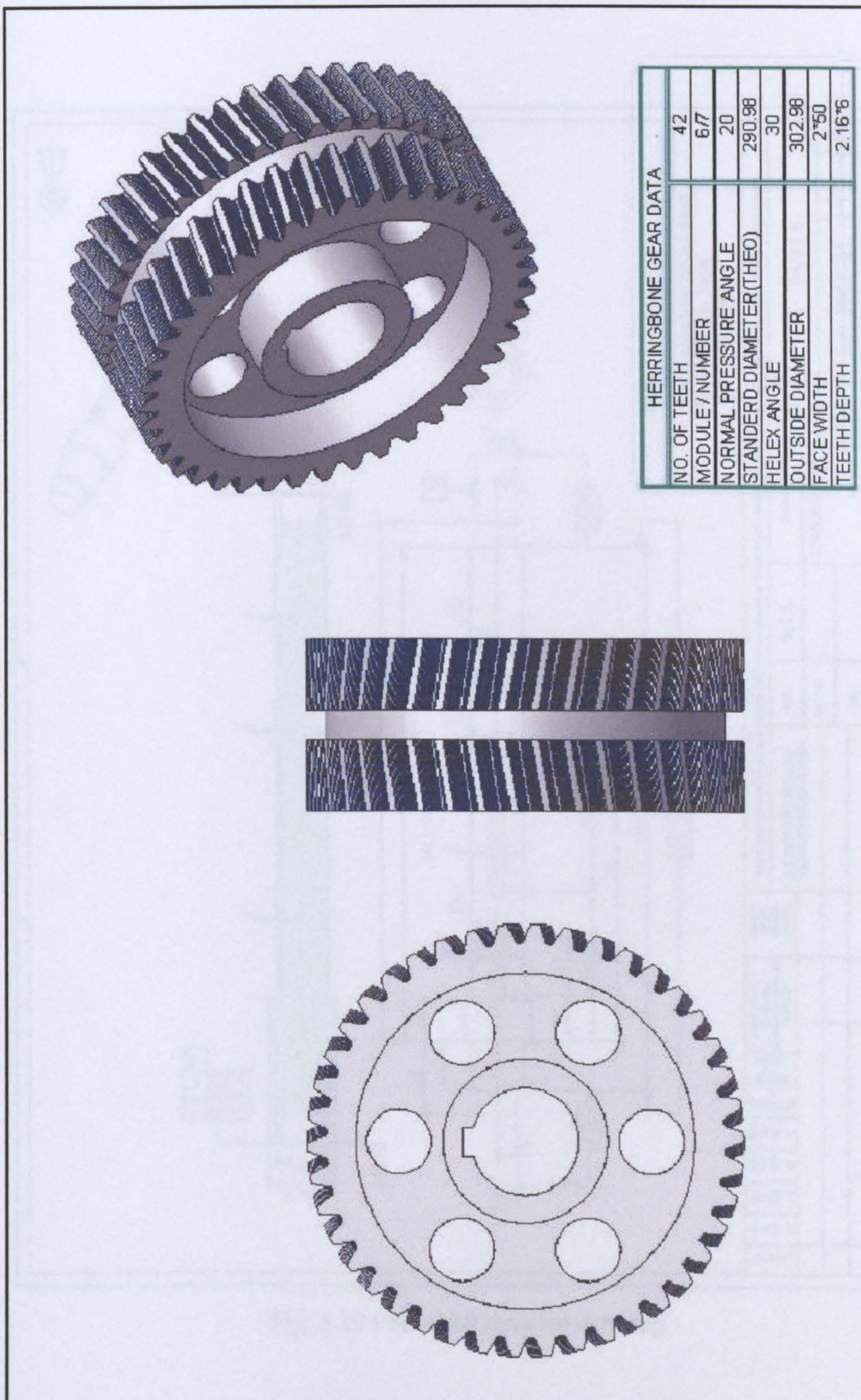

Fig. 5.18 Third Gear

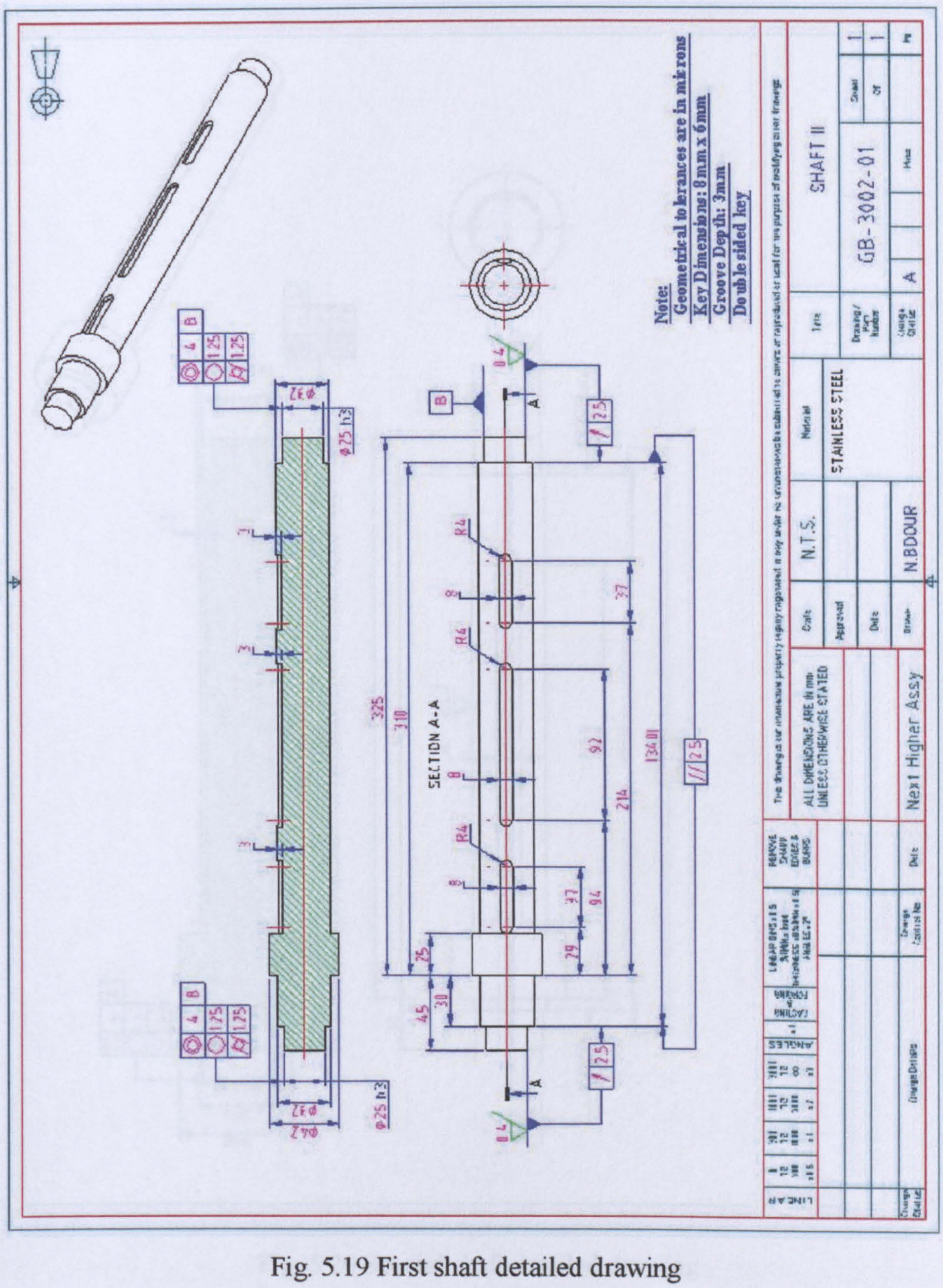

Fig. 5.19 First shaft detailed drawing

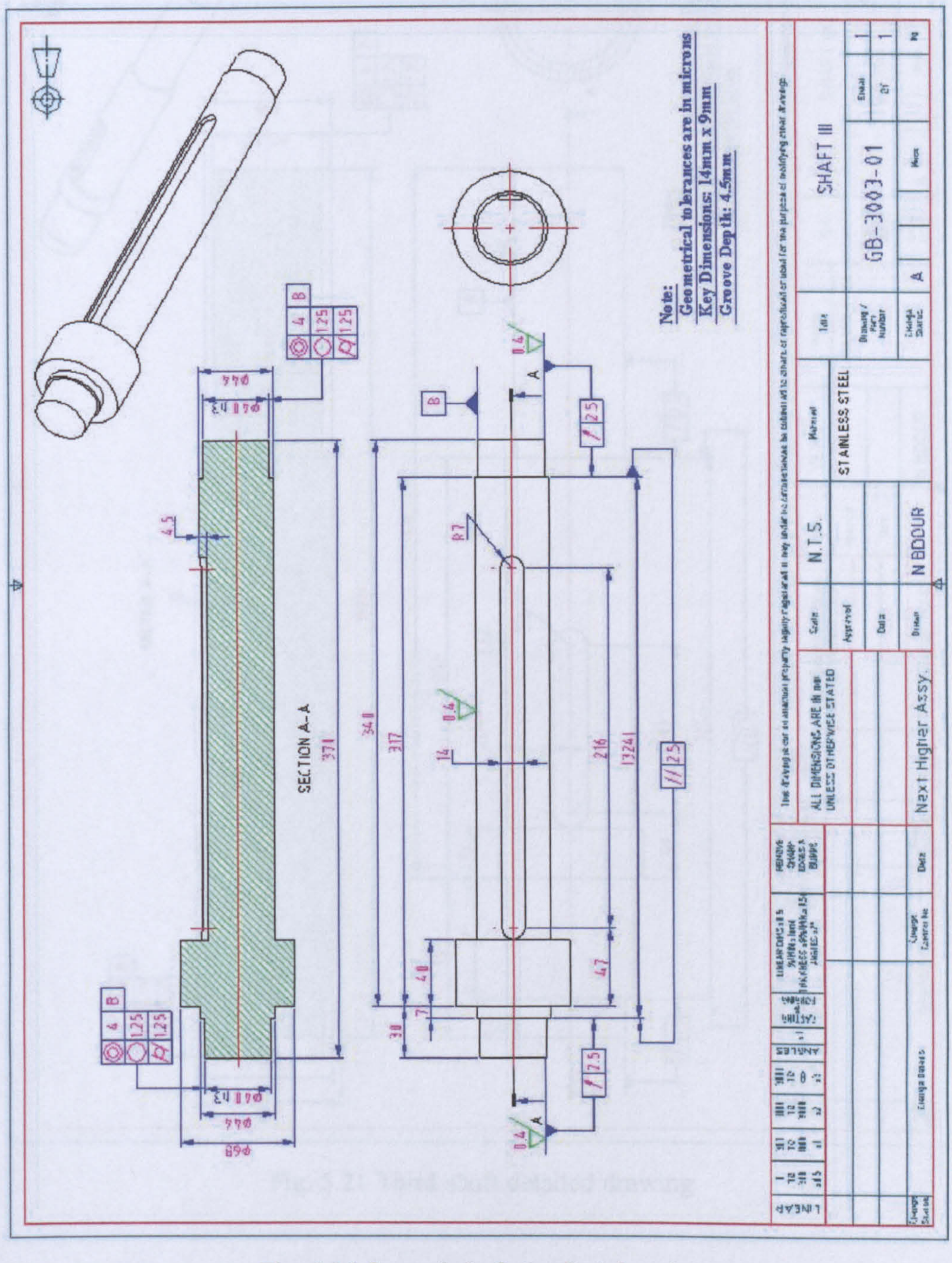

Fig. 5.20 Second shaft detailed drawing

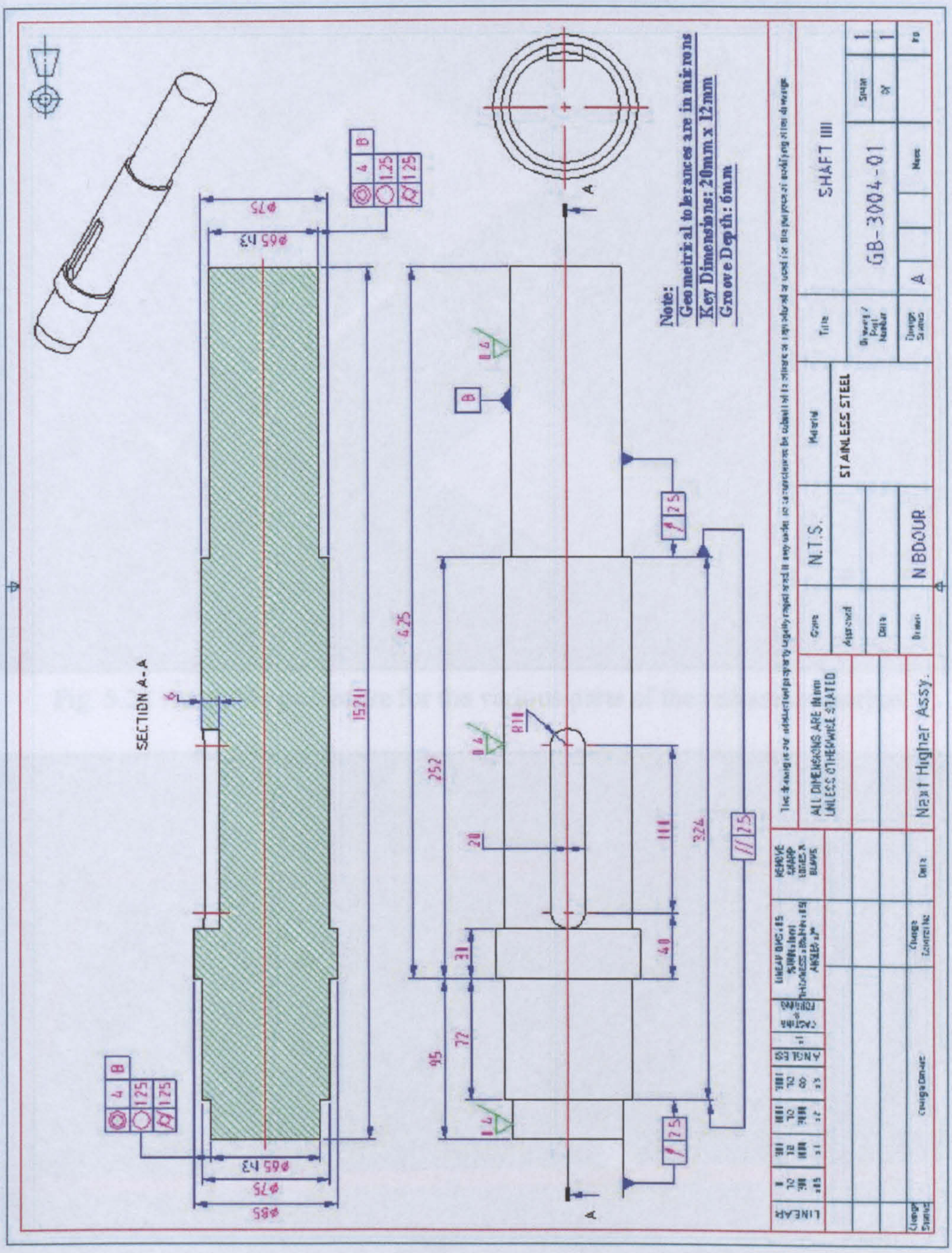

Fig. 5.21 Third shaft detailed drawing

The assembly procedure for the various parts of the reduction gearbox is shown in Fig. 5.22 and the complete machined reduction gearbox is depicted in Fig. 5.23.

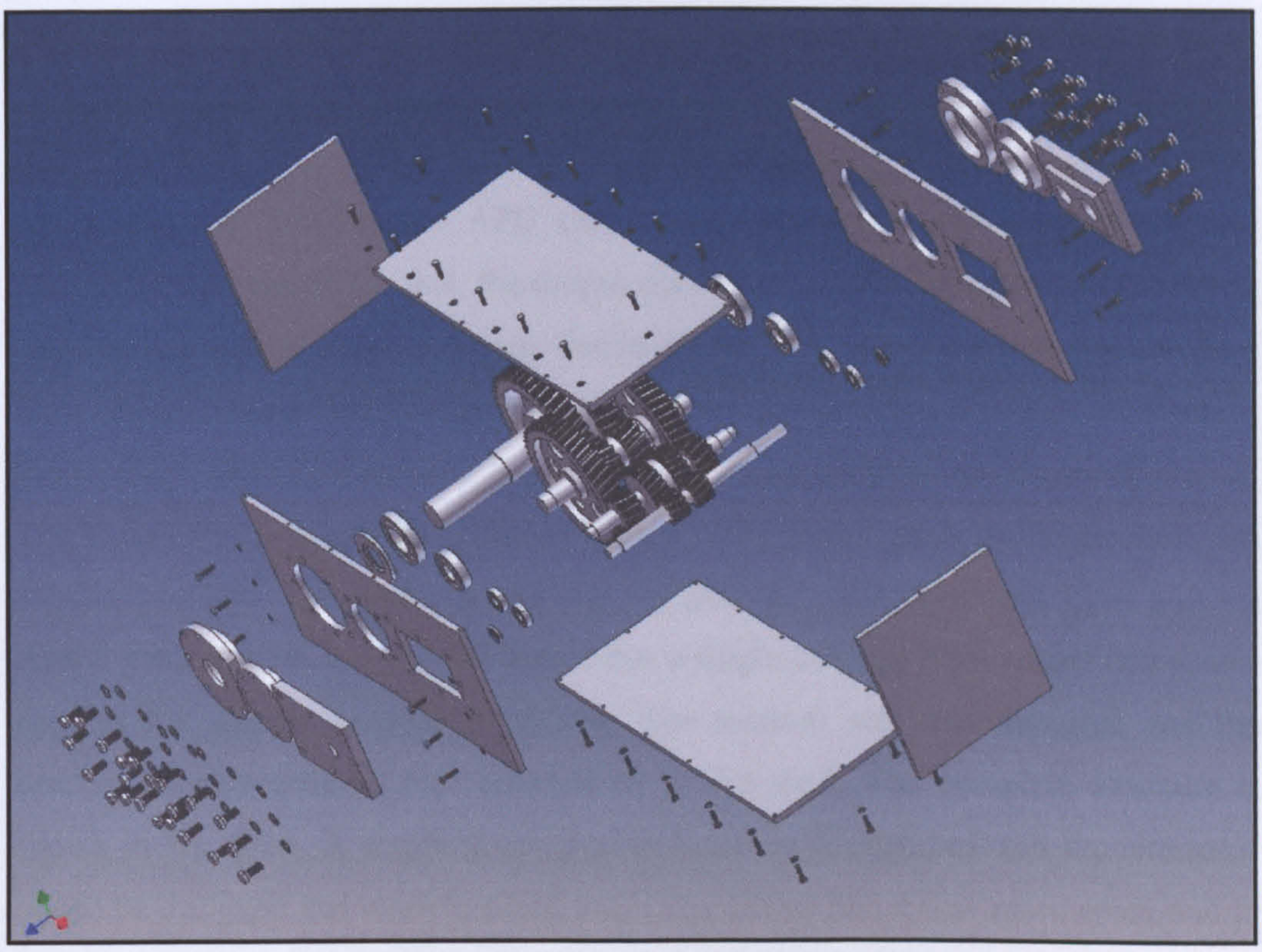

Fig. 5.22 Assembly procedure for the various parts of the reduction gearbox

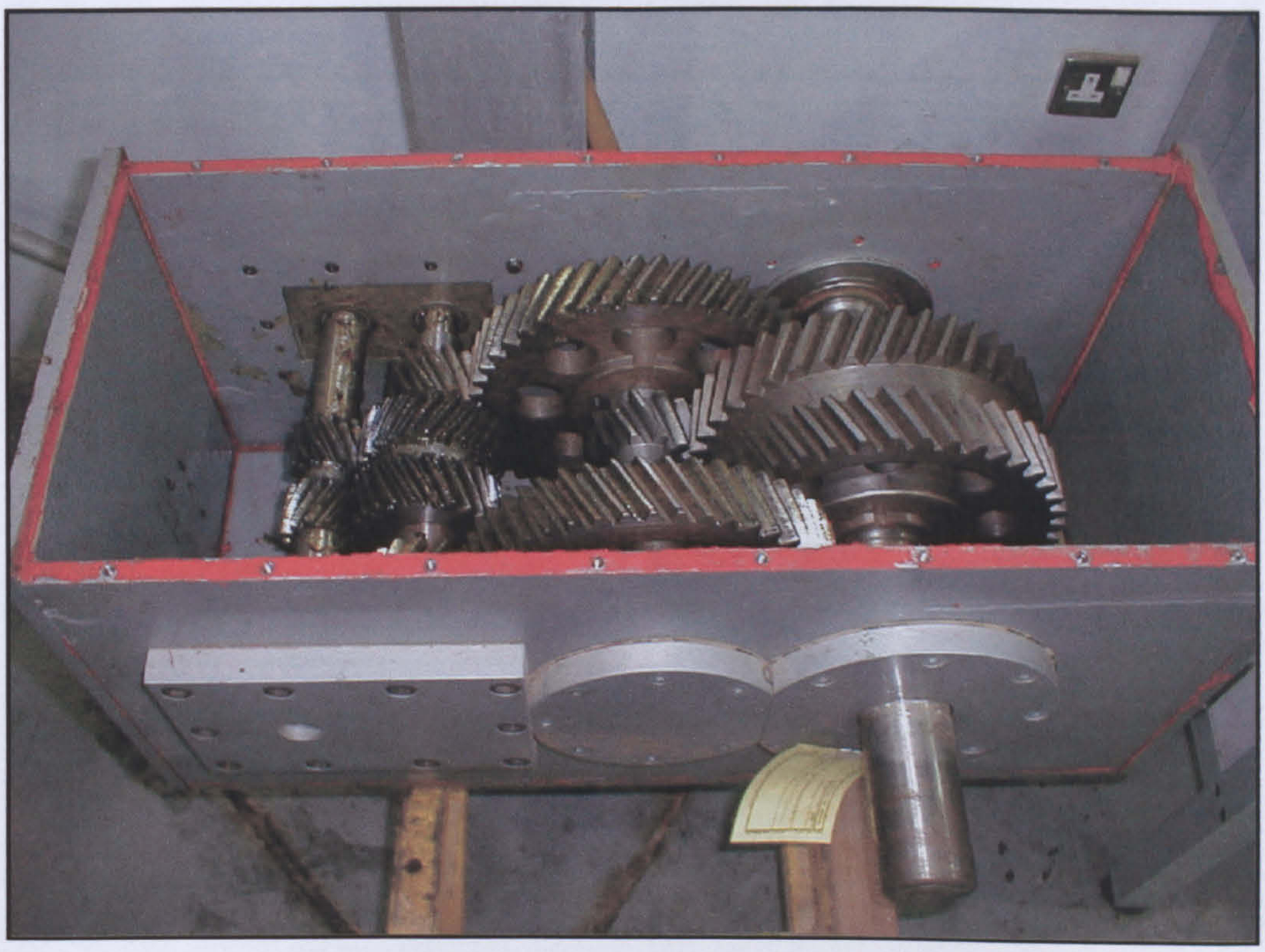

Fig. 5.23 The complete machined reduction gearbox

5.2.2 Modifying the APU Stand for the Adaptation of the Reduction Gearbox and the Electrical Generator

The connection between the APU stand and the gearbox was a straightforward procedure. The reason for that, the output shaft of the APU was a female spline shaft and this was considered in the early design of the input shaft of the gearbox to be a male spline so that direct coupling can be achieved.

The connection between the alternator side and the output shaft of the gearbox was another problem. The problem was that the alternator was taken out from a diesel engine generator set and this alternator has a single bearing. This means that a new support for another bearing is needed. The support was manufactured and the bearing housing (pillow) was selected to fit the shaft. The complete structure is shown in Fig. 5.24. A coupling component between the gearbox and the alternator has to be designed and manufactured but it was found that it was more economic to buy a ready made one. This coupling component is shown in Fig. 5. 25.

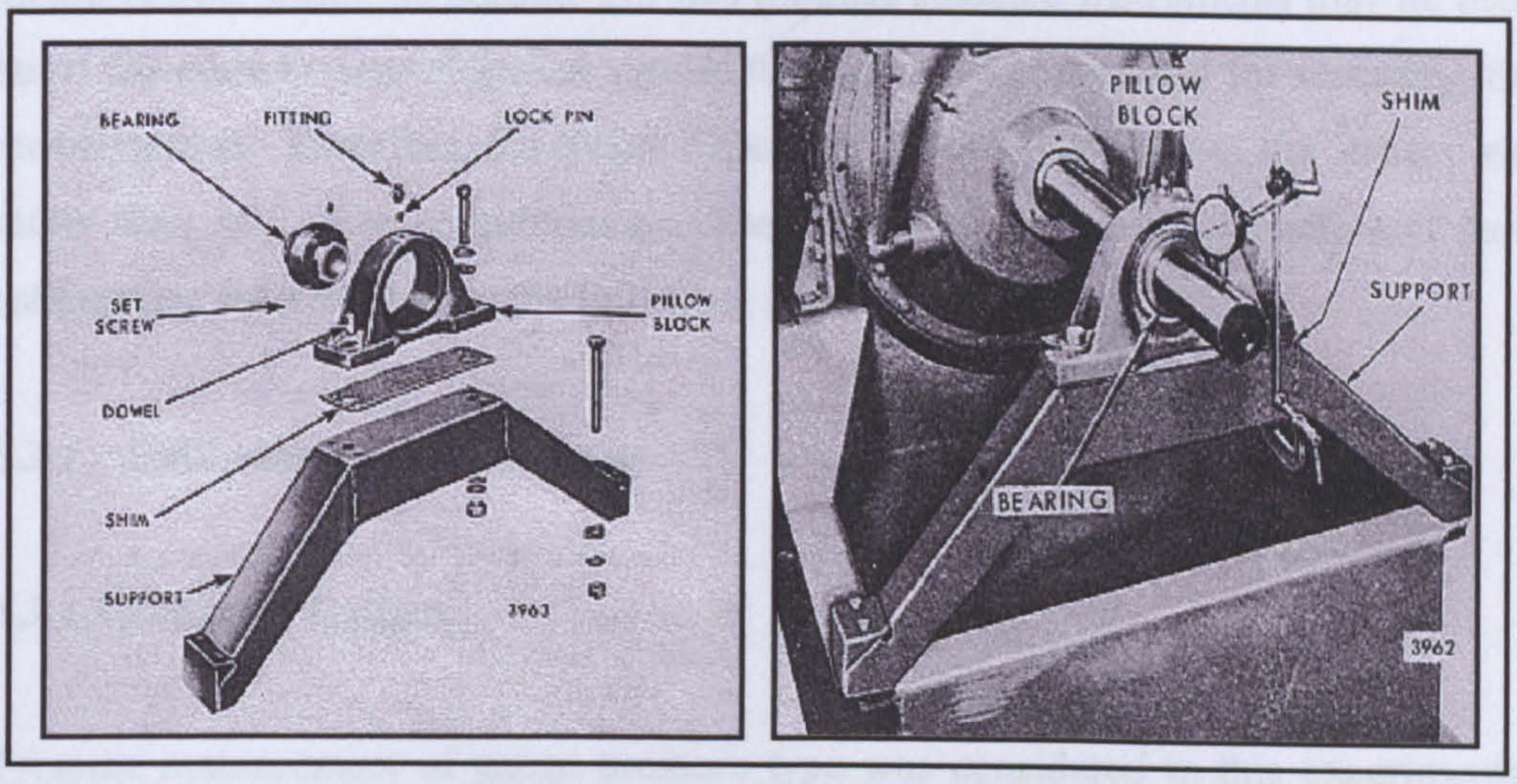

Fig. 5.24 Complete structure of support and bearing housing for the electrical alternator

Fig. 5.25 Main shaft Coupling

5.3 Instrumenting the Test Facility

The measurements needed to determine experimentally the performance of the gas turbine engine are usually pressures, temperatures, mass flow rates and rotational speed at various locations as shown on the test rig, Fig. 5.1. The quantities to be measured were not likely to change with time therefore only steady state measurements would be needed. For this purpose standard instruments may be used but if the outputs were electrical signals it would very convenient for recording the measurements. Therefore, the choice depended on the availability of the instruments rather than any other considerations. The details of all the instruments and their calibrations are described in the following sections.

5.3.1 Calibration of Instruments

5.3.1.1 Pressure Gauges

Pressure measurement of gauge pressure type was considered in this experimental work. Their calibration was carried out using a highly pressurised air bottle connected to a calibrated mercury-filled U-tube manometer and a calibrated pressure standard indicator. The calibrated pressure standard indicator is a calibrated pressure transducer uses a 4-digit digital display. The justification for using two calibrated pressure instrument to provide more accuracy to the calibrated process.

The inlet pressure port of the pressure gauge was connected to the inlet of both the calibrated pressure standard indicator and the calibrated mercury-filled U-tube manometer via an X-connection (Fig. 5.26). A regulated valve provided between the pressurised air bottle and the rest of the calibration set. This was used to regulate the air pressure going to the calibration set and to facilitate data reading at intermediate stations (mercury column height versus pressure gauge output). The whole calibration set up is depicted in Fig. 5.26.

The air pressure was changed using the regulator valve and the pressure readings of the three instruments when air pressure stabilized were recorded. Since the pressure gauge readings were in pounds per square inch (PSI) and the manometer readings were in millimetre mercury (mmHg), the manometer readings were converted to PSI using the following equation:

$$\Delta P = \rho g L \tag{5.15}$$

where ΔP is the pressure difference in *Pascal*

ρ is the mercury density in kg/m^3

g is the gravitational acceleration in m/s^2

L is the length of the mercury column in the manometer in m

and $1\ Pascal = 1.45 \times 10^{-4}\ psi$

The pressure gauge was calibrated by adjusting the gauge pointer referenced according to both the manometer readings and the calibrated pressure standard indicator readings. However, the three instruments calibration process was repeated again for all pressure gauges to make sure that pressure gauges give the same outputs.

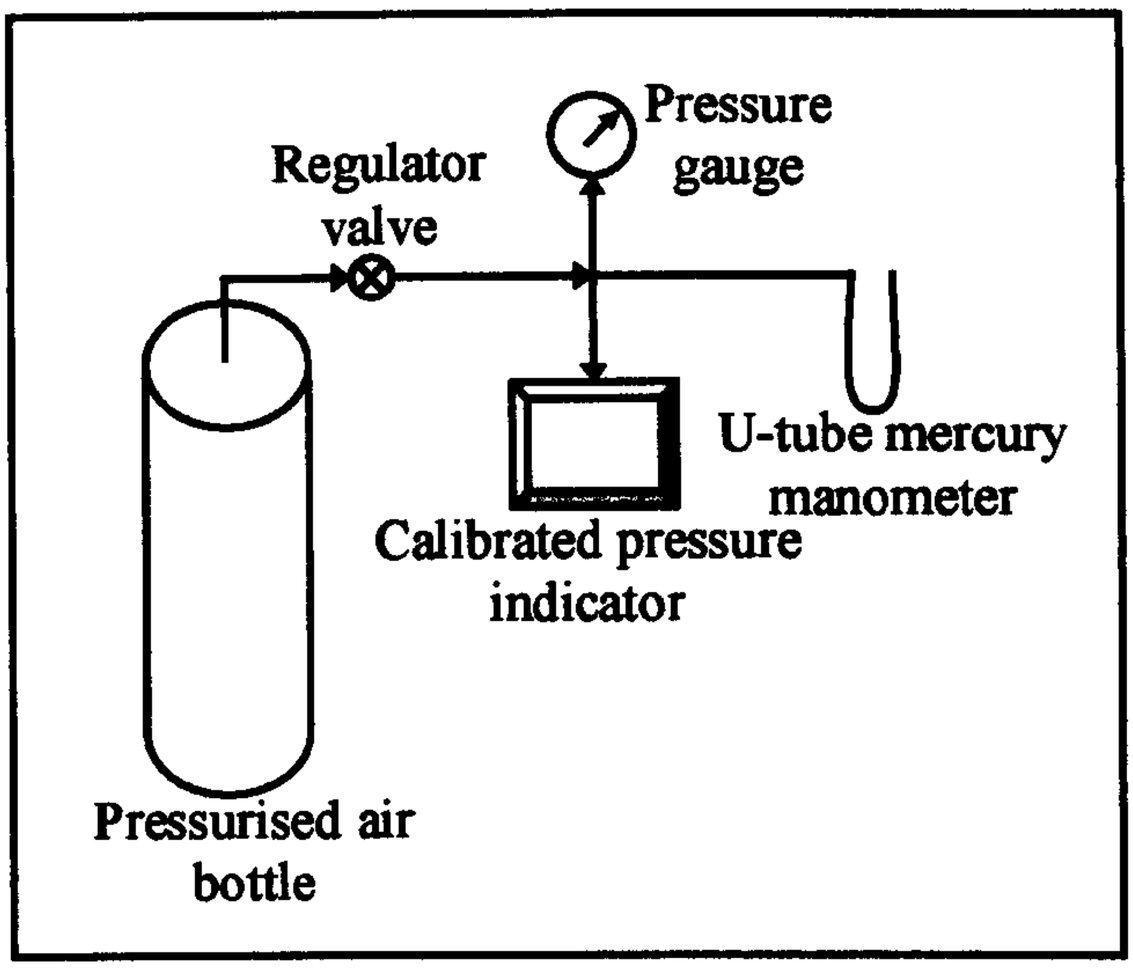

Fig. 5.26 Calibration equipment set for the pressure gauges

5.3.1.2 Temperature Transducers (Thermocouples)

A thermocouple is a temperature-measuring device made of two dissimilar wires. When those pair of wires is joined together at one end, a temperature difference between this end and the other end of the wires produces a voltage between the wires (Fig. 5.27). The magnitude of this voltage depends on the materials used for the wires and the amount of temperature difference between the joined ends and the other ends.

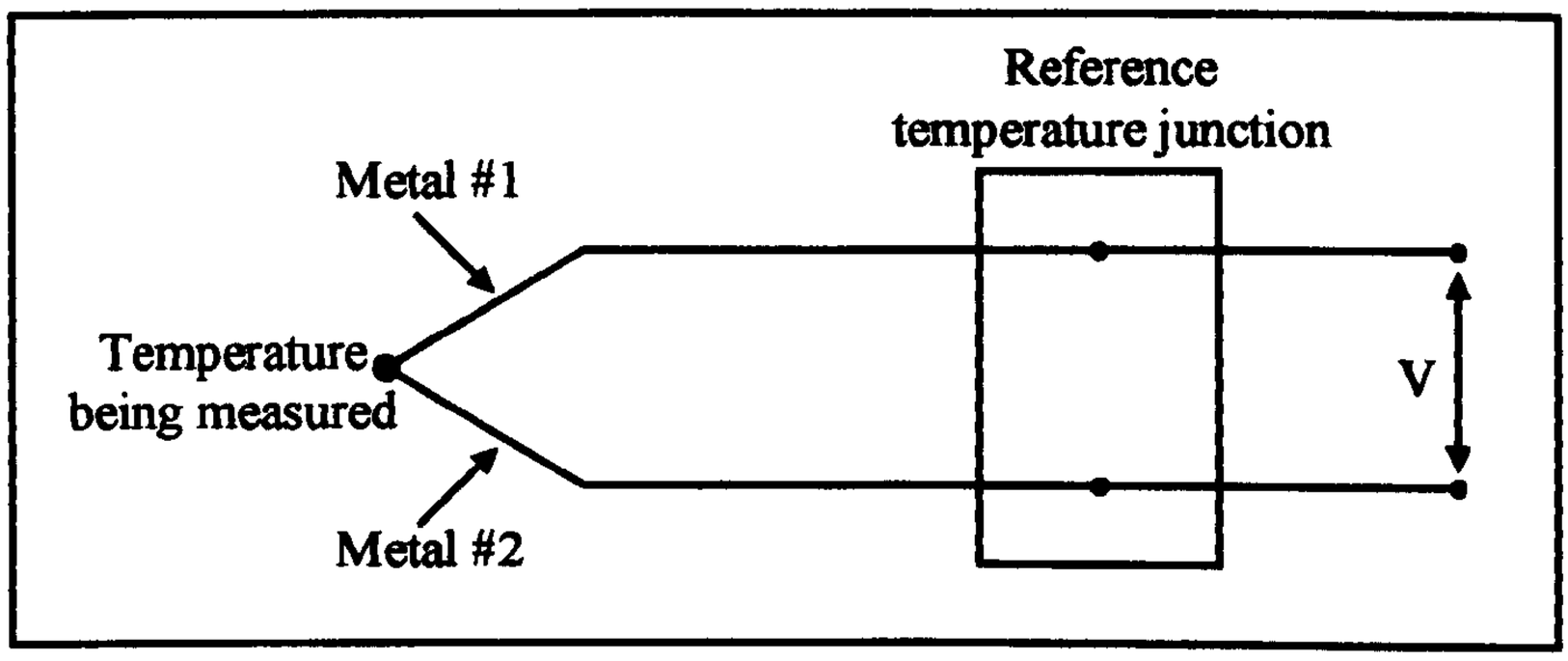

Fig. 5.27 Schematic representation of a thermocouple assembly

The thermocouples used in the experimental work are of "K" type thermocouples (Fig. 5.27). This type of thermocouples are made of chromel/Alumel alloy that has a working range from -200° C to 1372° C[44].

Fig. 5.27 "K" type thermocouple

The calibration process was carried out using an electrical heat source and a standard calibrated resistance temperature detector (RTD), which is considered an accurate temperature-measuring device. Both the thermocouple and the calibrated RTD were inserted in the same electrical heat source well. The calibrated RTD was connected to its equivalent temperature indicator while the thermocouple leads were connected to a calibrated 4-digit digital voltmeter. The equipment set up is depicted in Fig. 5.28. The electrical heat source temperature was controlled by the calibrated RTD in order to stabilise the required heat source well temperature and to facilitate the data reading of instruments.

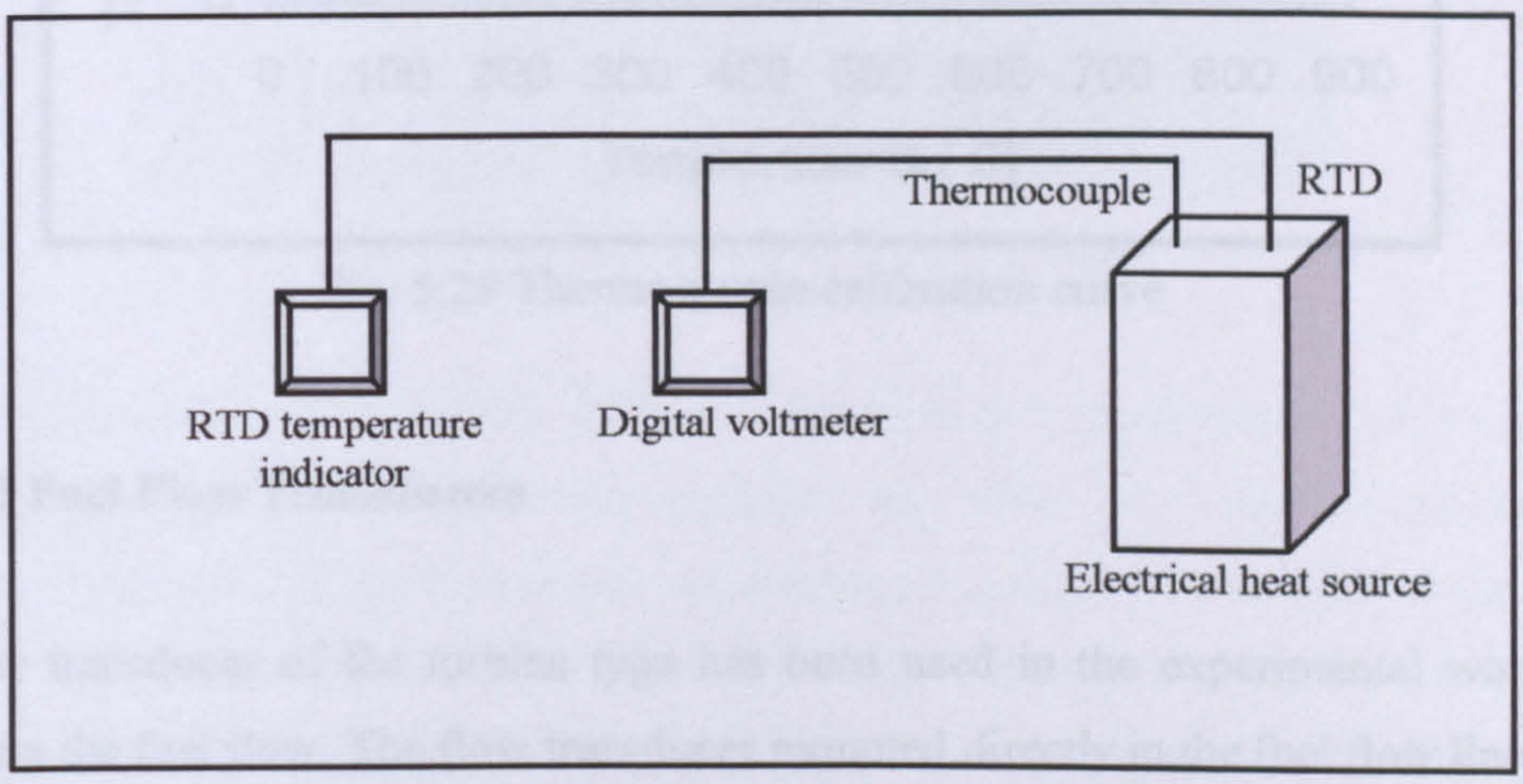

Fig. 5.28 Thermocouple calibration equipment set up

The process of calibration was carried as follows, the electrical heat source was switched on and set at a temperature of 50° C, when the heat source reached the desired stabilized temperature then the calibrated RTD temperature (in ° C) was recorded against the thermocouple output (in mV). This process was repeated in steps of 50° C until reaching the upper limit of the electrical heat source of 800° C. The recorded results have been tabulated in Table 5.4 and used to plot the thermocouple calibration curve as shown in Fig. 5.29.

Temp. (°C)	50	100	150	200	250	300	350	400
Volt (mV)	0.9865	3.043	5.094	7.096	9.1	11.14	13.24	15.33
Temp. (°C)	450	500	550	600	650	700	750	800
Volt (mV)	17.325	19.385	21.418	23.456	25.486	27.528	29.575	31.634

Table 5.4 Recorded results for thermocouple calibration

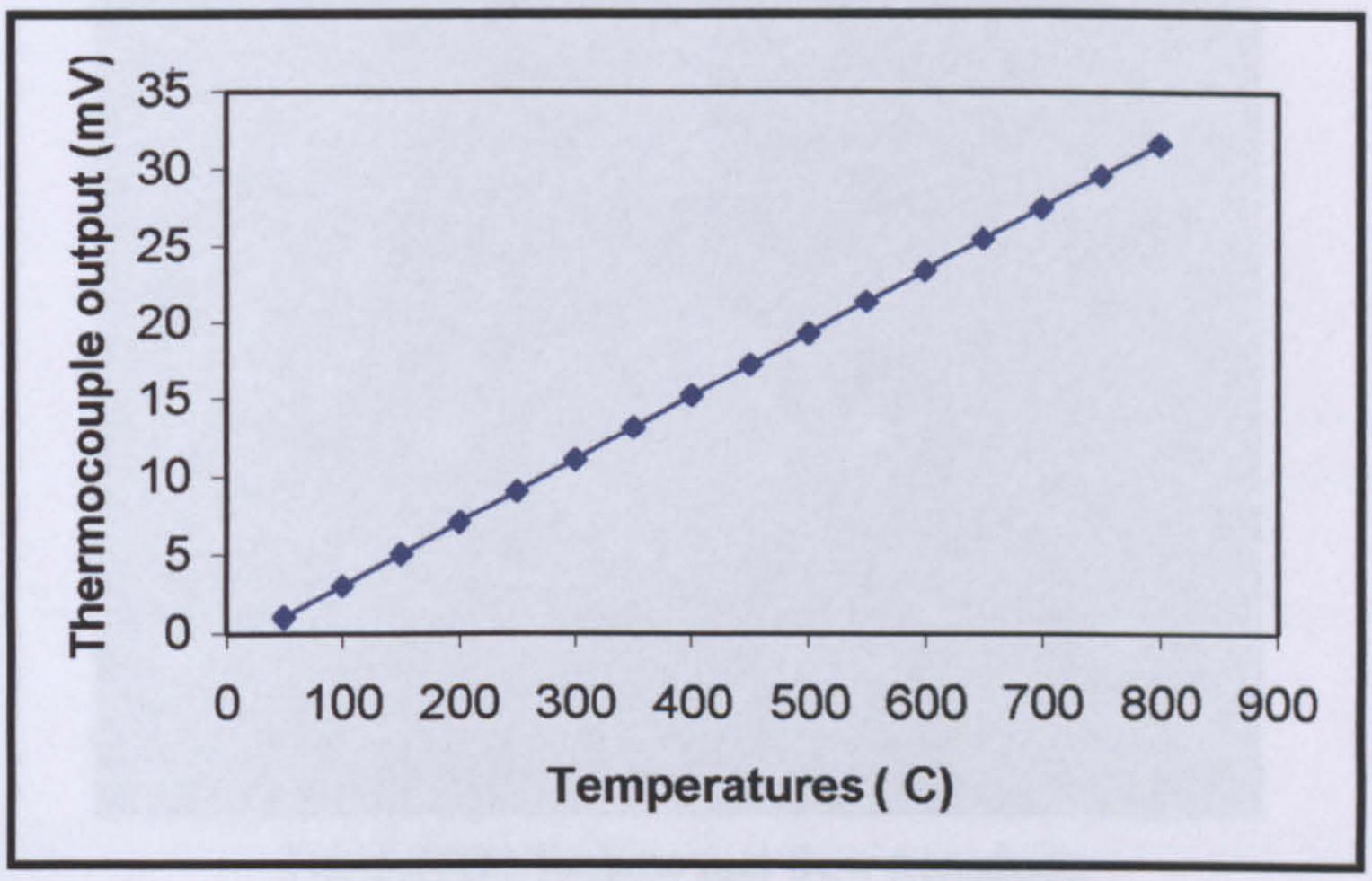

Fig. 5.29 Thermocouple calibration curve

5.3.1.3 Fuel Flow Transducers

A flow transducer of the turbine type has been used in the experimental work to measure the fuel flow. The flow transducer mounted directly in the fuel flow line and consists of cylindrically bored housing, flow straightners and a ferromagnetic turbine

assembly, and a magnetic pickoff. The components of fuel flow transducer are shown in Fig. 5.30(a) and fuel flow transducer is shown in Fig. 5.30(b).

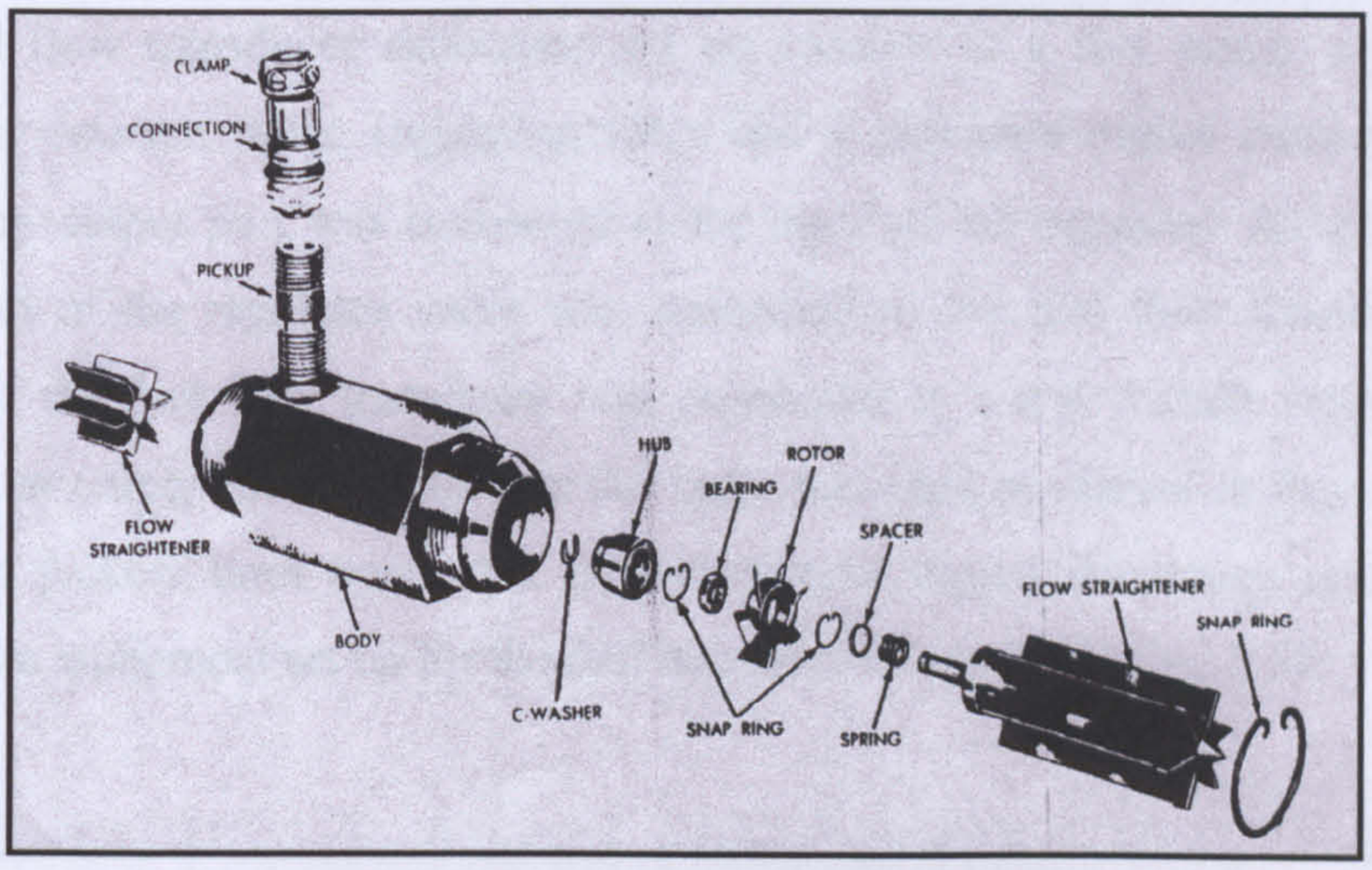

Fig. 5.30(a) Main components of turbine fuel flow transducer

Fig. 5.30(b) Turbine fuel flow transducer

Fluid passing through the turbine causes it to revolve at a speed directly proportional to the fluid velocity. As each ferromagnetic rotor passes the magnetic pickoff, it varies the magnetic pickoff reluctance, producing an ac signal. Since turbine speed is directly proportional to the fluid velocity, which produces ac signal, i.e. signal frequency, therefore, frequency is proportional to the rate of the flow $\dot{m}_f$. The output

signal can be fed into various types of instruments, to indicate the rate of flow, such as a frequency counter, a frequency converter or a voltmeter.

The fuel flow transducer calibration set up consists of a fuel pump, a calibrated frequency counter, timer, regulating valve and a calibrated digital mass scale. The fuel pump output port was connected to the input of the regulator valve where the other port of the regulator valve was connected to the fuel flow transducer. The output of the fuel flow transducer was connected to 2-way switch valve directed towards an empty fuel container or the main fuel tank as shown in Fig. 5.31. The magnetic pickoff lines connected to a calibrated digital frequency counter. The calibration equipment set up for the fuel transducer is shown in Fig. 5.31.

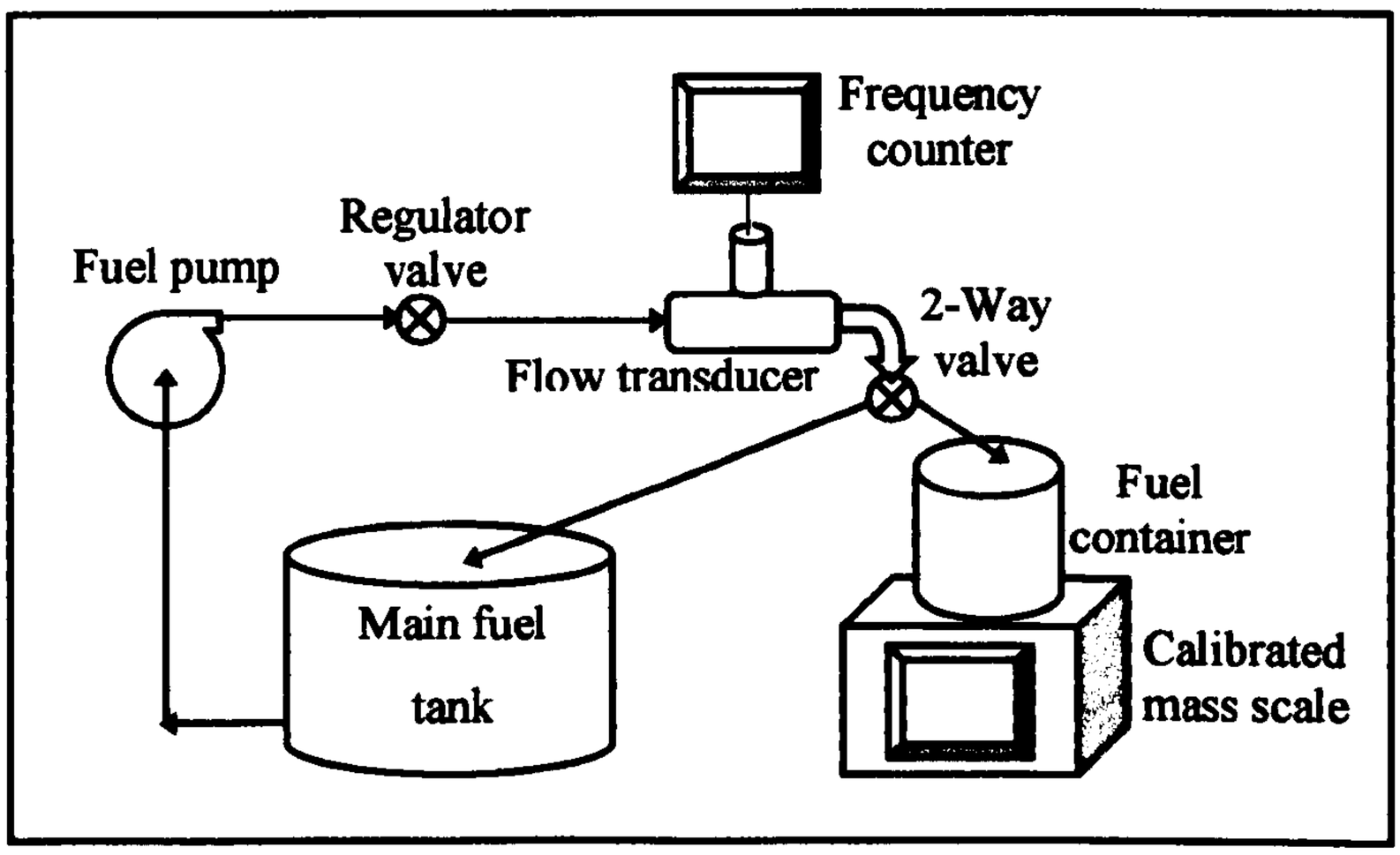

Fig. 5.31 The equipment set up for the fuel flow transducer

The process of calibration was carried out as follows: the fuel pump started while the regulator valve was fully opened and the 2-Way valve directed towards the fuel main tank. Time was given to the flow to stabilise then the flow directed towards the empty container as the timer started. During the next 20 seconds the frequency counter reading recorded then as the pump switched off the timer stopped and the fuel collected during the process weighed using the calibrated scale. The same process has been repeated every time the regulating valve partially closed. The measured frequencies, weight of fuel and time recorded have been tabulated, using

the tabulated data the flow rate calculated and added to the tabulated data at Table 5.5.

Measured			Calculated
Frequency (Hertz)	Weight (kg)	Time (seconds)	Flow rate (kg/s)
1500	2.835	19.25	0.147273
1200	2.268	19.25	0.117818
900	1.701	19.25	0.088364
600	1.134	19.2	0.059063
480	0.907	19.21	0.047215
360	0.68	19.26	0.035306
240	0.454	19.32	0.023499
180	0.34	19.32	0.017598
120	0.227	19.31	0.011756
90	0.17	19.22	0.008845
73	0.138	19.19	0.007191

Table 5.5 Recorded and calculated data for fuel flow transducer

The data measured and calculated has been used to plot the calibration curve that shown in Fig. 5.32.

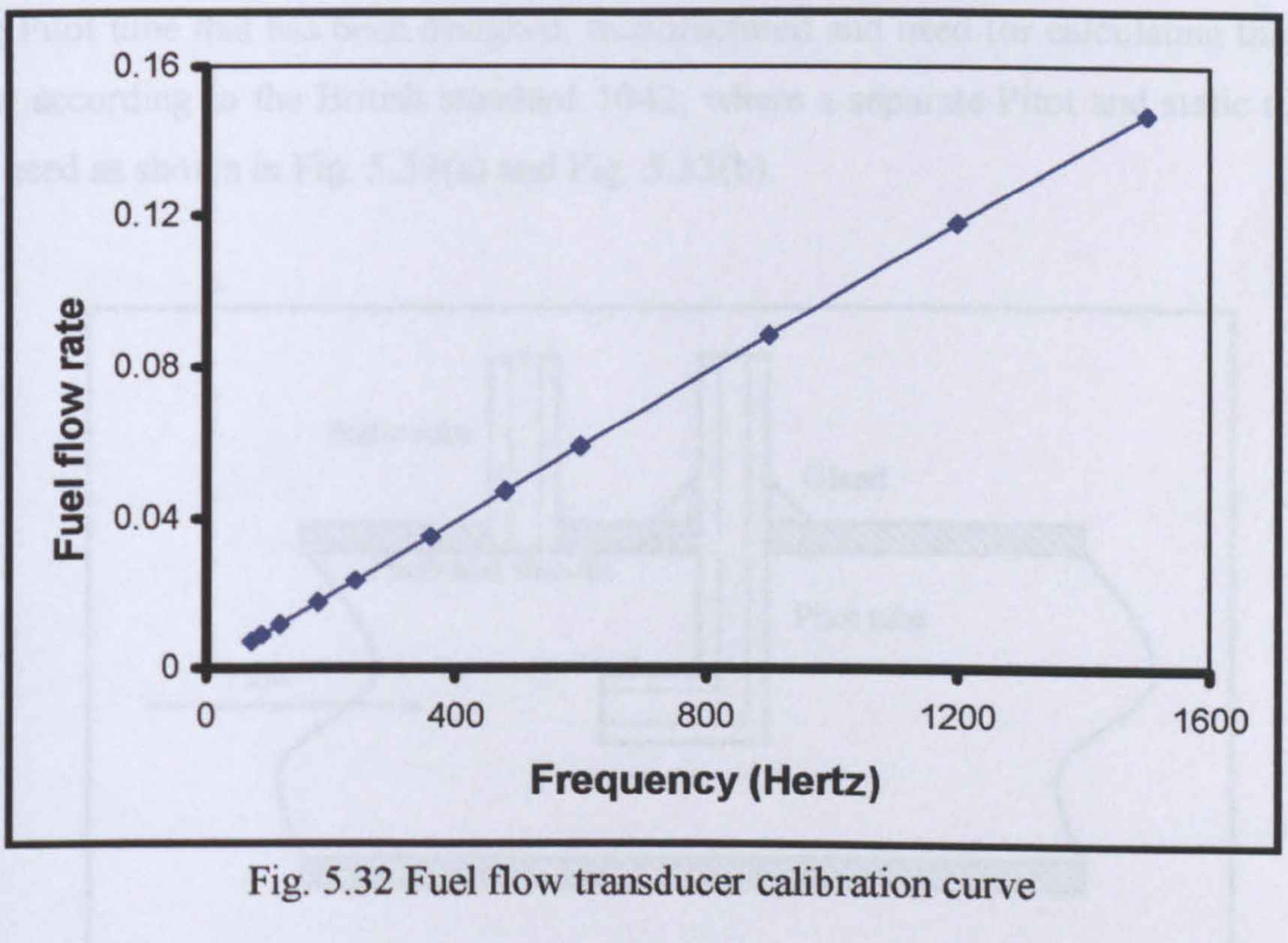

Fig. 5.32 Fuel flow transducer calibration curve

5.3.1.4 Gas Flow Pitot Tube

A Pitot tube was chosen to measure the gas flow rate in the current experimental work for the following reasons:

i. The Pitot tube can be easily manufactured and installed in the test rig.
ii. The Pitot tube produces no appreciable pressure loss.
iii. The Pitot tube can be inserted through comparatively small hole into the main gas stream without the necessity for shutting off the system.
iv. The Pitot tube can be used to measure local velocities at different points in the test rig.

The Pitot tube consists essentially of a tube with an open end placed in a direction to face a stream of fluid. The stream of fluid will produce an impact pressure in the tube derived from the loss of the fluid kinetic energy. This tube will give the sum of impact (dynamic) and static pressure; a Pitot tube must work in conjunction with a means of measuring the static pressure. This might be incorporated in the Pitot tube itself or in a simple connection in the wall of the main stream.

The Pitot tube that has been designed, manufactured and used for calculating the gas flow according to the British standard 1042, where a separate Pitot and static tubes are used as shown in Fig. 5.33(a) and Fig. 5.33(b).

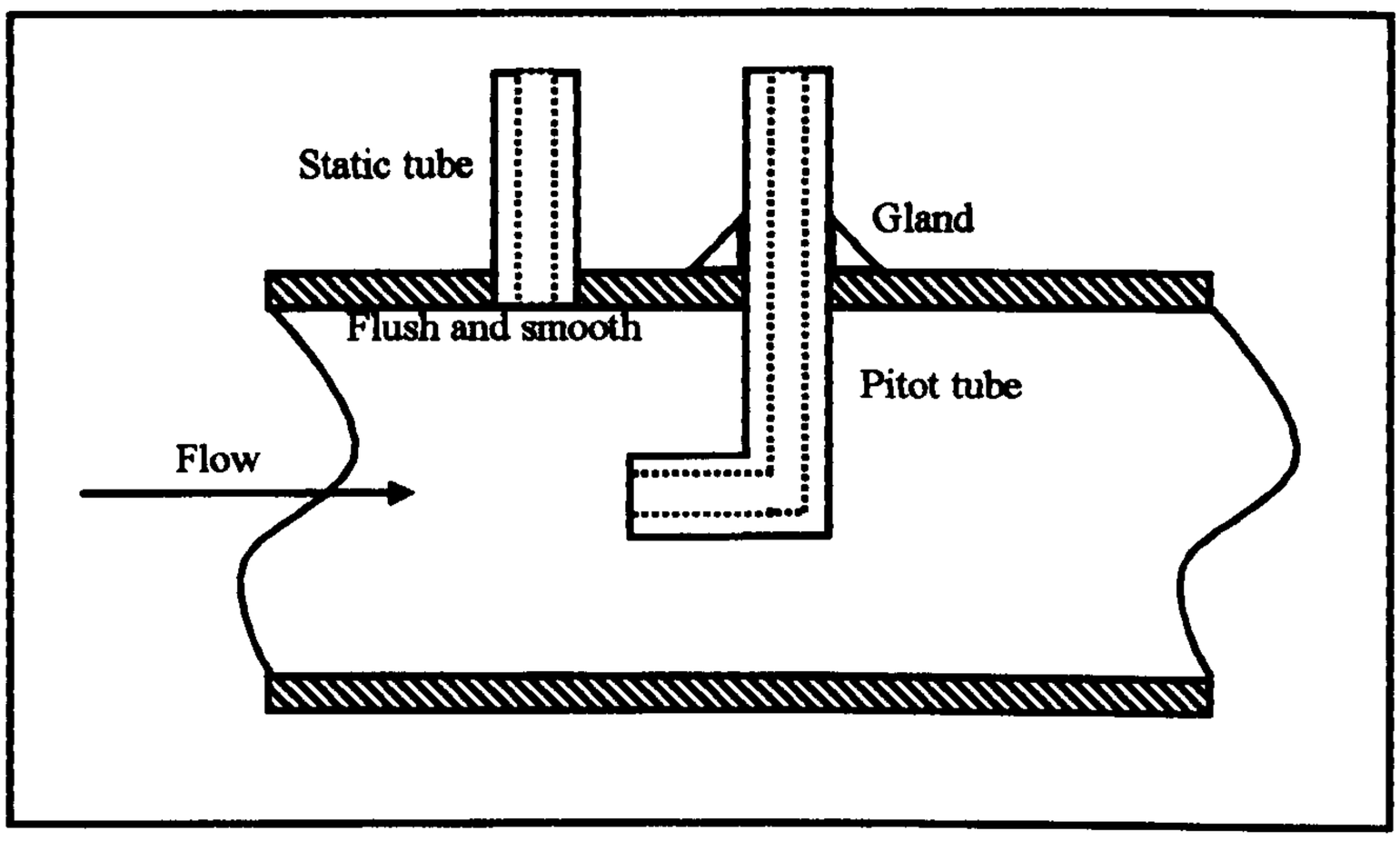

Fig. 5.33(a) Single hole static tube with separate total pressure tube

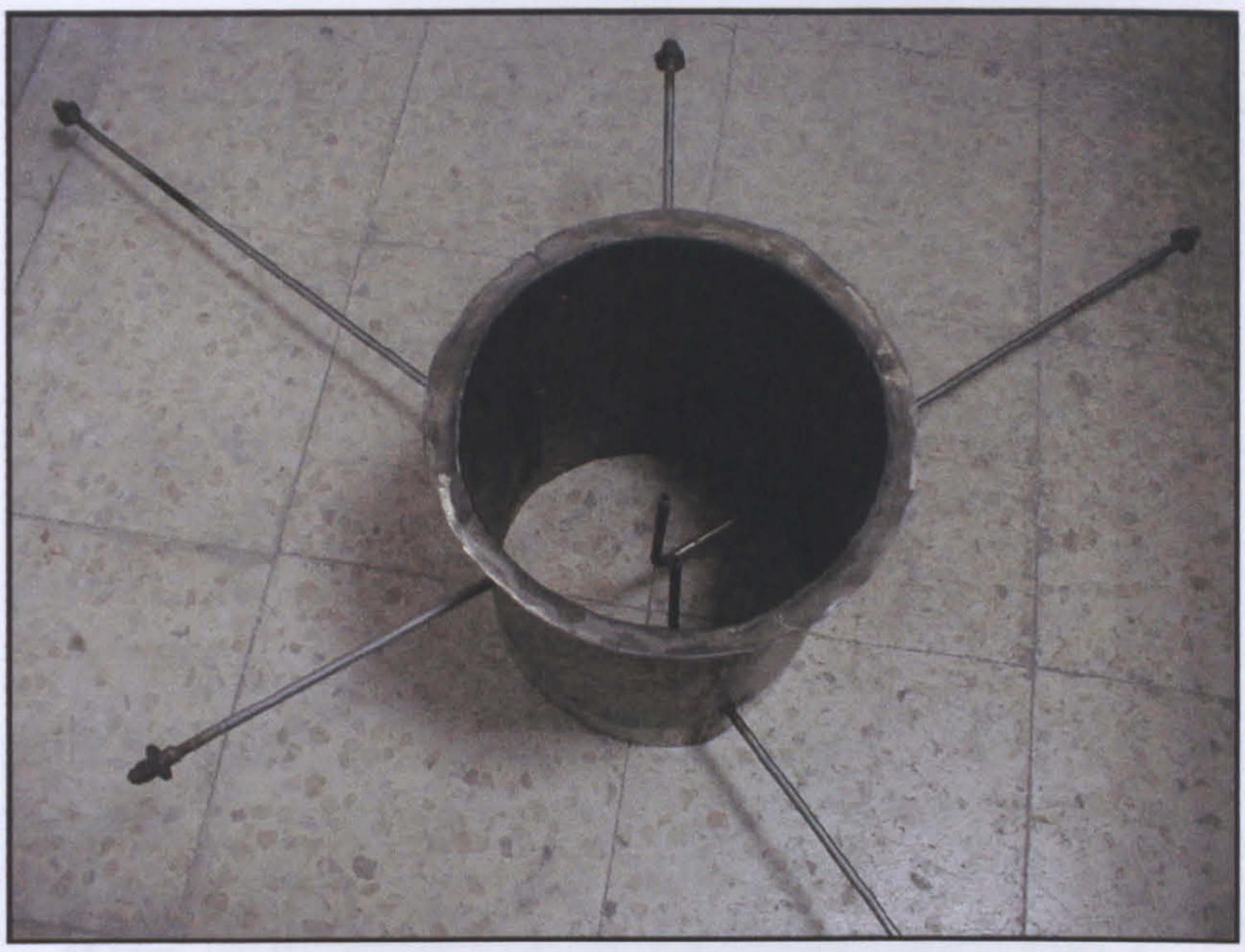

Fig. 5.33(b) Static tubes with separate total pressure tubes

If the two pressures are connected across a U-tube manometer, the difference between the total (static and dynamic) pressure head and the static pressure head at that local point can be measured. This pressure difference will be equal to the velocity head or pressure head produced by the loss of kinetic energy at that local point.

$$\Delta P = \frac{1}{2}\rho_{gas} V_{local}^2 \tag{5.15}$$

$$V_{local} = \sqrt{\frac{2\Delta P}{\rho_{gas}}} \tag{5.16}$$

in case of using a mercury manometer

$$\Delta P = \rho_{mercury} g L \tag{5.17}$$

where $\rho_{mercury}$ is the density of mercury in kg/m^3

g is the acceleration due to gravity in m/s^2

L is the manometer pressure head in m

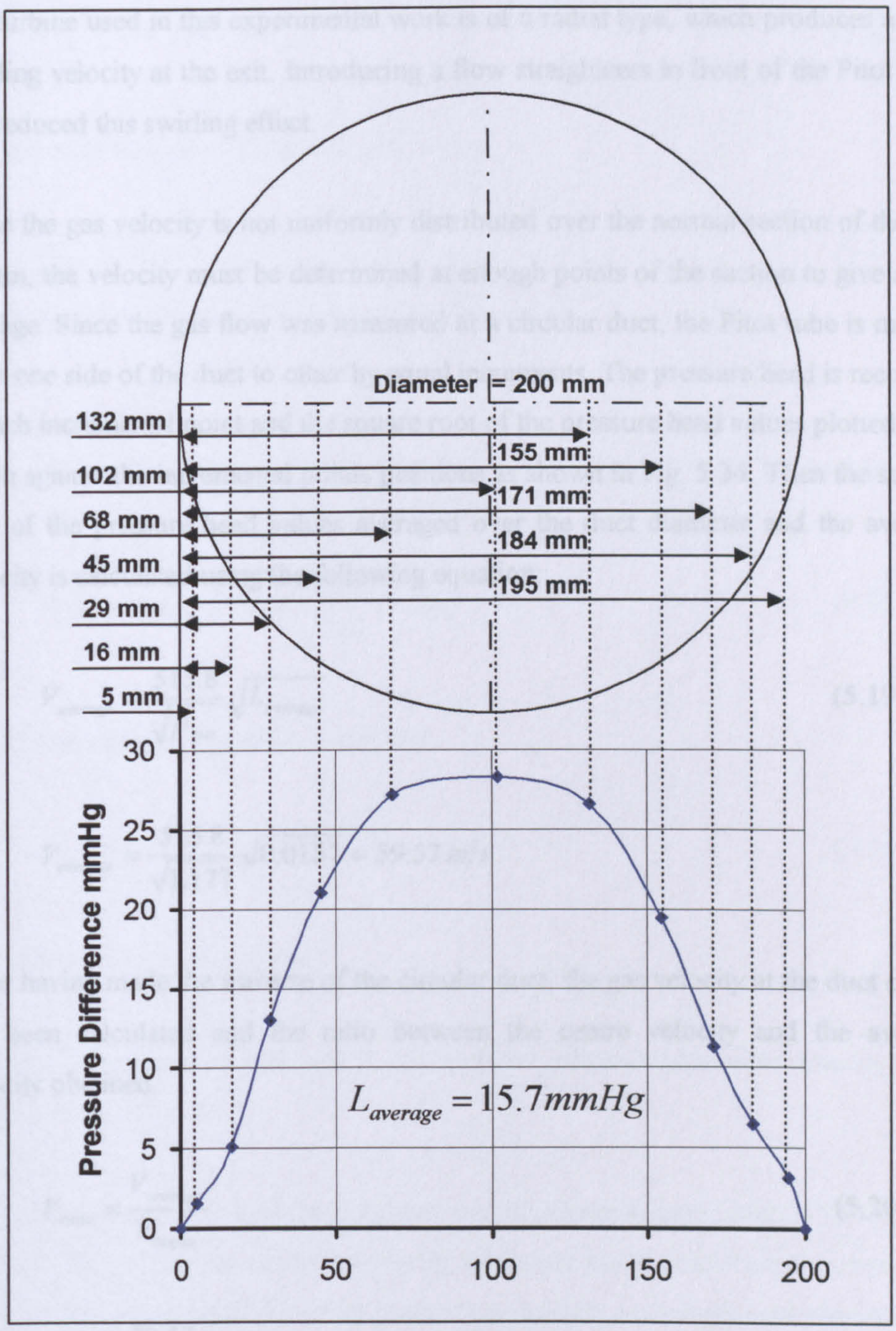

Fig. 5.34 Methods of making traverses at the Pitot tube

$$V_{local} = \frac{515.8}{\sqrt{\rho_{gas}}}\sqrt{L} \tag{5.18}$$

The gas turbine exhaust has been used to measure the gas flow rate using the Pitot tube because of the difficulty of inserting the Pitot tube in the compressor inlet. The gas turbine used in this experimental work is of a radial type, which produces a high swirling velocity at the exit. Introducing a flow straightners in front of the Pitot tube has reduced this swirling effect.

Since the gas velocity is not uniformly distributed over the normal section of the gas stream, the velocity must be determined at enough points of the section to give a fair average. Since the gas flow was measured at a circular duct, the Pitot tube is moved from one side of the duct to other by equal increments. The pressure head is recorded at each incremental point and the square root of the pressure head values plotted on a graph against the incremental points positions as shown in Fig. 5.34. Then the square root of the pressure head values averaged over the duct diameter and the average velocity is calculated using the following equation:

$$V_{average} = \frac{515.8}{\sqrt{\rho_{gas}}} \sqrt{L_{average}} \qquad (5.19)$$

$$V_{average} = \frac{515.8}{\sqrt{1.177}} \sqrt{0.0157} = 59.57\, m/s$$

After having made the traverse of the circular duct, the gas velocity at the duct centre has been calculated and the ratio between the centre velocity and the average velocity obtained.

$$V_{ratio} = \frac{V_{average}}{V_{centre}} \qquad (5.20)$$

$$V_{ratio} = \frac{59.57}{79.56} = 0.74875$$

Finally the Pitot tube is fixed at the duct centre and the velocity ratio used to obtain the average velocity from the centre reading according to the following equation:

$$V_{average} = V_{ratio} \times V_{centre} \tag{5.21}$$

$$V_{average} = 0.74875 \times V_{centre} \tag{5.22}$$

The gas mass flow then calculated as follows:

$$\dot{m}_{gas} = \rho_{gas} A V_{average} \tag{5.23}$$

where A is the cross sectional area of the flow in m^2

$$\dot{m}_{gas} = \rho_{gas} A V_{ratio} V_{centre} \tag{5.24}$$

$$\dot{m}_{gas} = \rho_{gas} \frac{\pi}{4} D^2 V_{ratio} \frac{515.8}{\sqrt{\rho_{gas}}} \sqrt{L_{centre}} \tag{5.25}$$

If the cross sectional diameter is 200 mm

$$\dot{m}_{gas} = 12.133 \sqrt{\rho_{gas}} \sqrt{L_{centre}} \tag{5.26}$$

5.3.1.5 Pressure Transducers

Pressure transducers of both gauge and absolute pressure type were considered in this experimental work.

The calibration of the absolute pressure type transducer (ranges from 0 to 15 psia), shown in Fig. 5.35, was carried out using a vacuum pump connected to a mercury-filled U-tube manometer. The inlet pressure port of the transducer was connected to the same side of the manometer via a T-connection (Fig. 5.36), while the output of the transducer was measured on a calibrated digital voltmeter accurate to 4 significant figures in the design range of the transducer output (1-6 volts). A shut-off valve was provided between the vacuum pump and the manometer (after the transducer connection point). This was used to re-pressurise the system gradually

and facilitate data reading at intermediate stations (mercury column height versus transducer output). The whole calibration set up is depicted in Fig. 5.36.

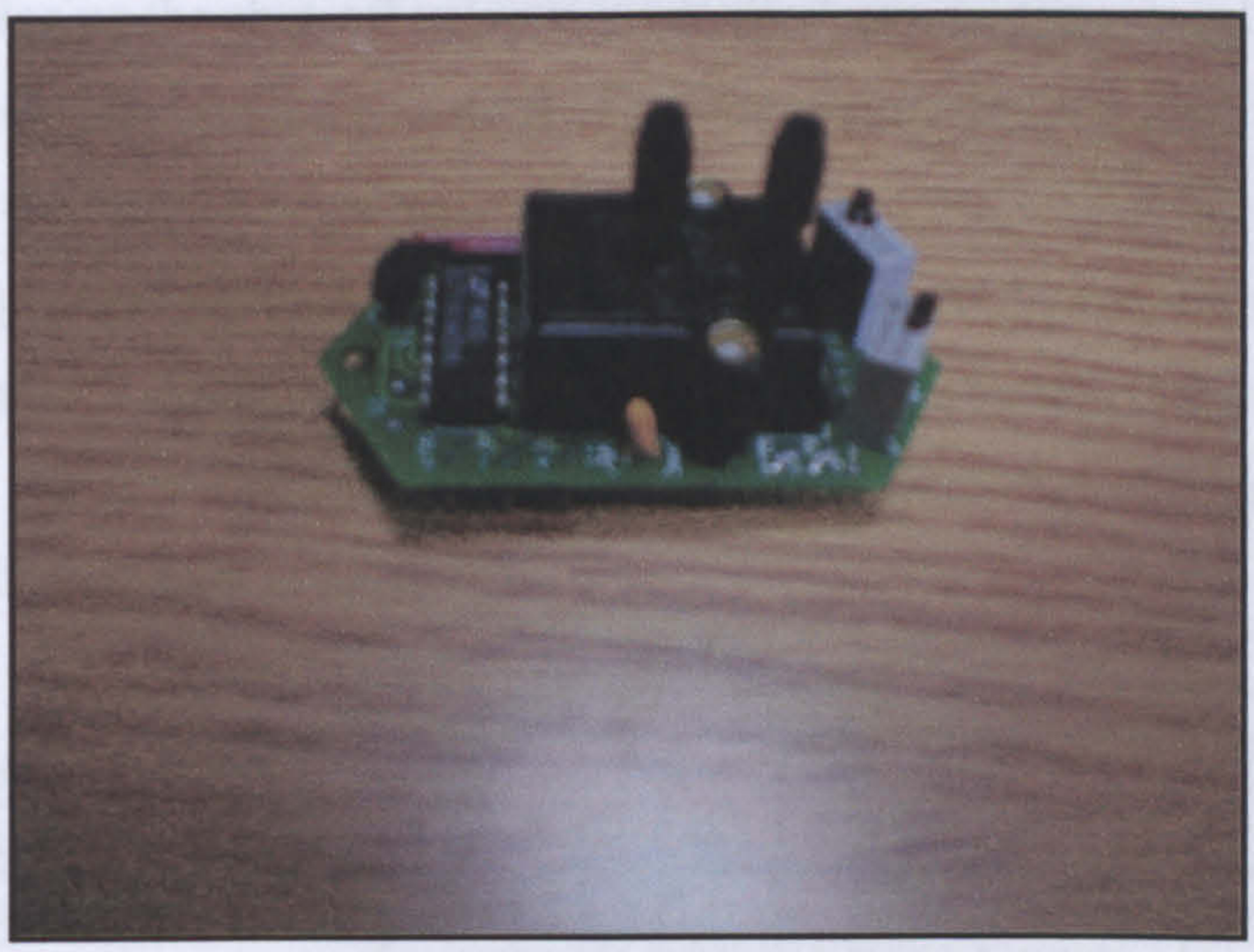

Fig. 5.35 Absolute pressure transducer (0-15 psia)

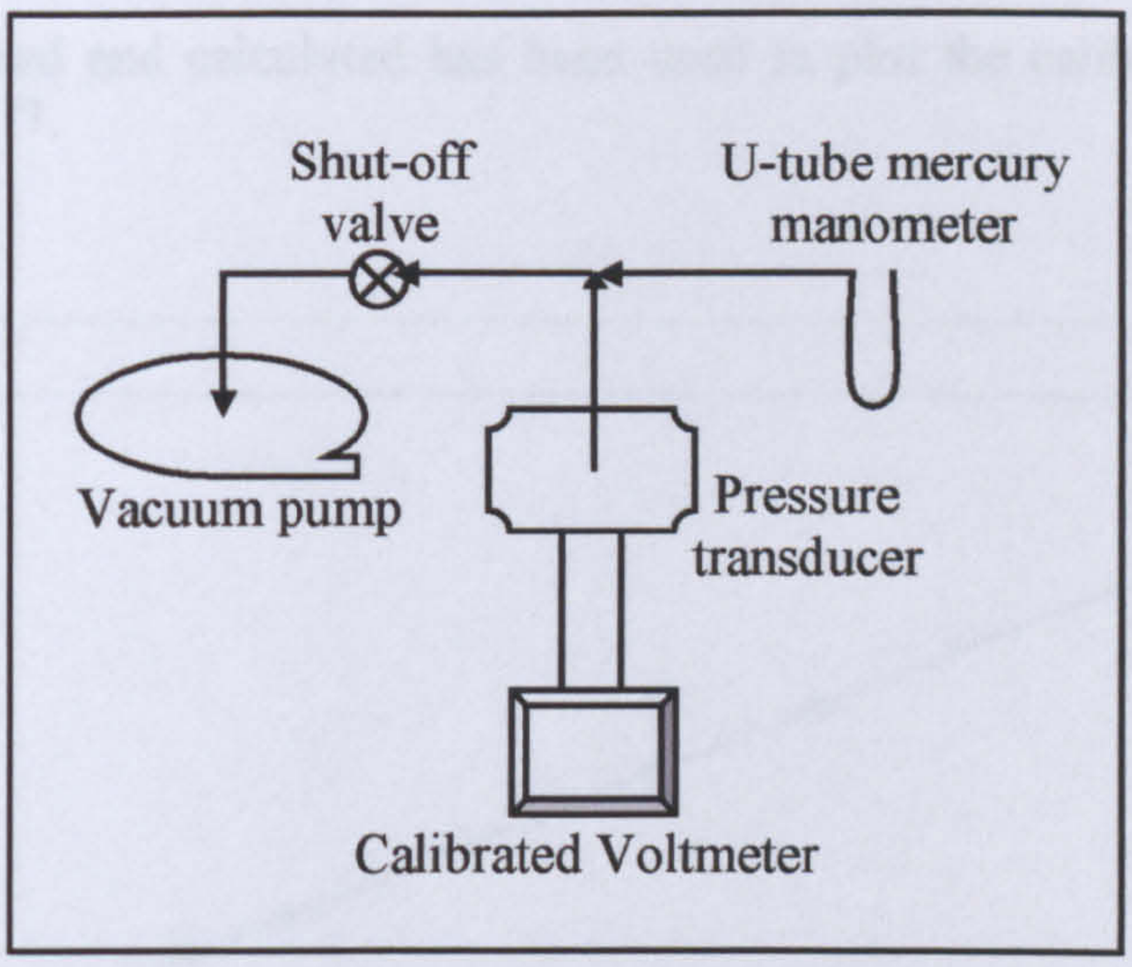

Fig. 5.36 Calibration equipment set for the absolute pressure transducer

The vacuum pump was started while the shut-off valve was open, and was run for a sufficient time until the difference in the mercury columns was at the maximum achievable (after a 30-minute run the difference in mercury height was hardly changing). The shut-off valve was then closed and the vacuum pump stopped.

The mercury height reached (in mm Hg) was recorded against the transducer voltage output (in volts), then the shut-off valve was slightly opened and closed very quickly and the new mercury height and transducer reading were recorded. The process of opening and closing the shut-off valve was repeated several times until zero mercury height difference between the two sides of the U-tube manometer was restored.

Height readings were subtracted from the value of the atmospheric pressure (which was equivalent to 748mm Hg, on the day of day of calibration), the results which represent the absolute pressure value tabulated against the equivalent pressure transducer voltage output in Table 5.6.

Manometer reading (mmHg)	6	53	96	160	210	295
Transducer output (Volts)	1.0339	1.3347	1.6099	2.0195	2.3395	2.8835
Manometer reading (mmHg)	350	414	504	580	690	740
Transducer output (Volts)	3.2355	3.6451	4.2211	4.7075	5.4115	5.7315

Table 5.6 Recorded results for the absolute pressure transducer

The data measured and calculated has been used to plot the calibration curve that shown in Fig. 5.37.

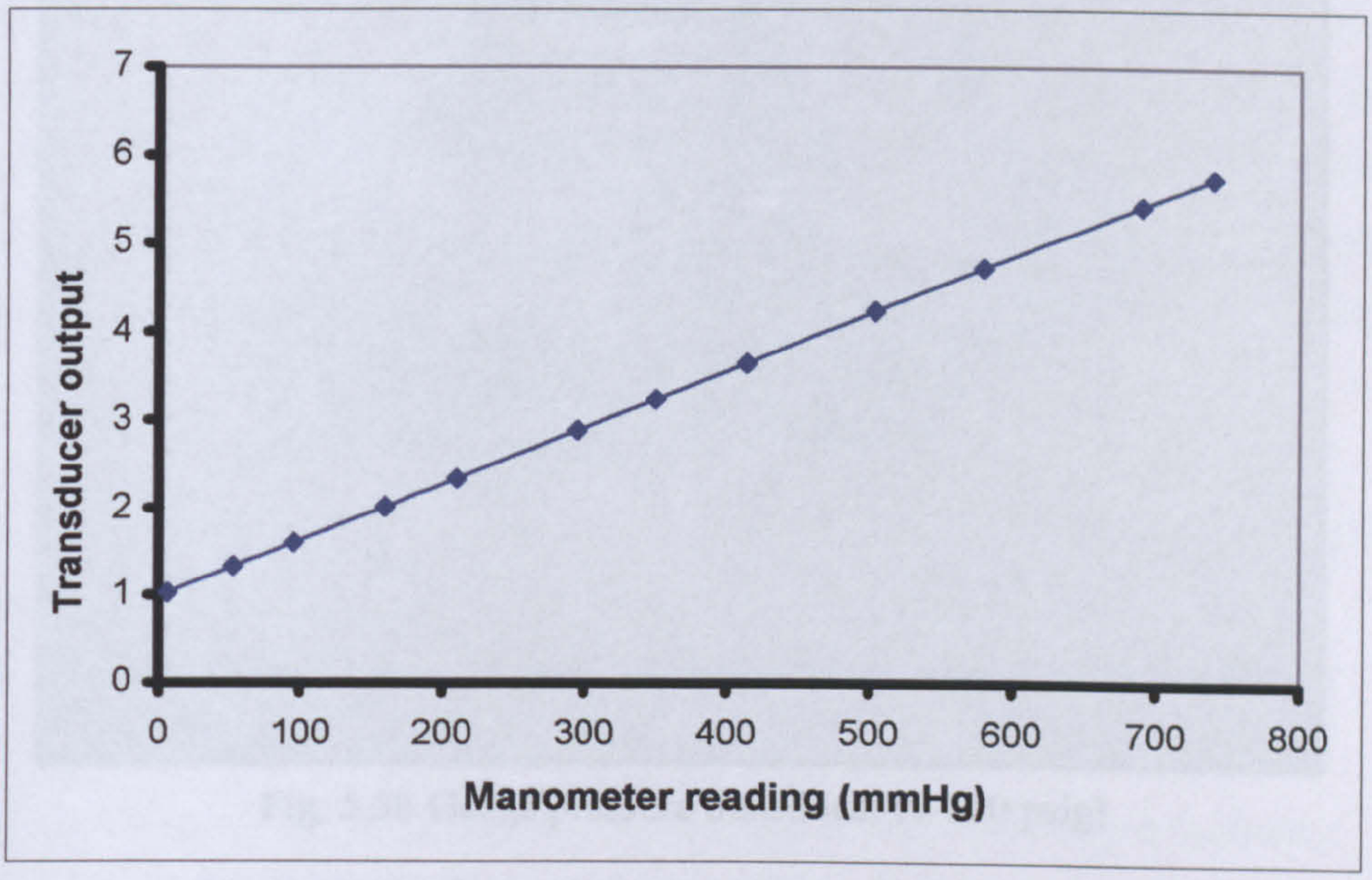

Fig. 5.37 Absolute pressure transducer calibration curve

The calibration of the gauge pressure transducer (ranges from 0 to 100 psig), shown in Fig. 5.38, was carried out using the same procedure and equipment set of the pressure gauges described in section 5.3.1.1. The only difference of the equipment set was that the output of the pressure transducer was measured on a calibrated digital voltmeter accurate to 4 significant figures in the design range of the transducer output (0-10 volts). The measured voltage and the equivalent manometer readings have been tabulated in Table 5.7. The data measured and calculated has been used to plot the calibration curve that shown in Fig. 5.39.

Manometer reading (mmHg)	5	112	252	362	443	567
Transducer output (Volts)	0.00967	0.2166	0.4873	0.6999	0.8566	1.0964
Manometer reading (mmHg)	642	728	819	894	962	984
Transducer output (Volts)	1.2414	1.4077	1.5837	1.7287	1.8602	1.9027

Table 5.7 Recorded results for the gauge pressure transducer

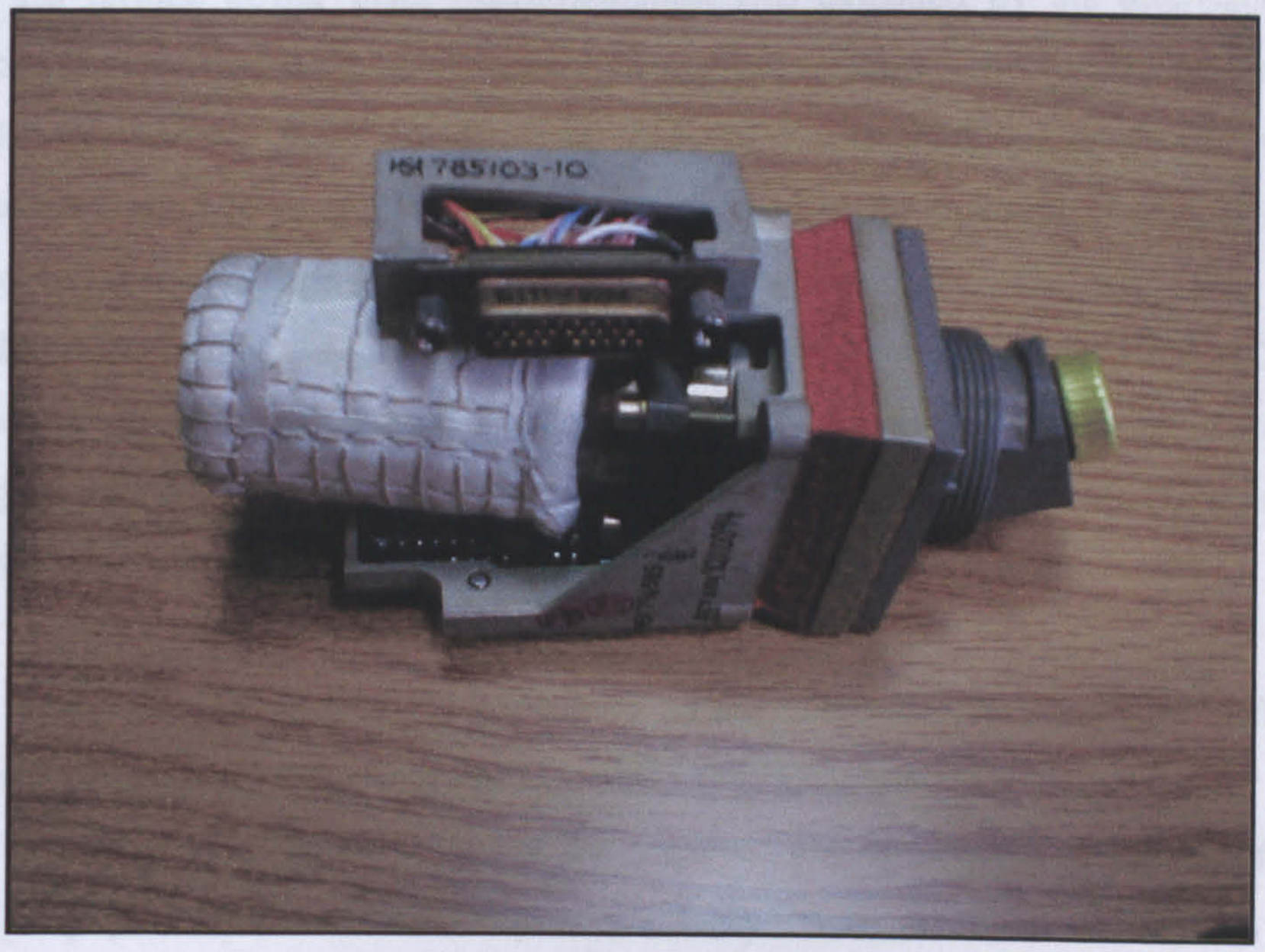

Fig. 5.38 Gauge pressure transducer (0-100 psig)

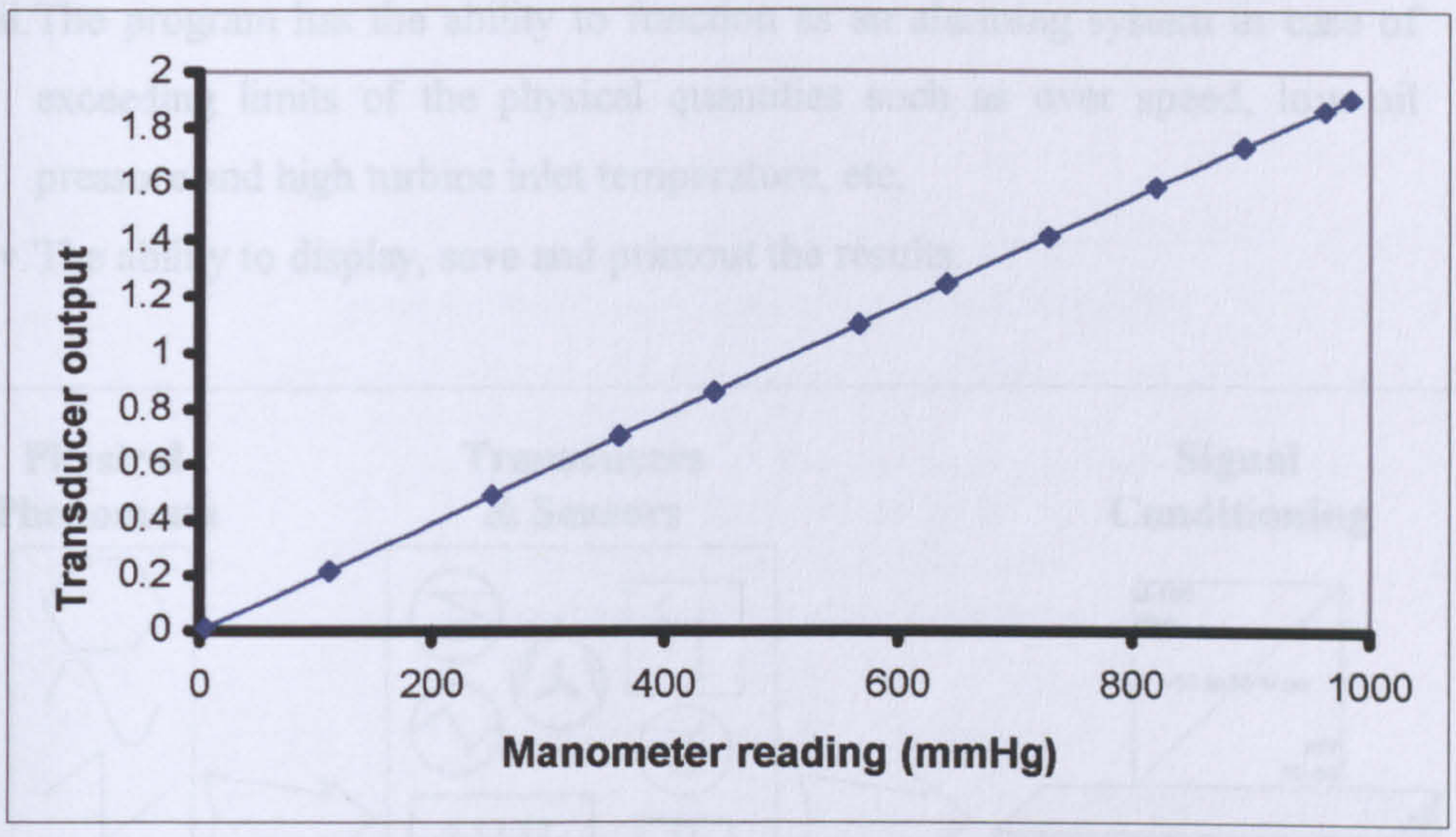

Fig. 5.39 Gauge pressure transducer calibration curve

5.4 PC Based Gas turbine Plant Data Acquisition System

The gas turbine power plant instrumentation was extended by the digitisation of building a personal computer based data acquisition system. The various parameters of the gas turbine plant performance such as temperature, pressure etc. which considered as physical quantities can be converted to an analogue electrical signal using active or passive transducers as shown in Fig. 5.40. The next step is to condition the analogue signals to a specified direct current voltage (± 10 V DC) and converted to digital signal by DAQ card. The Final acquired data can be processed using a personal computer and a print out can be extracted. Figure 5.40 illustrates the gas turbine plant data acquisition system.

This acquired data has to be processed again. Therefore, a computer software program was developed to carry out the following functions:

i. Converting the digital values of the acquired data into readable values of the physical quantities such as pressure, temperature, etc.
ii. The program has the ability to use the acquired converted data to calculate various performance parameters such as power output, thermal efficiency, torque and specific fuel consumption.

iii. The program has the ability to function as an alarming system in case of exceeding limits of the physical quantities such as over speed, low oil pressure and high turbine inlet temperature, etc.

iv. The ability to display, save and printout the results.

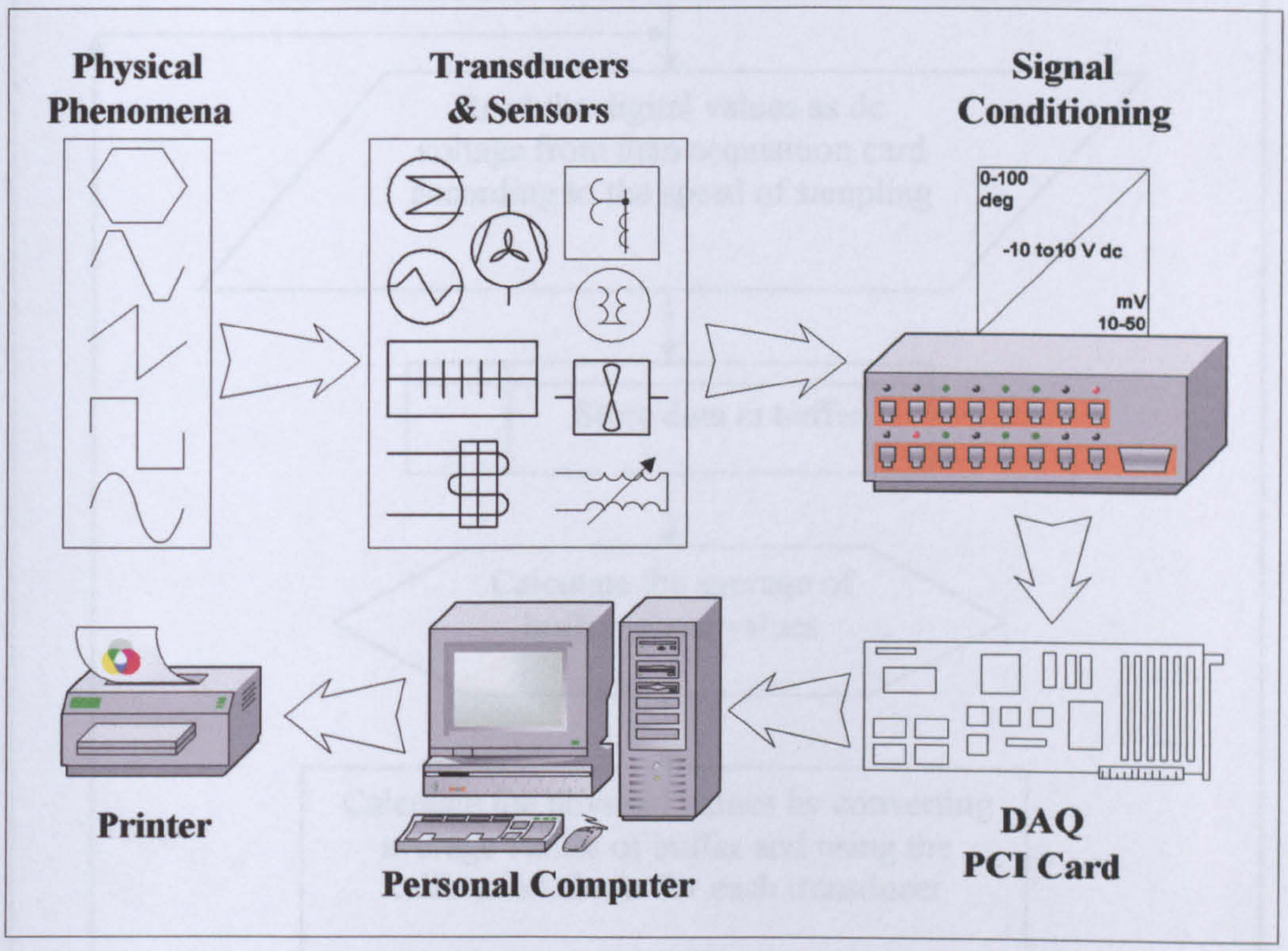

Fig. 5.40 Illustration of gas turbine plant data acquisition system

This program was written using *Data Translation Measure Foundry* software. A flow chart of this program is shown in Fig. 5.41. The main window of the developed program is depicted in Fig. 5.42.

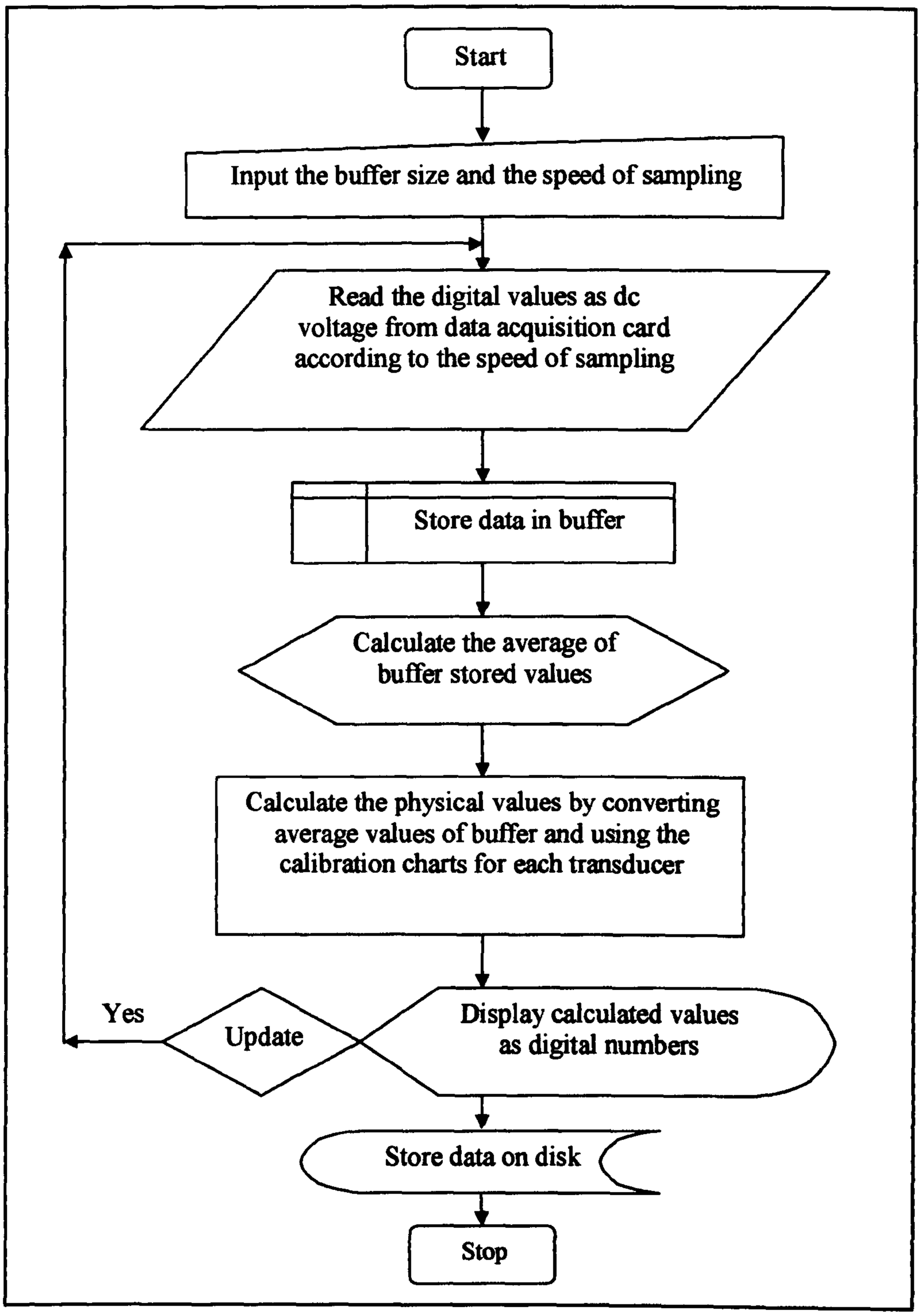

Fig. 5.41 Flowchart of computer data acquisition software program

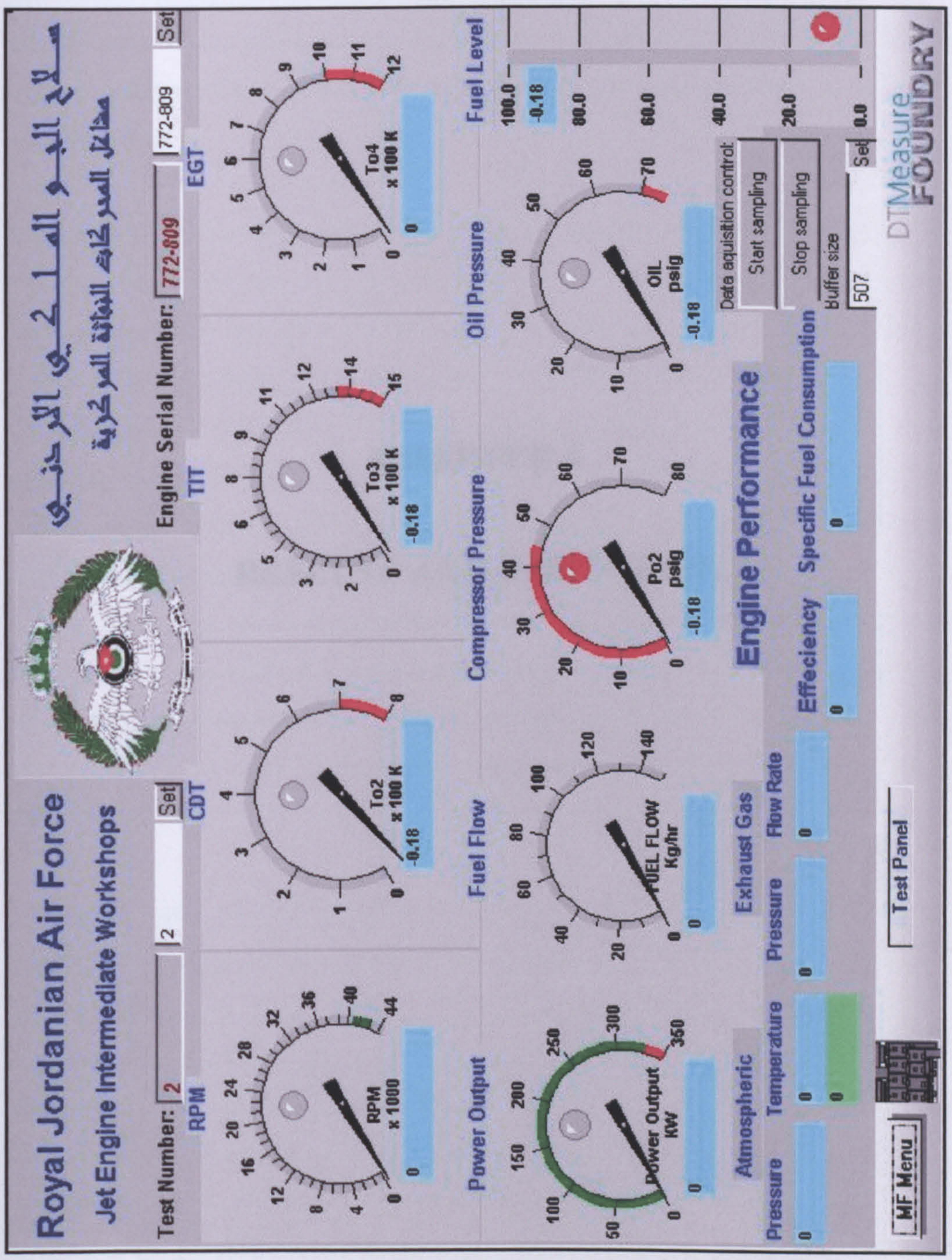

Fig. 5.42 The main window of the developed testing software

CHAPTER 6

RESULTS AND DISCUSSION

6.1 Introduction

The results of the research programme reported in this thesis have been divided broadly into two categories, namely: (a) Results of parametric study of the gas turbine cycles and the combined power and power (CPP) cycles and (b) Results of modelling and simulation.

The primary purpose of the parametric study was to show the influence of either the principal design variables and cycle configurations or the operating conditions on the performance of the gas turbine engine working in series with a steam turbine engine as a part of the combined power and power or CPP plant. It was hypothesised that a combination of a particular set of the design parameters, cycle configuration or the operating conditions that might produce the optimum performance when the gas turbine engine was used of its own for electrical power generation, might not be optimum if the same engine worked in series with a steam turbine in a CPP plant. The reason which gave rise to this hypothesis was that in the CPP plant environment, the factor that must be taken into consideration would be the grade of the thermal energy of gas turbine exhaust indicated by its temperature. The theory of the parametric study was developed in chapter 3; the results obtained by applying that theory are given in this chapter.

Parametric study is a very powerful tool for the initial stages of optimisation but it would be restricted only to design point performance. In order to investigate off design performance of gas turbine engines, it would be necessary to either run the engines and measure actual performance or use modelling techniques to obtain performance through computer simulation. Various modelling techniques have been developed by researchers and designers of gas turbine engines. Almost all such techniques rely on real experimental data, but they depart only in the method of using these data for matching the components and the load. There are two most widely used techniques; in one the data would be used to produce equations with the help of the available curve fitting techniques and in the other *Lookup Tables* would be produced

on which the matching criteria would be satisfied by using interpolation or extrapolation methods.

Alternatively, matching conditions between the compressor and the turbine, for example, might be met by superimposing the turbine performance characteristics on the compressor performance characteristics. This graphical approach, if computerised, can be very useful tool for simulating gas turbine engines. The procedure used for developing this technique was explained in chapter 4; the results of simulation are discussed in this chapter.

6.2 Discussion of Results of Parametric Study

Theoretical investigations, which included parametric studies, were carried out on the computer using the simulation computer program and the assumed parameters' values tabulated in Table 3.1 of chapter 3. The outputs of the computer programs developed for the parametric study were used to generate Fig. 6.1 to Fig. 6.6 for the performance of the gas turbine cycles and Fig. 6.8 to Fig. 6.23 for the performance of the combined power and power cycles.

6.2.1 Results of Parametric Study of the Gas Turbine Cycles

The relationship between the gas turbine efficiency η_{gt} and specific work w_{gt} at constant pressure ratio r and turbine inlet temperature T_{o3} are shown in Fig. 6.1. It can be seen that the maximum efficiency points and the maximum specific work output points at different values of constant temperature or pressure ratio are not coincident. The design choice can be either to opt for maximum efficiency (industrial applications with low operating cost) or maximum specific work output (military applications with high power/weight ratio) or any other point that may represent the optimum choice for a particular application.

Figure 6.2 depicts the relationship between the pressure ratio r and the gas turbine exhaust temperature T_{o4} at constant turbine inlet temperature T_{o3}. It can be seen that

raising the turbine inlet temperature T_{o3} as well as lowering the compressor pressure ratio r can increase the gas turbine exhaust temperature T_{o4}. It is worth noting that the maximum specific work output points have a higher turbine exhaust temperatures than the maximum efficiency points. Furthermore, the higher the pressure ratio the greater would be the difference between the points of maximum thermal efficiency and maximum specific work output. This is because of the increasing divergence between the maximum thermal efficiency and maximum specific work output lines with increasing cycle pressure ratio.

Reheating the gas turbine cycle increases the specific work output with some reduction of thermal efficiency. This is because reheating of exhaust gas after the first expansion does not contribute in any way to the cycle pressure ratio, as shown in the T-S diagram, Fig. 6.7, consequently the thermal efficiency reduces. Reheating also tends to reduce the difference between the maximum efficiency points and the maximum specific work points. Hence, for the reheated gas turbine cycle at constant turbine inlet temperature there is only one point for both maximum thermal efficiency and maximum specific work output at each cycle pressure ratio as illustrated in Fig. 6.3.

The exhaust gas temperature of the reheat gas turbine cycle can also be plotted against pressure ratio, Fig. 6.4. An increase in the exhaust temperature is expected due to reheating but the change in exhaust temperature with the pressure ratio is totally different than that for the simple gas turbine cycle especially at lower values of T_{o3}.

The effect of cooling the air before it enters the compressor on the gas turbine exhaust gas temperature is shown in Fig. 6.5. As would be expected, at a constant value of the turbine entry temperature the exhaust gas temperature decreases as the cycle pressure ratio is increased. From the point of view of the combined power and power cycle this is an undesirable feature. However, both the specific work output and the thermal efficiency increase with increasing cycle pressure ratio. This can be seen in Fig. 6.6 which gives a comparison between the simple gas turbine cycle, reheat cycle and the pre-cooling cycle.

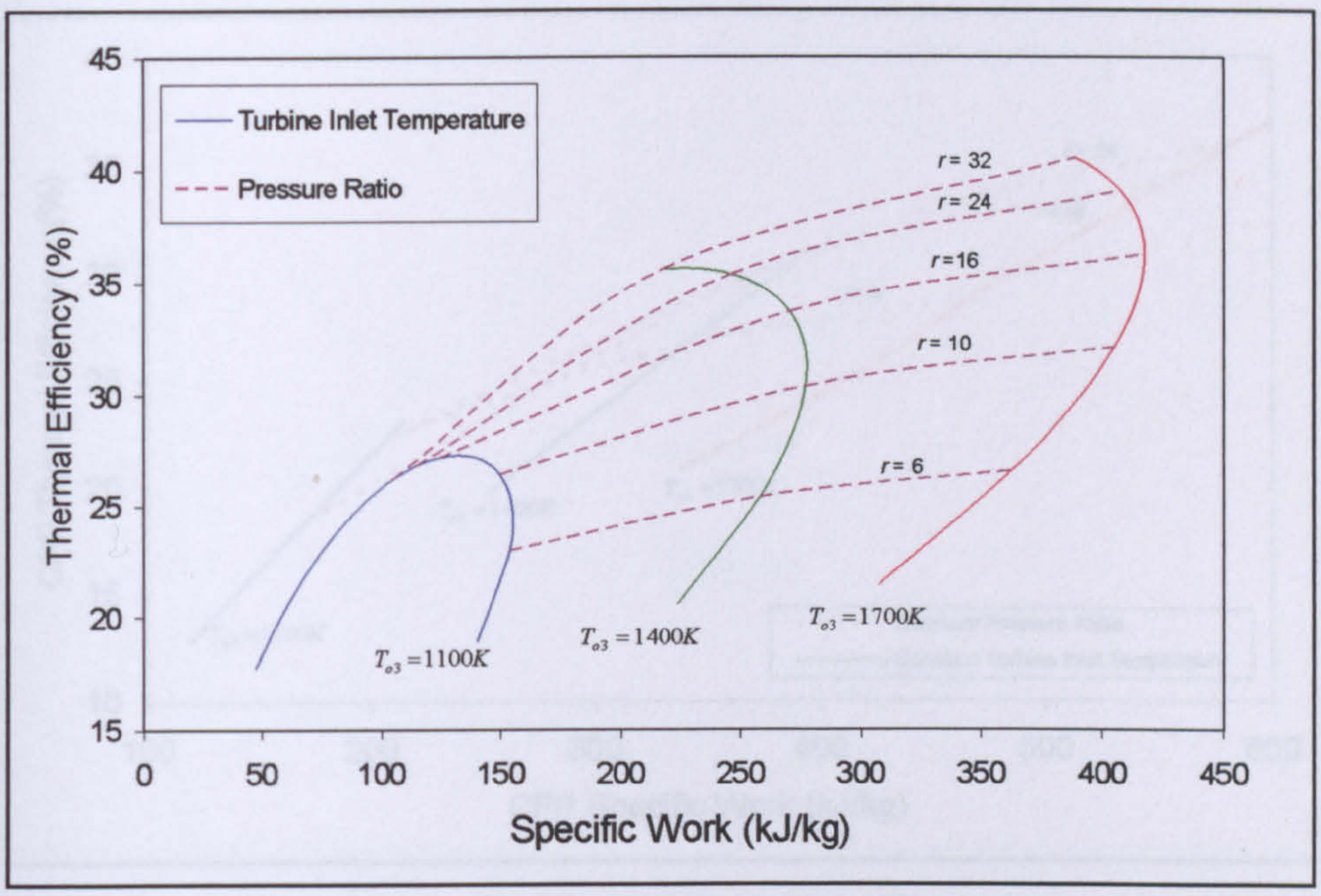

Fig. 6.1 Gas turbine efficiency versus specific work output at constant turbine inlet temperatures and pressure ratios

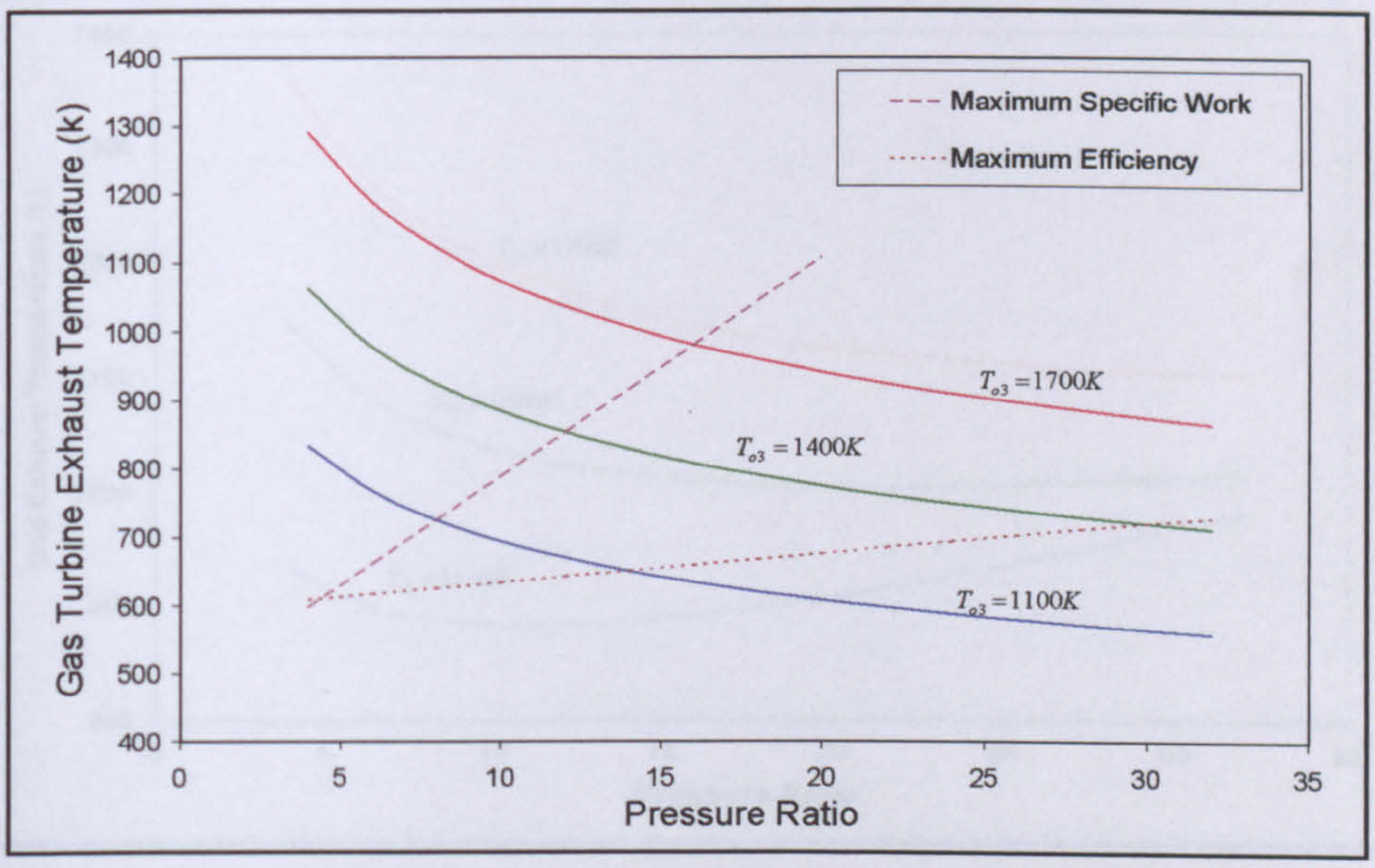

Fig. 6.2 Gas turbine exhaust temperature versus pressure ratio at constant turbine inlet temperatures

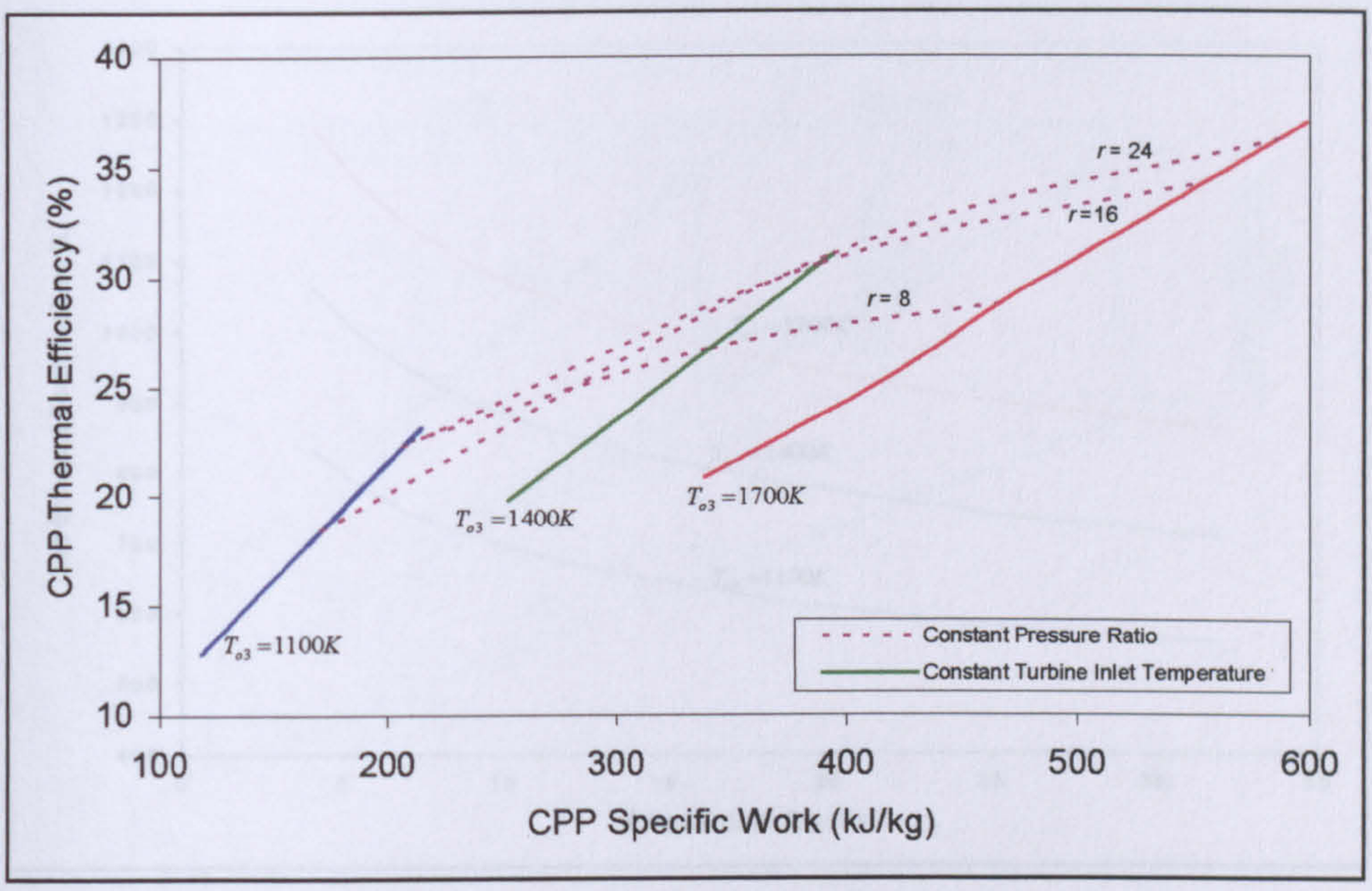

Fig. 6.3 Gas turbine reheat cycle efficiency versus specific work at constant turbine inlet temperatures and pressure ratios

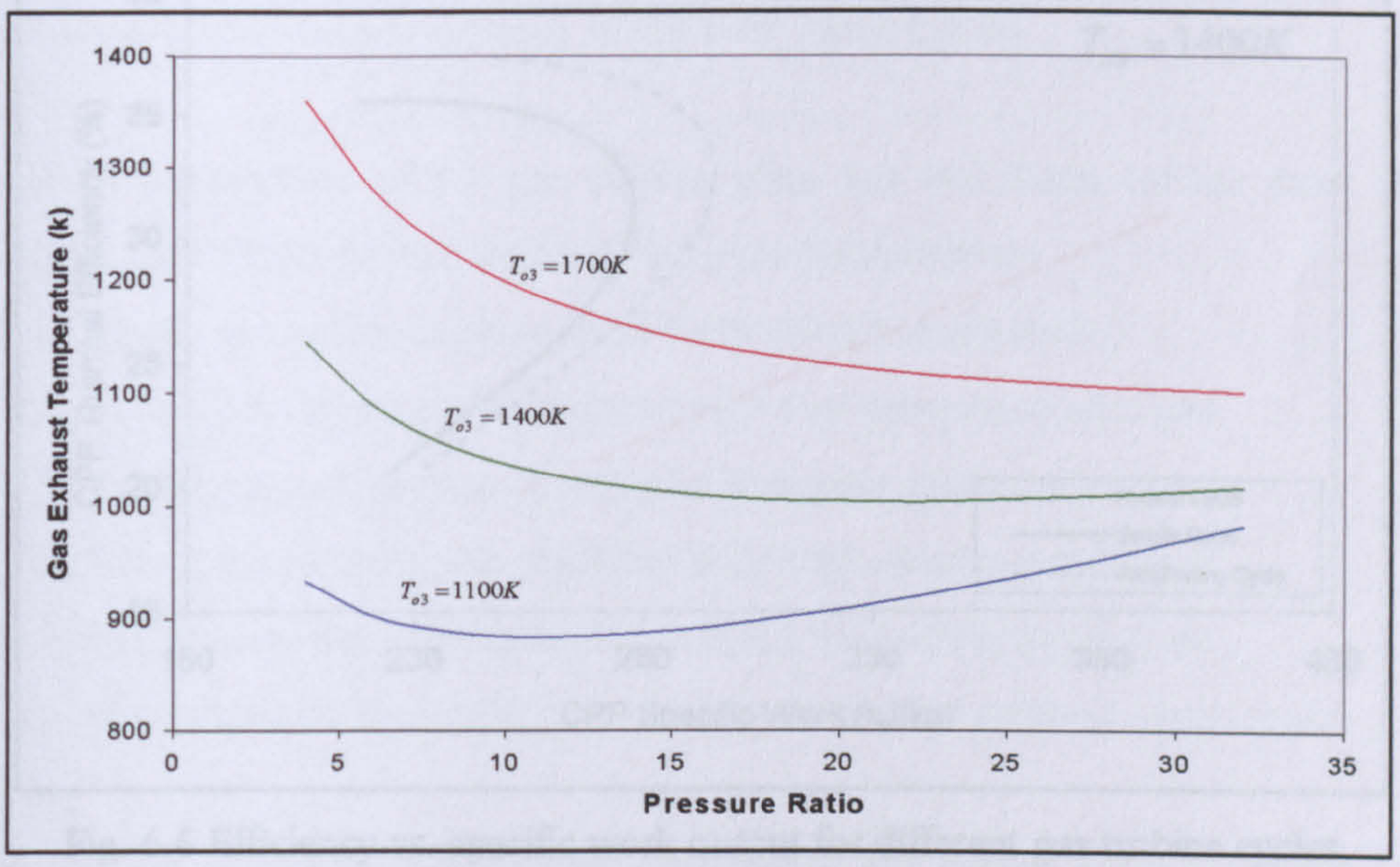

Fig. 6.4 Exhaust temperature of gas turbine reheat cycle versus pressure ratio at constant turbine inlet temperatures

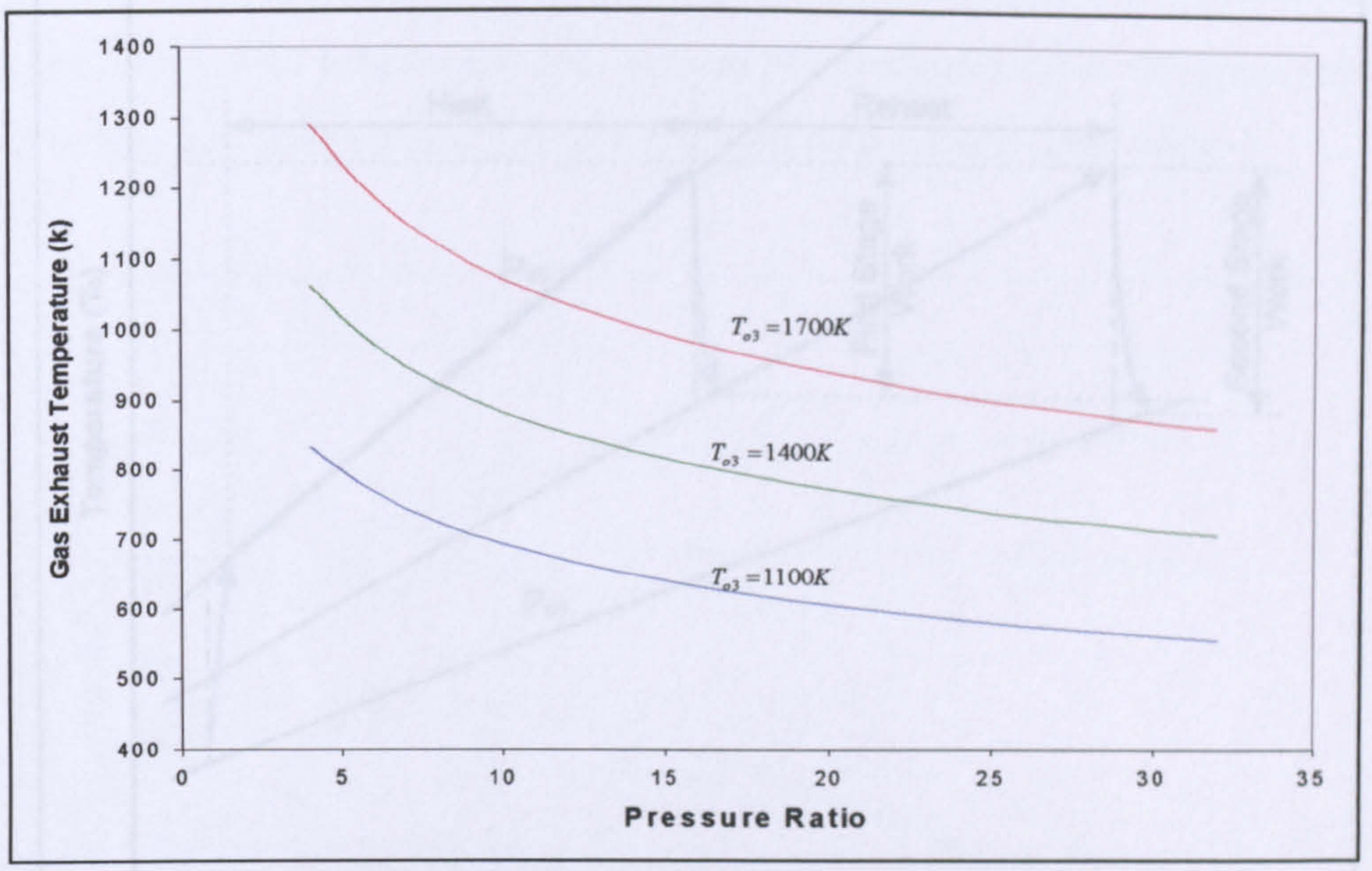

Fig. 6.5 Exhaust temperature of gas turbine pre-cooling cycle versus pressure ratio at constant turbine inlet temperatures

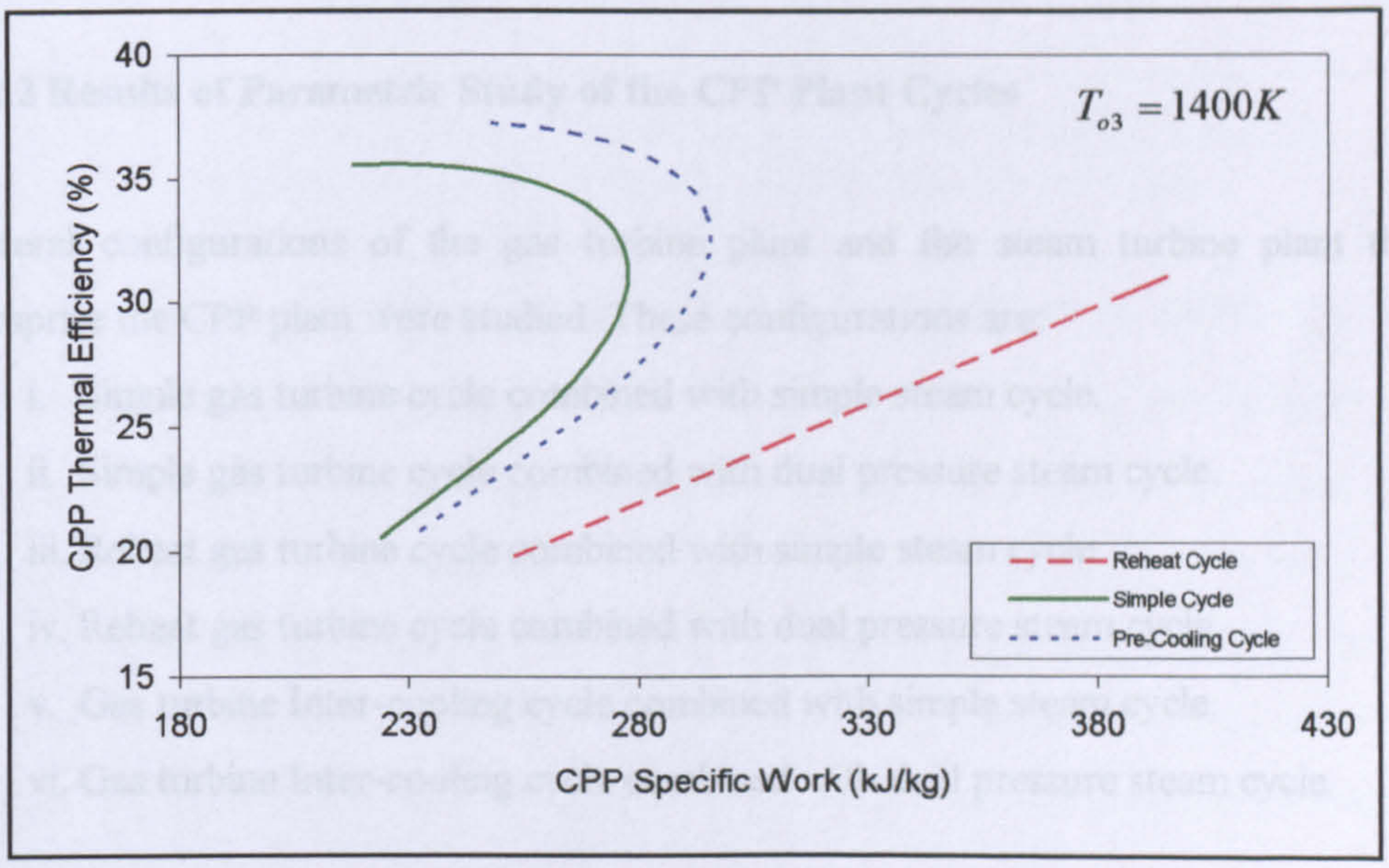

Fig. 6.6 Efficiency vs. specific work output for different gas turbine cycles

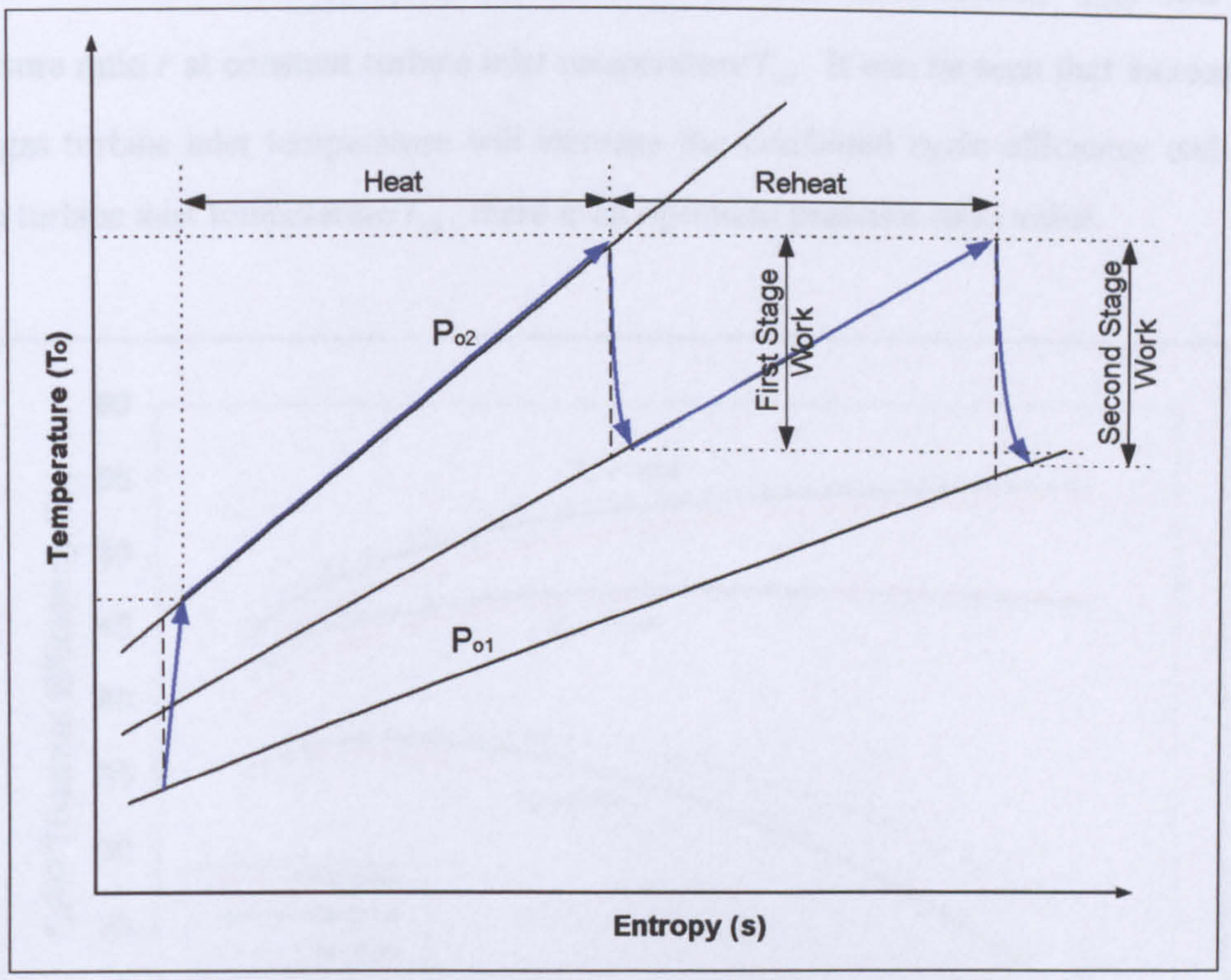

Fig 6.7 Temperature-Entropy diagram of reheat gas turbine cycle

6.2.2 Results of Parametric Study of the CPP Plant Cycles

Several configurations of the gas turbine plant and the steam turbine plant that comprise the CPP plant were studied. These configurations are:

i. Simple gas turbine cycle combined with simple steam cycle.
ii. Simple gas turbine cycle combined with dual pressure steam cycle.
iii. Reheat gas turbine cycle combined with simple steam cycle.
iv. Reheat gas turbine cycle combined with dual pressure steam cycle.
v. Gas turbine Inter-cooling cycle combined with simple steam cycle.
vi. Gas turbine Inter-cooling cycle combined with dual pressure steam cycle.

The first set of results, which covers the simple gas turbine cycle combined with simple steam turbine cycle, is given in Figs. 6.8 to 6.12. The conditions for calculating the relevant data are shown on each figure.

Figure 6.8 shows the relationship between the CPP thermal efficiency η_{CPP} and the pressure ratio r at constant turbine inlet temperature T_{o3}. It can be seen that increasing the gas turbine inlet temperature will increase the combined cycle efficiency and for each turbine inlet temperature T_{o3}, there is an optimum pressure ratio value.

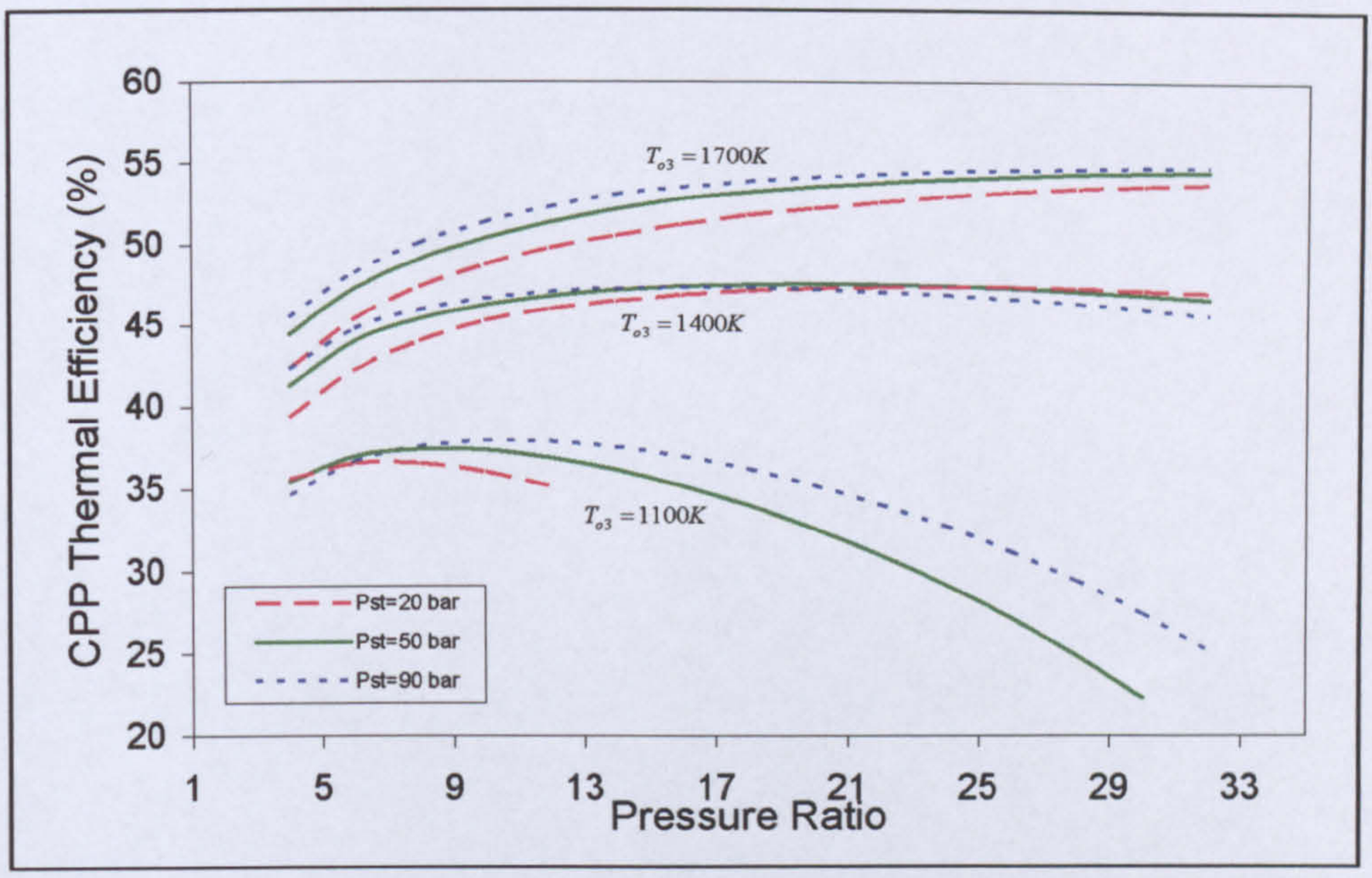

Fig. 6.8 Combined efficiency versus pressure ratio at constant turbine inlet temperatures and boiler pressures (simple combined cycle)

Figure 6.9 depicts the relationship between the CPP specific work output w_{CPP} and the pressure ratio r at constant turbine inlet temperature T_{o3}. It can be seen that increasing the gas turbine inlet temperature will increase the specific work output. The maximum specific work output at each turbine inlet temperature will be at low pressure ratio values. This is due to the fact at these values of pressure ratio, the gas turbine cycle will have a higher exhaust temperatures; hence the steam cycle will produce more power output. Consequently the CPP specific work output increases.

Figure 6.10 is a combination of Fig. 6.8 and Fig. 6.9, which shows the relationship between the CPP thermal efficiency η_{CPP} and the CPP specific work output w_{CPP} at various turbine inlet temperature T_{o3}. It is noticeable that the maximum efficiency points and the maximum specific work output points do not coincide.

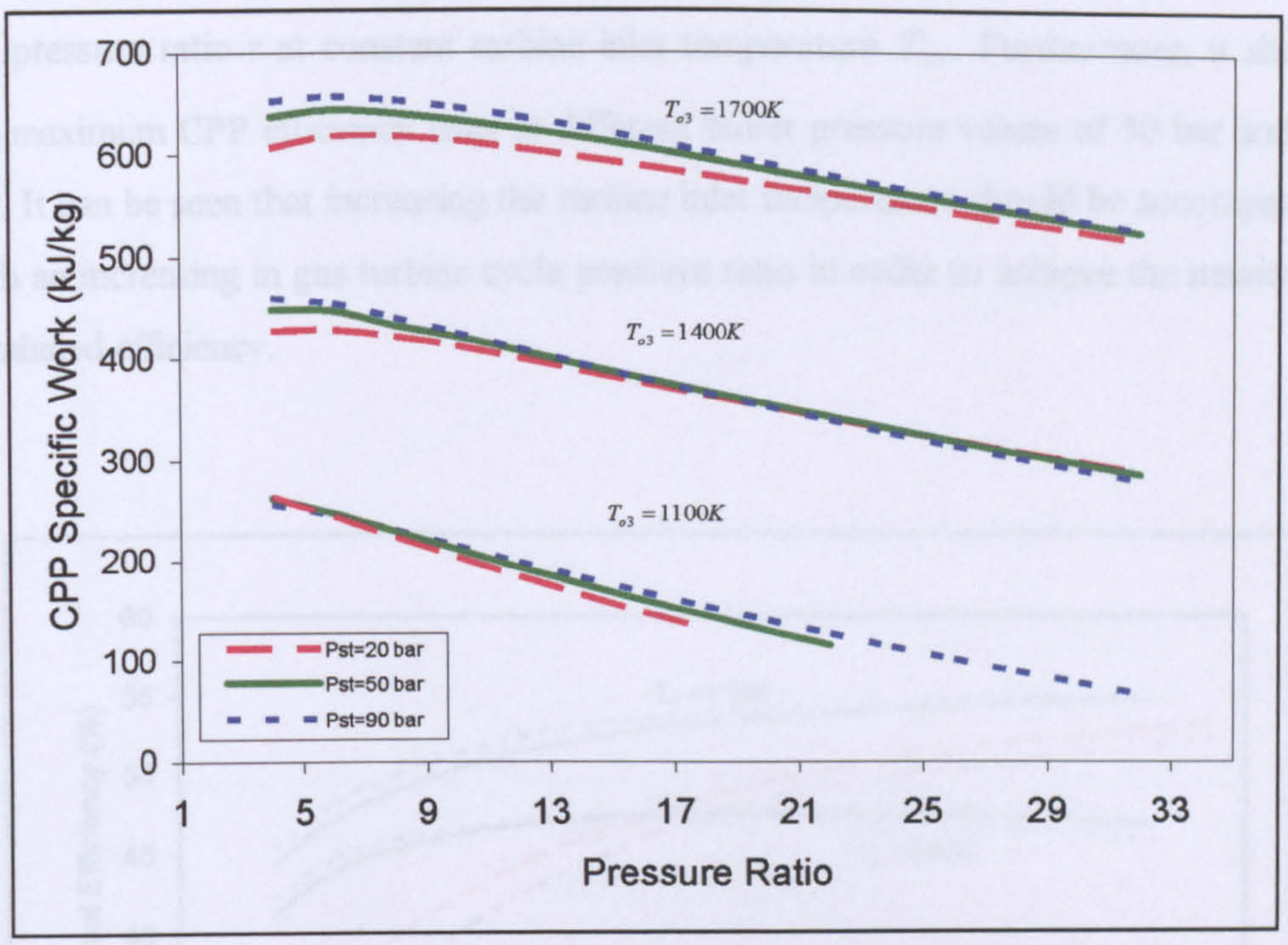

Fig. 6.9 Combined specific work output versus pressure ratio at constant turbine inlet temperatures and boiler pressures (simple combined cycle)

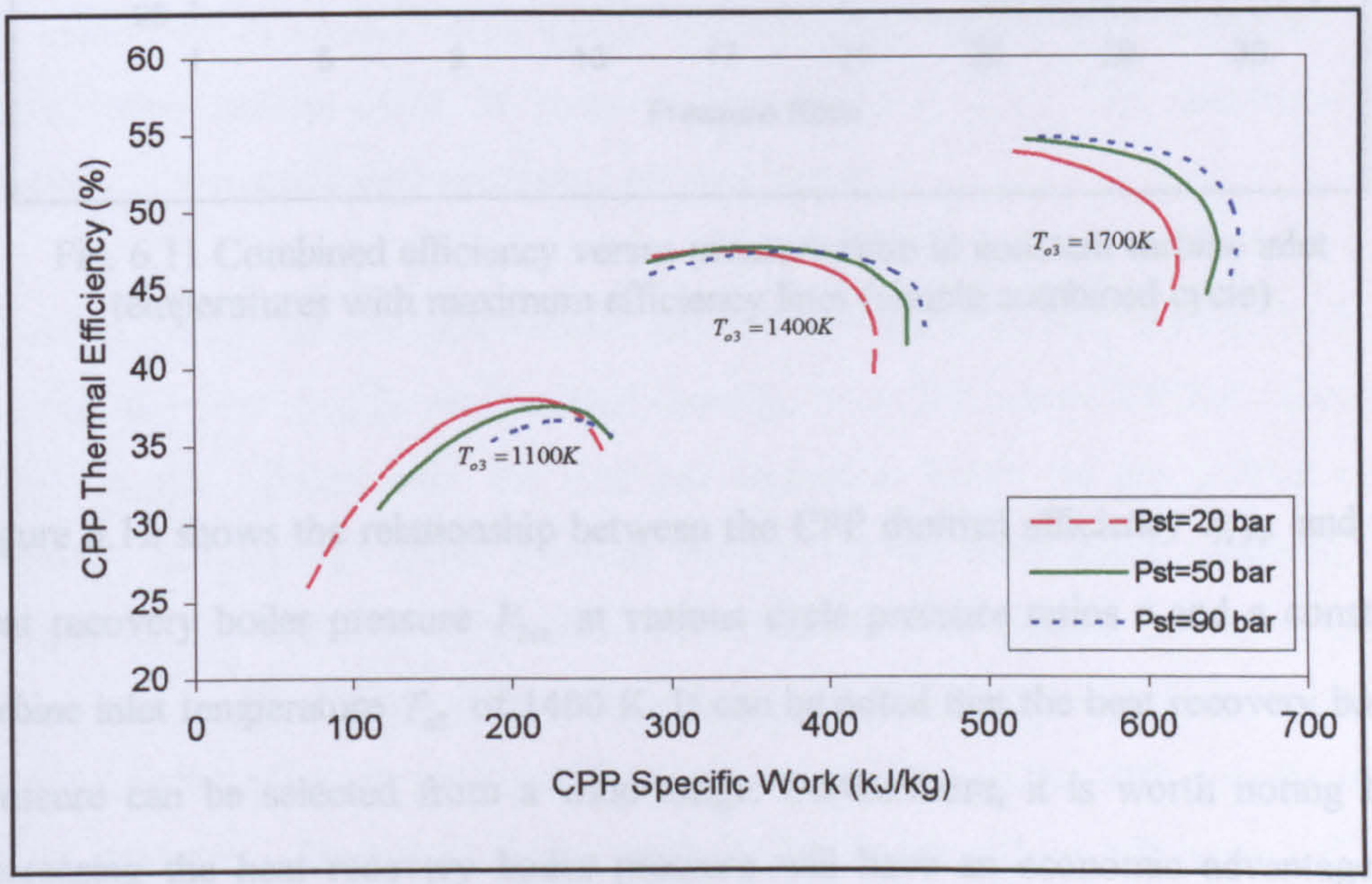

Fig. 6.10 Combined specific work output versus combined efficiency at constant turbine inlet temperatures and boiler pressures (simple combined cycle)

Figure 6.11 shows again the relationship between the CPP thermal efficiency η_{CPP} and the pressure ratio r at constant turbine inlet temperature T_{o3}. Furthermore, it shows the maximum CPP efficiency lines at different boiler pressure values of 50 bar and 90 bar. It can be seen that increasing the turbine inlet temperature should be accompanied with an increasing in gas turbine cycle pressure ratio in order to achieve the maximum combined efficiency.

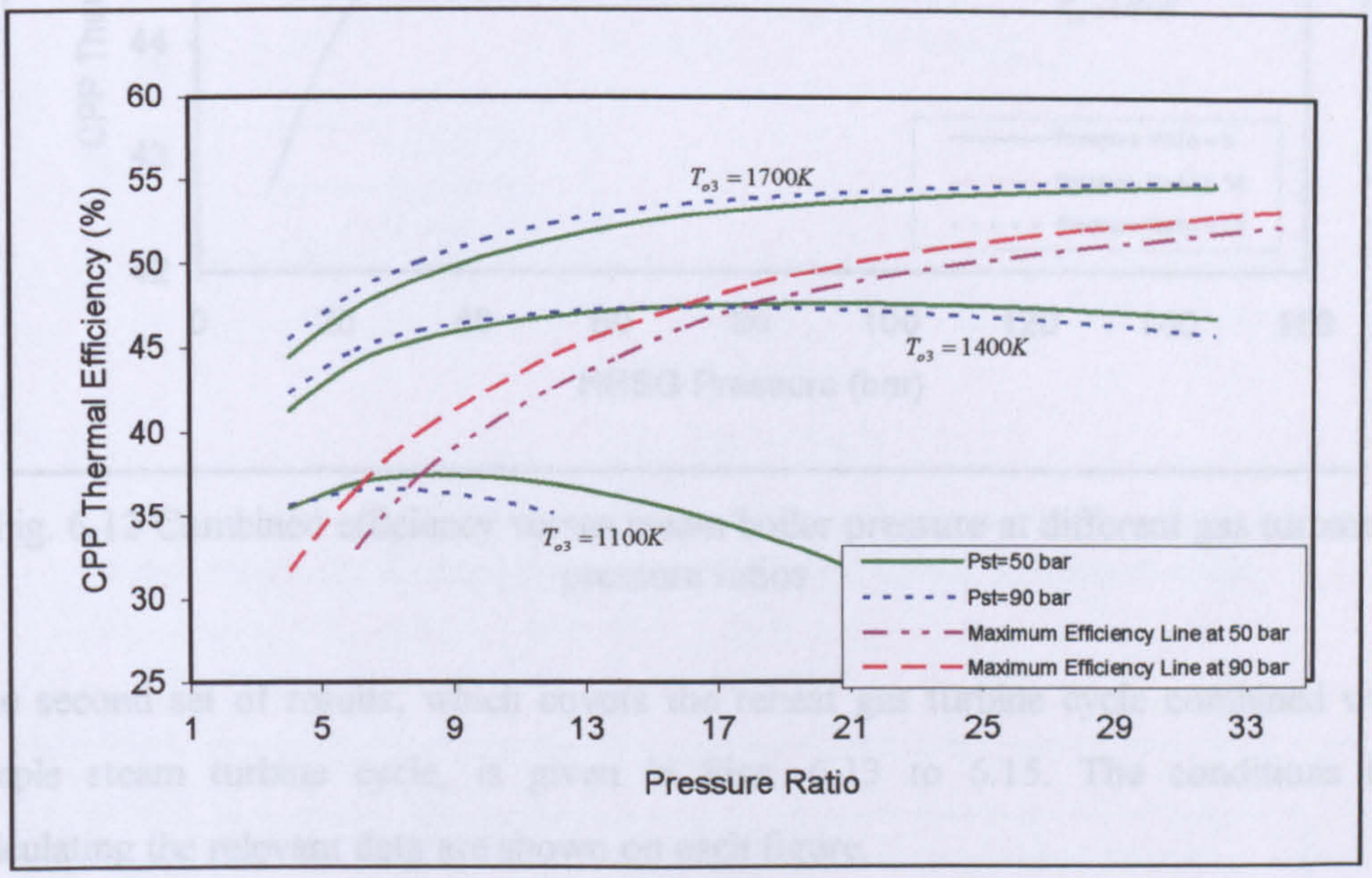

Fig. 6.11 Combined efficiency versus pressure ratio at constant turbine inlet temperatures with maximum efficiency lines (simple combined cycle)

Figure 6.12 shows the relationship between the CPP thermal efficiency η_{CPP} and the heat recovery boiler pressure P_{2st} at various cycle pressure ratios r and a constant turbine inlet temperature T_{o3} of 1400 K. It can be noted that the heat recovery boiler pressure can be selected from a wide range. Furthermore, it is worth noting that decreasing the heat recovery boiler pressure will have an economic advantage of lowering the combined plant total cost. In particular, the capital cost of building the heat recovery steam generator.

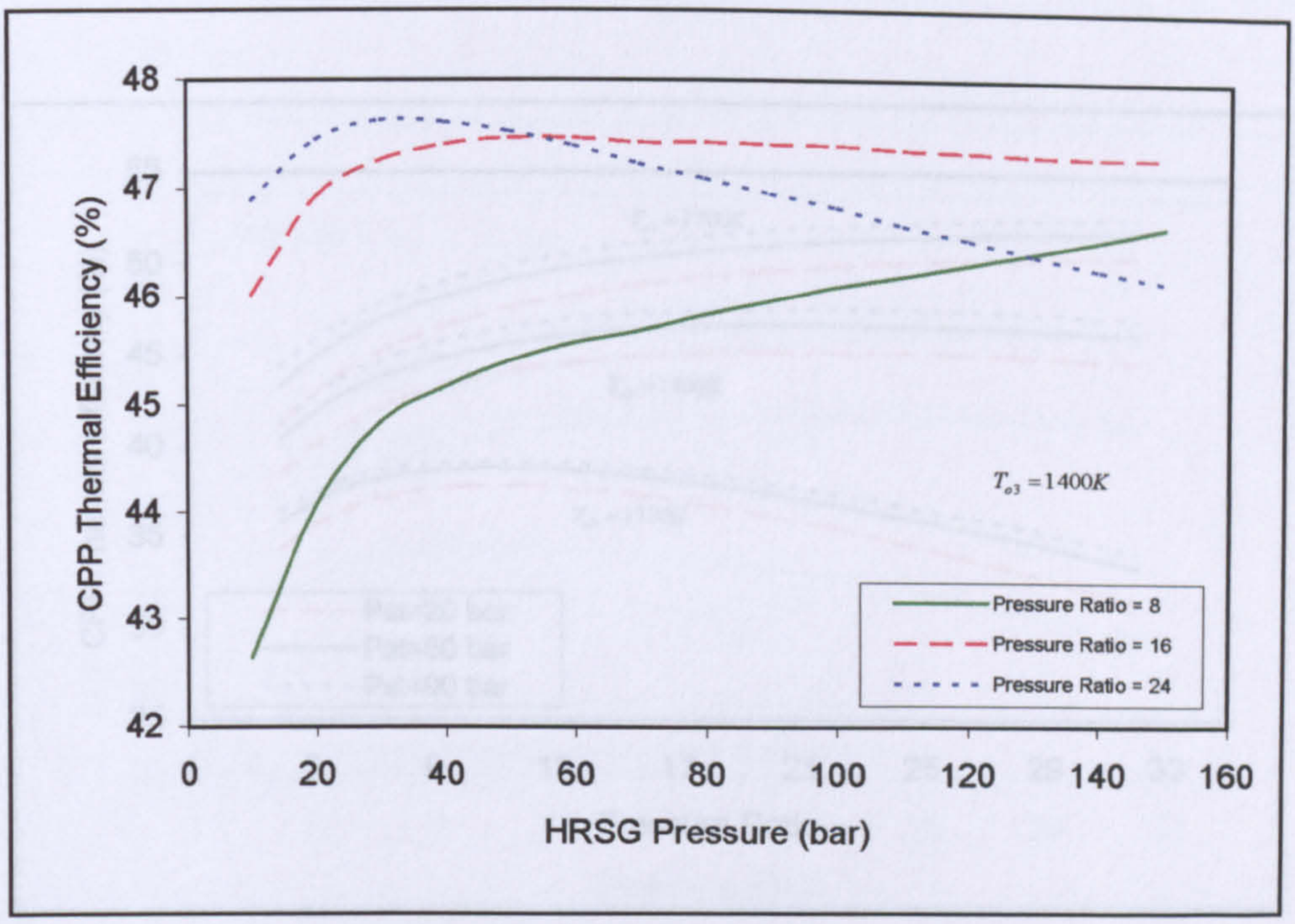

Fig. 6.12 Combined efficiency versus steam boiler pressure at different gas turbine pressure ratios

The second set of results, which covers the reheat gas turbine cycle combined with simple steam turbine cycle, is given in Figs. 6.13 to 6.15. The conditions for calculating the relevant data are shown on each figure.

Reheating the gas turbine cycle reduces the CPP thermal efficiency, see Fig. 6.13 and increases the CPP specific work output, see Fig. 6.14. The reason for that, reheating of gas turbine exhaust after the first gas expansion lower the gas turbine cycle efficiency, as explained in the previous section. On the other hand, reheating will increase the gas turbine cycle specific work output and the exhaust gas temperature. Consequently, higher gas turbine exhaust temperature will increase both the steam turbine thermal efficiency and specific work output. Hence, the CPP specific work output increases. However, the increase in the steam turbine efficiency will not compensate for the reduction of gas turbine efficiency, consequently the CPP thermal efficiency reduces, refer to Fig. 6.15.

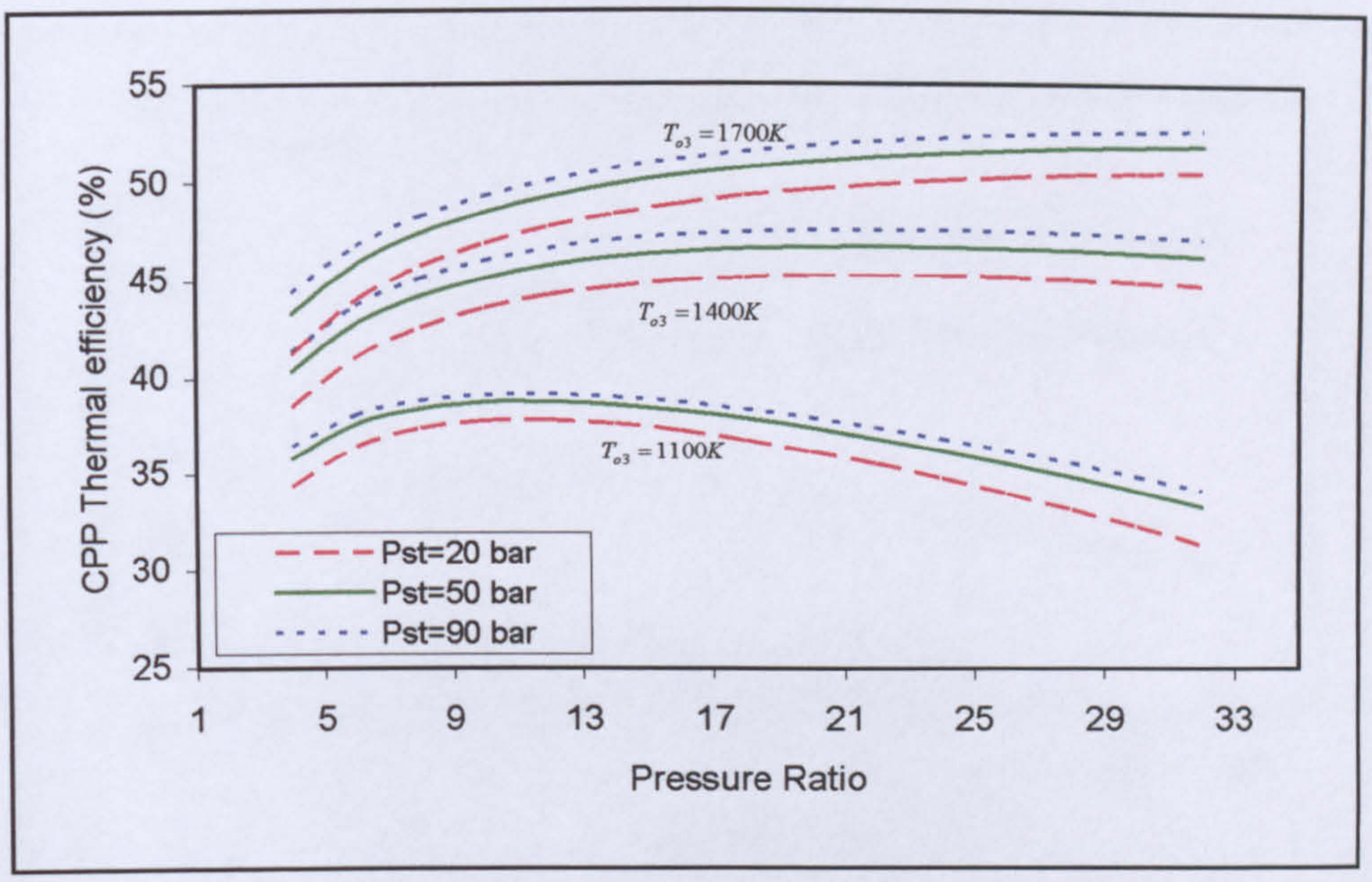

Fig. 6.13 Combined efficiency versus pressure ratio at constant turbine inlet temperatures and steam boiler pressures (gas reheat combined cycle)

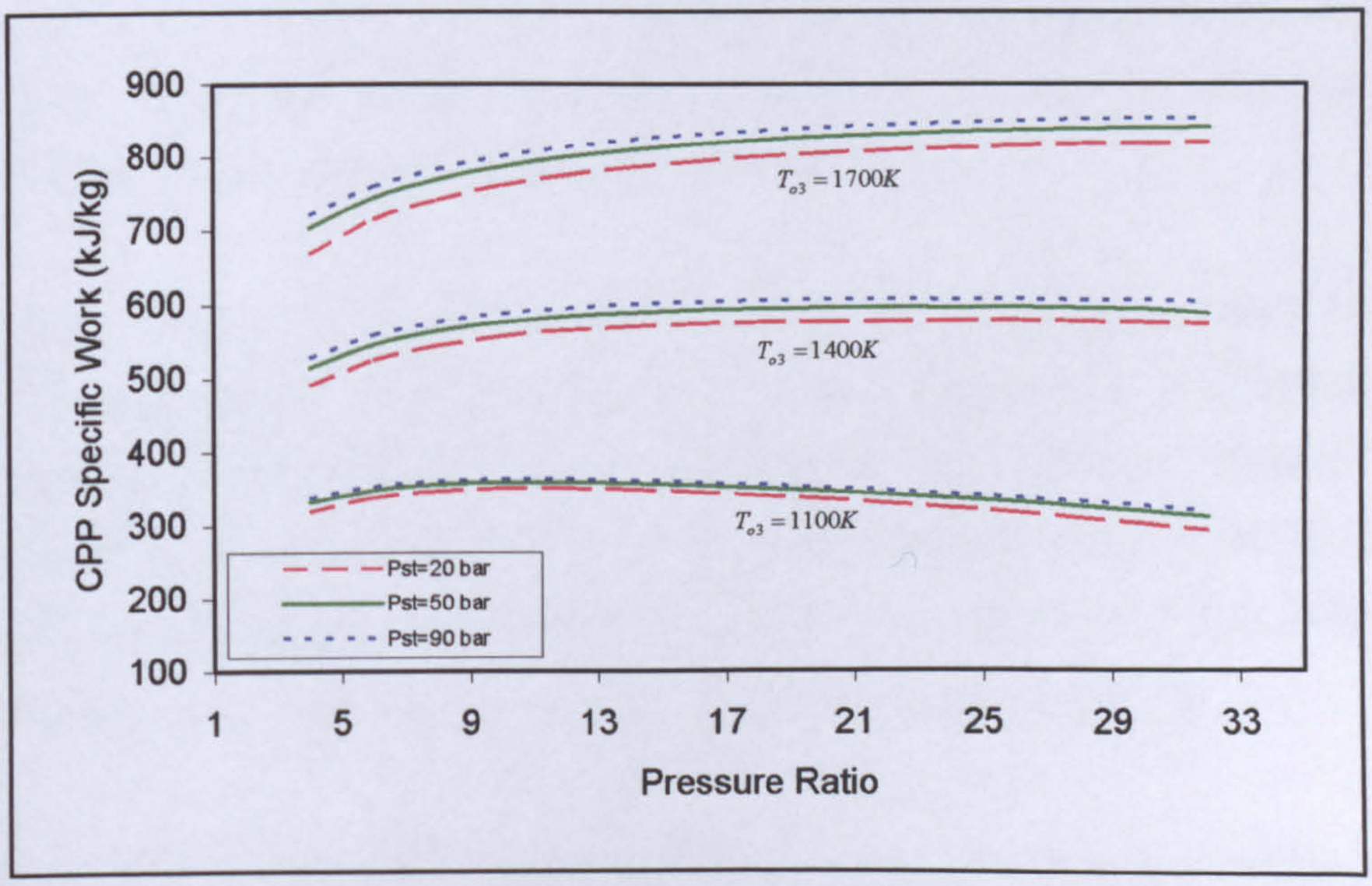

Fig. 6.14 Combined specific work versus pressure ratio at constant turbine inlet temperatures and steam boiler pressures (gas reheat combined cycle)

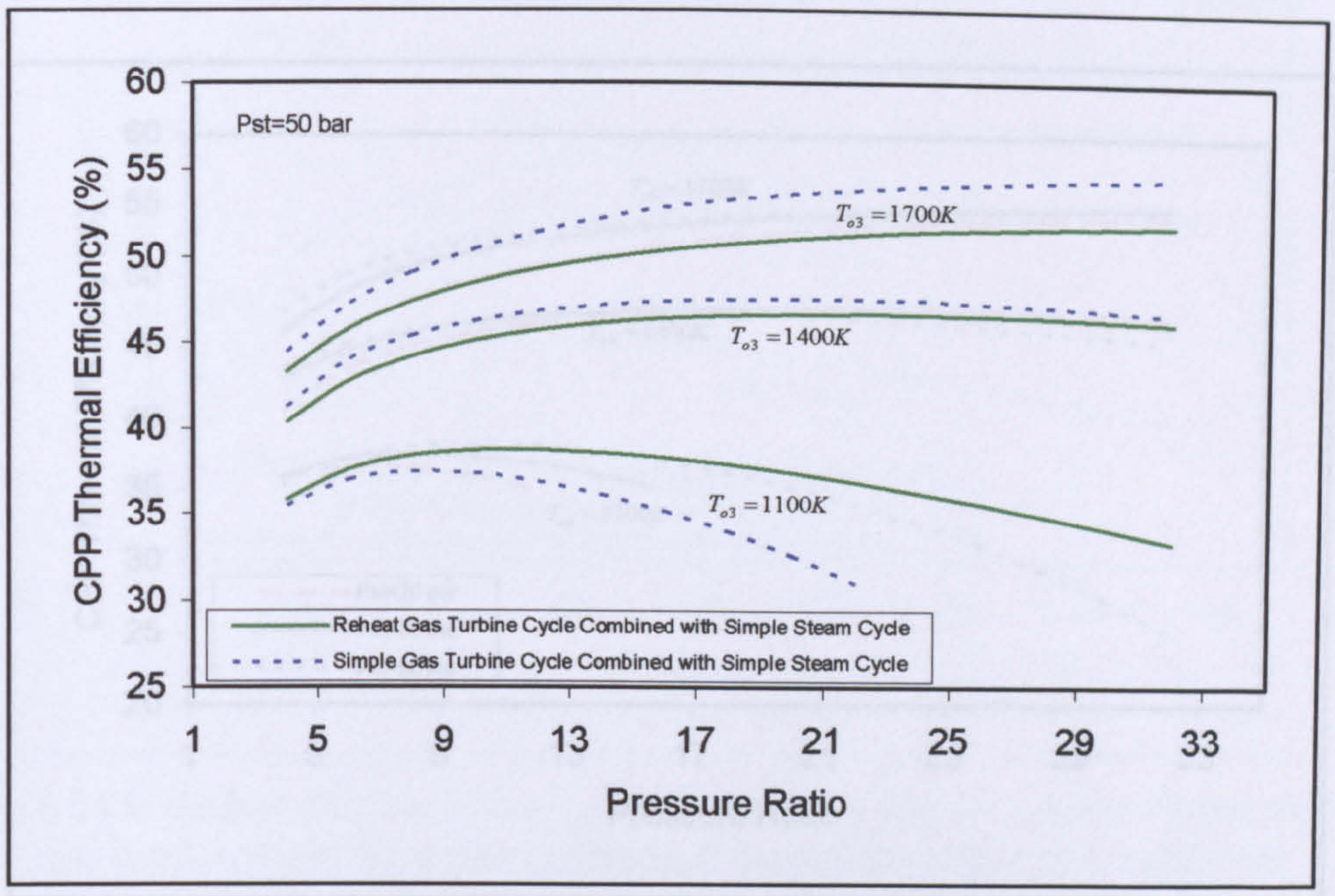

Fig. 6.15 Combined efficiency versus pressure ratio at constant turbine inlet temperatures for simple combined cycle and gas reheat combined cycle

The third set of results, which covers the simple gas turbine cycle combined with dual pressure steam turbine cycle, is given in Figs. 6.16 to 6.18. The conditions for calculating the relevant data are shown on each figure.

Figures 6.16 and 6.17 show that the dual pressure steam cycle will increase both the CPP thermal efficiency and CPP specific work output. It can be also noted that raising the turbine inlet temperature will also increase both the CPP thermal efficiency and CPP specific work output. Furthermore, the effect of higher values of pressure ratio on CPP thermal efficiency is fairly small at constant T_{o3} higher than 1400 K, while the CPP specific work output showed similar trends at all temperatures of T_{o3}.

Figure 6.18 shows the comparison of various cycles; (a) Simple gas turbine cycle combined with simple steam cycle; (b) Simple gas turbine cycle combined with dual pressure steam cycle; and (c) Reheat gas turbine cycle combined with simple steam

cycle. The trends of CPP thermal efficiency lines for theses cycles are similar. It also shows that Simple gas turbine cycle combined with simple steam cycle has the highest thermal efficiency.

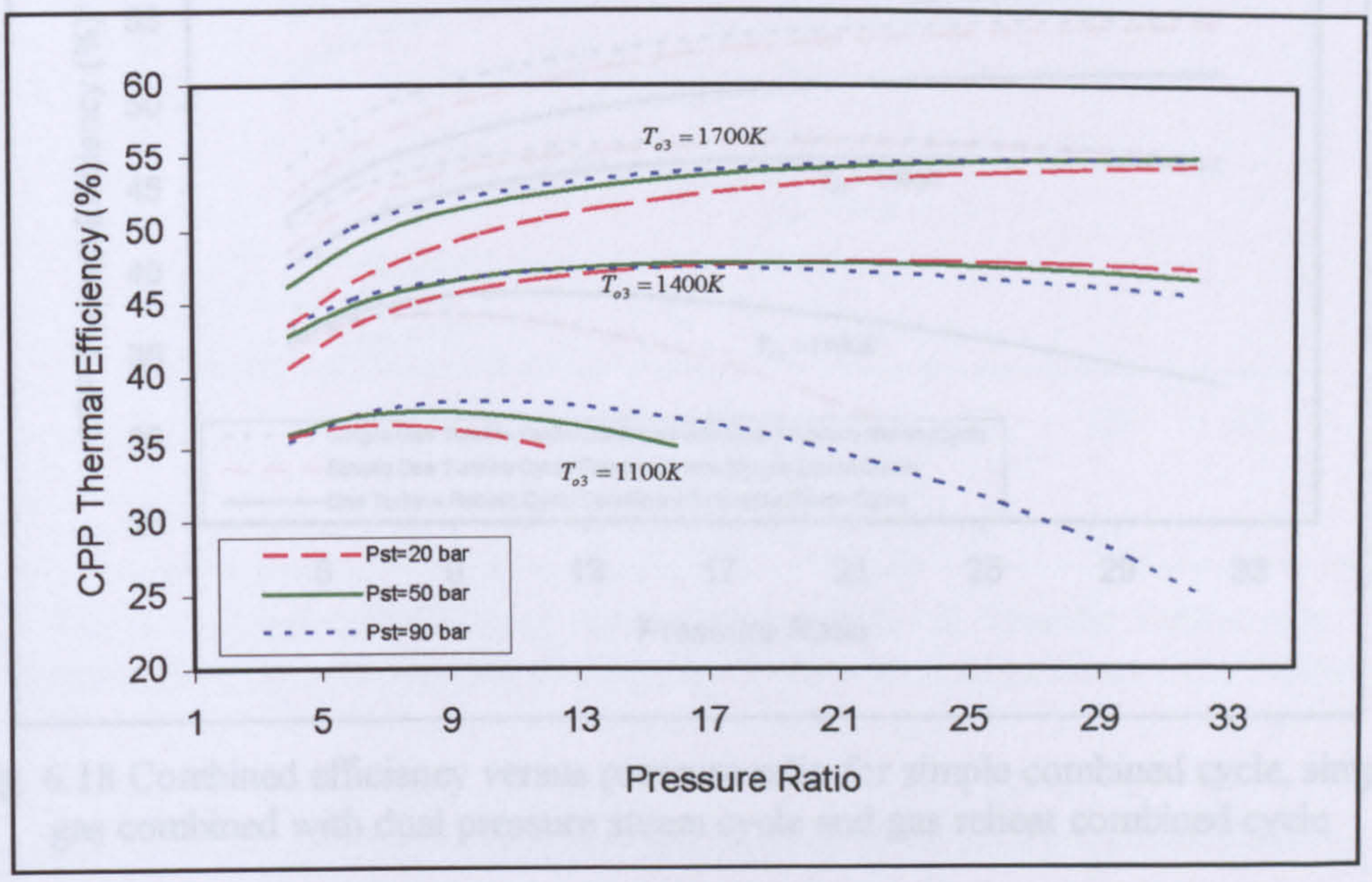

Fig. 6.16 Combined efficiency versus pressure ratio at constant turbine inlet temperatures (simple gas and dual pressure steam combined cycle)

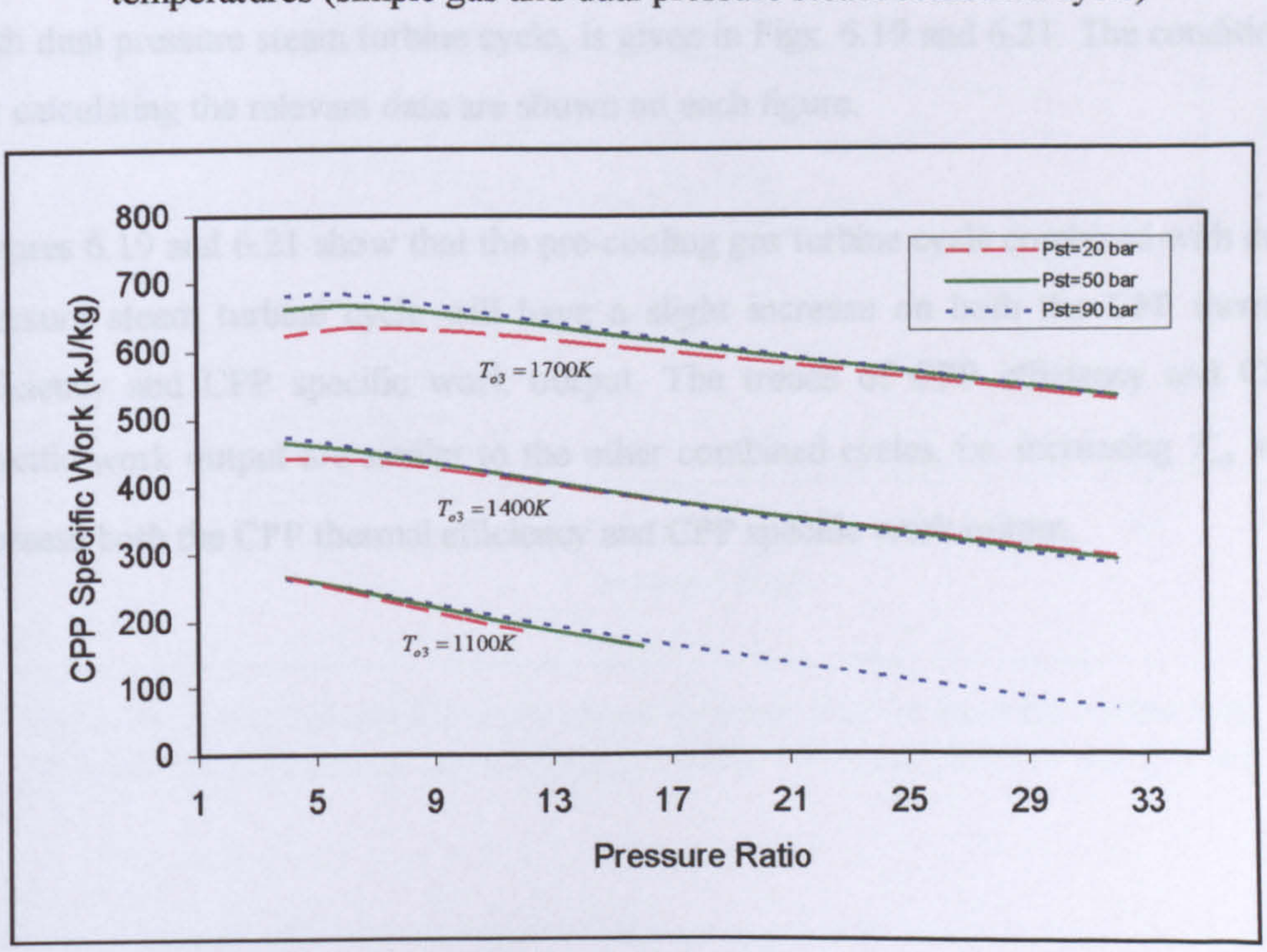

Fig. 6.17 Combined specific work output versus pressure ratio at constant turbine inlet temperatures (simple gas and dual pressure steam combined cycle)

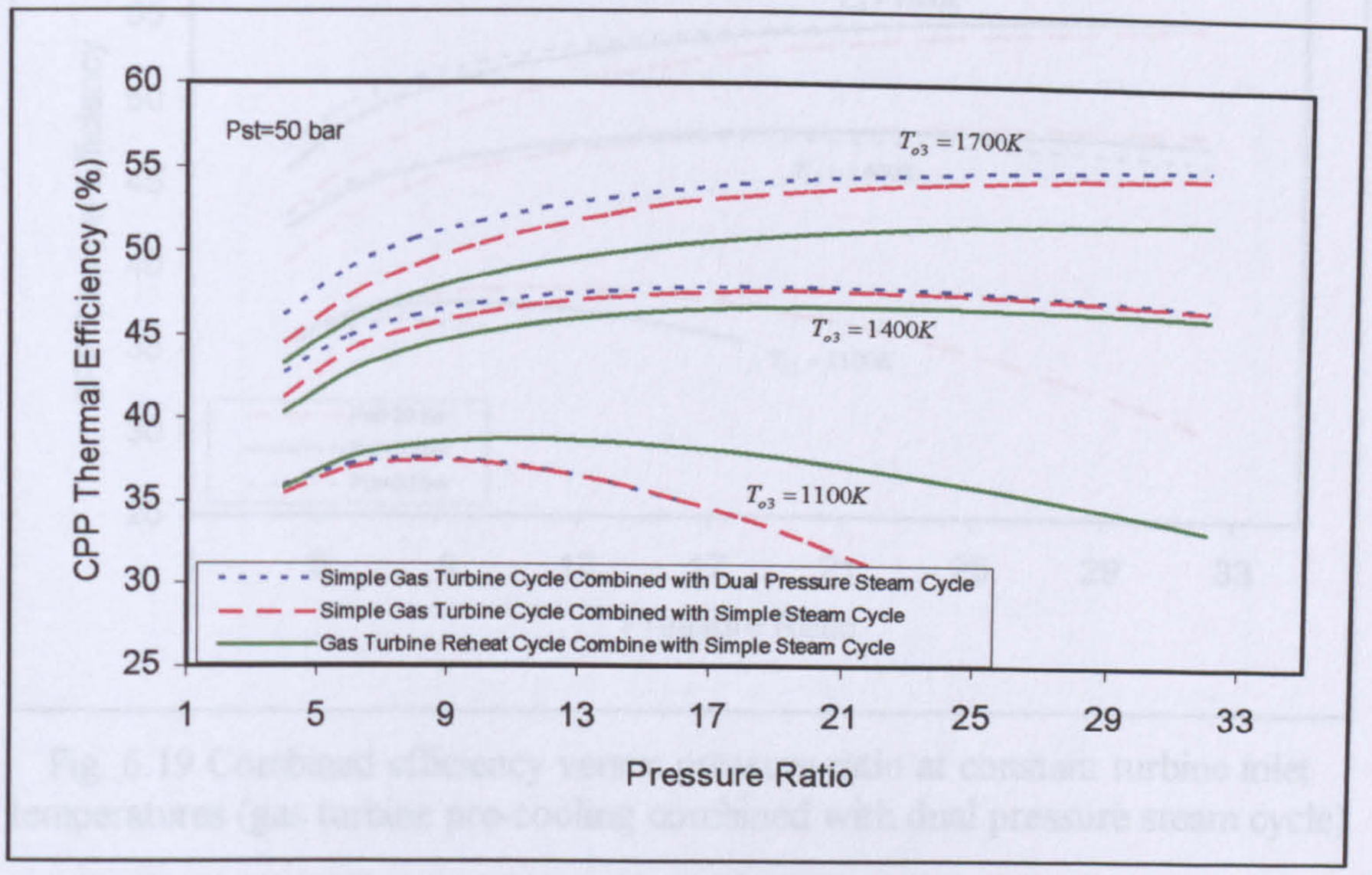

Fig. 6.18 Combined efficiency versus pressure ratio for simple combined cycle, simple gas combined with dual pressure steam cycle and gas reheat combined cycle

The fourth set of results, which covers the pre-cooling gas turbine cycle combined with dual pressure steam turbine cycle, is given in Figs. 6.19 and 6.21. The conditions for calculating the relevant data are shown on each figure.

Figures 6.19 and 6.21 show that the pre-cooling gas turbine cycle combined with dual pressure steam turbine cycle will have a slight increase on both the CPP thermal efficiency and CPP specific work output. The trends of CPP efficiency and CPP specific work output are similar to the other combined cycles, i.e. increasing T_{o3} will increase both the CPP thermal efficiency and CPP specific work output.

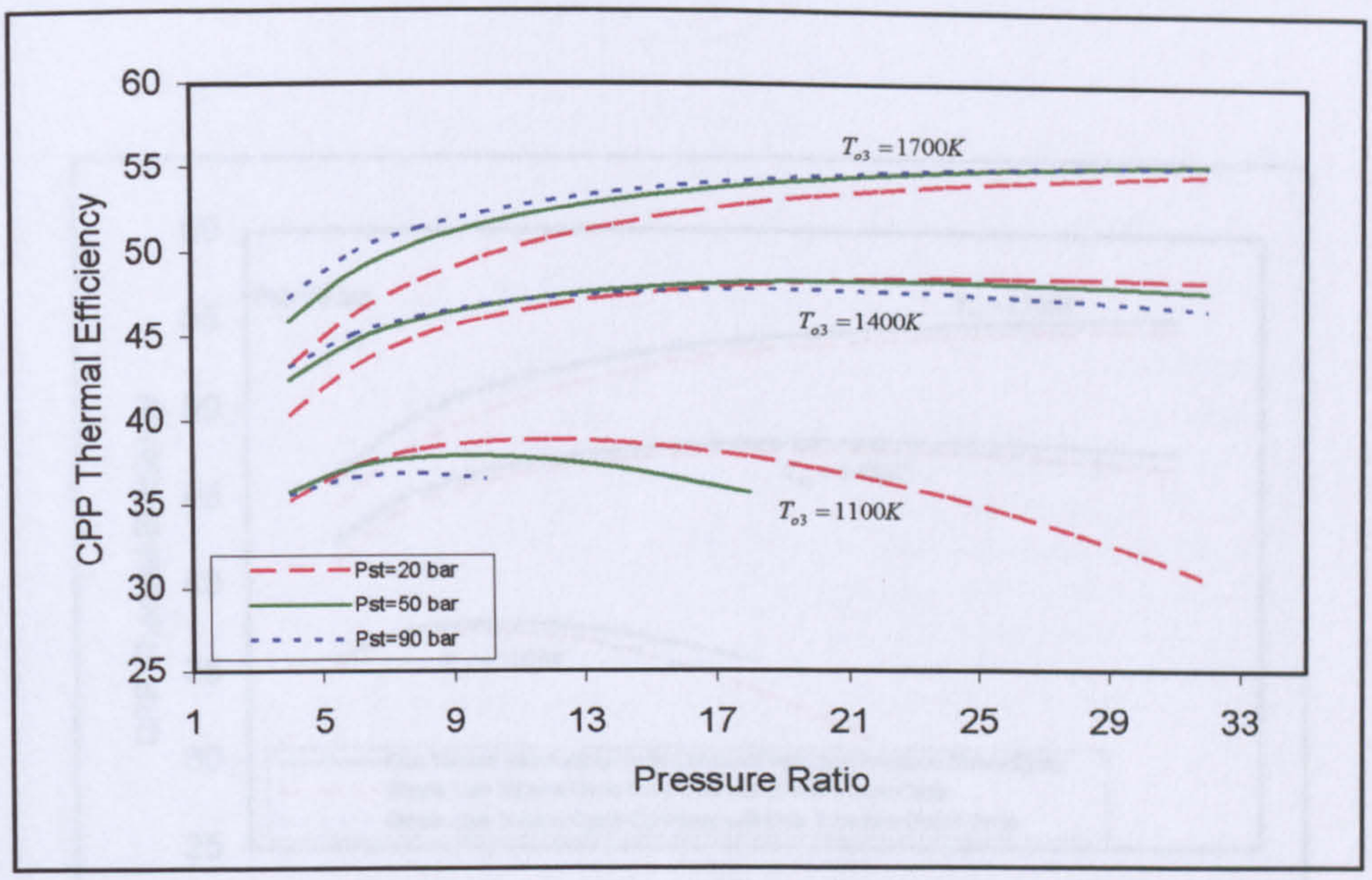

Fig. 6.19 Combined efficiency versus pressure ratio at constant turbine inlet temperatures (gas turbine pre-cooling combined with dual pressure steam cycle)

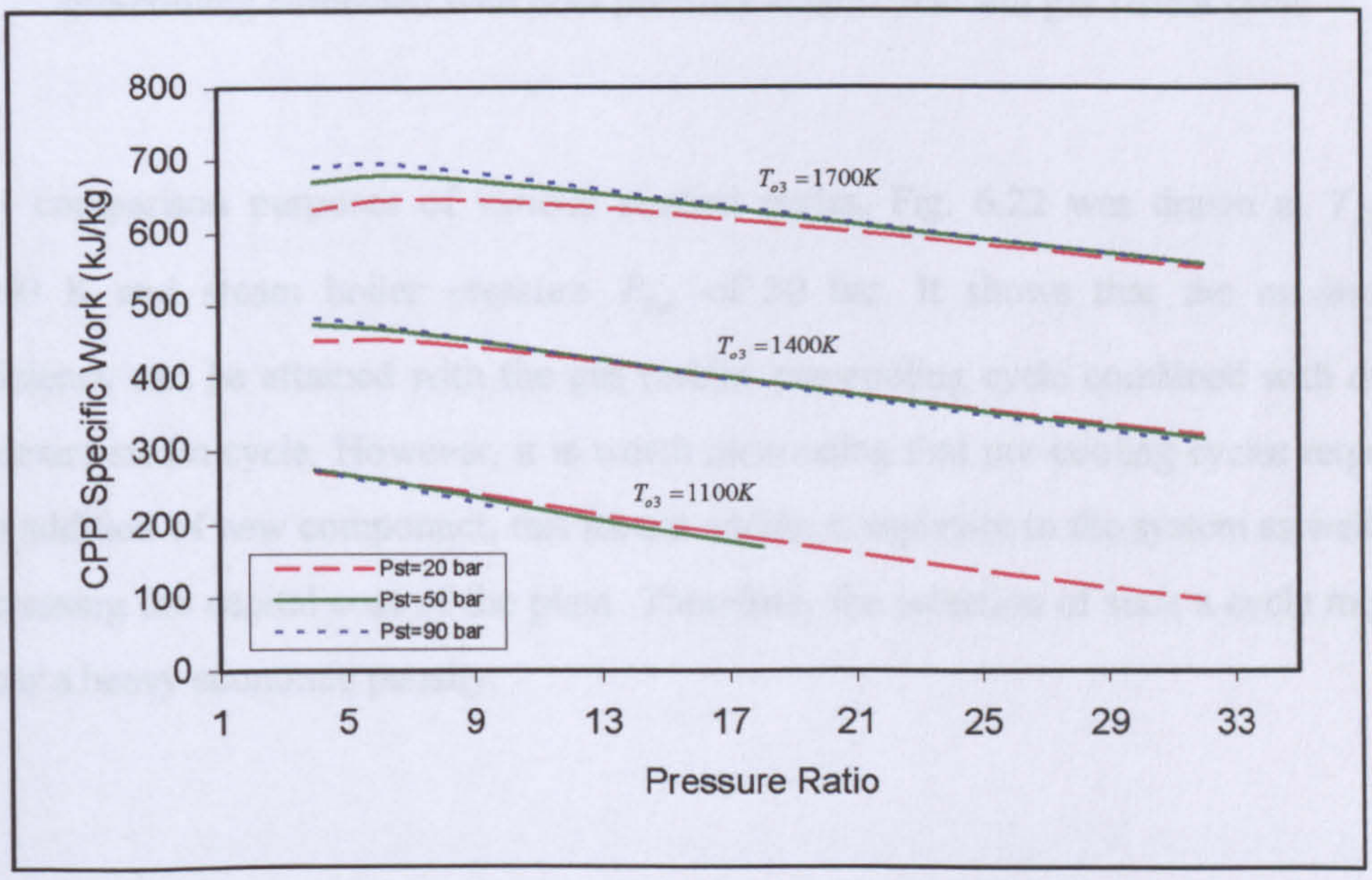

Fig. 6.20 Combined specific work versus pressure ratio at constant turbine inlet temperatures (gas turbine pre-cooling combined with dual pressure steam cycle)

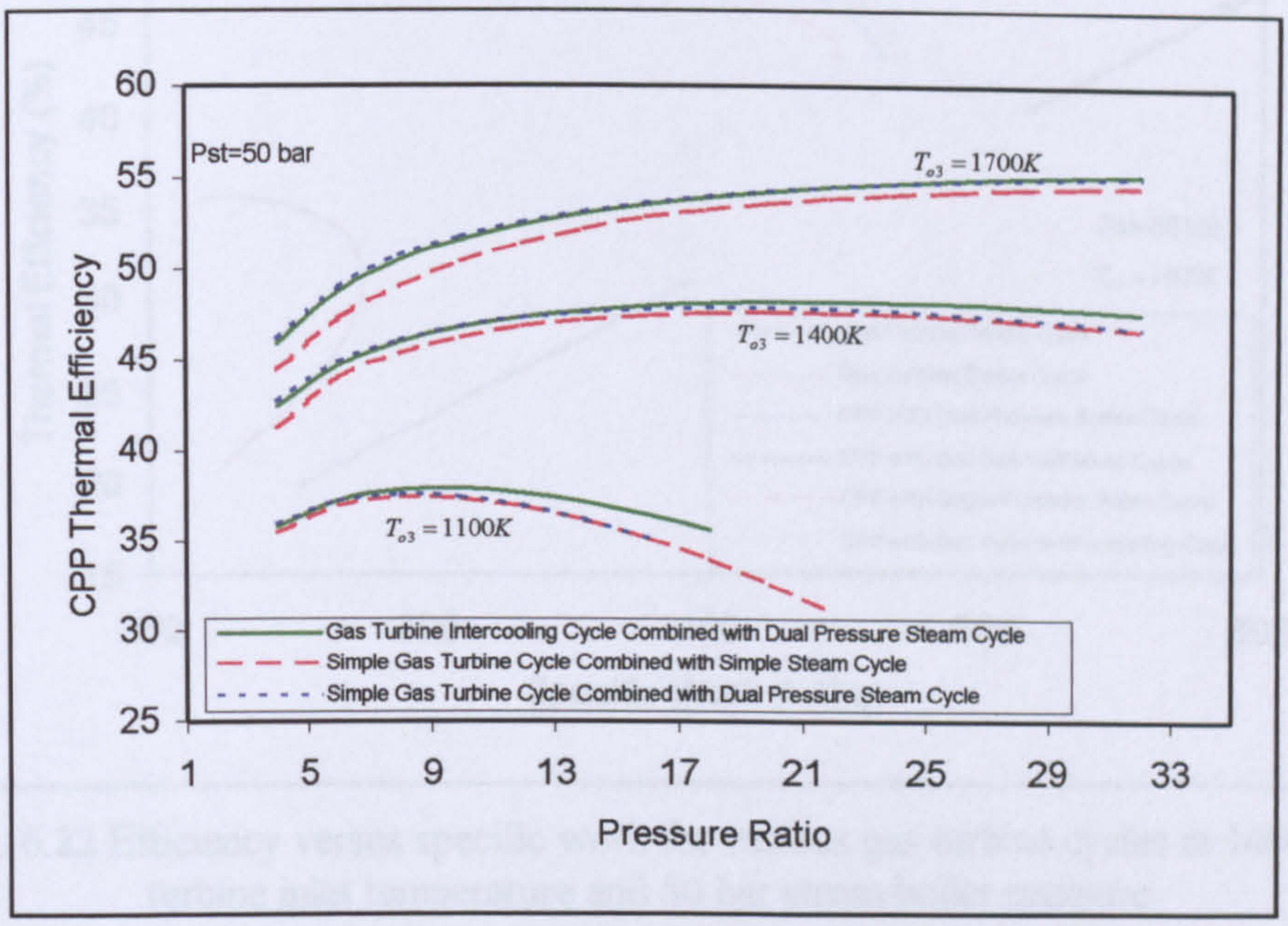

Fig. 6.21 Combined efficiency versus pressure ratio for simple combined cycle, gas pre-cooling combined with dual pressure steam cycle and gas reheat cycle

For comparison purposes of various studied cycles, Fig. 6.22 was drawn at T_{o3} of 1400 K and steam boiler pressure P_{2st} of 50 bar. It shows that the maximum efficiency can be attained with the gas turbine pre-cooling cycle combined with dual pressure steam cycle. However, it is worth mentioning that pre-cooling cycles require the addition of new component, this means adding complexity to the system as well as increasing the capital cost of the plant. Therefore, the selection of such a cycle might incur a heavy economic penalty.

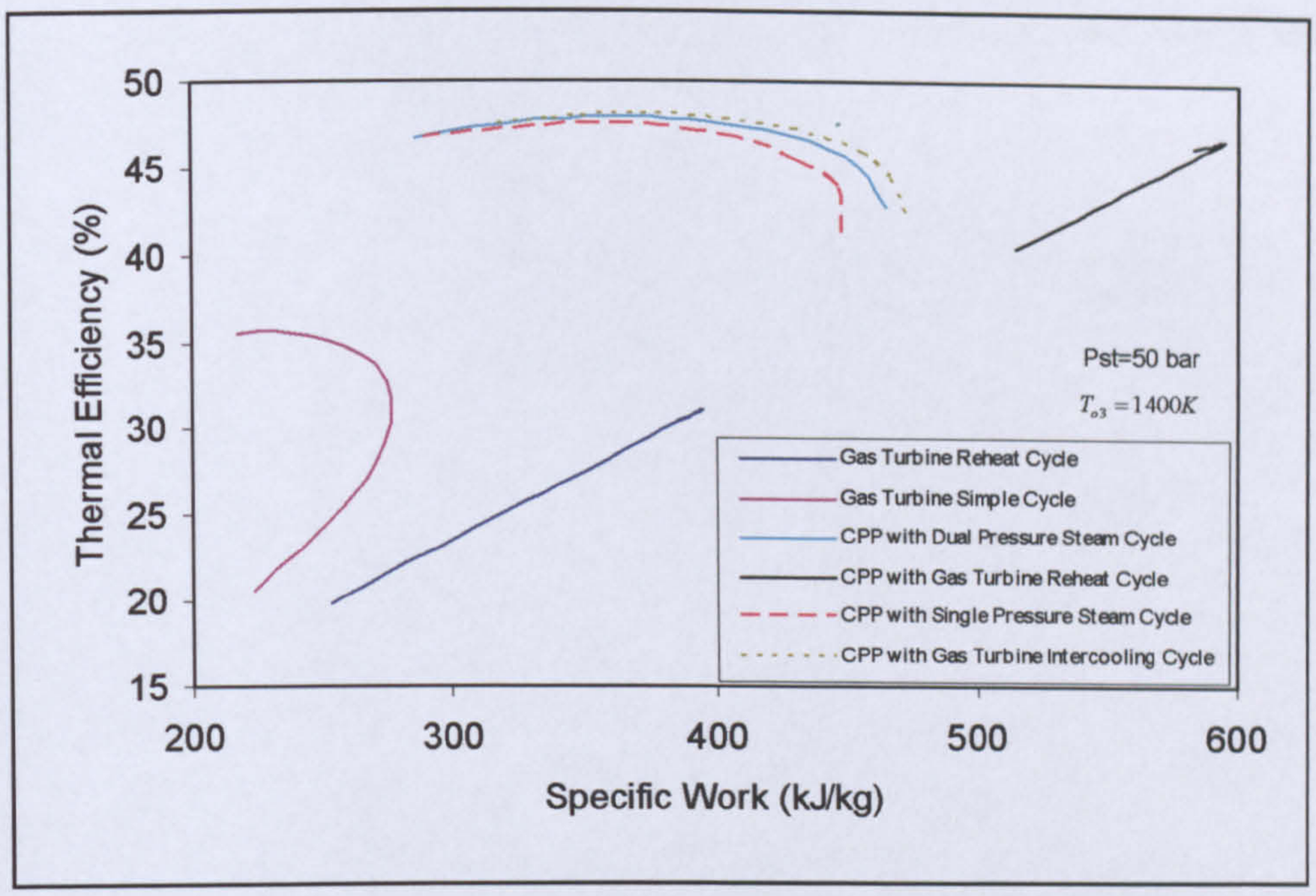

Fig. 6.22 Efficiency versus specific work for various gas turbine cycles at 1400 K turbine inlet temperature and 50 bar steam boiler pressure

6.3 Results of Modelling and Simulation

It was shown previously in chapter 4 a new methodology for matching and simulation of simple gas turbine engine used for power generation application. The output results of methodology are illustrated graphically in Figs 6.23 to 6.32.

Figures 6.23 and 6.24 show complete typical performance characteristics of a centrifugal compressor and complete typical performance characteristics of a radial turbine[42], respectively.

In order to match the turbine with the compressor Figs. 6.23 and 6.24 have to be reproduced by introducing the matching parameter, refer to chapter 4 section 4.3. The outcomes of this transformation are shown in Figs. 6.25 and 6.26. For the compressor it is worth noticing that the constant speed lines were shifted apart, nevertheless the trends stay the same. For the turbine, the trend of the constant speed lines has changed. The reason is due to the fact that the turbine inlet temperature T_{o3} is not

constant along any constant speed line while for the compressor case, the compressor inlet temperature T_{o1} is constant.

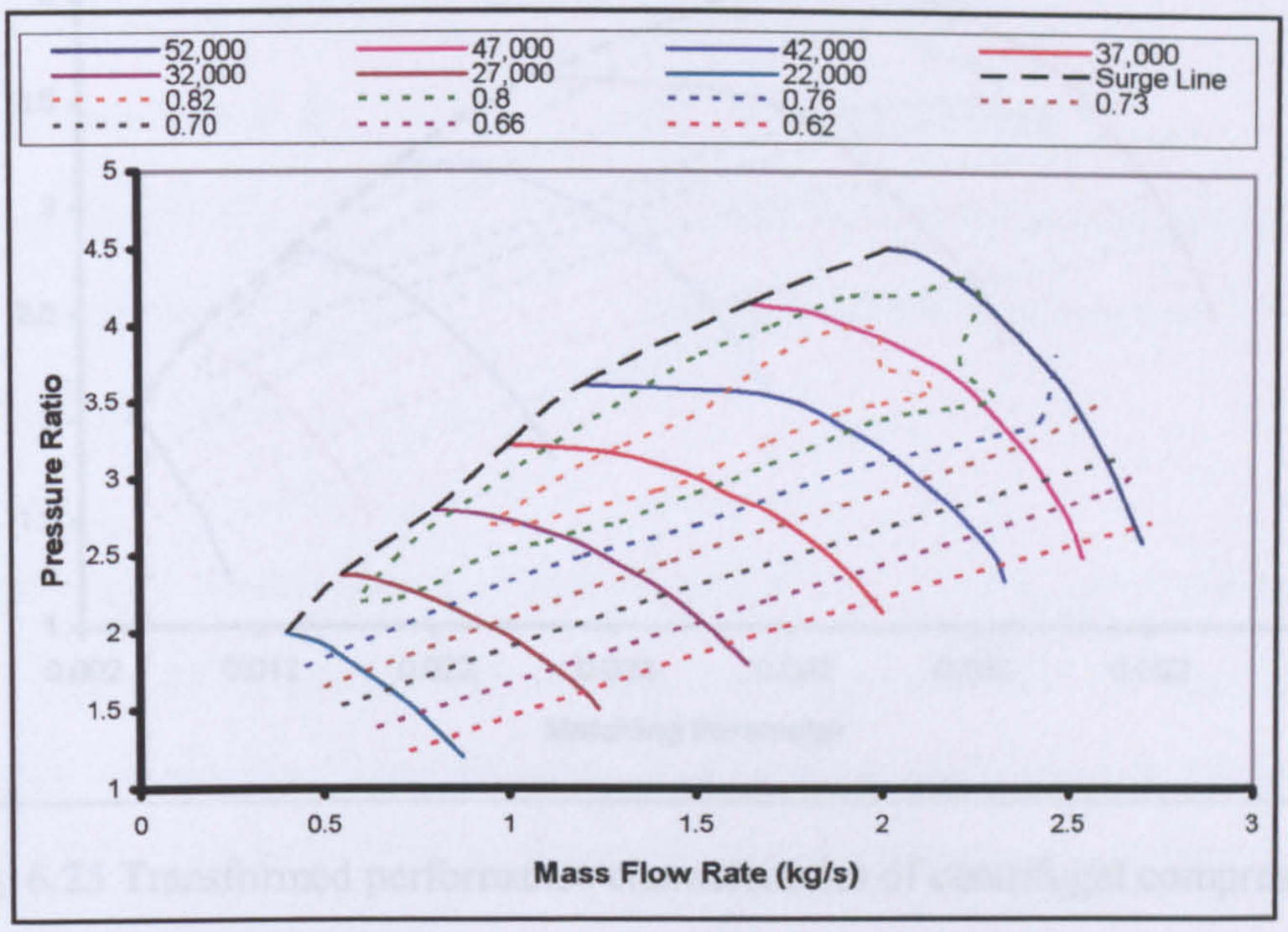

Fig. 6.23 Complete performance characteristics of a centrifugal compressor[42]

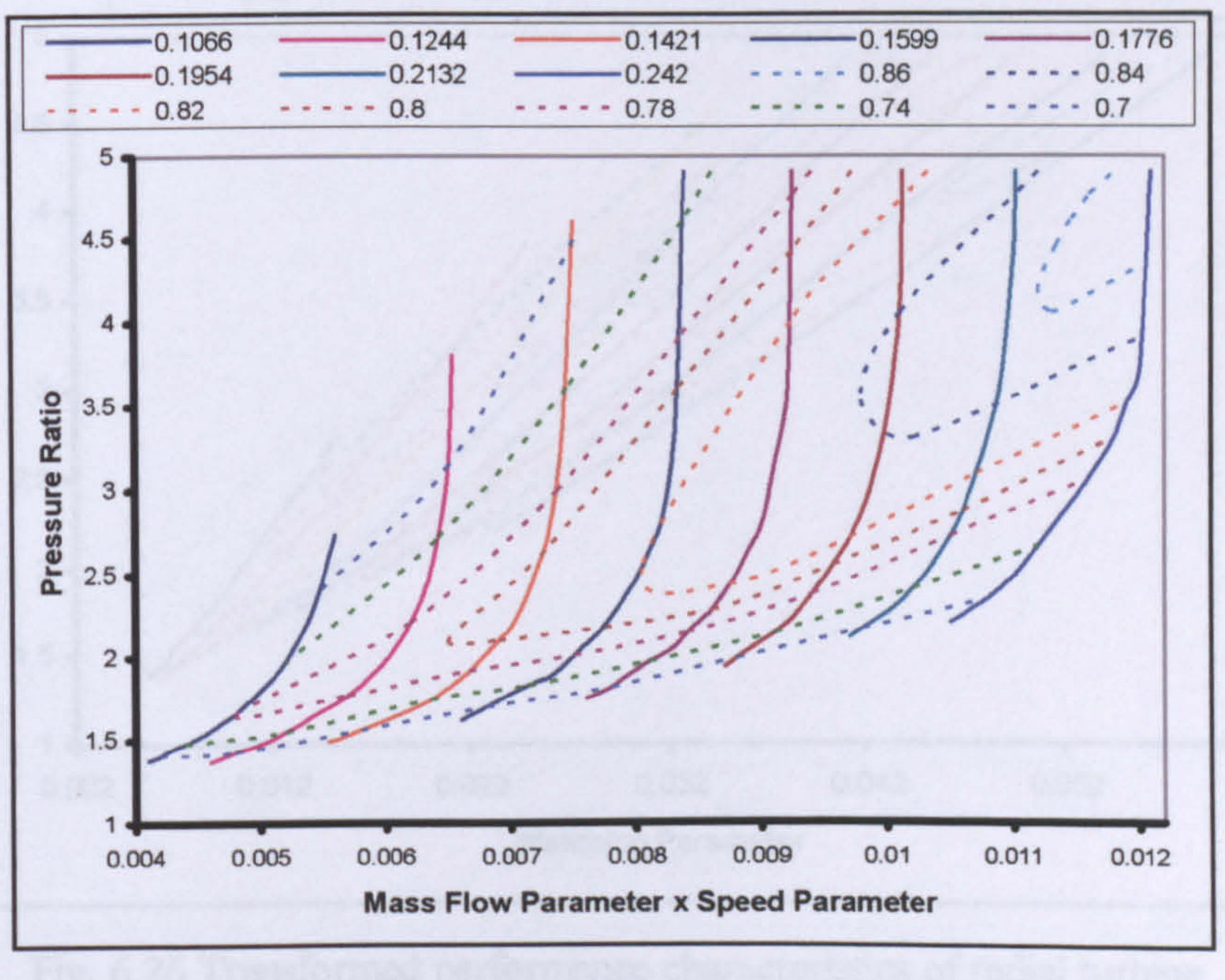

Fig. 6.24 Complete performance characteristics of a radial turbine[42]

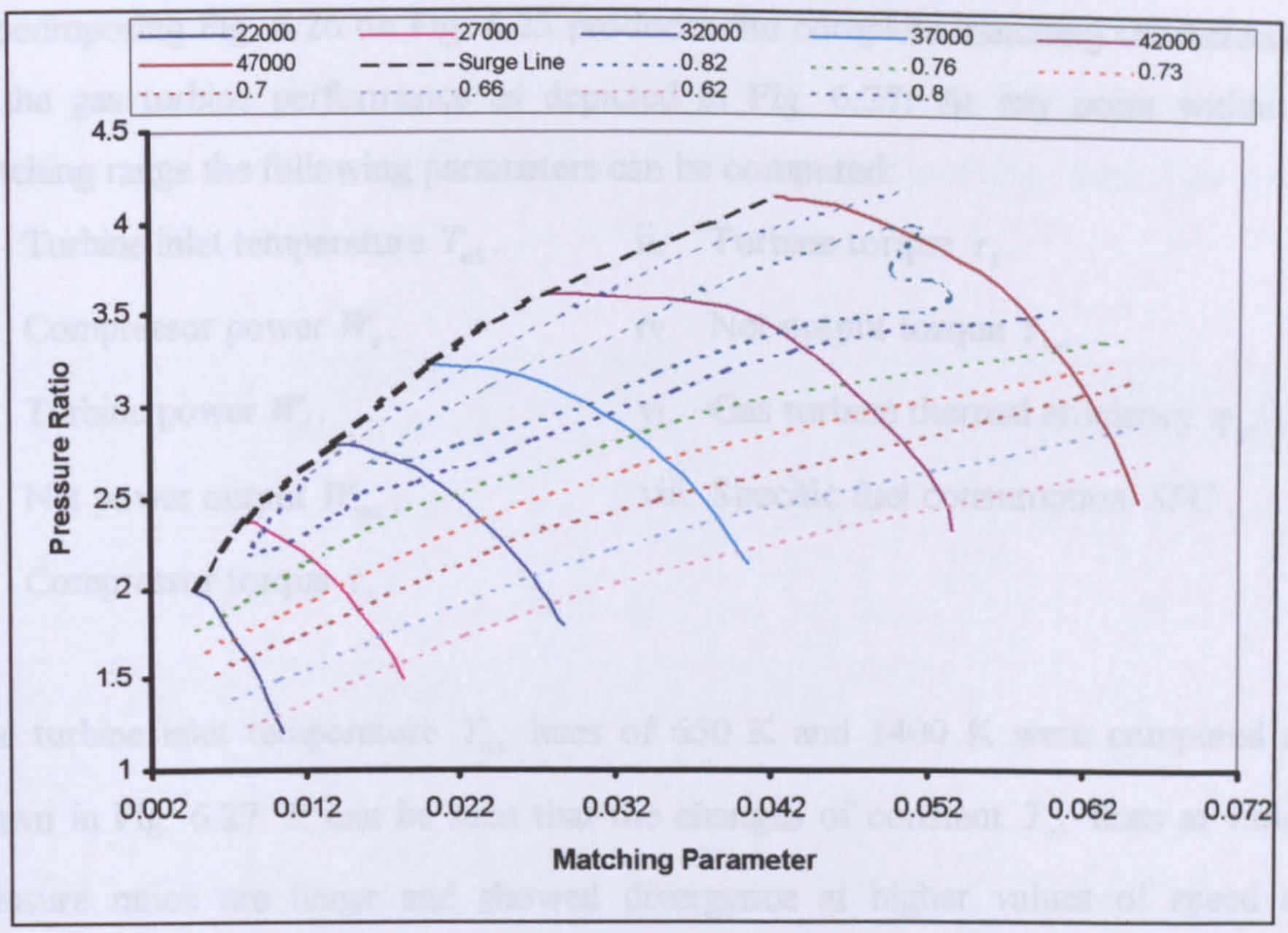

Fig. 6.25 Transformed performance characteristics of centrifugal compressor

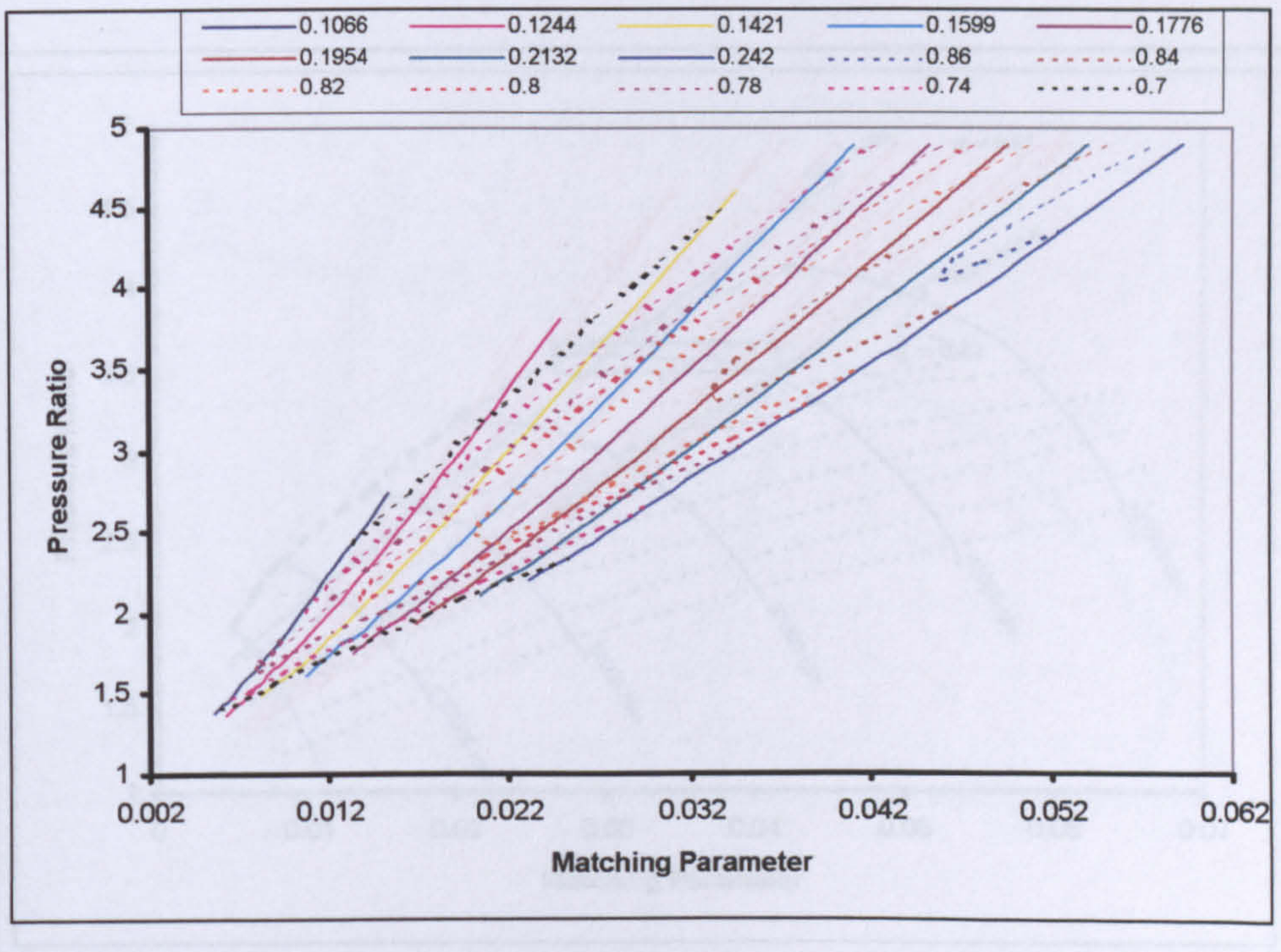

Fig. 6.26 Transformed performance characteristics of radial turbine

Superimposing Fig. 6.26 on Fig. 6.25 produces the complete matching characteristics of the gas turbine performance as depicted in Fig. 6.27. At any point within the matching range the following parameters can be computed:

i. Turbine inlet temperature T_{o3}.
ii. Turbine torque τ_t.
iii. Compressor power W_c.
iv. Net output torque τ_{net}.
v. Turbine power W_t.
vi. Gas turbine thermal efficiency η_{gt}.
vii. Net power output W_{net}.
viii. Specific fuel consumption SFC.
ix. Compressor torque τ_c.

The turbine inlet temperature T_{o3} lines of 650 K and 1400 K were computed and drawn in Fig. 6.27. It can be seen that the changes of constant T_{o3} lines at various pressure ratios are linear and showed divergence at higher values of speed and pressure ratios. The area between these two lines represents the accepted working range for the gas turbine engine.

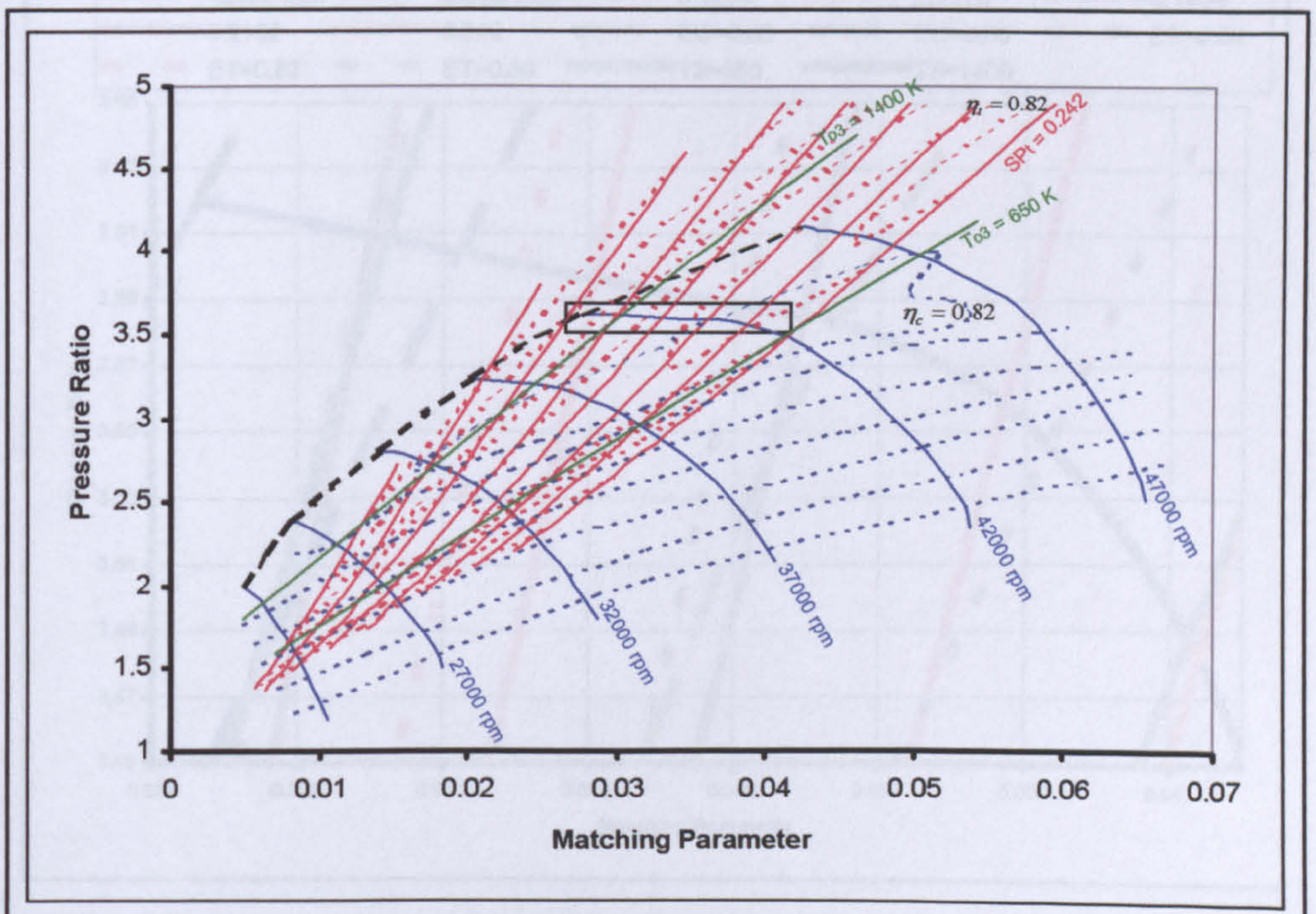

Fig. 6.27 Complete matching characteristics of the gas turbine performance

For a power generation driven by gas turbine engine, let's consider any running line for example a speed of 42000 rpm as shown in Fig. 6.28. Based on the graphical analysis, the above parameters can be calculated within the specified working range. The output results are given in Table 6.1.

#	Matching Parameter	r	Turbine Speed	η_c	η_t	T_{o2}	T_{o3}	T_{o4}	W_c
1	0.0413	3.483	0.242	83	82	436.82	651.97	508.69	268.24
2	0.0387	3.558	0.2132	83.2	84.5	439.48	840	647.02	255.85
3	0.0359	3.585	0.1954	81.8	84.5	443.17	1000	769.1	243.12
4	0.0331	3.597	0.1776	80.8	82.8	445.58	1210.52	936.02	227.64
5	0.03	3.61	0.1599	79.5	80	448.7	1493.34	1165.4	210.4
#	W_t	W_{net}	Fuel/Air Ratio	$\dot{m}_f$	η_{gt}	SFC	τ_c	τ_t	τ_{net}
1	296.79	28.55	0.00611	0.01095	6.37	0.7699	203.39	225.04	21.65
2	374.59	118.74	0.01143	0.01921	15.1	0.4264	194	284.04	90.04
3	415.78	172.66	0.01596	0.02488	16.95	0.3327	184.35	315.27	130.92
4	455.72	228.08	0.02205	0.03169	17.57	0.3281	172.61	345.55	172.94
5	493.48	283.08	0.03036	0.03955	17.48	0.3861	159.54	374.19	214.65

Table 6.1 Calculated parameters within the specified working range of 42000 rpm

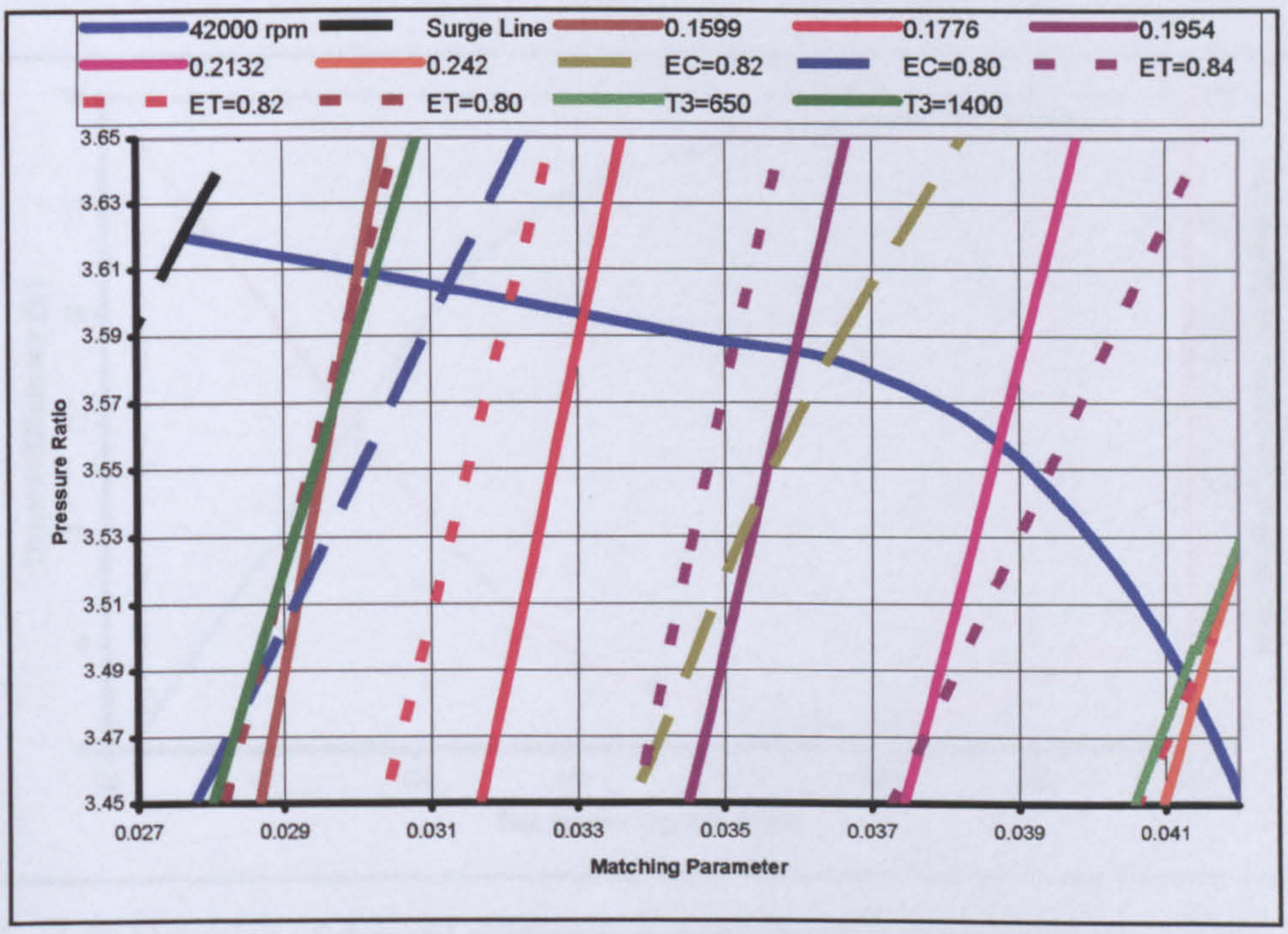

Fig. 6.28 Matching characteristics at running line of 42000 rpm

Using the results in Table 6.1, the relationship between thermal efficiency and specific fuel consumption with the net power output are drawn in Fig. 6.29. It shows that the

maximum thermal efficiency of 17.57% is attained, which corresponds to a net power output of 228 kW and minimum specific fuel consumption of 0.3327 kg/kW.hr.

Figure 6.30 shows that the gas mass flow rate is decreasing with increasing the net power output. At the same time the gas exhaust temperature is increasing under the same condition. This can be explained due to the fact that the turbine is considered a constant volumetric flow component, i.e. the turbine will passes the same amount of volume turbine flow rate. Increasing the turbine work output at constant speed can be achieved by raising the turbine inlet temperature T_{o3}. In order to accommodate the same amount of volumetric mass flow at this higher T_{o3}, the mass flow rate must decrease. Consequently the gas exhaust temperature increases.

In combined power and power cycles, the input conditions of the steam power plant are based on the two parameters, which are the gas mass flow rate and the gas exhaust temperature. These parameters can be extracted from Fig. 6.30.

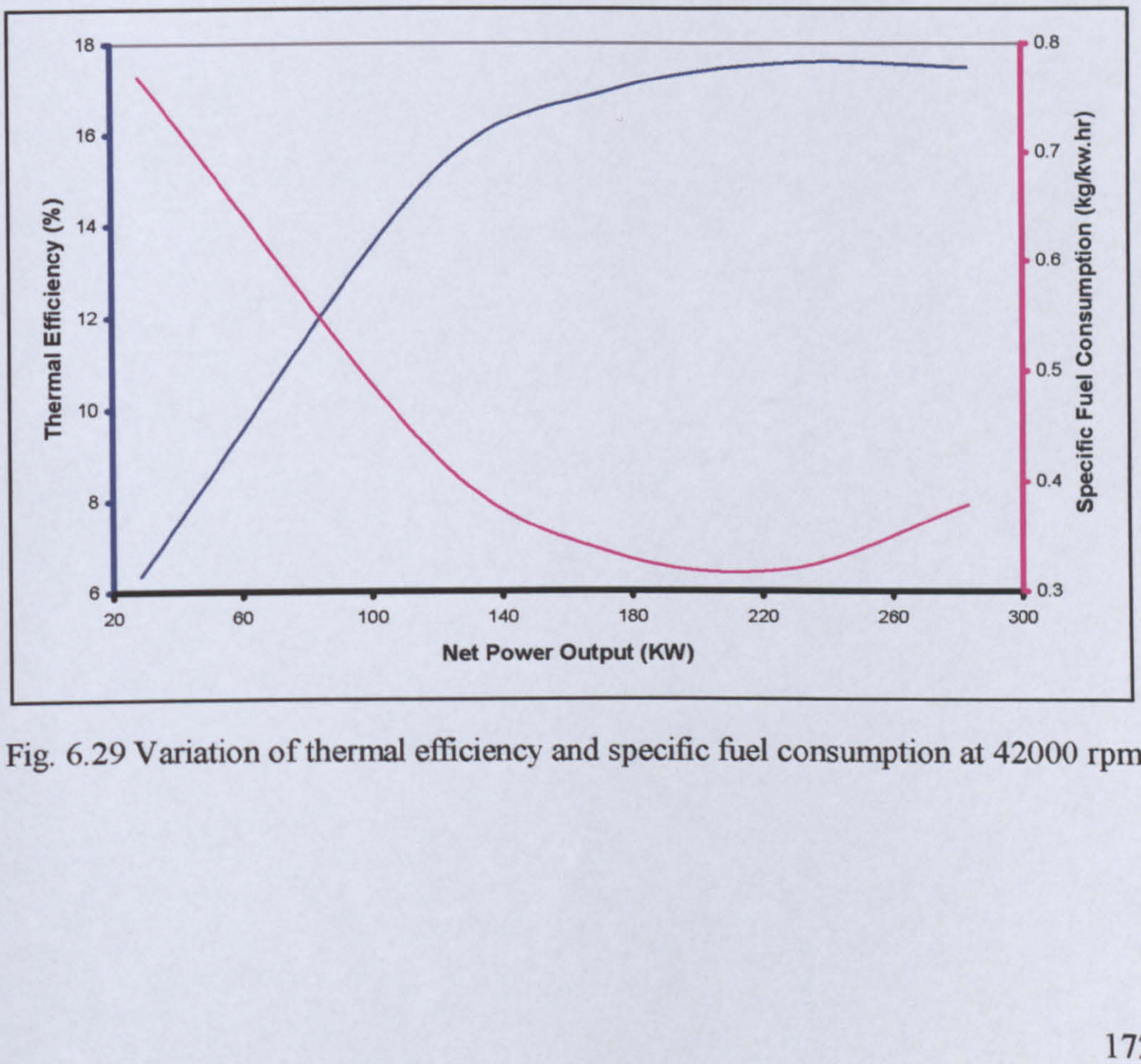

Fig. 6.29 Variation of thermal efficiency and specific fuel consumption at 42000 rpm

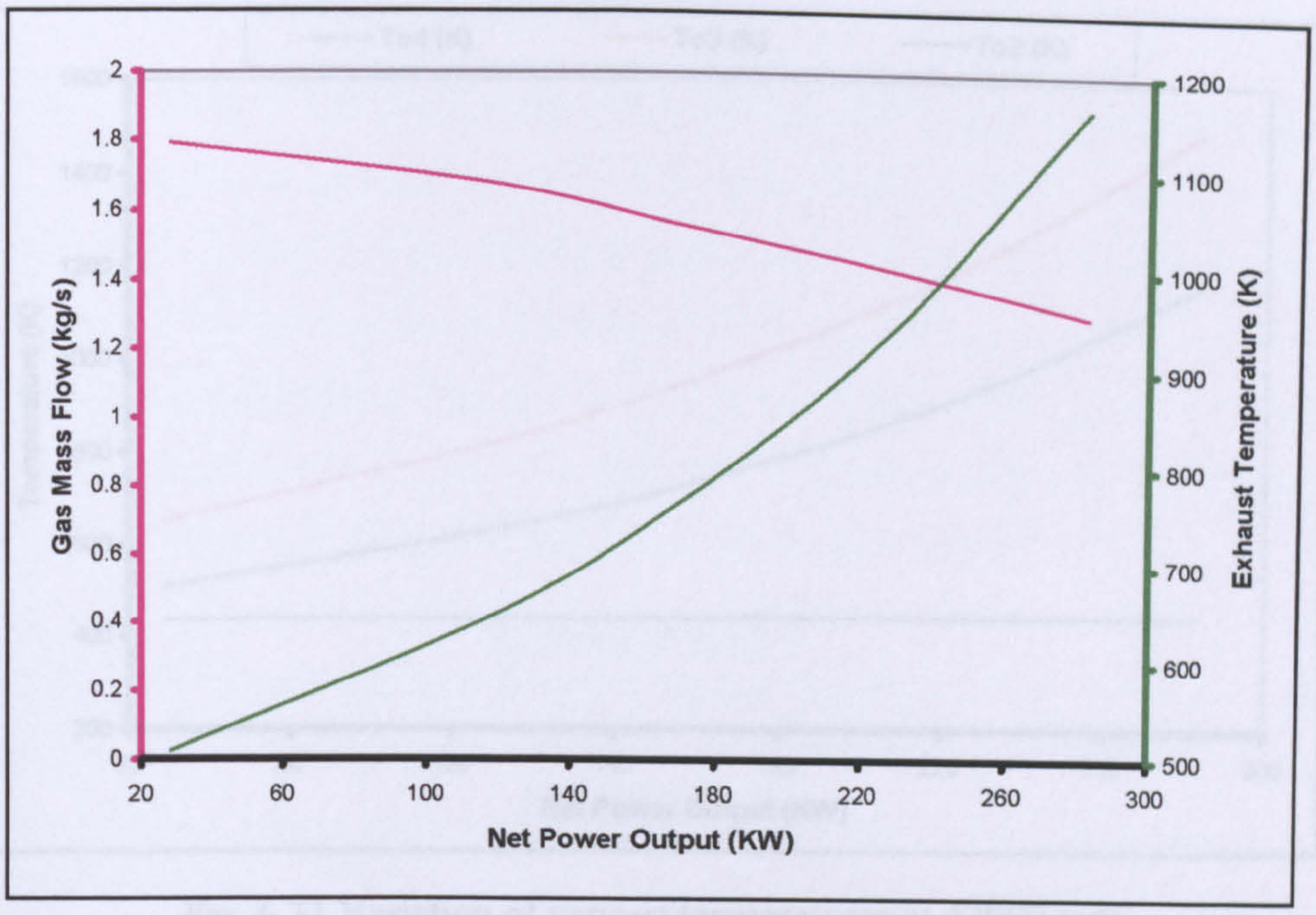

Fig. 6.30 Variation of exhaust mass flow and temperature at 42000 rpm

Figure 6.31 shows the variation of temperatures T_{o2}, T_{o3} and T_{o4} with the net power output. It can be seen that the variation of T_{o2} is fairly small because T_{o2} depends on the compressor pressure ratio and within the working range of the constant speed of 42000, the pressure ratio variation is small (see Fig. 6.28).

Figure 6.32 shows the relationship between the turbine and compressor torque with net power output of the gas turbine engine at constant speed of 42000 rpm. It can be noticed that the variation of torque and net power output is linear and increases at a constant rate.

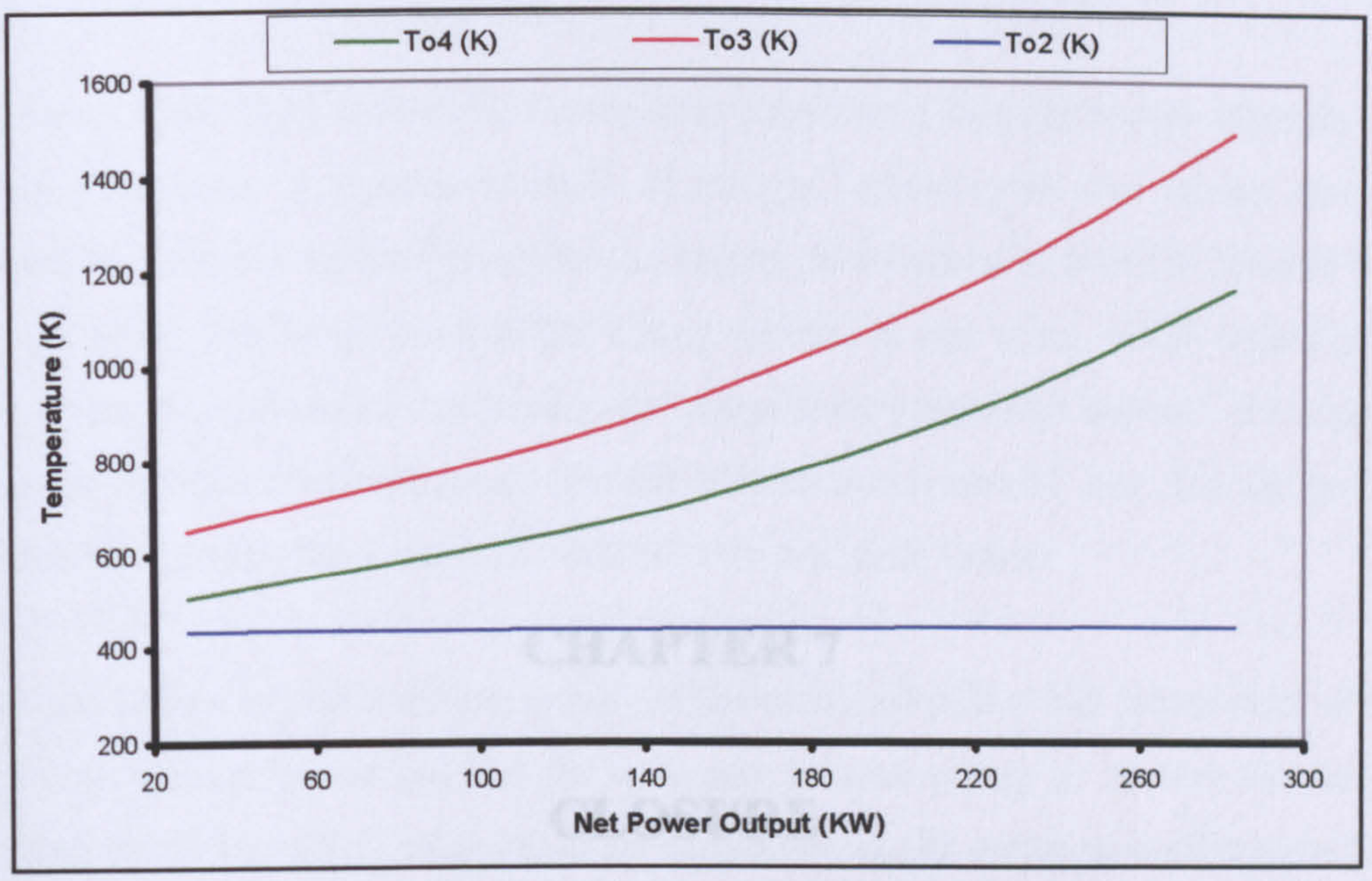

Fig. 6.31 Variation of various temperatures at 42000 rpm

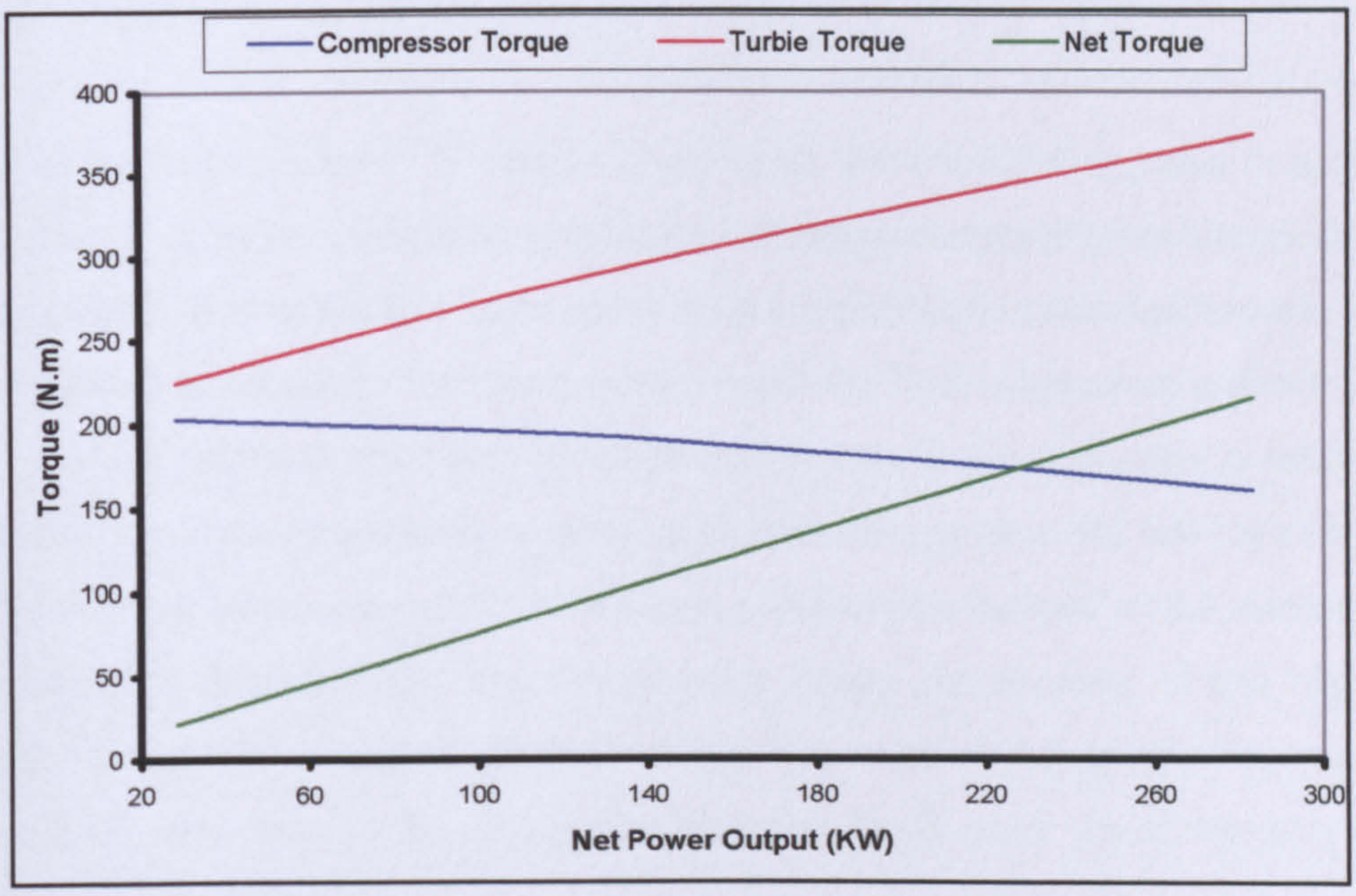

Fig. 6.32 Variation of torque values at 42000 rpm

CHAPTER 7

CLOSURE

7.1 Conclusions

The gas turbine plant represents a complex system where its performance depends on many parameters. A parametric study of the gas turbine cycle was carried out to assess the influence of each parameter on engine performance in order to identify the design point. The design point in this case is defined as that point, which would give the optimum performance. Achieving the design point parameters depends on factors such as economic, technological, operational and environmental, etc. The design of gas turbine plants often requires a trade off between these factors.

The gas turbine engine operating as part of the combined power and power plant does not only produce power but also the necessary thermal energy to operate the steam turbine plant. Therefore, what might be considered as the optimum performance for the gas turbine plant may not necessarily be the optimum performance of the combined power and power or the CPP plant. The results of the parametric study confirm this hypothesis.

Gas turbine engine consists of various components that are linked together in such a way that there exists a mechanical and thermodynamic interdependence among these components. This means that some operational compatibility (matching) between the components is necessary for steady state operation. This requirement reduces the range of the operating conditions for these components. But it is possible to define a subset of the engine's operating envelope such that every point in this sub-region is at an equilibrium working point. These working points can be mapped on the respective components' characteristics. The design point values are elements of this region which yield the best thermal efficiency within the range of the specified operating conditions. Any point in the region other than the design point would represent an off-design condition.

The off-design problem may therefore be stated as the determination of a point in this region that corresponds to some specified conditions at which the equilibrium criteria would be satisfied but at reduced value of thermal efficiency. Since the operating

points of the individual components can be determined by using a set of values of some characteristic parameters, the off-design problem reduces to computing the values of these parameters that would satisfy the equilibrium criteria.

A computer program for simulating a gas turbine engine has been developed that can satisfy the necessary matching conditions analytically and thus achieve matching between the various components in order to produce the equilibrium running line. Representing the data for this line either in the form of *lookup tables* or an *equation* is known as modelling; solving that equation with the help of a computer is computer simulation. Thus modelling and simulation together satisfy all energy and mass balances, all equations of state of the working fluids, and the performance characteristics of all components.

The subject of this thesis "Design criteria and performance of gas turbines in a combined power and power (CPP) plant for electrical power generation" was an ambitious programme as the intention originally was to adopt a full scale aircraft gas engine for the experimental work. As the work progressed, it became clear that using a full scale engine was not practical option for the following reasons:

(a) A matching alternator and a suitable gearbox to couple it to the engine were not available and purchasing these items especially for the purpose of this research was far beyond the research funds allocated originally.

(b) A suitable boiler and a steam turbine to absorb the waste heat from the gas turbine exhaust could not be found.

In view of these limitations, this research programme had to be modified without significantly altering its overall objective or scope. The emphasis then shifted to theoretical work and the development of computer programs to verify the hypothesis, which simply states that a different philosophy would be required to design a gas turbine specifically for CPP plant than that used for designing either industrial or aero gas turbine engines.

The results of the work, presented in this thesis, led to the following conclusions:

i. For a simple gas turbine cycle, the maximum efficiency and the maximum specific work depend on different performance parameters, such as cycle pressure ratio or the dimensionless mass flow and speed parameters, while for a reheat gas turbine cycle, the maximum efficiency and the maximum specific work depend on identical performance parameters.

ii. Supplementary heating will always decrease the combined cycle efficiency except in the case that the supplementary heating significantly increases the steam turbine cycle efficiency.

iii. Increasing the gas turbine inlet temperature at constant cycle pressure ratio will increase the combined cycle efficiency and the combined specific work.

iv. The higher the gas turbine inlet temperature the greater the influence of the pressure ratio difference on the combined cycle efficiency of any combined cycle configurations.

v. Gas turbine reheating can be justified only if the turbine inlet temperature is low (low gas exhaust temperatures) and/or higher combined specific work output.

vi. Although gas turbine pre-cooling improves the gas turbine performance, it has a slight effect on the combined cycle efficiency and the combined specific work output.

vii. In the combined power and power cycle, the combined cycle maximum efficiency depends on neither the gas turbine maximum efficiency parameters nor the gas turbine maximum specific work parameters, but on new parameters that are closer to the gas turbine maximum specific work parameters.

viii. Matching conditions between the compressor and the turbine may be met by superimposing the turbine performance characteristics on the compressor performance characteristics with suitable transformation of the co-ordinates.

ix. The computer simulation program can help in investigating the effects of the components performance characteristics on the performance of the complete engine. This investigation can be carried out at the design

stage without bearing the cost of manufacturing and testing an expensive prototype.

x. The computer simulation program can also serve as a valuable tool for investigating the performance of the gas turbine at off-design conditions. This investigation can help in designing an efficient control system for the gas turbine engine of a particular application including being an identical of the CPP plant.

7.2 Recommendations for Further Work

The results of the theoretical studies have demonstrated the interactions between the gas turbine and the steam turbine do limit the freedom of choice of the principal design parameter to a narrow range for optimum performance of the CPP plant. However, solid experimental evidence is needed to convince the potential users that the overall efficiency of CPP plant can be raised. Further work is needed to put together a full scale plant to provide the all important evidence that based on experimental data.

The present study has not considered the control problems in sufficient detail. Therefore, it is felt that further research is needed to study the problems of controlling the CPP plant to achieve optimum performance. The potential user of the CPP plant would be interested to know whether it would be more profitable to dedicate the steam turbine to handle the base load and use the gas turbine to deal with load variations or vice versa. The initial studies of the various control strategies may be carried out by using the simulation program developed for present research and described in this thesis.

Finally, further work would also be valuable to investigate, by means of experimental work, the validity of the matching concept that has been developed in this thesis.

REFERENCES

References

[1] Horlock, J. H. *"Combined power plants; including combined cycle gas turbine (CCGT) plants"*. Pergamon Press, Oxford, 1992.

[2] Cohen, H., Rogers, G. F. C. and Saravanamuttoo, H. I. H. *"Gas turbine theory"*. 4th edition, Longman, London, 1996

[3] Kehlhofer, R. *"Combined cycle gas turbine and steam turbine power plants"*. Fairmont Press, Lilburn GA, 1991.

[4] Haywood, R. E. *"Analysis of engineering cycles"*. 4th edition, Pergamon Press, Oxford, 1991.

[5] Sonntag, R. E. *"Fundamentals of thermodynamics"*. 5th edition, Wiley, New York, 1998.

[6] Watson, J. *"The technology that drove the 'dash for gas'"*. Power engineering journal, Feb. 1997, PP 11-19.

[7] Wunsch, A. *"Highest efficiencies possible by converting gas turbine plants into combined cycle plants"*. Brown Boveri review, Oct. 1985, PP 455-463.

[8] Horlock, J. H. *"Aero-engine derivative gas turbines for power generation: Thermodynamic and economic perspectives"*. Trans. ASME Journal of Engineering for gas turbines and power, Vol.119, No.1, PP 119-123, 1997.

[9] Horlock, J. H. *"Combined power plants: past, present and future"*. Trans. ASME Journal of Engineering for gas turbines and power, Vol.117, No.4, PP 608-616, 1995.

[10] Horlock, J. H. *"The optimum pressure ratio for a combined cycle gas turbine plant"*. Proc. Inst. Mechanical Engineering Part A: Journal of power and energy, Vol.209, PP 259-264, 1995.

[11] El-Masri, M. A. and Chin, W. W. *"Exergy Analysis of Combined Cycles: Part 2 -Analysis and Optimisation of Two-Pressure Steam Bottoming Cycles"*. Trans. ASME Journal of Engineering for gas turbines and power, Vol.109, No.1, PP 237-243, 1987.

[12] El-Masri, M. A. *"Exergy Analysis of Combined Cycles: Part 1 -Air cooled Brayton Cycle gas turbines"*. Trans. ASME Journal of Engineering for gas turbines and power, Vol.109, No.2, PP 228-236, 1987.

[13] El-Masri, M. A. *"On thermodynamics of gas turbine Cycles: Part 1 –Second law analysis of combined Cycles"*. Trans. ASME Journal of Engineering for gas turbines and power, Vol.107, No.4, PP 880-236, 1985.

[14] Cerri, G. *"Parametric Analysis of Combined Gas-Steam Cycles"*. Trans. ASME Journal of Engineering for gas turbines and power, Vol.109, No.1, PP 46-55, 1987.

[15] Rufli, P. *"A systematic analysis of the combined gas/steam cycle"*. ASME COGEN-TURBO I, Montreux, 1987.

[16] Dvidson, B. J. and Keely, K. R. *"The thermodynamics of practical combined cycles"*. Proc. Inst. Mechanical Engineering conference on combined cycle gas turbines, PP 28-50, 1991.

[17] Bhinder, F. S. and Mango, O. I. K. *"A parametric study of the combined power and power (CPP) plant for generating electricity"*. ASME Turbo Cogeneration. Vienna, 1995.

[18] Hawthorne, W. R. and Davis, G. de V. *"Calculating gas turbine performance"*. Engineering, No.181, PP 461, 1956.

[19] Bannister, R. L., Cheruvu, N. S., Little, D. A. and McQuiggan, G. *"Development requirements for an advanced gas turbine system"*. Trans. ASME Journal of Engineering for gas turbines and power, Vol.117, No.4, PP 724-733, 1995.

[20] Bannister, R. L., Briesch, M. S., Diakunchak, I. S. and Huber, D. J. *"A Combined Cycle Designed to achieve greater than 60 % Efficiency"*. Trans. ASME Journal of Engineering for gas turbines and power, Vol.117, No.4, PP 734-741, 1995.

[21] Taft, M. *"A comprehensive classification of combined cycle and cogeneration plant"*. Proc. Inst. Mechanical Engineering, Vol.205, PP 145-159, 1991.

[22] Dhar, P. L., Seyedan, B., Guar, R. R. and Bindra, G. S. *"Computer Simulation of a Combined Cycle Power Plant"*. Journal of Heat Recovery Systems & CHP. Vol.15, No.7, PP 619-630, 1995.

[23] Golinski, J. A. *"A conceptual design for a Combined Cycle Power Plant Comprising Modified Exhaust-Heated Gas Turbine and A Steam Turbine Plant"*. ASME Turbo Cogeneration. Vol.9, PP 215-236, Vienna, 1994.

[24] Bhinder, F. S. and Ismail, I. H. *"Simulation of aircraft gas turbine engines"*. Trans. ASME Journal of Engineering for gas turbines and power, Vol.113, No.1, PP 95-99, 1991.

[25] Bhinder, F. S., Poole, C., Salsi, A. G. and Kumar, S. *" A software environment for the modelling, simulation and control of industrial gas turbine engines"*. Proc. Of international gas turbine and aeroengine congress and exposition, Orlando, 1991.

[26] Roy-Aikins, J. E. A. *"BRAKINE: a programming software for the performance of Brayton and Rankine cycle plants"*. Proc. Inst. Mechanical Engineering, Vol.209, PP 281-286, 1995.

[27] Perz, E. *"A computer method for thermal power cycle calculation"*. Trans. ASME Journal of Engineering for gas turbines and power, Vol.113, No.2, PP 148-189, 1991.

[28] El-Masri, M. A. *"GASCAN: An interactive code for thermal analysis of gas turbine systems"*. Trans. ASME Journal of Engineering for gas turbines and power, Vol.110, No.2, PP 201-209, 1988.

[29] Dechamps, P. J., Pirard, N. and Mathieu, Ph. *"Part load operation of Combined Cycle Power plant"*. Trans. ASME Journal of Engineering for gas turbines and power, Vol.117, No.2, PP 475-483, 1995.

[30] Gyarmthy, G. *" On load control methods for combined cycle plants"*. Proc. ASME COGEN-TURBO III, PP 39-50, 1989.

[31] Frutschi, H. U. *"Control methods for cogeneration with gas turbines and combined cycles"*. Proc. ASME COGEN-TURBO I, PP 263-268, 1987.

[32] Susta, M. R. and Luby, P. *"Combined cycle power plant efficiency: A prognostic extrapolation"*. Modern power systems review, Apr. 1997, PP 21-24.

[33] Yonghong, W. *"A new method of predicting the performance of gas turbine engines"*. Trans. ASME Journal of Engineering for gas turbines and power, Vol.113, No.1, PP 106-111, 1991.

[34] Bettocchi, R., Spina, P. R. and Alliney, S. *"Resolution method for gas turbine mathematical models"*. Proc. ASME COGEN-TURBO, PP 361-369, 1994.

[35] Farmer, R. *"See 57% net efficiency combined cycles powered by 2400 °F '3A' series turbines"*. Gas turbine world, Jan. 1995, PP 18-28.

[36] Hirose, F. and Azuhata, S. *"Completion of a 1300 °C class high efficiency gas turbine"*. Hitachi review, Vol.42, No.1, PP 5-10, 1993.

[37] Rogers, G. F. C. and Mayhew, Y. R. *"Thermodynamic and transport properties of fluids "*. 4th edition, Basil Blackwell, 1988.

[38] Chappel, M. S. and Cockshutt, E. P. *"Gas Turbine cycle calculations: Thermodynamic data tables for Air and combustion products for three systems of units"*. NRC No. 14300, Ottawa, 1974.

[39] Najjar, Y. S. H., Lamfon, N. J. and Akyurt, M. "Modelling and simulation of *gas turbine engine, part 1: Design point performance at ISO conditions"*. International Journal of power and energy systems, Vol.15, No.2, PP 61-67, 1995.

[40] Herbert, M. V. *"A Method Of Performance Prediction for Centrifugal Compressors"*. Aeronautical Research Council, R&M No. 3843, 1980.

[41] Ainley, D. G and Mathieson, G C. R. *"A method of oerformance estimation for axial-flow turbines"*. Aeronautical Research Council, 1957.

[42] Kurzke, J., *"How to get component maps for aircraft gas turbine performance calculations"*. ASME paper 96-GT-164, 1996.

[43] Traupel, W., *"Thermische Turbomaschinen"*. Vol I, Springer Verlag, Berlin, 1977.

[44] Jones, L. and Chin, A. *"Electronic Instruments and Measurements"*. 2nd edition, Prentice-Hall, New Jersey, 1991.

[45] Najjar, Y. S. H., Lamfon, N. J. and Akyurt, M. "Modelling and simulation of *gas turbine engine, part 2: Impact of ambient conditions on gas turbine performance"*. International Journal of power and energy systems, Vol.15, No.3, PP 94-103, 1995.

[46] Najjar, Y. S. H., Lamfon, N. J. and Akyurt, M. *"Modelling and simulation of gas turbine engine, part 2: Analysis of part-load performance"*. International Journal

of power and energy systems, Vol.16, No.1, PP 29-35, 1995.

[47] Facchini, B. *"A simplified approach to off-design performance evaluation of single shaft heavy duty gas turbines"*. Proc. ASME COGEN-TURBO 7th, PP 189-197, 1993.

[48] Kail, C. *"Evaluation of advanced combined cycle power planst"*. Proc. Inst. Mechanical Engineering Part A: Journal of power and energy, Vol.212, PP 1-12, 1998.

[49] Sarabchi, K. and Polley, G. T., *"Thermodynamical optimisation of a combined cycle plant performance"*. ASME paper 94-GT-304, 1994.

[50] Erbes, M. R., Gay, R. R. and Cohn, A., *"GATE: A simulation code for analysis of gas-turbine power plants"*. ASME paper 89-GT-39, 1989.

[51] Bonzani, G., Mennucci, M., Scaia, M. and Sormani, G. *"Technical and economical optimisation of a 450 MW combined cycle plant"*. Proc. ASME COGEN-TURBO IGTI-Vol. 6, PP 131-143, 1991.

[52] Kurzke, J., *"Gas turbine cycle design methodology: A comparison of parameter variation with numerical optimisation"*. ASME paper 98-GT-343, 1998.

[53] *"AGMA information sheet: Strength of spur, helical, herringbone and bevel gear teeth"*. AGMA 225.01.

[54] *"AGMA information sheet: Surface durability (pitting) of spur, helical, herringbone and bevel gear teeth"*. AGMA 215.01.

[55] Mott, R. L. *"Machine elements in mechanical design "*. Charles E. Merrill Publishing Company, 1988.

[56] Deutschman, A., Michels, W. and Wilson, C. *"Machine design theory and practice "*. Collier-Macmillan Publishing Company, 1975.

APPENDIX A

SAMPLE OF THERMODYNAMIC CALCULATIONS

Appendix A

A set of the following parameters will be used to give a sample for the numerical calculations of combined gas/steam cycle:

Pressure ratio (r) = 8

$P_{2(st)} = 50$ bar

$T_{atm} = 293$

$\eta_c = 0.86$

$\eta_{cc} = 0.98$

$\eta_{t(st)} = 0.87$

$\xi = 0.07$

$\eta_{mec} = 0.98$

PP = 20 K

T_{o3} =1400 K

P_{con} = 0.2 bar

P_{atm} = 101.3 kPa

$\eta_{t(gt)} = 0.88$

$\eta_P = 0.85$

$\eta_B = 0.85$

LCV = 42400 kJ/kg

$PP_{\min} = 20$ K

$\varepsilon_{sup} = 0.9$

i. <u>Gas turbine cycle performance calculations</u>

For $\dot{m}_a = 1$ kg/s and from equation (3.2)

Using subroutine AIRPROP the following has been calculated:

$$C_{Pa} = 1018.24 \quad kJ/kgK$$

$$C_{va} = 718.0 \quad kJ/kgK$$

$$\gamma_a = 1.4182$$

Using Eqn. 3.41,

$$T_{02} = 293 + \frac{293}{0.86}\left[\left(\frac{8}{1}\right)^{1.4182-1/1.4182} - 1\right] = 581.3 \ K$$

Using Eqn. 3.39

$$W_c = 1 \times 1.0184 \times 10^3 \times \frac{293}{0.86} \times \left[(8)^{\frac{1.4182-1}{1.4182}} - 1 \right] = 277.84 \quad \text{kW}$$

Using subroutine FARATIO, the following has been calculated:

$$C_{Pg} = 1159 \quad kJ/kgK$$

From Eqn. 3.44

$$F = \frac{1}{\frac{0.98 \times 42400 \times 10^3}{1.159 \times 10^3 (1400 - 581.3)} - 1} = 0.02336$$

From Eqn. 3.45

$$P_{o3} = (1 - 0.07) \times 8 \times 101.3 = 753.672 \quad \text{kPa}$$

Using subroutine GASPROP, the following has been calculated:

$$C_{Pg} = 1147 \quad kJ/kgK$$

$$C_{vg} = 860 \quad kJ/kgK$$

$$\gamma_g = 1.334$$

If $P_{o4} = 109.3$ kPa then

From Eqn. 3.46

$$W_t = (1 + 0.02336) \times 1 \times 1.147 \times 10^3 \times 0.88 \times 1400 \left[1 - \left(\frac{109.3}{753.672} \right)^{\frac{1.334-1}{1.334}} \right]$$

$$W_t = 557.5 \quad \text{kW}$$

From Eqn. 3.47

$$T_{o4} = 1400 - 0.88 \times 1400 \times \left[1 - \left(\frac{109.3}{753.672}\right)^{\frac{1.334-1}{1.334}}\right] = 928.27 \quad \text{K}$$

From Eqn. 3.48

$$\eta_{gt} = \frac{(557.5 - 277.84) \times 10^3}{0.02336 \times 1 \times 42400 \times 10^3} = 0.2838$$

From Eqn. 3.50

$$w_{gt} = \frac{(557.5 - 277.84)}{1} = 279.66 \quad \text{kJ/kg}$$

ii. <u>Heat recovery steam generator performance calculations</u>

From Eqn. 3.53 and at $P_{2(st)} = 50$ bar

$$T_{2(st)} = 0.9 \times (928.27 - 537.05) + 537.05 = 889.148 \quad \text{K}$$

From the steam tables and using Eqn. 3.54

$$h_{2(st)} = 3703 \quad \text{kJ/kg}$$

From Eqn.

$$T_{o(evp)} = 20 + 537.05 = 557.05 \quad \text{K}$$

From Eqn. 3.56

$$\dot{m}_{st} = \frac{1 \times (1+F) \times 0.85 \times 1.140 \times 10^3 \times (928.27 - 557.05)}{(3703 - 1147) \times 10^3} = 0.14636 \quad \text{kg/s}$$

From the compressed water tables and using Eqn. 3.57

$$h_{1(st)} = 258 \quad \text{kJ/kg}$$

From Eqn. 3.58

$$T_{o6} = 557.05 - \frac{0.14636 \times (1140 - 258) \times 10^3}{1 \times (1 + 0.02336) \times 1.140 \times 10^3} = 445.97 \quad \text{K}$$

From the steam tables and using Eqn. 3.59

$$h_{3(st)} = 2407.79 \quad \text{kJ/kg}$$

From the steam tables and using Eqn. 3.60

$$h_{4(st)} = 251 \quad \text{kJ/kg}$$

iii. <u>Steam turbine cycle performance calculations</u>

From the steam tables and using Eqn.3.62

$$W_P = \frac{0.14636}{0.85} \times (258 - 251) \times 10^3 = 1.205 \quad \text{kW}$$

From the steam tables and using Eqn. 3.63

$$W_{t(st)} = 0.14636 \times 0.87 \times (3703 - 2407.79) \times 10^3 = 164.92 \text{ kW}$$

From Eqn. 3.64

$$\eta_{st} = \frac{(164.92 - 1.205) \times 10^3}{1 \times (1 + 0.02324) \times 1.155 \times 10^3 \times (928.27 - 445.97)} = 0.2872$$

iv. Combined cycle performance calculations

From the calculated values and using Eqn. 3.66

$$\eta_{CPP} = \frac{(279.66 + 163.715) \times 10^3}{1 \times 0.02324 \times 42400 \times 10^3} = 0.45$$

From the calculated values and using Eqn. 3.67

$$w_{CPP} = \frac{(279.66 + 163.715) \times 10^3}{1} = 443.375 \text{ kJ/kg of air}$$

APPENDIX B

THE STEADY- FLOW ENERGY EQUATION

Appendix B

At the instant when the mass $\delta\dot{m}$ reaches the boundary of the open system , let the fluid within the open system possess a quantity of internal energy U . This internal energy U includes the kinetic and potential energy of the fluid element within the boundary of the open system

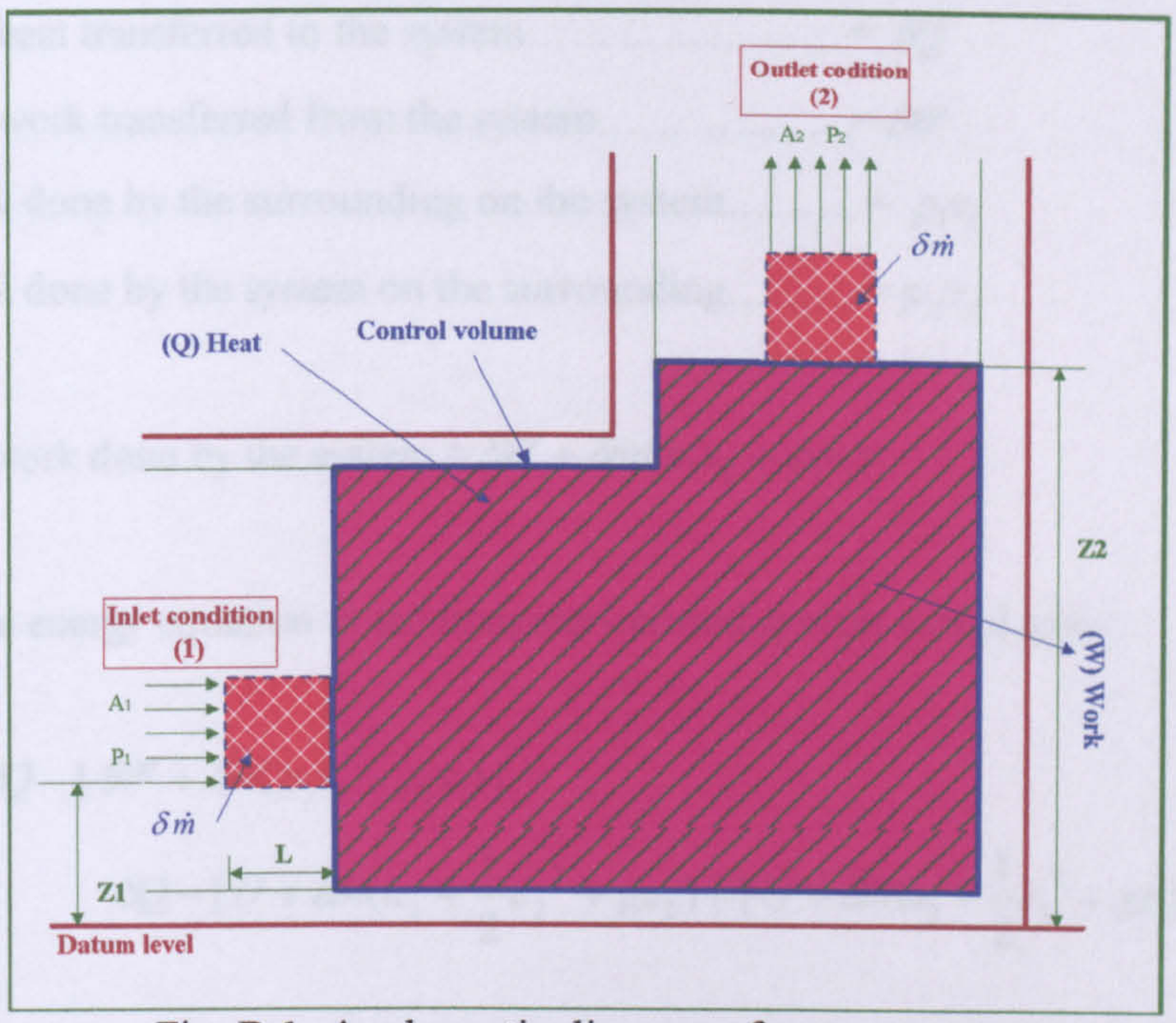

Fig. B.1 A schematic diagram of an open system

If the element is moving with a velocity c_1 at a height z_1 above some reference level as shown in **Fig. B.1**, it possesses an internal energy U, kinetic energy $\delta\dot{m}c_1^2/2$ and potential energy $\delta\dot{m}gz_1$.

$$U_1 + \frac{1}{2}\delta\dot{m}c_1^2 + \delta\dot{m}gz_1 \qquad \text{(B.1)}$$

If it is assumed that the element is small enough for the thermodynamic properties to be uniform throughout its extent , the equation C.1 becomes equal:

$$\text{The total energy of the mass} = \delta\dot{m}(u_1 + \frac{1}{2}c_1^2 + gz_1) \qquad \text{(B.2)}$$

The total energy at inlet condition 1 $= U + \delta\dot{m}(u_1 + \frac{1}{2}c_1^{\,2} + gz_1)$ **(B.3)**

The total energy at outlet condition 2 $= U + \delta\dot{m}(u_2 + \frac{1}{2}c_2^{\,2} + gz_2)$ **(B.4)**

Assume heat transferred to the system..... $= \delta Q$

Assume work transferred from the system..... $= \delta W$

The work done by the surrounding on the system..... $= p_1 v_1$

The work done by the system on the surrounding..... $= p_2 v_2$

The net work done by the system $= \delta W + \delta\dot{m}(p_2 v_2 + p_1 v_1)$ **(B.5)**

Apply the energy equation to the imaginary closed system would give :

$$\delta Q - [\,\delta W + \delta\dot{m}(p_2 v_2 + p_1 v_1)\,] = \quad \textbf{(B.6)}$$

$$\delta Q - [U + \delta\dot{m}(u_2 + \frac{1}{2}c_2^{\,2} + gz_2)\,] - [U + \delta\dot{m}(u_1 + \frac{1}{2}c_1^{\,2} + gz_1)\,]$$

The quantity U cancels , and by writing the enthalpy $h = u + pv$, the Eqn. B.6 reduces to

$$\delta Q - \delta W = \delta\dot{m}(h_2 + \frac{1}{2}c_2^{\,2} + gz_2) - \delta\dot{m}(h_1 + \frac{1}{2}c_1^{\,2} + gz_1) \quad \textbf{(B.7)}$$

For the total mass of fluid $\dot{m}$ per unit time with heat and work associated with this flow $\dot{m}$ of mass , the energy steady-flow equation B.7 can be rearranged and written as follows :

$$\dot{Q} - \dot{W} = (h_2 - h_1) + \frac{1}{2}(c_2^{\,2} + c_1^{\,2}) + g(z_2 + z_1) \quad \textbf{(B.8)}$$

where $\dot{Q}$ and $\dot{W}$ describe the heat and work transfers per unit mass flowing through the system.

The assumptions upon which equation B.8 is based on, may be summarized as follows:

i. The mass flow at inlet is constant with respect to time, and equal to the mass flow at outlet.
ii. The properties at any point within the open system do not vary with time.
iii. Any work or heat crossing the boundary does so at a uniform rate.

For turbomachinery flow where the process is adiabatic and there is no change in the potential energy term, then equation B.8 can be reduces to

$$\dot{W} = (h_2 - h_1) + \frac{1}{2}({c_2}^2 + {c_1}^2) = H_{02} - H_{01} \qquad \text{(B.9)}$$

APPENDIX C

TORSION OF A SOLID CIRCULAR SHAFT

Appendix C

The solid circular shaft of Fig. C.1, has a length L and radius a in the cross-section. When equal torques τ are applied at each end about a longitudinal axis, one can assume the following:-

i. The twisting is uniform along the shaft.

ii. Cross-section remains plane during twisting.

iii. Radii remain straight during twisting.

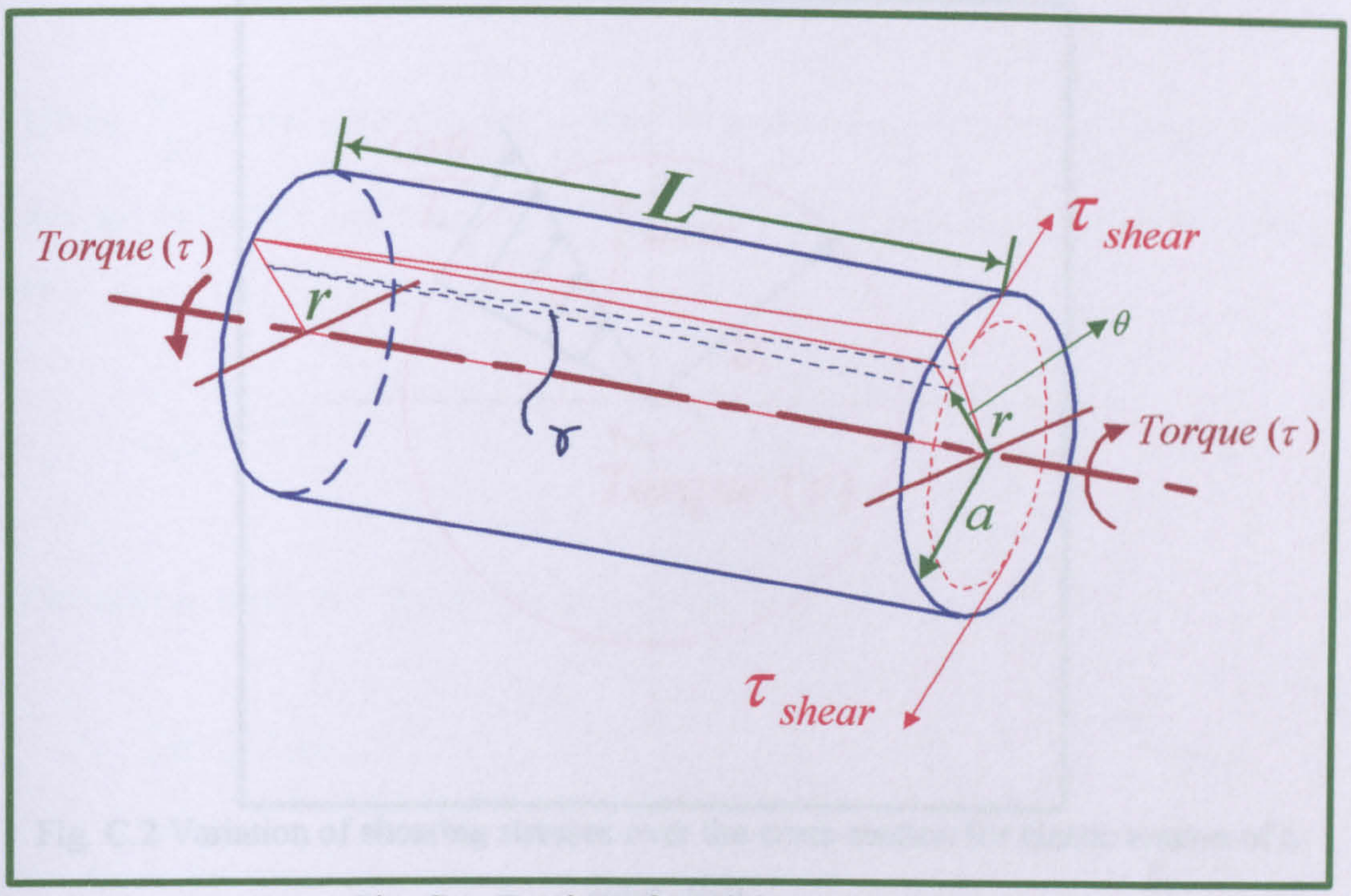

Fig C.1 Torsion of a solid circular shaft

If θ is the relative angle of twist of the two ends of the shafts, then the shearing strain γ of an elemental tube of thickness δr and at radius r is:

$$\gamma = \frac{r\theta}{L} \qquad \text{(C.1)}$$

If the material is elastic, and has a shearing modulus G, then the circumferential shearing stress on this elemental tube is :

$$\sigma_{shear} = G\gamma = \frac{Gr\theta}{L} \qquad \text{(C.2)}$$

It can be seen that σ_{shear} increases linearly from zero at the center of the shaft to $\frac{Gr\theta}{L}$ at the circumference. Along any radius of the cross-section, the shearing stresses are normal to the radius and in the plane of the cross section as shown in Fig. C.4.

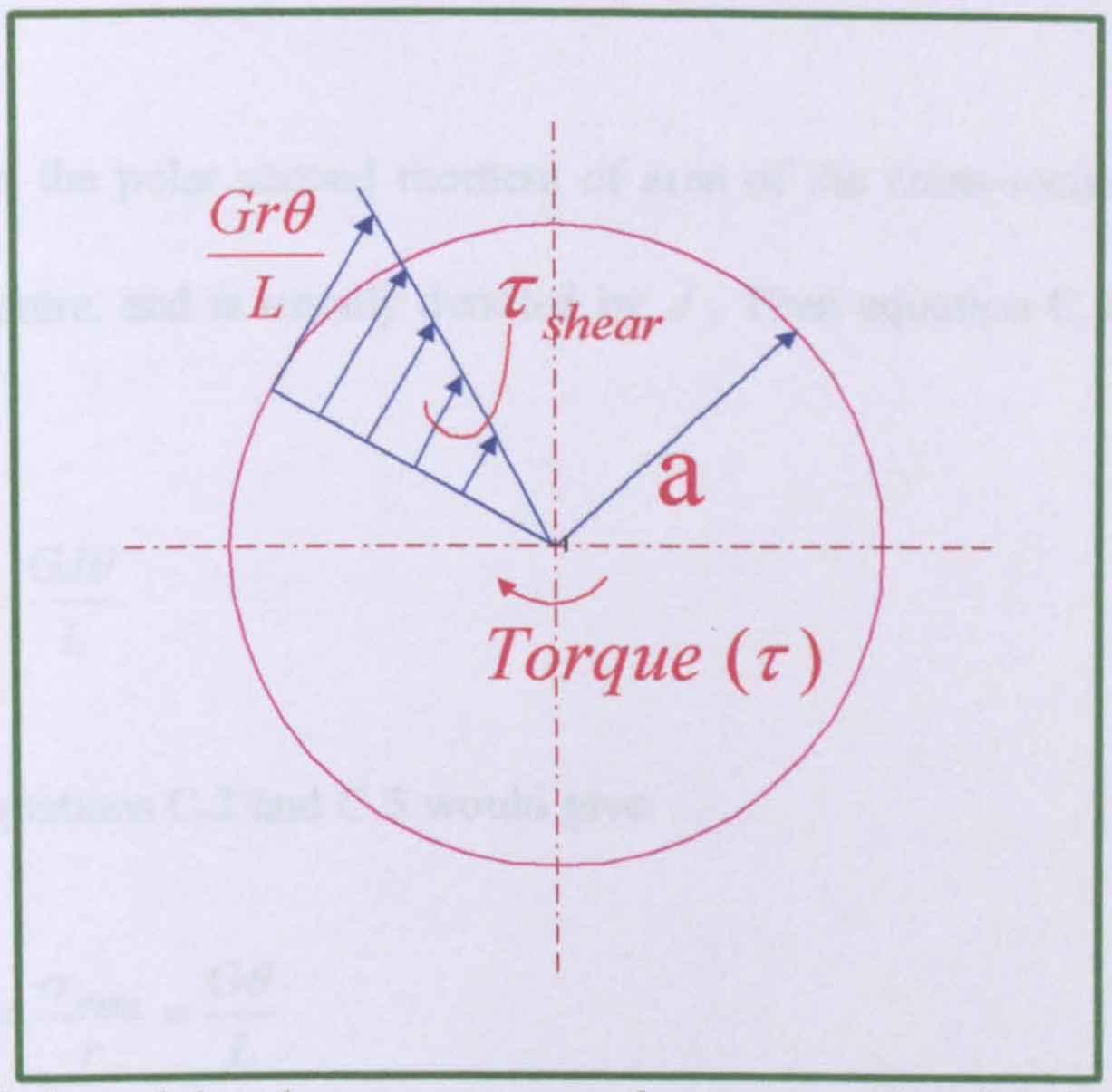

Fig. C.2 Variation of shearing stresses over the cross-section for elastic torsion of a solid shaft

The thickness of the elemental tube is δr, so the total torque on this tube is :

$$\tau_{tube} = \sigma_{shear}(2\pi r\,\delta r)r = \sigma_{shear}2\pi r^2\delta r$$

The total torque on the solid shaft is then :

$$\tau_{shaft} = \int_0^a \sigma_{shear}2\pi r^2 dr \qquad \text{(C.3)}$$

Substituting equation C.2 into equation C.3 gives :

$$\tau_{shaft} = 2\pi\left(\frac{G\theta}{L}\right)\int_0^a r^3 dr$$

$$= 2\pi\left(\frac{G\theta}{L}\right)\left(\frac{a^4}{4}\right)$$

$$= \left(\frac{G\theta}{L}\right)\left(\frac{\pi a^4}{4}\right) \qquad \textbf{(C.4)}$$

Where $\frac{\pi a^4}{2}$ is the polar second moment of area of the cross-section about an axis through the centre, and is usually denoted by J. Then equation C.4 may be written as :

$$\tau_{shaft} = \frac{GJ\theta}{L} \qquad \textbf{(C.5)}$$

Combining equations C.2 and C.5 would give:

$$\frac{\tau_{shaft}}{J} = \frac{\sigma_{shear}}{r} = \frac{G\theta}{L} \qquad \textbf{(C.6)}$$

Power developed of a rotational shaft is given by

$$P = \tau \times \omega \qquad \textbf{(C.7)}$$

From equation C.6, the torsion of a solid shaft is equal to

$$\tau_{shaft} = \frac{\sigma_{shear} \times J}{r} \qquad \textbf{(C.8)}$$

where J is the second polar of moment and for a solid shaft and is equal to $\frac{\pi d^4}{32}$

Therefore , equation C.8 becomes

$$\tau_{shear} = \frac{\sigma_{shear} \times \pi d^3}{64} \tag{C.9}$$

Therefore, comboning equations C.7 and C.8 and re-arranging for the solid diameter of the shaft d would give:

$$d = \left[(64)\left(\frac{P}{\omega}\right)\left(\frac{1}{(\pi)(\sigma_{shear})}\right)\right]^{1/3} \tag{C.10}$$

By considering the safety factor SF and apply it to equation C.10, an expression above would become equal to

$$d = (SF)\left[(64)\left(\frac{P}{\omega}\right)\left(\frac{1}{(\pi)(\sigma_{shear})}\right)\right]^{1/3} \tag{C.11}$$

Note that $(\sigma_{shear})_{material} = \frac{1}{3}(\sigma_{stress})$

APPENDIX D

DERIVATION OF BEAM STRENGTH OF SPUR GEAR

Appendix D

Referring to Fig. D.1 and by considering the tooth as a cantilever beam having its fixed end at BD, the stress can be expressed as follows:

$$\sigma = \frac{Mc}{I} = \frac{F_t L(t/2)}{bt^3/12} = \frac{6F_t L}{bt^2} \tag{D.1}$$

$$F_t = \frac{\sigma b t^2}{6L} \tag{D.2}$$

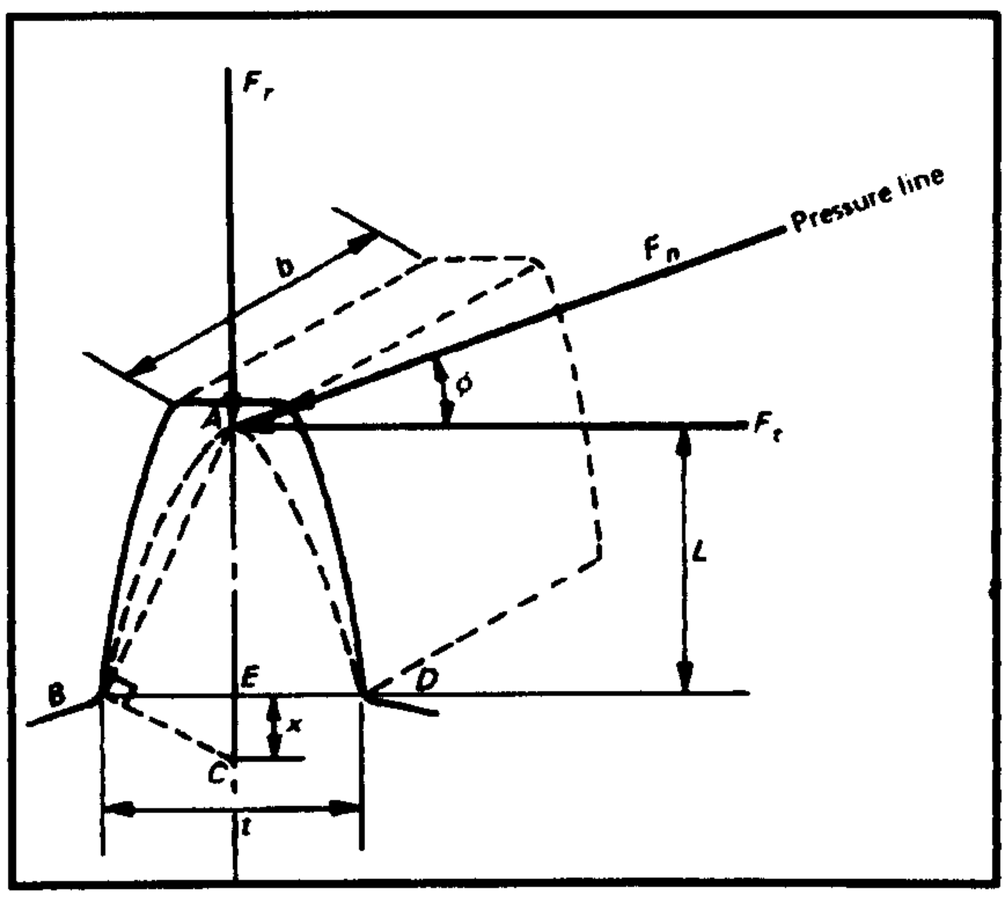

Fig. D.1 The geometric factors that are used to determine the Lewis form factor.

In a well-designed beam, the stress should be uniform in every section of the beam. In other words, in a gear tooth of uniform strength the stress is a constant, and since the gear width and gear load are also constants, Eqn. D.2 can be written as

$$L = \frac{\sigma b}{6F_t} t^2 = cons\tan t \times t^2 \tag{D.3}$$

Clearly this is the equation of a parabola. Referring to Fig. D.1, the weakest section of the tooth, BED, can be determined by inscribing the parabola through point A, and locating the points at which the parabola is tangent to the tooth profile, B and D. Equation. D.2 was therefore derived for the section having the maximum stress.

Triangle ABE is similar to triangle BCE and thus

$$\frac{x}{t/2} = \frac{(t/2)}{L} \; or \; L = \frac{t^2}{4x} \tag{D.4}$$

$$F_t = \frac{\sigma b t^3}{6t^2} 4x = \sigma b \frac{4x}{6} \tag{D.5}$$

Multiplying and dividing by the circular pitch P, gives

$$F_t = \sigma b \frac{4x}{6} \times \frac{P}{P} \tag{D.6}$$

Since x and P are geometric properties depending upon the size and shape of the tooth, it is possible to define a factor

$$y = \frac{2x}{3p} \tag{D.7}$$

y is the so-called Lewis form factor and therefore permits us to write the Lewis equation as

$$F_t = \sigma b y P \tag{D.8}$$

Because the diametral pitch, rather than circular pitch, is usually used to designate gears, the following substitution may be made: $p = \Pi/P$ and $Y = \Pi y$

$$F_t = \sigma b \frac{Y\Pi}{\Pi P} = \sigma b \frac{Y}{P} \tag{D.9}$$

Values for the Lewis form factor have been computed for standard gear systems and are found in Deutschman *et. al*[55]. A sample of Lewis form factor is given in Table D.1.

Appendix D

No. of Teeth	Load at Tips								Load Near Middle			
	14½ deg FD		20 deg FD		20 deg Stub		25 deg		14½ deg FD		20 deg FD	
—	Y	y	Y	y	Y	y	Y	y	Y	y	Y	y
10	0.176	0.056	0.201	0.064	0.261	0.083	0.238	0.076				
11	0.192	0.061	0.226	0.072	0.289	0.092	0.259	0.082				
12	0.210	0.067	0.245	0.078	0.311	0.099	0.277	0.088	0.355	0.113	0.415	0.133
13	0.223	0.071	0.264	0.083	0.324	0.103	0.293	0.093	0.377	0.120	0.443	0.141
14	0.236	0.075	0.276	0.088	0.339	0.108	0.307	0.098	0.399	0.127	0.468	0.149
15	0.245	0.078	0.289	0.092	0.349	0.111	0.320	0.102	0.415	0.133	0.490	0.156
16	0.255	0.081	0.295	0.094	0.360	0.115	0.332	0.106	0.430	0.137	0.503	0.160
17	0.264	0.084	0.302	0.096	0.368	0.117	0.342	0.109	0.446	0.142	0.512	0.163
18	0.270	0.086	0.308	0.098	0.377	0.120	0.352	0.112	0.459	0.146	0.522	0.167
19	0.277	0.088	0.314	0.100	0.386	0.123	0.361	0.115	0.471	0.150	0.534	0.170
20	0.283	0.090	0.320	0.102	0.393	0.125	0.369	0.118	0.481	0.153	0.544	0.173
21	0.289	0.092	0.326	0.104	0.399	0.127	0.377	0.120	0.490	0.156	0.553	0.177
22	0.292	0.093	0.330	0.105	0.404	0.129	0.384	0.122	0.496	0.158	0.559	0.178
23	0.296	0.094	0.333	0.106	0.408	0.130			0.502	0.160	0.565	0.180
24	0.302	0.096	0.337	0.107	0.411	1.032	0.396	0.126	0.509	1.062	0.572	0.183

Table D.1 Sample of Lewis form factor

An examination of equation D.9 shows that the maximum allowable tangential or transmitted load can now be determined if the allowable stress for the gear material is used. In order to avoid confusion, the usual procedure is to designate the allowable load based on bending as F_b. Therefore, we will write the Lewis equation as

$$F_b = Sbyp = Sb\frac{Y}{P} \tag{D.10}$$

At this point it would be well to consider the effect of another assumption made in deriving the Lewis equation. It was assumed that the full transmitted load F_t acted at the tip of the tooth. Because most gears are designed with a contact ratio of 1.2 and 1.6, it is clear that when the load acts on the tip of one tooth is still in contact, and the full load does not act on the number one tooth.

In Fig. D.2, the load has been moved away from the tooth tip to point near the middle of the tooth (the second tooth has gone out of contact, and the full load does

act on the tooth shown). As can be seen from the diagram, the derivation of the Lewis equation would follow exactly as the previous one. The only difference would be in the values for the Lewis form factor.

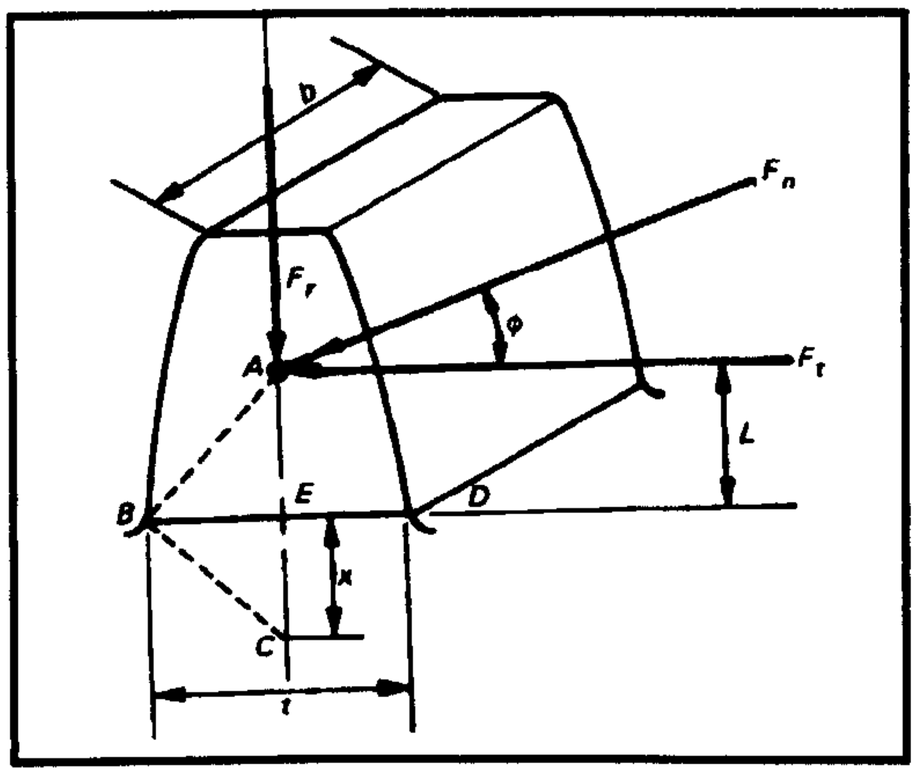

Fig. D.2 The load acts near the center of the tooth

At this point in our discussion, it is possible to design a gear, by using equation D.10 that will have the required strength, providing the proper allowable stress for the gear material is used. The allowable stresses presented in Table D.2 are based upon investigations of the performance of gears in actual use. Therefore, gears to be used for ordinary applications will give satisfactory service. However, a much better design is to use Eqn. D.10 and Table D.2 to come up with a preliminary design and then to check the gear for the items to be discussed in succeeding paragraphs.

AGMA Equation

The final strength equation to be presented is the AGMA modification of the Lewis equation. This equation is particularly useful to the designer because it applies correction factors to the original Lewis equation that compensate for some of the erroneous assumptions made in the derivation as well as for important factors not originally considered. Furthermore, since most of the factors are obtained empirically, the equation can be kept up to date by merely changing the values of the factors as more information about the gear behavior is obtained.

Appendix D

MATERIAL DESIGNATION *(AISI Number)*	CONDITION	TENSILE STRENGTH		YIELD STRENGTH		DUCTILITY *(Percent Elongation in 2 in)*	BRINELL HARDNESS *(HB)*
		Ksi	*MPa*	*Ksi*	*MPa*		
1020	Hot rolled	55	379	30	207	25	111
1020	Cold drawn	61	420	51	352	15	122
1020	Annealed	60	414	43	296	38	121
1040	Hot rolled	72	496	42	290	18	144
1040	Cold drawn	80	552	71	490	12	160
1040	OQT 1300	88	607	61	421	33	183
1040	OQT 400	113	779	87	600	19	262
1050	Hot rolled	90	620	49	338	15	180
1050	Cold drawn	100	690	84	579	10	200
1050	OQT 1300	96	662	61	421	30	192
1050	OQT 400	143	986	110	758	10	321
1117	Hot rolled	62	427	34	234	33	124
1117	Cold drawn	69	476	51	352	20	138
1117	WQT 350	89	614	50	345	22	178
1137	Hot rolled	88	607	48	331	15	176
1137	Cold drawn	98	676	82	565	10	196
1137	OQT 1300	87	600	60	414	28	174
1137	OQT 400	157	1083	136	938	5	352
1144	Hot rolled	94	648	51	352	15	188
1144	Cold drawn	100	690	90	621	10	200
1144	OQT 1300	96	662	68	469	25	200
1144	OQT 400	127	876	91	627	16	277
1213	Hot rolled	55	379	33	228	25	110
1213	Cold drawn	75	517	58	340	10	150
12L13	Hot rolled	57	393	34	234	22	114
12L13	Cold drawn	70	483	60	414	10	140
1340	Annealed	102	703	63	434	26	207
1340	OQT 400	285	1960	234	1610	8	578
1340	OQT 700	221	1520	197	1360	10	444
1340	OQT 1000	144	993	132	910	17	363
1340	OQT 1300	100	690	75	517	25	235
3140	Annealed	95	655	67	462	25	187
3140	OQT 400	280	1930	248	1710	11	555
3140	OQT 700	220	1520	200	1380	13	461
3140	OQT 1000	152	1050	133	920	17	311
3140	OQT 1300	115	792	94	648	23	233
4130	Annealed	81	558	52	359	28	156
4130	WQT 400	234	1610	197	1360	12	461
4130	WQT 700	208	1430	180	1240	13	415
4130	WQT 1000	143	986	132	910	16	302
4130	WQT 1300	98	676	89	614	28	202
4140	Annealed	95	655	60	414	26	197
4140	OQT 400	290	2000	251	1730	11	578
4140	OQT 700	231	1590	212	1460	13	461
4140	OQT 1000	168	1160	152	1050	17	341
4140	OQT 1300	117	807	100	690	23	235

Table D.2 Safe stresses and hardness numbers used in the Lewis equation

The equation is written as follows:

$$\sigma_t = \frac{F_t K_o P K_m}{K_v b J} \tag{D.13}$$

Where

σ_t = calculated stress at root of tooth, psi.

F_t = transmitted load, lb.

K_o = overload correction factor (application factor).

K_m = load distribution correction

K_v = dynamic factor

b = face width, in.

J = geometry factor

P = diametral pitch

As an aid in understanding and using the equation, the following discussion of the correction factors is presented.

The overload correction factor, K_o, accounts for the fact that, while F_t is an average value for the transmitted load, the actual maximum load may be as much as two times as great due to shock loading in either the driven or the driving system. Table D.3 gives some suggested values for K_o.

Power Source	Load on Driven Machine		
	Uniform	Moderate Shock	Heavy Shock
Uniform	1.00	1.25	1.75 or higher
Light shock	1.25	1.50	2.00 or higher
Medium shock	1.50	1.75	2.25 or higher

*For speed increasing drives of spur and bevel gears (but not helical and herringbone gears), add 0.01 $(n_G/n_p)^2$ to the factors in Table 10-4, where N_{tp} = number of teeth in pinion; N_{tg} = number of teeth in pinion;

SOURCE: AGMA

Table D.3 Overload correction factor

The load distribution factor K_m depends upon the combined effects of misalignment of axes of rotation due to machining error and bearing clearances; load deviations;

elastic deflection of shafts, bearing, and housing due to load. The AGMA information sheet presents tables and figures that give values for K_m when misalignment information is available. However, when estimated or actual misalignment is not known, the K_m factor for spur, helical, and herringbone gears as given in table D.4 may be used.

Condition of Support	Face Width							
	2-in. Face and under		6-in. Face		9-in. Face		16-in. Face and Over	
	Spur	Helical	Spur	Helical	Spur	Helical	Spur	Helical
Accurate mounting, low bearing clearances, minimum elastic deflection, precision gears	1.3	1.2	1.4	1.3	1.5	1.4	1.8	1.7
Less rigid mountings, less accurate gears, contact across full face	1.6	1.5	1.7	1.6	1.8	1.7	2.0	2.0
Accuracy and mounting such that less than full face contact exists	Over 2.0							

SOURCE: AGMA

Table D.4 Load distribution factor

The dynamic factor, K_v depends on the effect of tooth spacing and profile errors; effect of pitch line speed and revolution per minute; inertia and stiffness of all rotating elements; transmitted load per inch of face; tooth stiffness. K_v can be calculated from the following equations:

$$K_v = \left(\frac{A}{A + \sqrt{v_t}} \right)^B \tag{D.14}$$

Where

$$A = 50 + 56(1 - B)$$

$$B = \frac{(12 - Q_v)^{0.667}}{4}$$

Q_v = Transmission accuracy level number

The geometry factor J accounts for the effect of the shape of the tooth, the position at which the most damaging load is applied, the stress concentration, and the sharing of load between one or more pairs of teeth.

Tooth shape depends upon the geometry of the tooth system. In other words, such factors as pressure angle, number of teeth, whether full depth, stubbed, and so on. The position at which the most damaging load is applied depends upon how accurately the gears have been cut. For accurately cut teeth, the greatest stress will occur when the load acts at the greatest height for which only one pair of teeth are in contact. In other words, when the load acts at the tip of the tooth another pair of teeth is in contact and is sharing the load and thus the greatest stress does not occur at this position.

The geometry factor also includes the effect of stress concentration as well as tangential (bending stress) load and radial (compressive stress) load. Figure D.3 may be used to determine the geometry factor for 20-degrees spur gear.

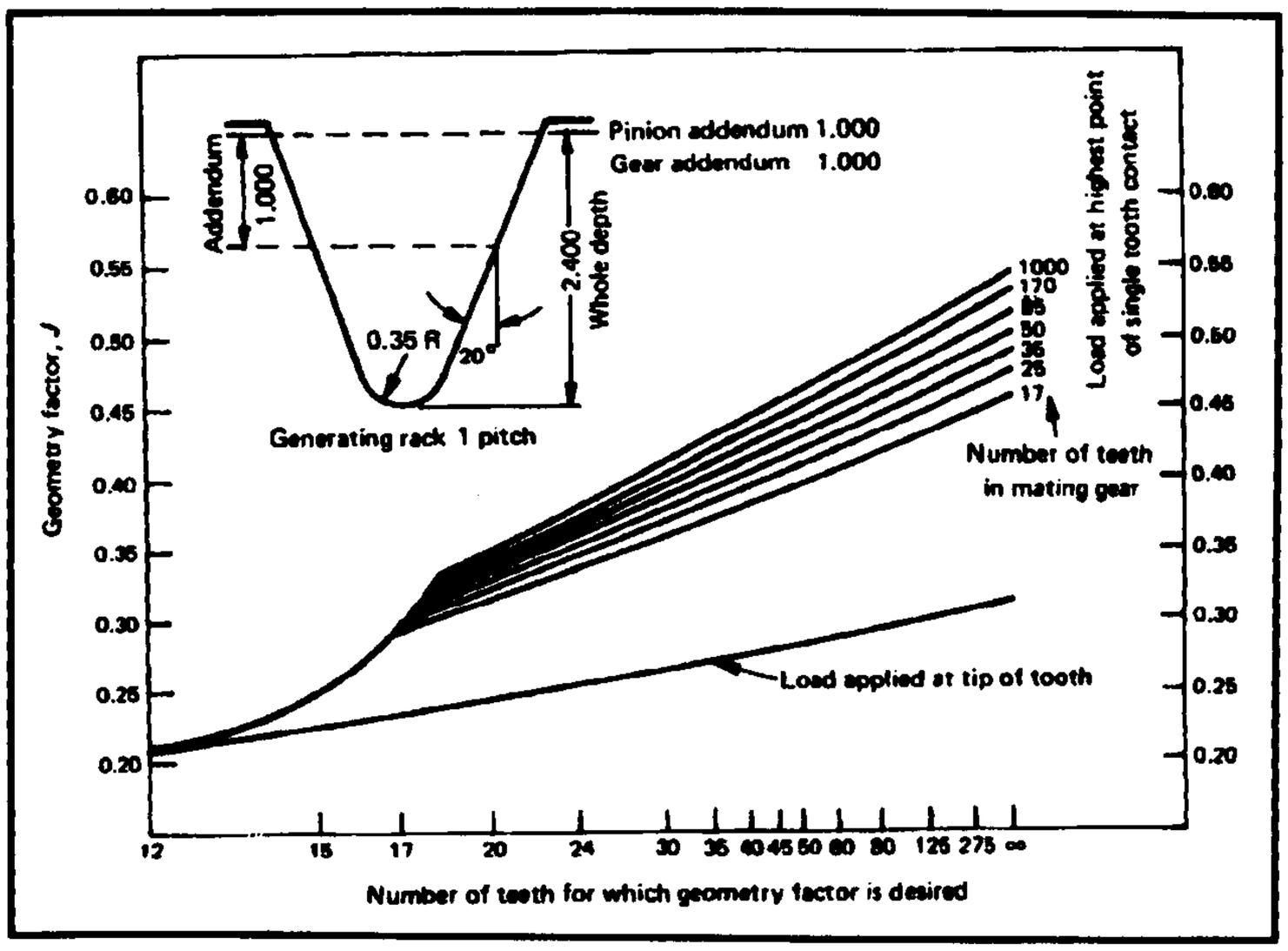

Fig. D.3 Geometry factor for 20-degree spur gear

For S.I units the AGMA equation can be expressed as follows:

$$\sigma_t = \frac{F_t K_o K_m}{M K_v b J} \tag{D.15}$$

It should be noted that the factors given in Eqn. D.15 are the same as in Eqn. D.13. The term M is referred to as the gear module.

APPENDIX E

"A PARAMETRIC STUDY TO INVESTIGATE THE INFLUENCE OF CYCLE PARAMETERS ON THE PERFORMANCE OF GAS TURBINE ENGINES IN A COMBINED POWER & POWER PLANT"

(SUBMITTED FOR PUBLICATION YEAR 2001)

A PARAMETRIC STUDY TO INVESTIGATE THE INFLUENCE OF CYCLE PARAMETERS ON THE PERFORMANCE OF GAS TURBINE ENGINES IN A COMBINED POWER & POWER PLANT

Qusai Z. Al-Hamdan
Omar A. Al-Quran
Royal Jordanian Air Force
Amman, JORDAN

and

S. H. Nasser
F. S. Bhinder

University of Hertfordshire
Hatfield, UK

ABSTRACT

The practical thermal efficiency of gas turbine engines ranges between 28% and 33%. In view of the rapidly depleting global reserves of fossil fuels, i.e. coal, oil and natural gas, this level of thermal efficiency is of serious concern to thermal power engineers. Several modifications to the thermodynamic cycle have been introduced to raise the thermal efficiency of gas turbine plants, including the Combined Heat and Power, CHP for short, plants. These plants recover the thermal energy from the exhaust of the gas turbine and use it for district heating. This concept improves the energy efficiency of the plant but it does not affect the thermal efficiency of the gas turbine.

In hot countries district heating is not necessary, but it is more beneficial if thermal energy recovered was used for producing additional electrical power. In this paper the results of a two part parametric study of the combined power and power, CPP for short, are presented. Part one deals with the recovery of thermal energy from the exhaust gas of the gas turbine engine to raise high-pressure superheated steam. The steam powers a steam turbine to generate additional electricity.

The results of the study show quite clearly that the values of the gas turbine cycle parameters that would produce optimum performance in the CPP plant are different from either the gas turbine or the CHP plant. Furthermore, overall thermal efficiency in the region of 55% may be achieved by using typical values for the cycle parameters, but further refinements may help to raise the efficiency to 60%. The results of this parametric study also show a significant reduction in the greenhouse effect.

In view of the growing worldwide concern for energy conservation and environmental protection, the authors feel that this paper would lead to a stimulating discussion.

NOMENCLATURE

Symbol	Meaning
C_p	Specific heat at constant pressure
C_v	Specific heat at constant volume
γ	Ratio of specific heats
$\dot{m}$	Mass flow rate
q,Q	Heat supplied or rejected
w,W	Specific work output, work output
P	Pressure
T	Temperature
S	Entropy
r	Pressure ratio
η	Efficiency
θ	Ratio of maximum to minimum temperature
h	Enthalpy
LCV	Lower calorific value
τ	Torque
PP	Pinch point temperature difference
f	Fuel to air ratio, function
ε	Effectiveness
D	Dryness factor
ξ	Pressure loss in combustion chamber
d	Diameter

Subscripts

1,2,3	State points in the cycles
gt	Gas turbine
st	Steam turbine
lq	liquid
s	Isentropic
∞	Polytropic
o	Stagnation
g	Gas
a	Air
c	Compressor
t	Turbine
cc	Combustion chamber

P	Pump
B	Boiler (Heat recovery steam generator)
con	Condenser
eco	Economiser
evp	Evaporator
sup	Superheater
sat	Saturation
mec	Mechanical
O	Overall
CPP	Combined power and power
max	Maximum
min	Minimum
atm	Atmospheric

Superscripts

.	Rate

INTRODUCTION

The world demand for electrical power is increasing sharply due to rising living standards, increasing world population and growing industries in many third world countries. In contrast the reserves of fossil fuels, coal, oil and natural gas, are depleting at an alarming rate. The contributions to the world's energy demand from the alternative sources of energy such as solar, wind, tidal, geothermal, etc., often described as renewable energy, are still insignificant in spite of the fact that much research effort is being directed globally to exploit these resources. In view of this scenario, conservation of fossil fuels by improving the efficiency of all thermal power plants, particularly those used for generating electricity, is of paramount importance.

Conventional power generation plants are powered by either steam turbines or gas turbines. The thermal efficiency of such plants is low. There have been many attempts to improve the efficiency of steam and gas turbines by reheating and regeneration or by using a mixture of working fluid inside the cycle in case of steam turbine. In spite of all these attempts the thermal efficiency of such plants is still low, thermal efficiency of gas turbine plants ranges between 28% and 33% and of steam turbine plants between 36% and 45%. Theoretical studies have shown that by recovering some of the low grade thermal energy from the exhaust gas of the gas turbine to produce high pressure steam and using this steam to power a steam turbine, which in turn, will produce additional electrical power, the overall thermal efficiency of the combined plant can be increased to as high as 60%. However, careful selection of the principal design parameters for the gas and steam turbines as well as proper scheduling of their control systems are of utmost importance for achieving optimum performance of CPP plants, particularly under part load conditions.

Generally, the power generating plants efficiencies can be increased either by the utilization of cogeneration cycle (Power and heat (CHP) plants) or by combined power and power (CPP) plants. Although the former is of simple structure and of higher thermal efficiency than the latter, this study is concerned mainly with latter type of plants (CPP). This is mainly due to the need for electricity and the hot climate nature of the developing countries.

The schematic diagram of the CPP plant can be shown in Fig.1 where the gas turbine exhaust will be used as the heat source of the steam power plant; an afterburner can be used to raise the gas turbine exhaust temperature.

THERMODYNAMIC ANALYSIS

Thermal efficiency and specific work can be used to represent the performance of the CPP plant.

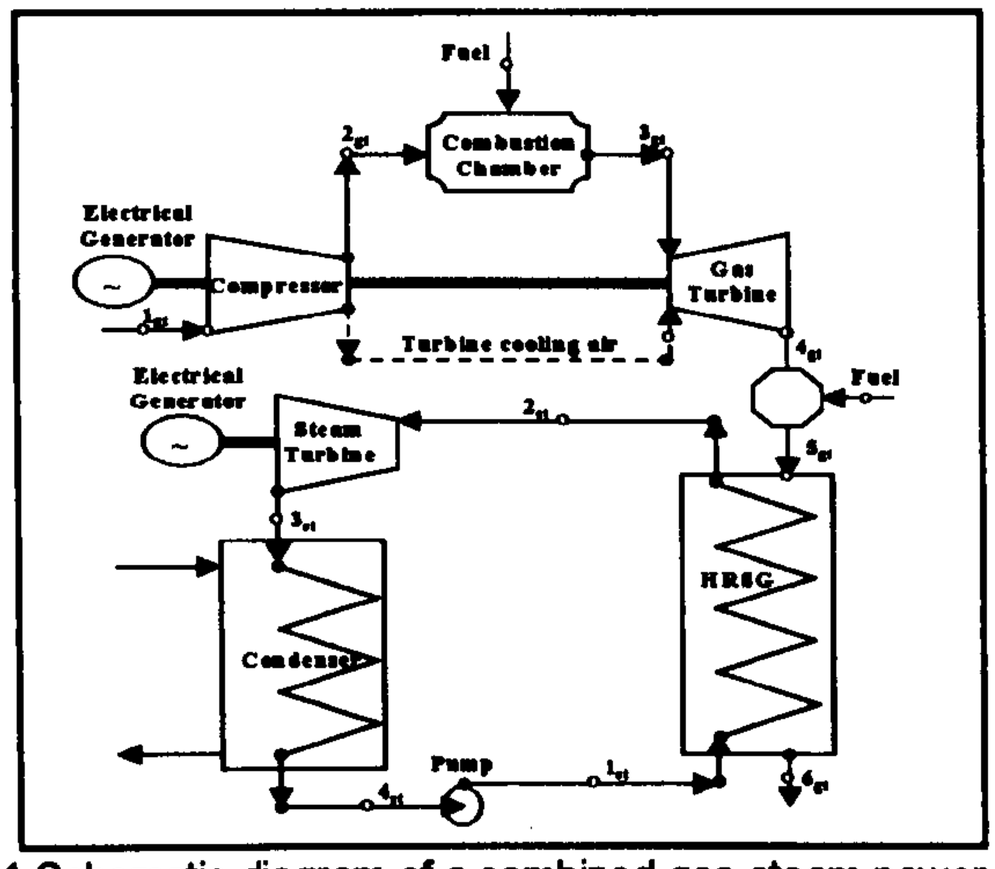

Fig.1 Schematic diagram of a combined gas-steam power plant with a heat recovery steam generator

The two plants in series

In a simple analysis, consider a cyclic power plant consists of combined gas turbine power plant and steam turbine power plant as shown in Fig.2. The gas turbine plant had a thermal efficiency of η_{gt}, absorbed heat of Q_H, rejected heat of Q_{HL} and work done of W_{gt}. The steam turbine plant had a thermal efficiency of η_{st}, absorbed heat of Q_L, rejected heat of Q_{Lstm} and work done of W_{st}. A supplementary heat (Q_{add}) can be added between the two power plants while a heat (Q_{loss}) can be lost at that point.

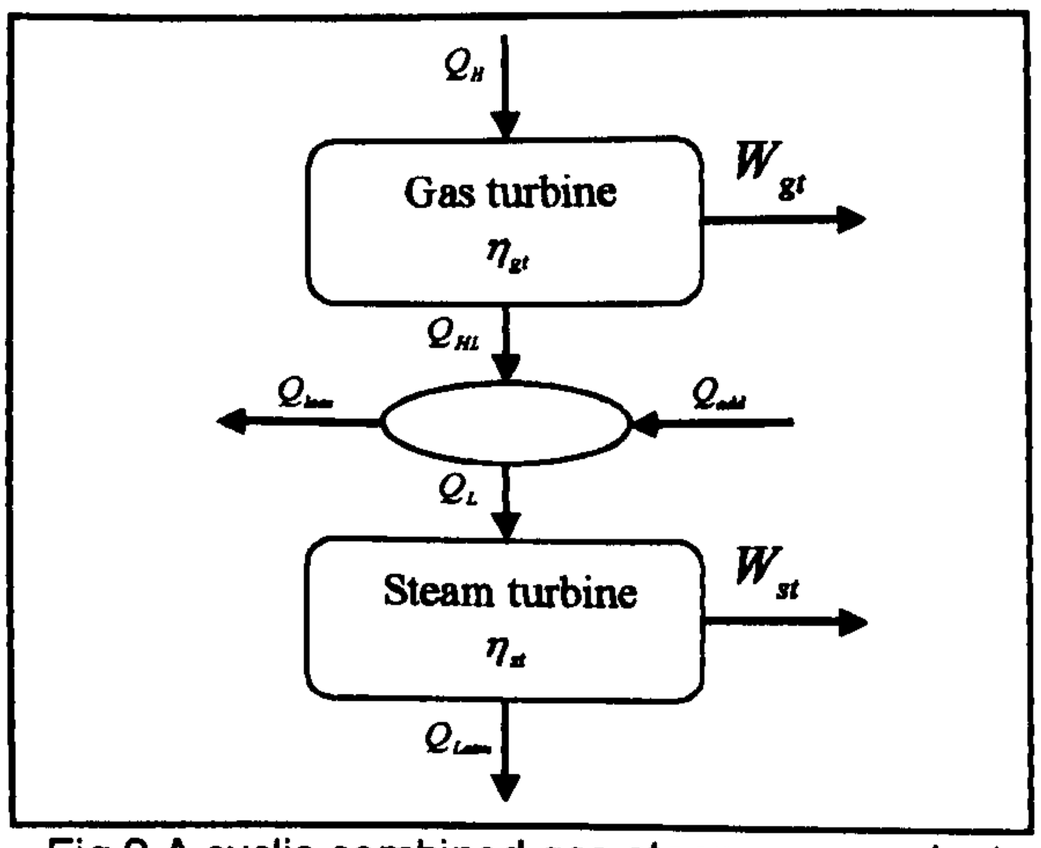

Fig.2 A cyclic combined gas-steam power plant

Thermal efficiency of gas turbine power plant is

$$\eta_{gt} = \frac{W_{gt}}{Q_H} \tag{1}$$

Thermal efficiency of steam turbine power plant is

$$\eta_{st} = \frac{W_{st}}{Q_L} \tag{2}$$

and the heat supplied to the steam power plant is

$$Q_L = Q_{HL} + Q_{add} - Q_{loss} \tag{3}$$

Thermal efficiency of the combined power plant is

$$\eta_{CPP} = \frac{W_{gt} + W_{st}}{Q_H + Q_{add}} \tag{4}$$

Using equations 1,2,3 and 4

$$\eta_{CPP} = \frac{\eta_{gt} + \eta_{st}\left(\frac{Q_{add}}{Q_H} + 1 - \eta_{gt} - \frac{Q_{loss}}{Q_H}\right)}{1 + \frac{Q_{add}}{Q_H}} \tag{5}$$

If there isn't any supplementary heating $(Q_{add} = 0)$ and no heat loss $(Q_{loss} = 0)$ then

$$\eta_{CPP} = \eta_{gt} + \eta_{st} - \eta_{gt}\eta_{st} \tag{6}$$

Using Equation 5, Fig.3 shows the value of the combined thermal efficiency (η_{CPP}) being calculated against the steam turbine thermal efficiency (η_{st}) with a constant gas turbine thermal efficiency (η_{gt}) of 0.3 at different constant values of supplementary heat ratios ($\frac{Q_{add}}{Q_H}$).

Without supplementary heating ($\frac{Q_{add}}{Q_H} = 0$) and by varying the gas turbine thermal efficiency (η_{gt}) between 0.0 and 0.6, Equation 5 has been used to calculate the steam turbine thermal efficiency (η_{st}) at two constant combined cycle efficiencies (η_{CPP}) of 0.5 and 0.6. The calculated results versus the gas turbine thermal efficiency plotted in Fig.4 at two constant heat loss percentages ($\frac{Q_{UN}}{Q_A}$) of 0% and 10%.

Using Fig.3 and Fig.4 the following observations can be made:

i. Supplementary heating will always decrease the overall combined power plant thermal efficiency except if the supplementary heating significantly increases the steam turbine thermal efficiency.

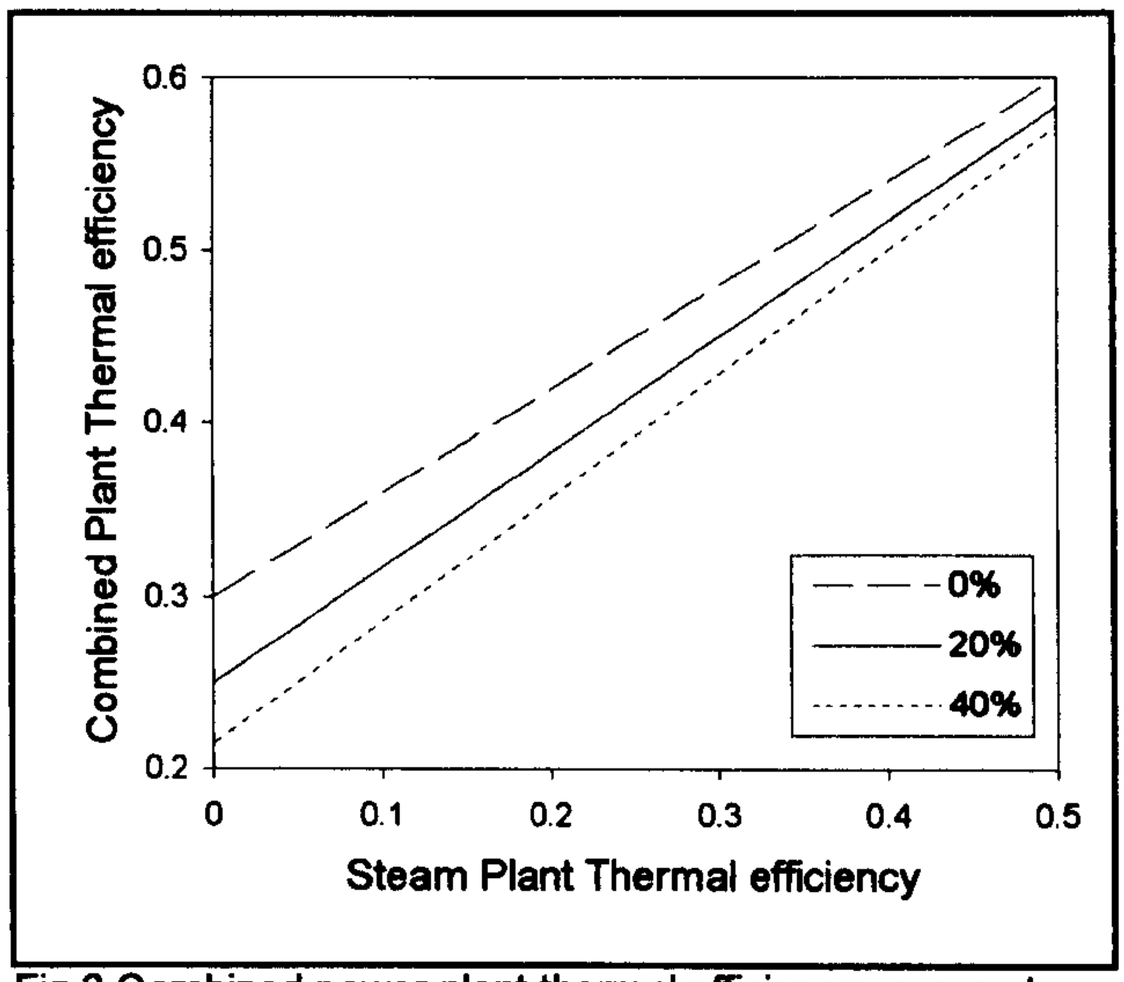

Fig.3 Combined power plant thermal efficiency versus steam plant thermal efficiency at constant supplementary heating ratios and 0.30 gas turbine plant thermal efficiency

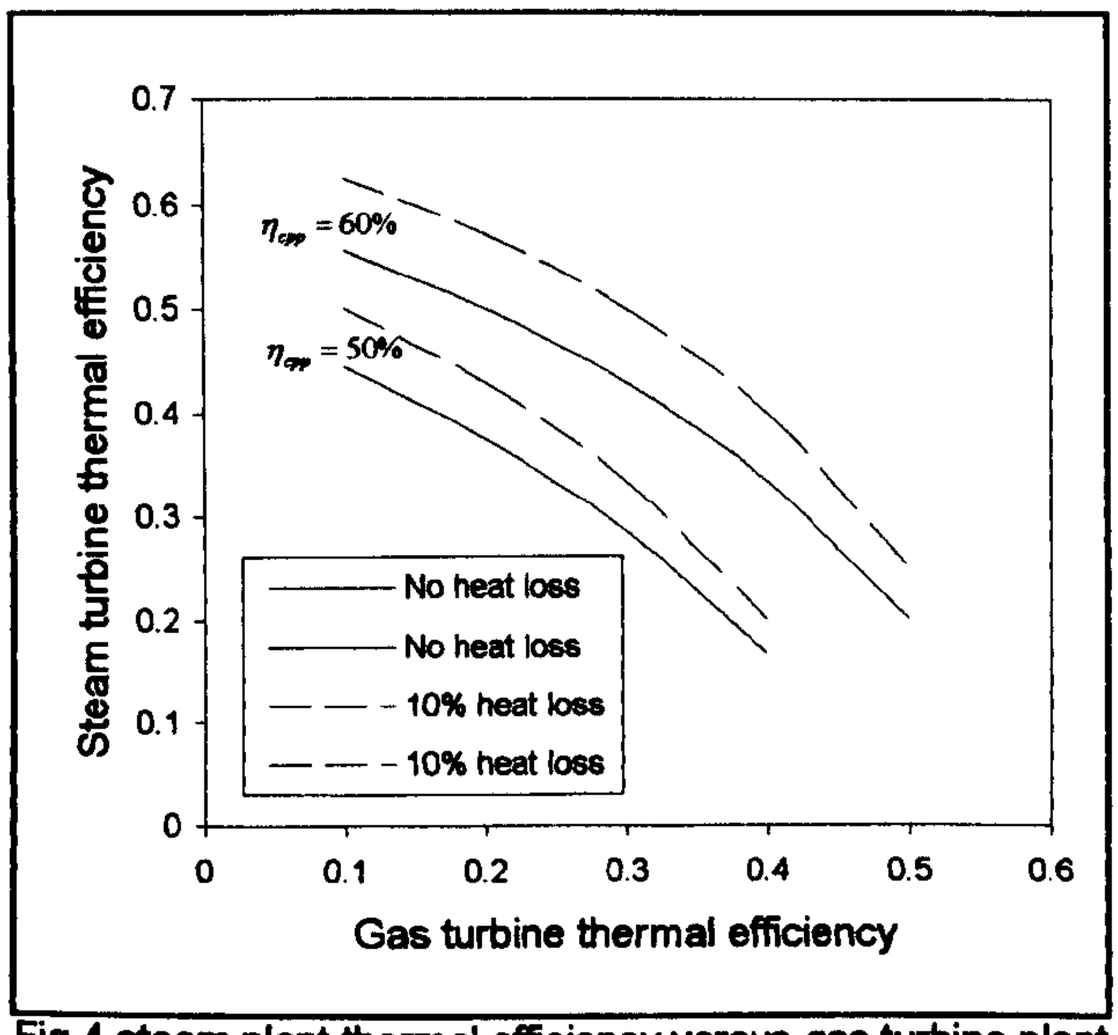

Fig.4 steam plant thermal efficiency versus gas turbine plant thermal efficiency at constant heat loss ratios for 0.60 and 0.50 Combined power plant thermal efficiency

ii. To exceed specified combined power plant thermal efficiency, a correct combination between the two plant's efficiencies should be chosen.

iii. The lost heat between the plants (Q_{loss}) increases the importance of gas turbine thermal efficiency on the combined power plant performance.

The CPP cycle thermodynamic analysis

Thermal efficiency and specific work of the CPP plant are function of many parameters:

$$\dot{W}_{CPP} = f(\theta, r, C_p, \eta_c, \eta_{cc}, \eta_{(gt)}, \eta_{mech}, P_{con}, T_{2st}, P_{2st}, \eta_{t(st)}, \eta_p, \ldots.) \quad (7)$$

$$\eta_{CPP} = f(\theta, r, C_p, \eta_c, \eta_{cc}, \eta_{(gt)}, \eta_{mech}, P_{con}, T_{2st}, P_{2st}, \eta_{t(st)}, \eta_p, \ldots.) \quad (8)$$

Mathematical solution of these two equations is very difficult. In this case a parametric study has been carried out to explore the effect of main gas turbine parameters on the performance of CPP plant.

The CPP cycle thermodynamic analysis can be simplified by making the following assumptions:

i. The air used by the gas turbine as well as the products of the combustion are perfect gases.
ii. The specific heat capacities can be constant through the process and represented at the average temperature of that process.
iii. The loss of stagnation pressure in the compressor inlet is a constant percentage of the compressor inlet pressure.
iv. The loss of stagnation pressure in the combustion chamber is a constant percentage of the combustion chamber inlet pressure.

The CPP cycle performance can be calculated through a step-by-step analysis for each component in the cycle.

Air and combustion gases properties

The thermodynamic properties of combustion gases and air at various stages throughout the gas turbine cycle are calculated by considering variable specific heats and no dissociation.

Chappel and Cockshutt[11] suggested the following equations to compute the specific heat values for air and combustion gases:

For air at low temperature range of 200 to 800 K

$$C_{Pa} = 1.0189\times10^{3} - 0.13784T_a + 1.9843\times10^{-4}T_a^{2} + 4.2399\times10^{-7}T_a^{3} - 3.7632\times10^{-10}T_a^{4} \quad (9)$$

For air at high temperature range of 800 to 2200 K

$$C_{Pa} = 7.9865\times10^{2} + 0.5339T_a - 2.2882\times10^{-4}T_a^{2} + 3.7421\times10^{-8}T_a^{3} \quad (10)$$

For specific heats of products of combustion

$$C_{Pg} = C_{Pa} + (F/(1+F))B_T \quad (11)$$

where B_T at low temperature range of 200 to 800 K

$$B_T = -3.59494\times10^{2} + 4.5164T_g + 2.8116\times10^{-3}T_g^{2} - 2.1709\times10^{-5}T_g^{3} + 2.8689\times10^{-8}T_g^{4} - 1.2263\times10^{-11}T_g^{5} \quad (12)$$

and B_T at high temperature range of 800 to 2200 K

$$B_T = 1.0888\times10^{3} - 0.1416T_g + 1.916\times10^{-3}T_g^{2} - 1.2401\times10^{-6}T_g^{3} + 3.0669\times10^{-10}T_g^{4} - 2.6117\times10^{-14}T_g^{5} \quad (13)$$

Air compression

The compression power (W_c) can be described as

$$W_c = \dot{m}_a C_{Pa} \frac{T_{o1}}{\eta_c}\left[\left(\frac{P_{o2}}{P_{o1}}\right)^{\gamma_a - 1/\gamma_a} - 1\right] \quad (14)$$

Where the finale stagnation temperature in the compression process (T_{o2}) equal

$$T_{o2} = T_{o1} + \frac{T_{o1}}{\eta_c}\left[\left(\frac{P_{o2}}{P_{o1}}\right)^{\gamma_a - 1/\gamma_a} - 1\right] \quad (15)$$

Combustion

The energy balance of the combustion chamber can be expressed as

$$\eta_{cc} f(LCV) = (1+f)C_{Pg}(T_{o3} - T_{o2}) \quad (16)$$

Therefore the fuel to air ratio (f) in the combustion chamber

$$f = \frac{1}{\frac{\eta_{cc}(LCV)}{C_{Pg}(T_{o3} - T_{o2})} - 1} \quad (17)$$

The pressure loss in the combustion chamber (ξ) is a percentage constant value from the inlet pressure where

$$P_{o3} = (1 - \xi_{cc})P_{o2} \quad (18)$$

Gas expansion

The turbine power (W_t) can be described as

$$W_t = (1+f)\dot{m}_a C_{Pg}\eta_t T_{o3}\left[1 - \left(\frac{P_{o4}}{P_{o3}}\right)^{\gamma_g - 1/\gamma_g}\right] \quad (19)$$

Where the exhaust stagnation temperature in the expansion process (T_{o4}) equal

$$T_{o4} = T_{o3} - \eta_t T_{o3}\left[1 - \left(\frac{P_{o4}}{P_{o3}}\right)^{\gamma_g - 1/\gamma_g}\right] \quad (20)$$

The efficiency of the gas turbine cycle (η_{gt}) can be described as

$$\eta_{gt} = \frac{W_t - W_c}{f\dot{m}_a(LCV)} \tag{21}$$

The specific work of the gas turbine cycle (w_{gt}) can be described as

$$w_{gt} = \frac{W_{gt}}{\dot{m}_a} = \frac{W_t - W_c}{\dot{m}_a} \tag{22}$$

Heat recovery steam generator calculations

The energy balance in the steam generator can be expressed as

$$\dot{m}_a(1+f)C_{Pg}(T_{o4(gt)} - T_{o6(gt)})\eta_B = \dot{m}_{st}(h_{2(st)} - h_{1(st)}) \tag{23}$$

The gas stack temperature ($T_{o6(gt)}$) should be kept as low as possible, but at the same time condensation should be avoided.

The fuel type used in the cycle determines the lowest stack temperature where the sulfuric fuels should have a higher stack temperature.

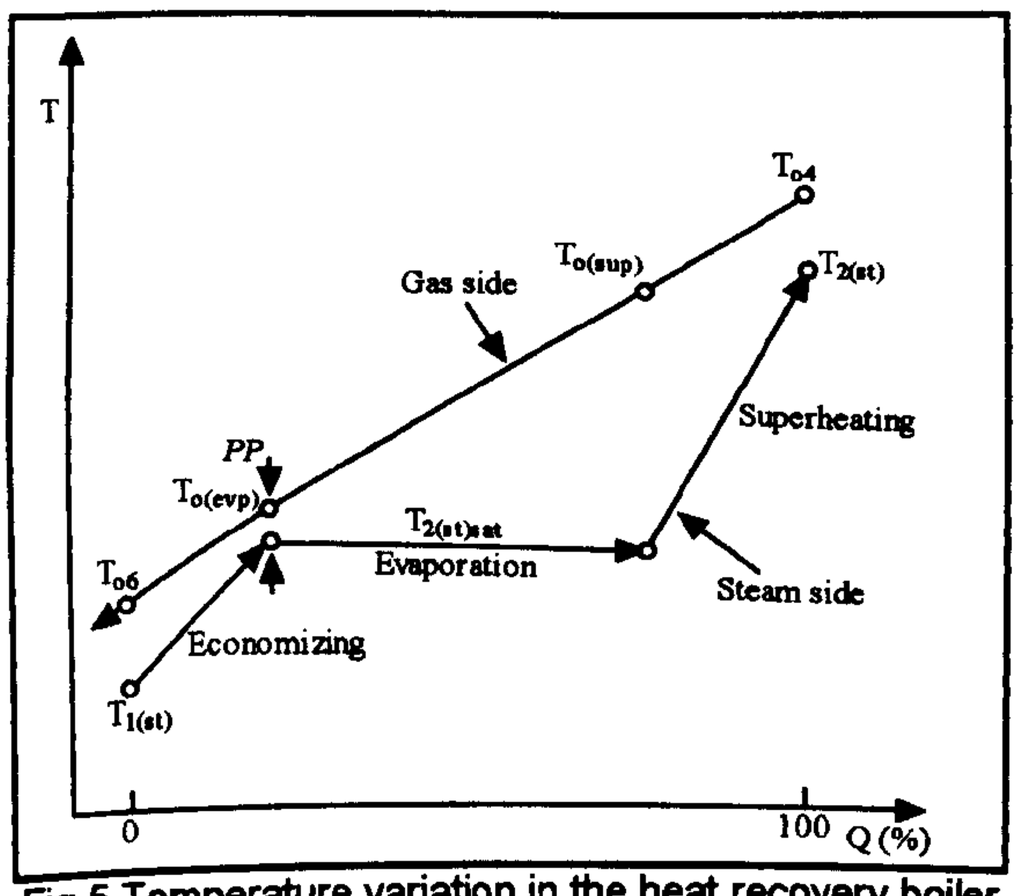

Fig.5 Temperature variation in the heat recovery boiler

The temperature-heat diagram of the heat recovery steam generator is shown in Fig.5. The heat absorbed by the water or the steam is carried out in three steps:

i. The economizing process where the temperature of water raises from $T_{1(st)}$ to the saturation liquid temperature at that boiler pressure.

ii. The evaporation process where the water absorbs heat at constant temperature to be converted to steam.

iii. The superheating step where the temperature of steam increases from the saturation temperature to the maximum temperature of the steam ($T_{2(st)}$).

$$T_{2(st)} = \varepsilon_{sup}(T_{o4(gt)} - T_{2(st)sat}) + T_{2(st)sat} \tag{24}$$

where $T_{2(st)sat}$ is the saturated temperature at the $P_{2(st)}$

The enthalpy of the steam at the exit of the boiler ($h_{2(st)}$) is

$$h_{2(st)} = f(T_{2(st)}, P_{2(st)}) \tag{25}$$

and

$$T_{o(evp)} = PP + T_{2(st)sat} \tag{26}$$

where $T_{o(evp)}$ is the gas temperature at the exit of the evaporator.

$$\dot{m}_{st} = \frac{\dot{m}_a(1+f)\eta_B C_{Pg}(T_{o4} - T_{o(evp)})}{h_{2(st)} - h_{2(lg)sat}} \tag{27}$$

where $h_{2(lg)sat}$ is the saturated liquid enthalpy at $P_{2(st)}$.

The enthalpy of the water at the exit of the pump ($h_{1(st)}$) is

$$h_{1(st)} = f(P_{1(st)}, S_4) \tag{28}$$

and

$$T_{o6} = T_{o(evp)} - \frac{\dot{m}_{st}(h_{2(lg)sat} - h_{1(st)})}{\dot{m}_a(1+f)C_{Pg}} \tag{29}$$

The enthalpy of the steam at the exit of the steam turbine ($h_{3(st)}$) is

$$h_{3(st)} = f(P_{4(st)}, S_3) \tag{30}$$

The enthalpy of the water at the exit of the condenser ($h_{4(st)}$) is

$$h_{4(st)} = f(P_{4(st)}) \tag{31}$$

The heating exchange process in a counter flow heat recovery steam generator must satisfy the following conditions:

i. The gas stack temperature ($T_{o6(gt)}$) must be greater than the inlet water temperature ($T_{1(st)}$).

ii. The gas temperature at the outlet of the evaporator ($T_{o(evp)}$) must be greater than the liquid saturation temperature of the steam ($T_{2(st)sat}$) by a minimum value (pinch point temperature difference (*PP*)).

iii. The superheated steam temperature ($T_{2(st)}$) must be less than the gas turbine exhaust temperature ($T_{o4(gt)}$).

Water pumping

The water pump power (W_p) can be described as

$$W_P = \frac{\dot{m}_{st}}{\eta_P}\left(h_{1(st)} - h_{4(st)}\right) \quad (32)$$

where the entropy at state 1 equals the entropy at state 4.

Steam expansion

The steam turbine power ($W_{t(st)}$) can be described as

$$W_{t(st)} = \dot{m}_{st}\eta_{t(st)}\left(h_{2(st)} - h_{3(st)}\right) \quad (33)$$

where the entropy at state 2 equals the entropy at state 3.

The efficiency of the steam turbine cycle (η_{st}) can be described as

$$\eta_{st} = \frac{W_{st}}{Q_B} = \frac{W_{t(st)} - W_P}{\dot{m}_a(1+f)C_{pg}(T_{o4} - T_{o6})} \quad (34)$$

Combined cycle performance

The combined cycle efficiency (η_{CPP}) can be described as

$$\eta_{CPP} = \frac{W_{Total}}{\dot{m}_f(LCV)} = \frac{W_{gt} + W_{st}}{\dot{m}_a f(LCV)} \quad (35)$$

The specific work of the combined cycle (w_{CPP}) can be described as

$$w_{CPP} = \frac{W_{Total}}{\dot{m}_a} = \frac{W_{gt} + W_{st}}{\dot{m}_a} \quad (36)$$

Considerations and limitations on the parametric analysis

The parameters can be varied according to the following thermodynamic conditions, technological factors and physical factors:

i. The temperature ratio can be assumed all the values from the ratio of (T_{o2}/T_{o1}) to a maximum value where the maximum value is tied to technological factors.

ii. The pressure ratio (r) can be assumed all the values from one to a maximum value where the specific work of the gas turbine is zero.

iii. The steam temperature can be assumed all the values from the saturation temperature at that pressure to a maximum value where the maximum value is tied to technological factors.

iv. The steam pressure and the condenser pressure are related to the wetness of the steam at the exit of the steam turbine, which has to be higher than a minimum acceptable value.

v. The exhaust gas temperature in the boiler should be higher than the temperature of the steam by a minimum value where this value dependent on the economic and the design parameters.

vi. The stack exhaust temperature should be higher than a minimum value where below this value a corrosive condensation can happen.

Using the thermodynamic analysis and parameters limitations, a computer program has been developed to calculate the specific work output and the thermal efficiency of the combined cycle.

RESULTS AND DISCUSSION

In the present parametric study the assumed ranges of values has been taken to be realistic and to compensate for any future developments. Table (1) gives the assumed values of the combined cycle parameters.

T_{o1}	293 K	$\eta_{t(gt)}$	0.88
P_{o1}	101.3 kPa	$\eta_{t(gt)}$	0.88
T_{o3}	(1100 - 1700) K	$\eta_{t(st)}$	0.87
r	(4 – 32)	η_B	0.85
$P_{2(st)}$	10 - 150 bar	η_P	0.85
$P_{1(st)}$	0.05 - 0.5 bar	η_{mec}	0.98
$T_{3(st)\,max}$	950 K	ξ	7%
PP	25 K	$\varepsilon_{superheater}$	0.9
D_{min}	0.88	LCV	42400 kJ/kg
η_c	0.86	η_{cc}	0.98

Table 1 Assumed parameters' values used in the parametric study

For a simple gas turbine cycle the thermal efficiency versus the specific work output is given in Fig.6 and the gas turbine exhaust temperature versus the pressure ratio is given in Fig.7. Fig.6 shows that the maximum gas turbine specific work points have different parameters than the maximum thermal efficiency points. Fig.7 shows that the gas turbine exhaust temperature is higher at lower gas turbine pressure ratio and that the maximum specific work points has a higher gas turbine exhaust temperature than the maximum efficiency points.

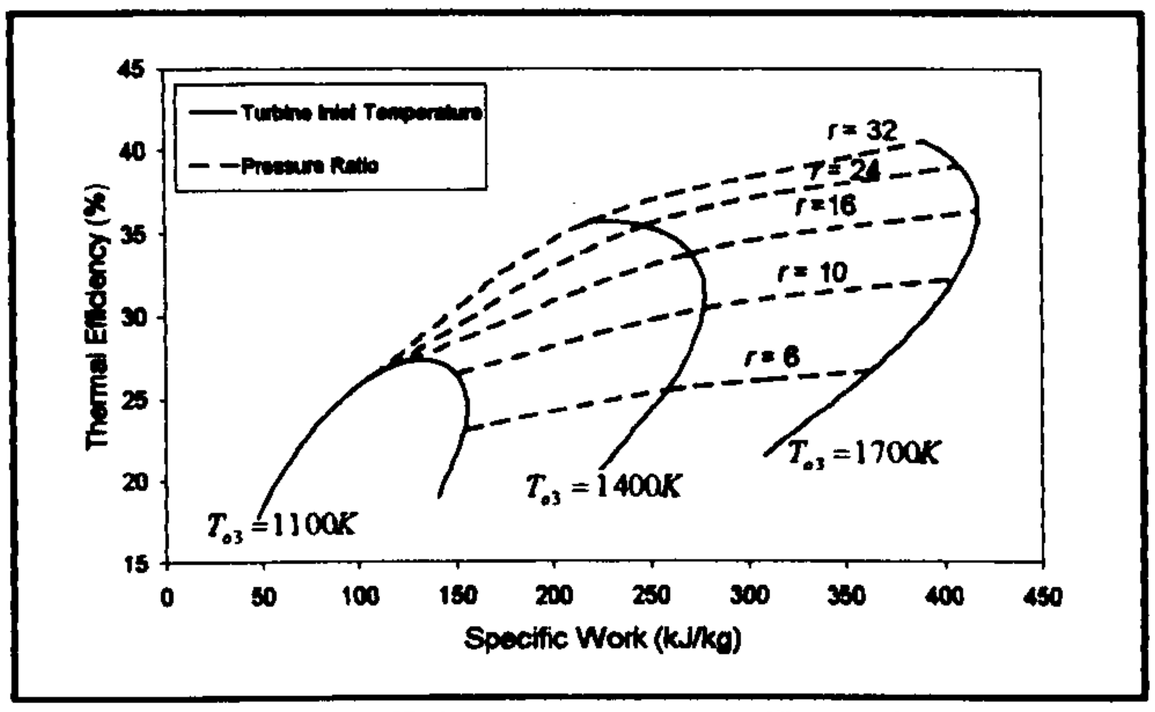

Fig.6 Gas turbine efficiency versus specific work at constant turbine inlet temperatures and pressure ratios

There are many gas/steam cycles configurations, In this study the following configurations has been considered:

i. Simple gas turbine cycle combined with simple steam cycle.

ii. Simple gas turbine cycle combined with dual pressure steam cycle.
iii. Reheat gas turbine cycle combined with simple steam cycle.
iv. Reheat gas turbine cycle combined with dual pressure steam cycle.

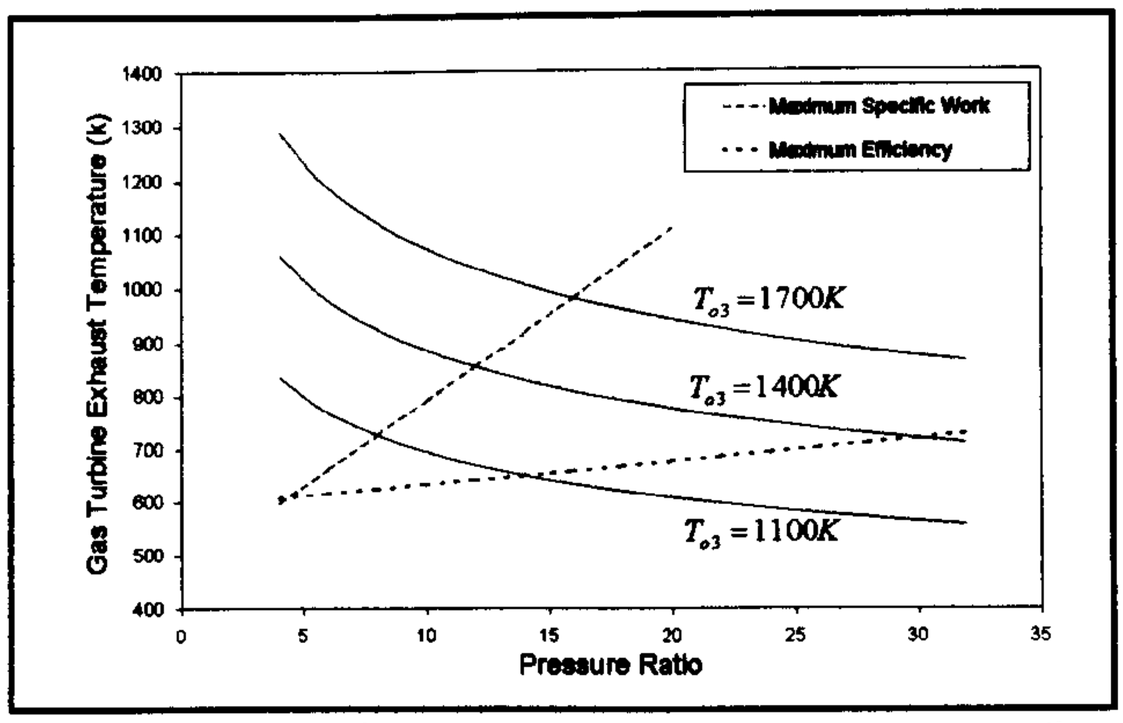

Fig.7 Gas turbine exhaust temperature versus pressure ratio at constant turbine inlet temperatures

v. Gas turbine Intercooling cycle combined with simple steam cycle.
vi. Gas turbine Intercooling cycle combined with dual pressure steam cycle.

Simultaneous variation of the main parameters in both cycles will show the effect of theses parameters on the combined cycle performance. While varying some parameters the other parameters should be taken as constants. Performance of combined cycle has been discussed with respect to the following parameters:

i. Gas turbine pressure ratio.
ii. Gas turbine inlet temperature.
iii. Gas turbine exhaust temperature.

Numerical results of the calculations performed according to the thermodynamic analysis of the cycles. The parameters varied according to the values in Table 1.

For a simple gas turbine cycle combined with simple steam cycle, combined cycle efficiency versus pressure ratio, keeping the gas turbine inlet temperature and the boiler pressure constants, is given in Fig.8. The corresponding specific work is given in Fig.9 and the combined efficiency versus the specific work is given in Fig.10. Combined efficiency versus pressure ratio with the maximum efficiency lines at 50 bar and 90 bar boiler pressure is given in Fig.11.

Combined cycle efficiency versus the boiler pressure at constant pressure ratio and for turbine temperature of 1400 K is given in Fig.12.

Combined cycle efficiency versus the steam air ratio for pressure ratio of 16 and turbine inlet temperature of 1400 K is given in Fig.13.

For a reheat gas turbine cycle with a simple pressure steam cycle, the reheat in the gas turbine cycle will increase the combined specific work at all turbine inlet temperatures but the combined efficiency will be increased at lower turbine inlet temperatures and decreased at higher turbine inlet temperatures. Combined cycle efficiency versus pressure ratio, keeping the gas turbine inlet temperature and the boiler pressure constants, is given in Fig.14. The corresponding specific work is given in Fig.15 and a comparison with the simple combined cycle efficiency is shown in Fig.16.

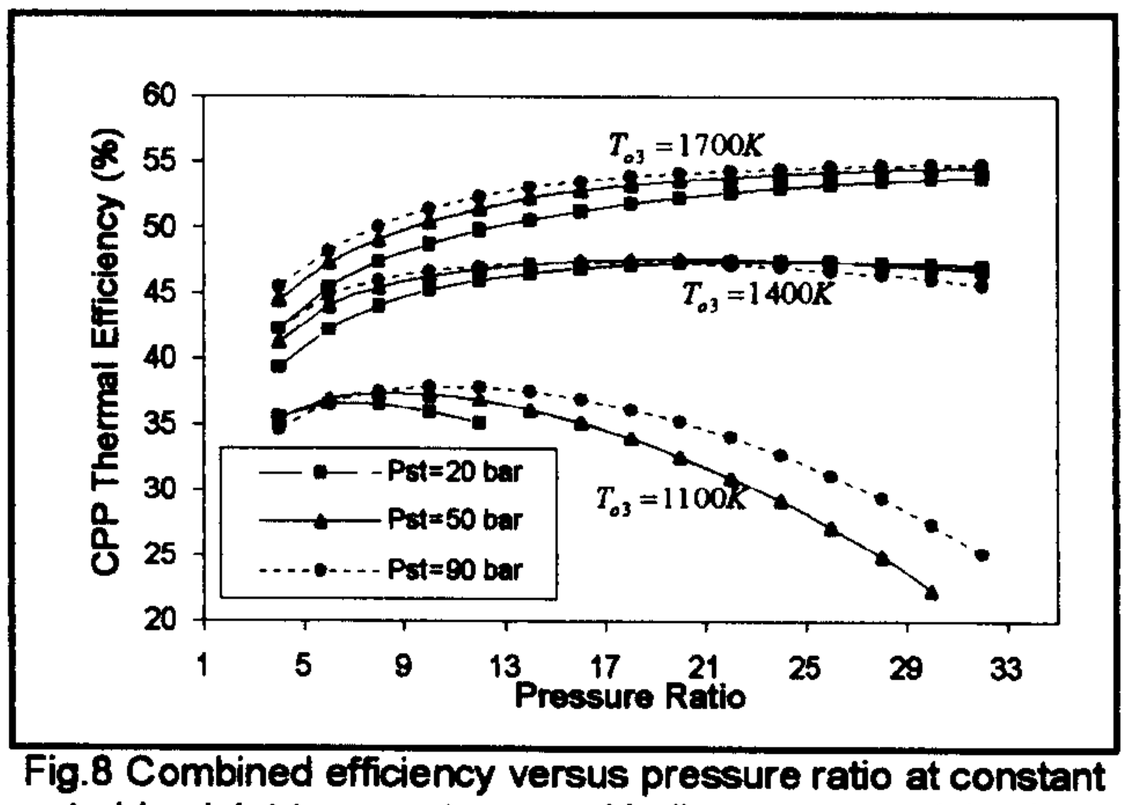

Fig.8 Combined efficiency versus pressure ratio at constant turbine inlet temperatures and boiler pressures (simple combined cycle)

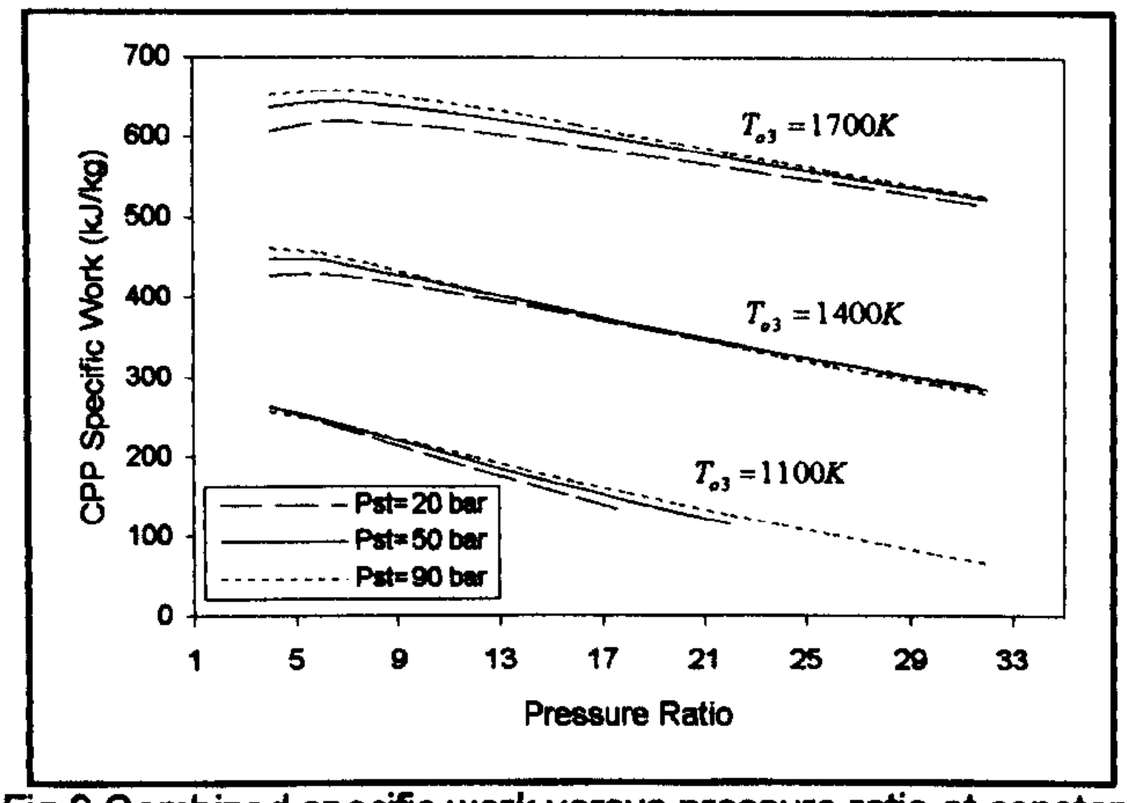

Fig.9 Combined specific work versus pressure ratio at constant turbine inlet temperatures and boiler pressures (simple combined cycle)

For a simple gas turbine cycle with a dual pressure steam cycle, the dual pressure steam cycle will increase both the combined efficiency and the combined specific work. Combined cycle efficiency versus pressure ratio, keeping the gas turbine inlet temperature and the boiler pressure constants, is given in Fig.17. The corresponding specific work is given in Fig.18 and a comparison with the simple combined cycle efficiency is shown in Fig.19.

For a Gas turbine Intercooling cycle combined with a dual pressure steam cycle, the gas intercooling cycle will increase the combined specific work and slightly increase the combined efficiency at higher values of pressure ratio. Combined cycle efficiency versus pressure ratio, keeping the gas turbine inlet temperature and the boiler pressure constants, is given in Fig.20. The corresponding specific work is given in Fig.21 and a comparison with the simple combined cycle efficiency is shown in Fig.22.

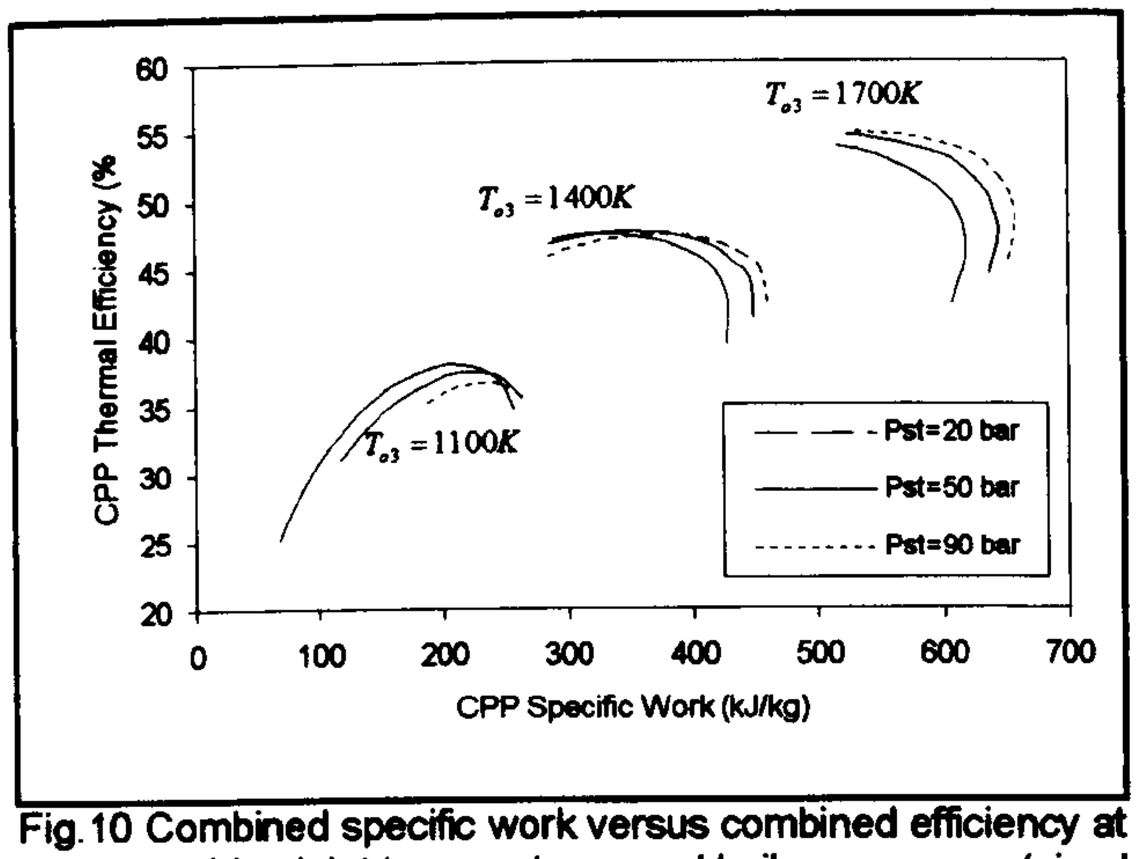

Fig.10 Combined specific work versus combined efficiency at constant turbine inlet temperatures and boiler pressures (simple combined cycle)

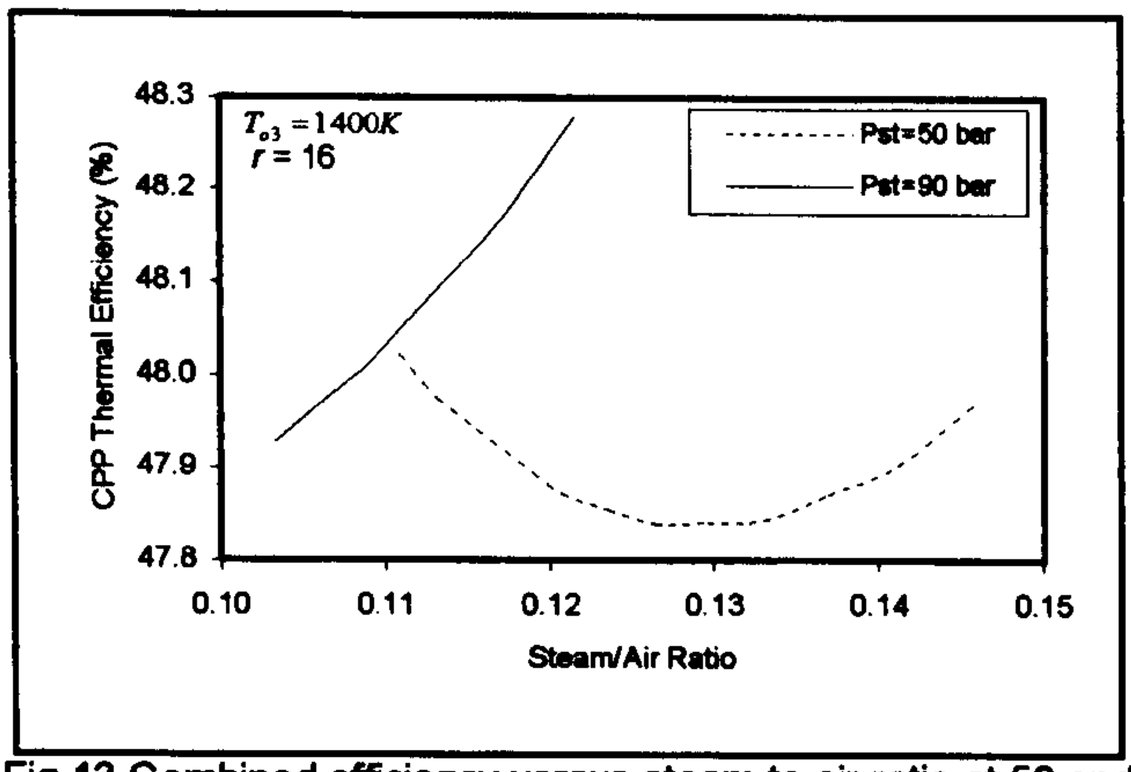

Fig.13 Combined efficiency versus steam to air ratio at 50 and 90 bar steam boiler pressure

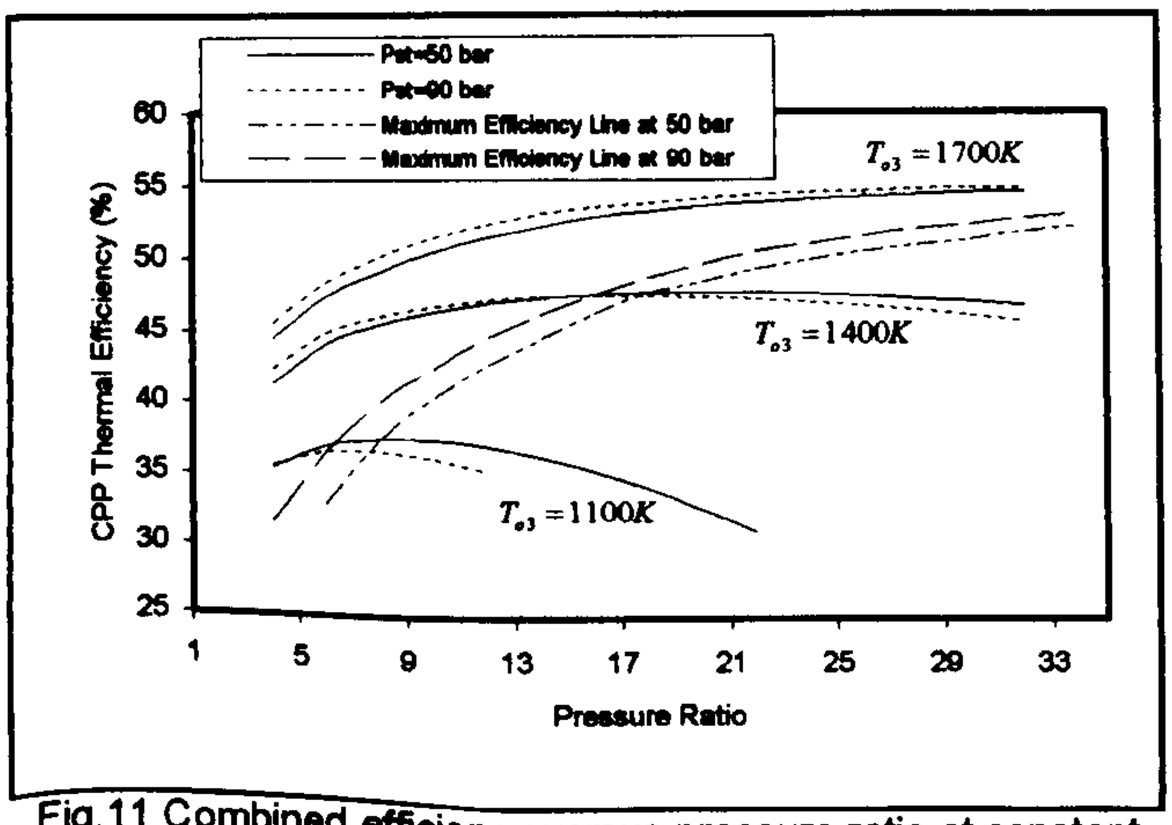

Fig.11 Combined efficiency versus pressure ratio at constant turbine inlet temperatures with maximum efficiency lines (simple combined cycle)

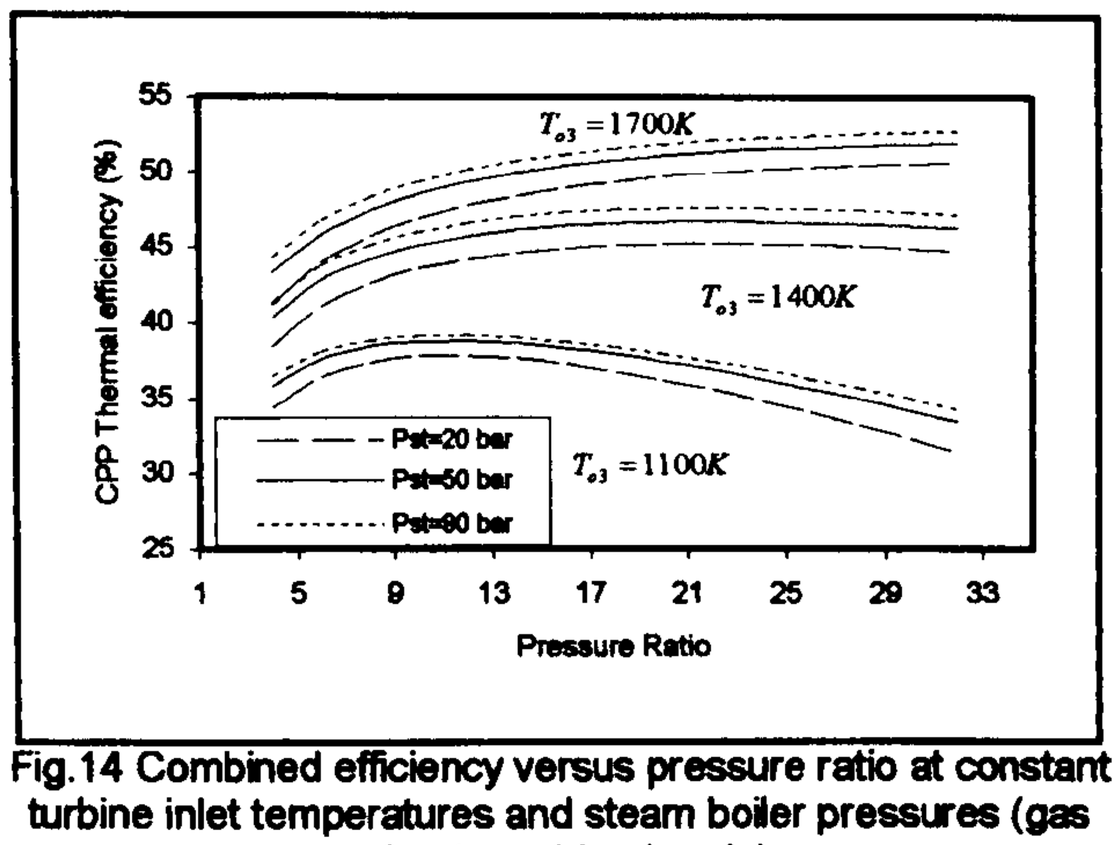

Fig.14 Combined efficiency versus pressure ratio at constant turbine inlet temperatures and steam boiler pressures (gas reheat combined cycle)

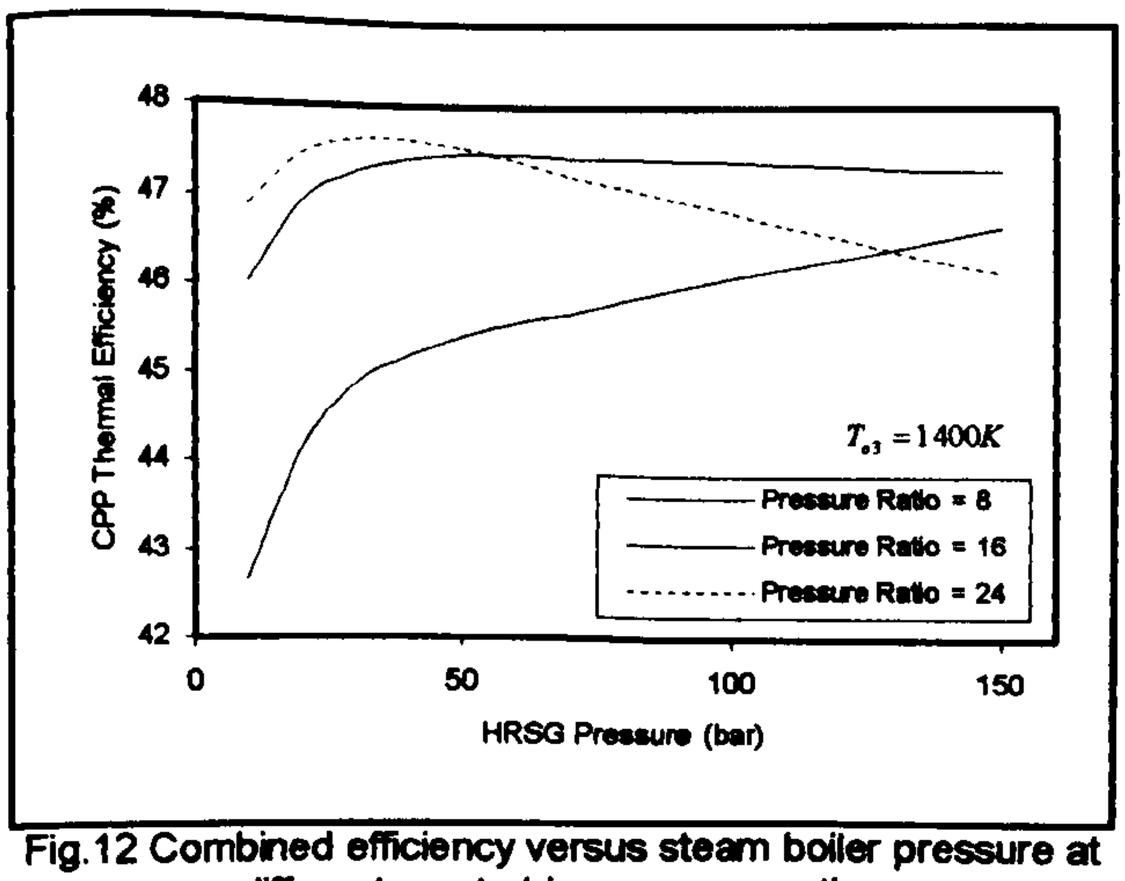

Fig.12 Combined efficiency versus steam boiler pressure at different gas turbine pressure ratios

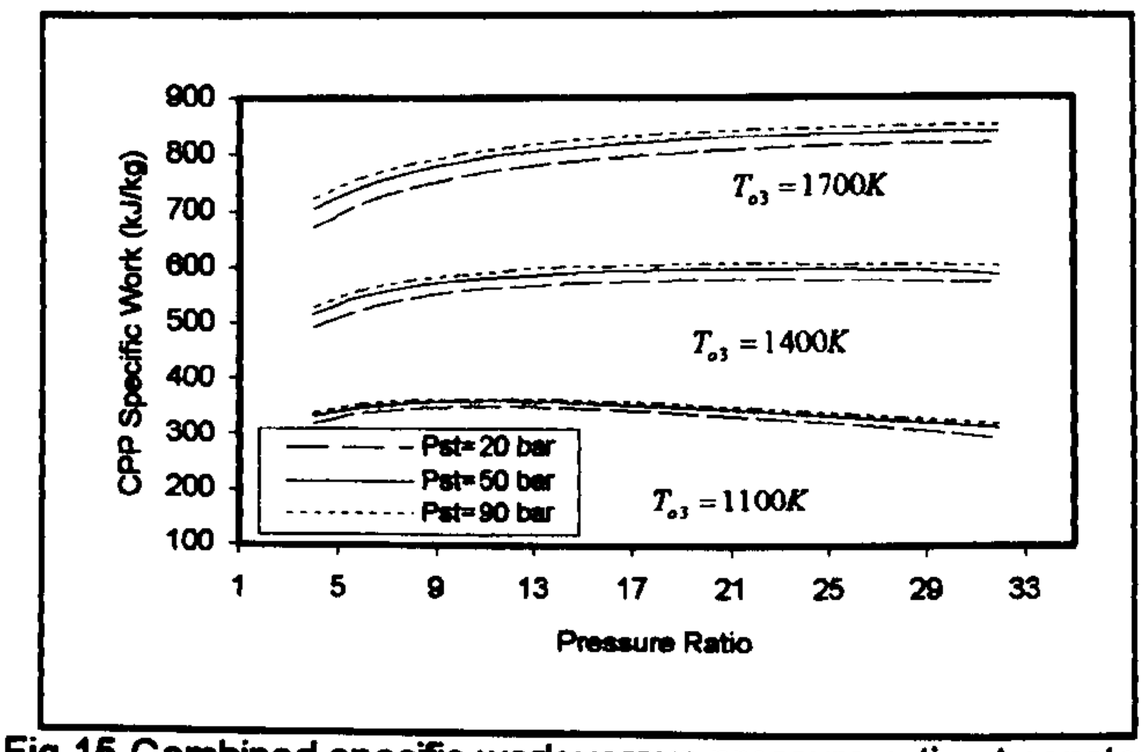

Fig.15 Combined specific work versus pressure ratio at constant turbine inlet temperatures and steam boiler pressures (gas reheat combined cycle)

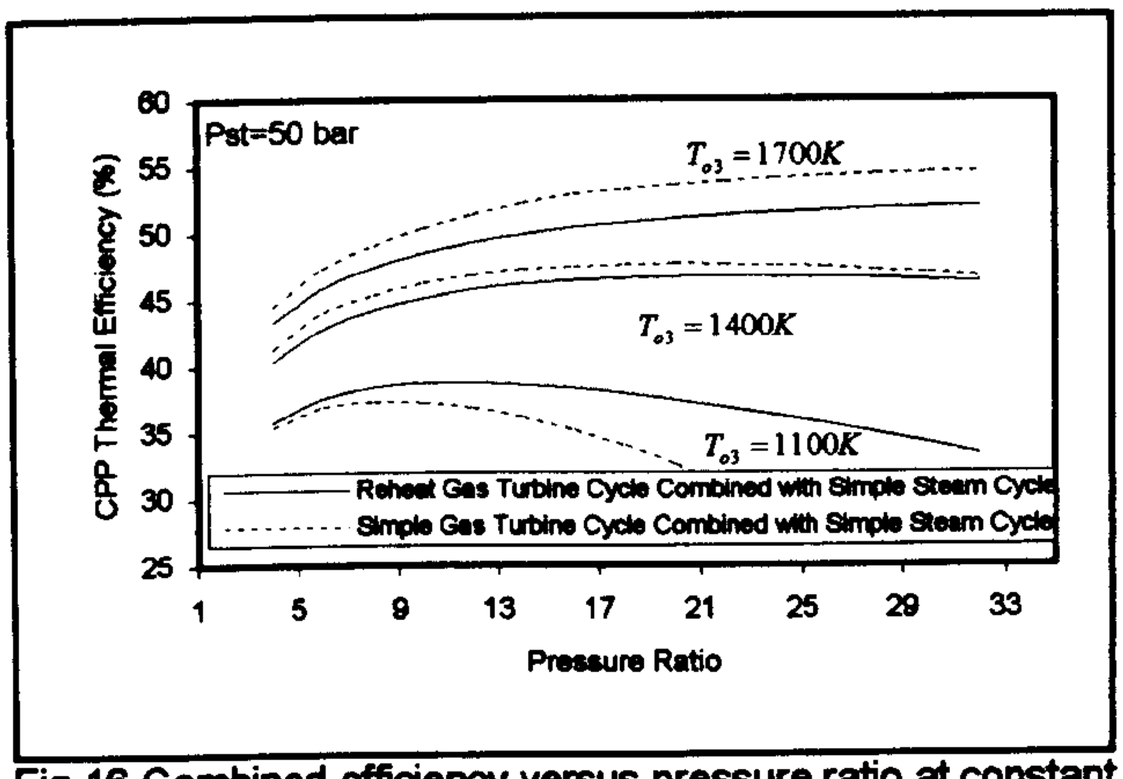

Fig.16 Combined efficiency versus pressure ratio at constant turbine inlet temperatures for simple combined cycle and gas reheat combined cycle

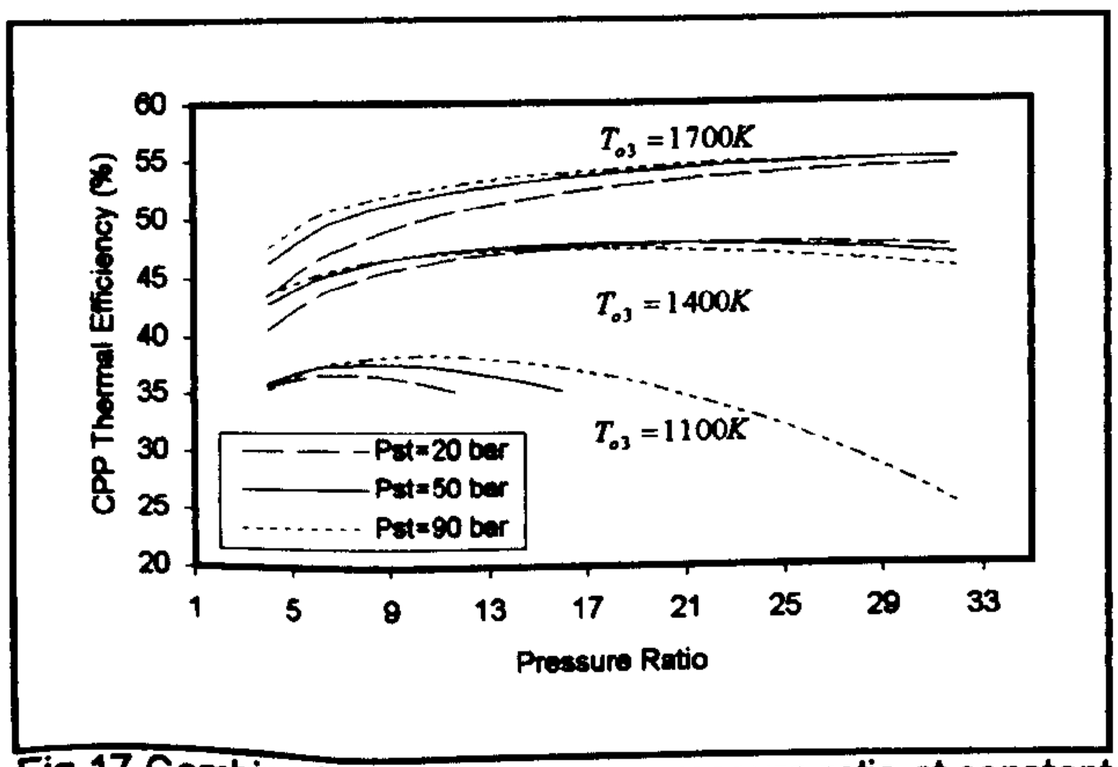

Fig.17 Combined efficiency versus pressure ratio at constant turbine inlet temperatures (simple gas and dual pressure steam combined cycle)

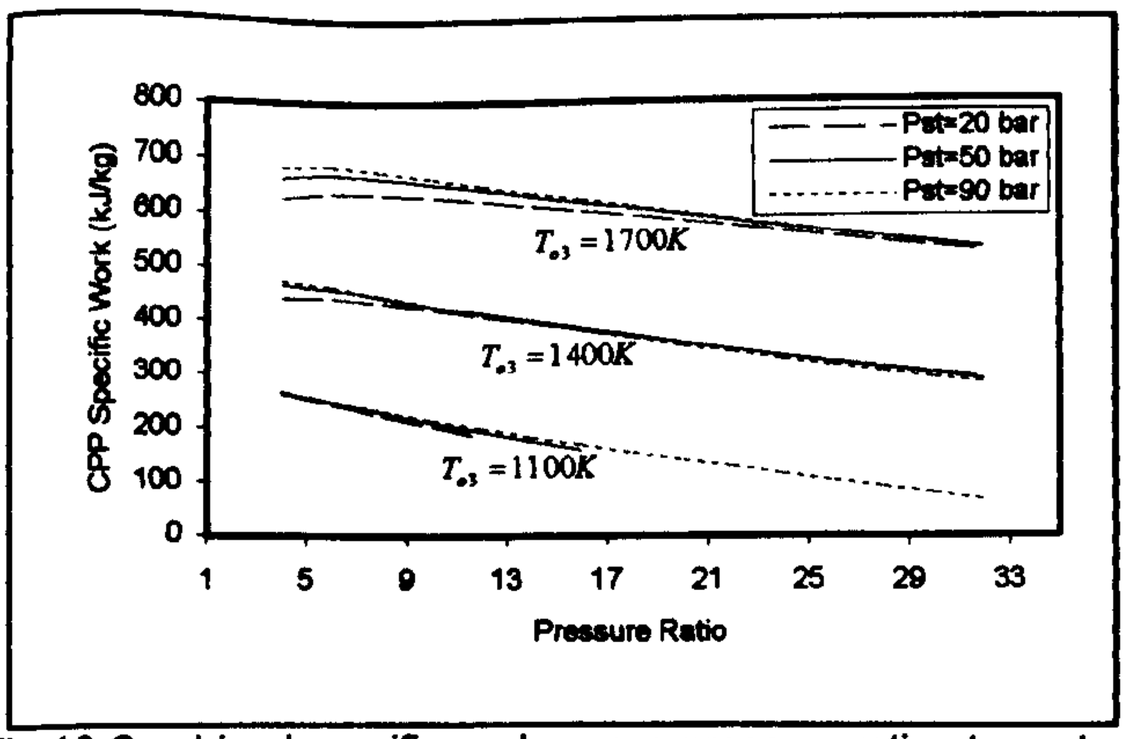

Fig.18 Combined specific work versus pressure ratio at constant turbine inlet temperatures (simple gas and dual pressure steam combined cycle)

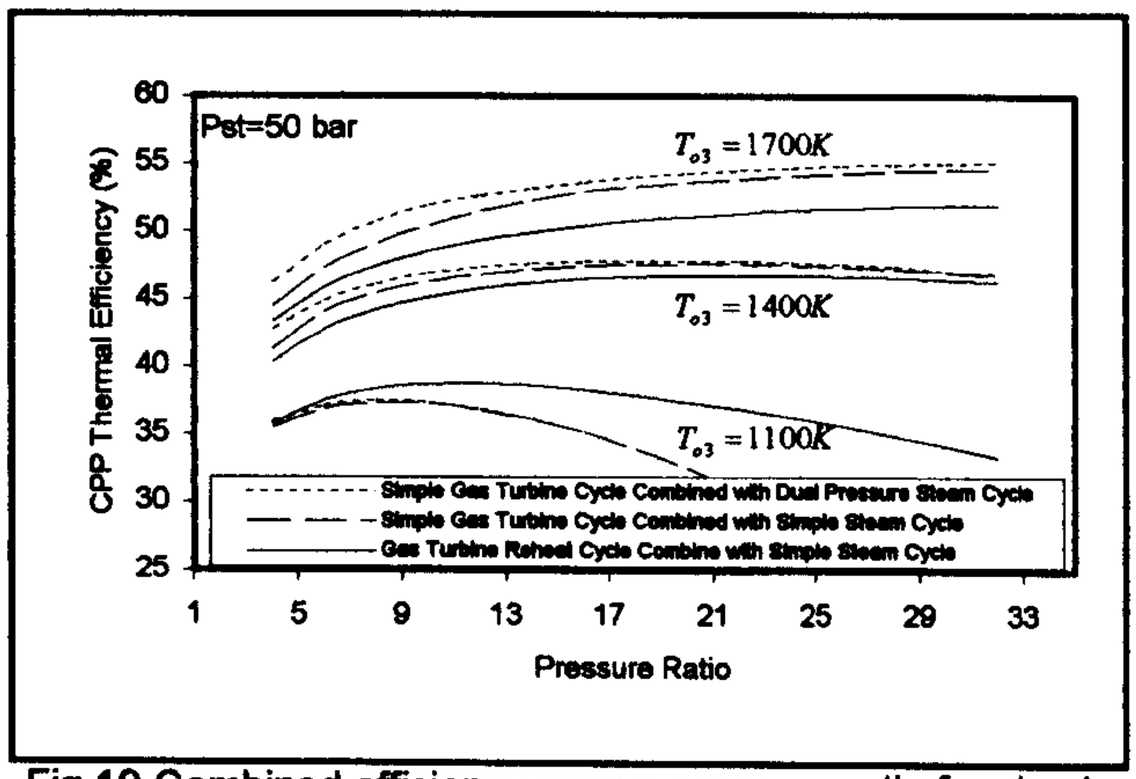

Fig.19 Combined efficiency versus pressure ratio for simple combined cycle, simple gas combined with dual pressure steam cycle and gas reheat combined cycle

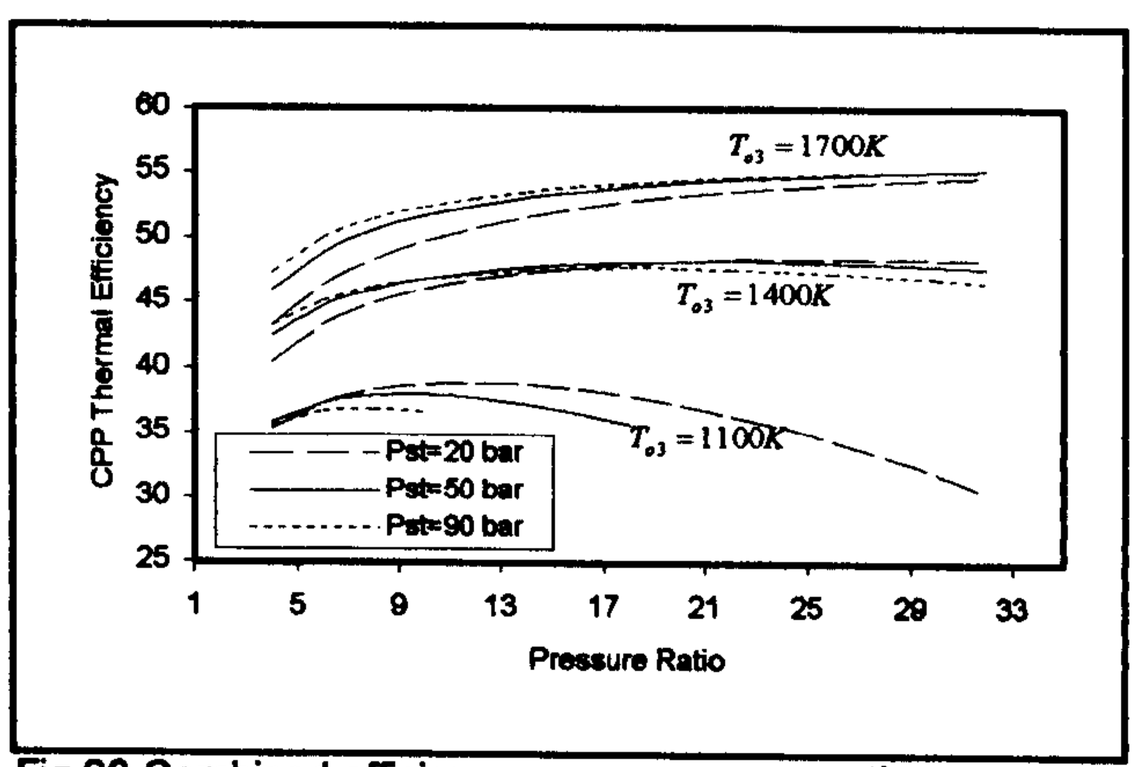

Fig.20 Combined efficiency versus pressure ratio at constant turbine inlet temperatures (gas turbine intercooling cycle combined with dual pressure steam cycle)

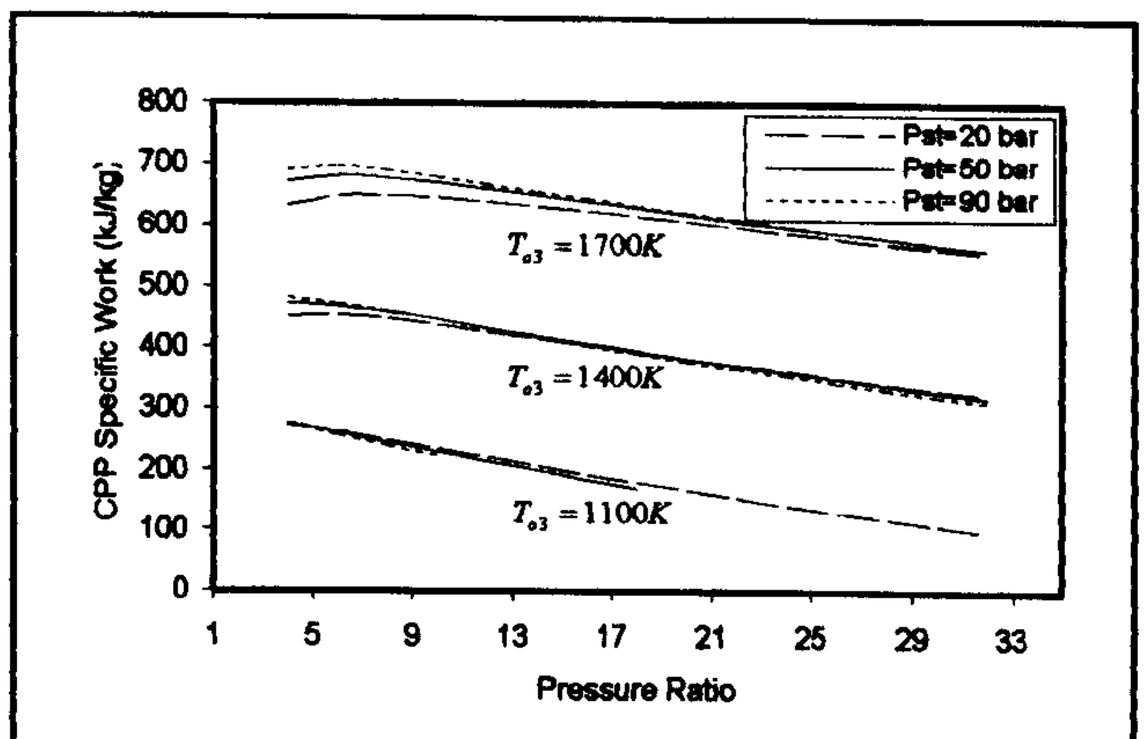

Fig.21 Combined specific work versus pressure ratio at constant turbine inlet temperatures (gas turbine intercooling cycle combined with dual pressure steam cycle)

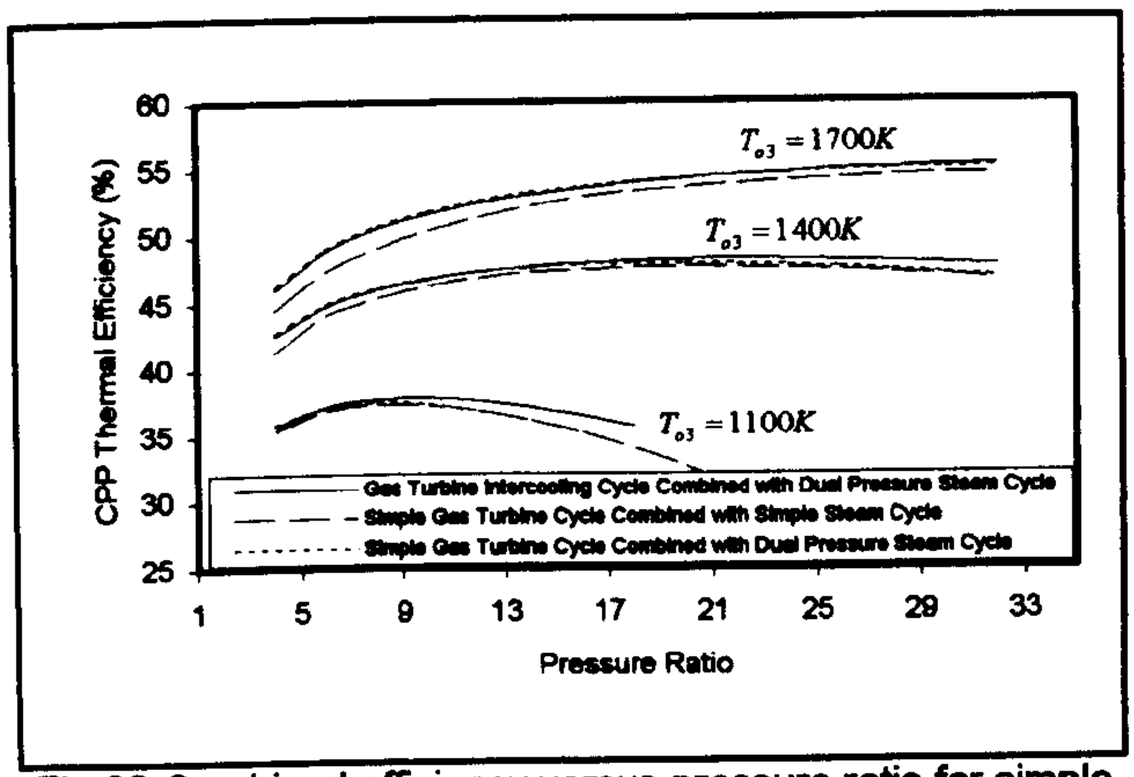

Fig.22 Combined efficiency versus pressure ratio for simple combined cycle, gas intercooling combined with dual pressure steam cycle and gas reheat cycle

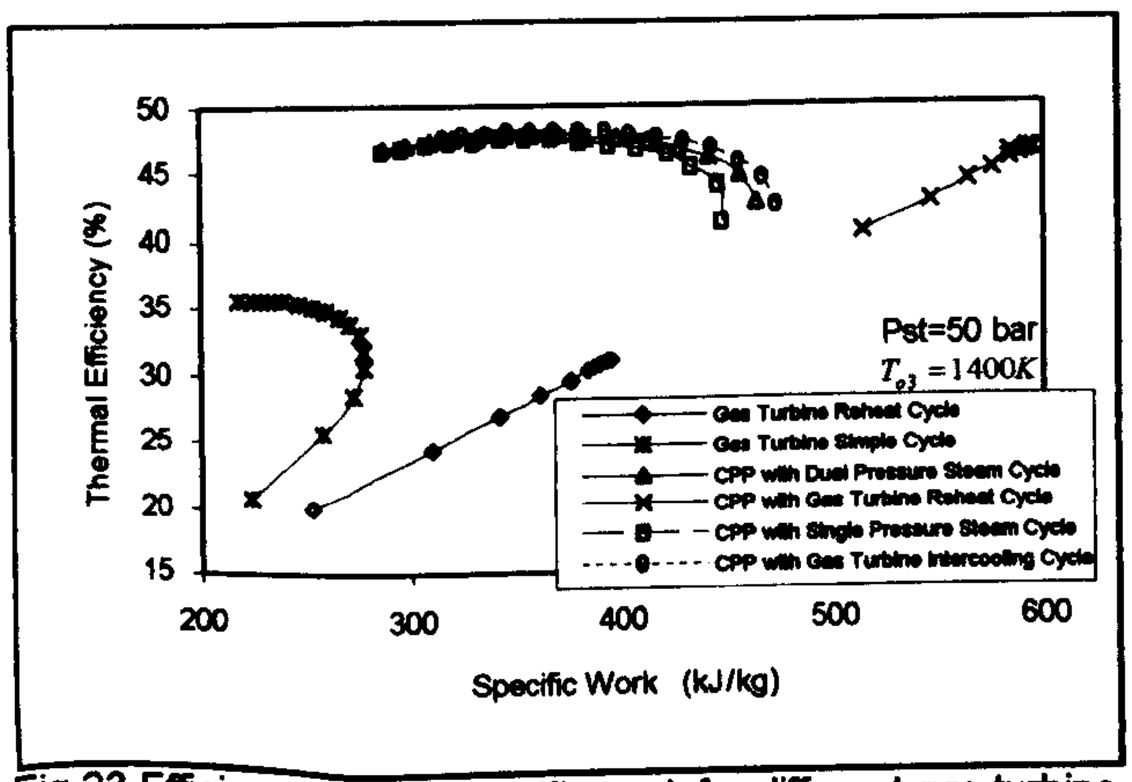

Fig.23 Efficiency versus specific work for different gas turbine cycles at 1400 K turbine inlet temperature and 50 bar steam boiler pressure

Fig.23 shows the efficiency versus the specific work for different configurations of a gas turbine cycle at 1400 K turbine inlet temperature and 50 bar boiler pressure.

CONCLUSION

From these results some important observations can be stated:

i. Increasing the gas turbine inlet temperature will always increase the combined cycle efficiency and the combined specific work.

ii. The higher the gas turbine inlet temperature the greater the influence of the pressure ratio difference on the combined cycle efficiency at any combined cycle configuration.

iii. High steam boiler pressure can be justified only with high exhaust temperatures (high turbine inlet temperature and/or low pressure ratio).

iv. Gas turbine reheating can be justified only with low turbine inlet temperatures (low gas exhaust temperatures) and/or higher combined specific work output.

v. Dual pressure steam will increase the combined cycle efficiency and the combined specific work output.

vi. Although gas turbine intercooling raises the gas turbine performance, it has a very slight effect on the combined cycle efficiency and the combined specific work output.

vii. The gas turbine cycle performance can be described by the gas turbine efficiency and the gas turbine specific work.

viii. The gas turbine inlet temperature and the compressor pressure ratio are the most influence parameters on the gas turbine cycle performance.

ix. For a simple gas turbine cycle, the maximum efficiency and the maximum specific work have a different performance parameters while for a reheat gas turbine cycle, the maximum efficiency and the maximum specific work have the same performance parameters.

x. Supplementary heating will always decrease the combined cycle efficiency except if the supplementary heating significantly increases the steam turbine cycle efficiency.

xi. Increasing the gas turbine inlet temperature will always increase the combined cycle efficiency and the combined specific work.

xii. The higher the gas turbine inlet temperature the greater the influence of the pressure ratio difference on the combined cycle efficiency at any combined cycle configuration.

xiii. Gas turbine reheating can be justified only with low turbine inlet temperatures (low gas exhaust temperatures) and/or higher combined specific work output.

xiv. Although gas turbine intercooling raises the gas turbine performance, it has a slight effect on the combined cycle efficiency and the combined specific work output.

xv. In the combined power and power cycle, the combined cycle maximum efficiency will not have neither the gas turbine maximum efficiency parameters nor the gas turbine maximum specific work parameters, but the new parameters are closer to the gas turbine maximum specific work parameters.

REFERANCES

[1] Bhinder, F. S. and Mango, O. I. K. "*A parametric study of the combined power and power (CPP) plant for generating electricity*". ASME Turbo Cogeneration. Vienna, 1995.

[2] Cohen, H., Rogers, G. F. C. and Saravanamuttoo, H. I. H. "*Gas turbine theory*". 4th edition, Longman, London, 1996

[3] Kehlhofer, R. "*Combined cycle gas turbine and steam turbine power plants*". Fairmont Press, Lilburn GA, 1991.

[4] Horlock, J. H. "*Combined power plants; including combined cycle gas turbine (CCGT) plants*". Pergamon Press, Oxford, 1992.

[5] Horlock, J. H. "*Aero-engine derivative gas turbines for power generation: Thermodynamic and economic perspectives*". Trans. ASME Journal of Engineering for gas turbines and power, Vol.119, No.1, PP 119-123, 1997.

[6] Horlock, J. H. "*Combined power plants: past, present and future*". Trans. ASME Journal of Engineering for gas turbines and power, Vol.117, No.4, PP 608-616, 1995.

[7] Horlock, J. H. "*The optimum pressure ratio for a combined cycle gas turbine plant*". Proc. Inst. Mechanical Engineering

Part A: Journal of power and energy, Vol.209, PP 259-264, 1995.
[8] Cerri, G. "*Parametric Analysis of Combined Gas-Steam Cycles*". Trans. ASME Journal of Engineering for gas turbines and power, Vol.109, No.1, PP 46-55, 1987.
[9] Rufli, P. "*A systematic analysis of the combined gas/steam cycle*". ASME COGEN-TURBO I, Montreux, 1987.
[10] Dvidson, B. J. and Keely, K. R. "*The thermodynamics of practical combined cycles*". Proc. Inst. Mechanical Engineering conference on combined cycle gas turbines, PP 28-50, 1991.
[11] Chappel, M. S. and Cockshutt, E. P. "*Gas Turbine cycle calculations: Thermodynamic data tables for Air and combustion products for three systems of units*". NRC No. 14300, Ottawa, 1974.